On the Dynamics of Low Tension Marine Cables

by

Waldir Terra Pinto

A thesis submitted for the degree of Doctor of Philosophy

in The Faculty of Engineering, University of London.

Department of Mechanical Engineering

University College London

January 1995

Abstract

This thesis is concerned with the dynamics of low tension marine cables. These cables are widely used in the ocean environment for signal and power transmission applications. There are two main issues in the dynamic analysis of such cables. When the tension is zero, which is often the situation encountered at the seabed during cable laying, the cable geometric stiffness matrix becomes singular. The other issue is that the transformation from local co-ordinates to global co-ordinates made through Euler angles leads to a greater number of unknowns than the number of differential equations. The former problem can be overcome by taking into account the flexural rigidity of the cable. The latter problem can be overcome by assuming that one of the Euler angles is known. However, this procedure can introduce singularities on the formulation of the problem.

A new three dimensional model for the dynamics of marine cables is presented in this thesis. The model takes into account the bending stiffness of the cable in order to overcome singularities in the geometric stiffness matrix. In order to overcome the problem owing to the use of Euler angles, a new displacement approach is introduced. This new displacement approach uses the differential geometry definition of curvature and torsion in order to establish the transformation from the local co-ordinates to the global co-ordinates.

The general formulation of the dynamics of marine cables presented in this thesis is applicable to a wide range of cases such as towed cables, cable installation and cable recovery. In order to illustrate this new formulation the cases of towed cables and cable installation are investigated in the some detail. Solutions for the differential equations of motion are presented for two and three dimensions. The two dimensional solution is obtained through a finite

element based technique which uses a weak Galerkin formulation for integration in space and the Newmark method for integration in time. The model's results are compared with full scale measurements. Simulations of the dynamic response of marine cables to vessel wave induced motions and vessel changes in speed are also presented. The three dimensional solution is obtained by expressing the equations of motion as functions of the Euler angles. The space integration is also performed by a finite element model but it uses a finite difference scheme for the time integration. This solution is then used to study the influence of sheared cross-currents in the cable's configuration. Finally, conclusions and suggestions for further research are presented.

TO MY FAMILY

Acknowledgements

I would like to express my gratitude to my supervisor, Dr J. A. Witz, for his encouragement and valuable suggestions throughout this work.

I very grateful to my sponsors, The British Council, Brazilian Post-Graduate Federal Agency (CAPES) and University of Rio Grande for their financial support throughout this research.

I am very indebted to my wife, Vera, and my son, Humberto, for their love, support and encouragement.

I am also very indebted to my parents, Francisco and Irene, and my sister Rosa for their love.

I would like to specially thank my friend, Janito, for his valuable help.

Finally I would like to thank colleagues and staff from the Department of Mechanical Engineering, University College London, for their support.

Table of Contents

List of Figures

List of Tables

Nomenclature

The notation and symbols used in this thesis are defined in the text. To further assist the reader the following list is provided:

A	cross-sectional area of the cable
$\mathbf{a}$	absolute acceleration vector
$\mathbf{a}_N$	normal acceleration vector
$\mathbf{a}_r$	relative acceleration
a	absolute acceleration magnitude
a_{rt}, a_{rn}, a_{rb}	components of the relative acceleration vector with reference to the local frame of reference
a_{rx}, a_{ry}, a_{rz}	components of the relative acceleration vector with reference to the vessel frame of reference
a_t, a_n, a_b	components of the absolute acceleration vector with reference to the local frame of reference
a_{vx}, a_{vy}, a_{vz}	components of the vessel acceleration vector with reference to the vessel frame of reference
a_x, a_y, a_z	components of the absolute acceleration vector with reference to the vessel frame of reference.
C_D	normal drag coefficient
C_M	added mass coefficient
C_T	tangential drag coefficient
d	cable's diameter
EA	cable's axial stiffness
EI	cable's flexural rigidity
$\mathbf{e}_t, \mathbf{e}_n, \mathbf{e}_b$	unit vectors of the local frame of reference affected by the sign of the curvature
$\mathbf{F}$	global force vector
$\mathbf{f}$	element force vector

$\mathbf{f}_b$	element force vector due to the bending stiffness
$\mathbf{f}_d$	element force vector due to the drag forces
$\mathbf{f}_{ext}$	external force vector
$\mathbf{f}_g$	element force vector due to the geometric stiffness
$\mathbf{f}_m$	element force vector due to forces
$\mathbf{f}_w$	element force vector due to the self-weight and buoyance forces
f	just fill slack
f_{at}, f_{an}	tangential and normal components of the added mass force per unit length
f_{mt}, f_{mn}	tangential and normal components of the inertia force per unit length
f_t, f_n	tangential and normal components of the drag force per unit length
$\mathbf{H}$	angular momentum (chapter 3) Hessian matrix (chapter 4)
H	hydrodynamic constant
h	water depth
$\mathbf{I}, \mathbf{J}, \mathbf{K}$	unit vectors for the inertial frame of reference
$\mathbf{i}, \mathbf{j}, \mathbf{k}$	unit vectors for the vessel frame of reference
$\mathbf{L}$	linear momentum per unit length
l	cable length
l_{dp}	amout of cable deployed on the seabed
l_k	finite element length
l_{po}	amount of cable paid out
$\mathbf{M}$	bending moment vector
$\mathbf{M}_T$	twisting moment vector
M	bending moment magnitude
M_T	twisting moment magnitude
m	physical mass per unit length
p	stretched arc length

$\mathbf{Q}$	shear force vector
Q	shear force magnitude
q	distributed load on a beam
$\mathbf{R}$	residual vector quantity
R_s	residual scalar quantity
$\mathbf{r}$	vector position of an element of cable with reference to the vessel frame of reference
$\mathbf{r}_c$	vector position of an element of cable with reference to the inertial frame of reference
$\mathbf{r}_v$	vector position of the vessel with reference to the inertial frame of reference
s	unstretched arc length
$\mathbf{T}$	tension vector
T	tesnion magnitude
T_0	tension at the boundary
$\mathbf{t},\mathbf{n},\mathbf{b}$	unit vectors for the local frame of reference
t	time
t_0	initial time
$\mathbf{U}$	global unknown vector
U	fluid velocity
U_{fx},U_{fy},U_{fz}	components of the fluid velocity in the vessel frame of reference
U_{fX},U_{fY},U_{fZ}	components of the fluid velocity in the inertial frame of reference
U_t,U_n,U_b	components of the fluid velocity in the local frame of reference
$\mathbf{u}$	local unknown vector
$\mathbf{V}$	velocity vector
$\mathbf{V}_c$	absolute velocity vector of an element of cable
$\mathbf{V}_N$	normal velocity vector in two dimensions
$\mathbf{V}_{RN}$	normal velocity vector in three dimensions
$\mathbf{V}_T$	tangential velocity vector
V_{ct},V_{cn},V_{cb}	components of the velocity in the local frame of reference

V_{cx}, V_{cy}, V_{cz}	components of the velocity in the vessel frame of reference
V_{po}	pay out rate
V_{rt}, V_{rn}, V_{rb}	components of the relative velocity in the local frame of reference
V_{rx}, V_{ry}, V_{rz}	components of the relative velocity in the vessel frame of reference
$\overline{V}_{vx}, \overline{V}_{vy}, \overline{V}_{vz}$	components of the mean vessel velocity with reference to the vessel frame of reference
V_0	vessel initial forward speed
$\overline{\mathrm{W}}$	weighting functions
w	subemerged weight per unit length
$\overline{X}_v, \overline{Y}_v, \overline{Z}_v$	co-ordinated of the mean vessel path with reference to the vessel frame of reference
X, Y, Z	co-ordinates of an element of cable with reference to the inertial frame of reference.
x, y, z	co-ordinates of an element of cable with reference to the vessel frame of reference
x_v, y_v, z_v	vessel co-ordinates with reference to the inertial frame of reference
x_w, y_w, z_w	surge, heave and sway wave induced vessel motions
$\tilde{y}$	approximation for the y-co-ordinate
α	approximation for slope Newmark parameter
$\boldsymbol{\beta}_a$	vector which contains Newmark's coefficients for acceleration
$\boldsymbol{\beta}_v$	vector which contains Newmark's coefficients for velocity
β	seabed slope angle which defines the tangent to the vessel mean path
δ	Newmark parameter differential operator
$\boldsymbol{\varepsilon}$	vector wich contains the term neglected in Taylor expansion
ε	strain

	slack
ε_b	bottom slack
ε_s	vessel slack
ζ	coefficient which defines the finite difference algorthm for time integration
θ	slope
θ_0	slope at the boundary
$\theta_1, \theta_2, \theta_3$	Euler rotations
κ	curvature
$\tilde{\kappa}$	approximation for curvature
ξ	normalised arc length
τ	geometric torsion
ψ	shape functions

1 - Introduction

This thesis investigates the dynamics of low tension marine cables. Cables are a class of structure with very low flexural rigidity compared with their axial stiffness. As a consequence, their ability to react transverse loads comes almost entirely from their geometric stiffness. In general, cables can not withstand compressive loads without experiencing instabilities and undergoing large three dimensional deflections. The behaviour of a cable under load has been the subject of considerable attention over centuries. Virtually all models for cables assume that the cable is perfectly flexible. Perhaps one of the most elegant ways of describing cable behaviour is that attributed to James Bernoulli: " The action of any part of the line upon its neighbour is purely tangential" (Irvine, 1981).

Cable structures have been used in a wide range of applications in the marine environment. Examples are marine cables for signal and power transmission, wire ropes and chains for numerous applications such as mooring systems, flexible pipes for risers and flow lines, and umbilicals for combined tether, signal and power duties for remotely operated semisubmersible vehicles, amongst others.

In recent years the demand for marine cables for signal and power transmission applications has increased substantially. The main reasons for this are, on the one hand, the advent of optical fibre technology which made communication systems based on optical fibre cables a viable alternative to celestial communication systems. As a result, the oceans and seas are rapidly being crossed by a large number of these cable communication systems. This growth is illustrated in Table 1.1. On the other hand, as a result of the need for the hydrocarbon industry to exploit oil and gas in ever deeper waters and increasingly hostile environments, production systems are shifting from fixed platforms to floating production systems. One of the most important features of

these floating production systems are their station keeping where cables play a very important role. In addition, cable structures such as flexible risers and dynamic umbilicals play important functions in floating production systems where they provide the means to bring oil to the surface and permit control of subsea equipment. Other offshore exploration and construction activities such as the installation of pipelines require the use of remotely operated vehicles in which cables are also very important members. These three applications are illustrated in Figures 1.1 to 1.3.

Marine cables can be classified into two main groups according to their mechanical behaviour. The first group corresponds to cables subject to high tension such as mooring lines. In this case the dynamic configuration is close to the quasi-static configuration. The second group corresponds to cables subject to low tensions. In this case the dynamic and static tensions can be of the same order of magnitude. Furthermore, since the tension is low, the geometric stiffness of the cable is also low. As a consequence, even small transverse loads applied to the cable can lead to large displacements. Another feature of low tension cables is that they can exhibit instability, experiencing large three dimensional deflections which may result in loop formation and kinking (Coyne, 1990, Tan and Witz, 1992a, b). A looped marine cable is shown in Figure 1.4. In order to address this looping behaviour both the global dynamic behaviour and the local structural behaviour need to be understood.

The structural behaviour of a cable under load is complex. Cables exhibit a torsional response under axial load as a consequence of the helical armour wires and a non-linear relationship between applied bending moment and curvature. This complex behaviour is the result of the interaction between the cable's component layers with the associated tribological conditions and the non-linear behaviour associated with polymeric materials and the geometry of the helix used for the conductors and armour layers. This structural behaviour

has been the subject of extensive research (Costello,1990, Jolicoeur and Cardou, 1991, Knapp et al, 1991, Feld et al, 1992 and Witz and Tan, 1992a,b) and is itself a topic beyond the scope of this thesis.

As a result of the coupled axial-torsional structural behaviour of cables, twist can be readily built up along a cable as a result of manufacturing techniques, handling procedures and the loading experienced. This induced twist is known as residual twist. The accumulation of residual twist leads to loop formation. As the loop forms, part of the torsional strain energy stored as a result of the residual twist is released and converted into flexural strain energy which leads to large deflections. This often occurs when the tension is temporarily relaxed as the twist is released. The cable may be damaged during loop formation if plastic deformations occur. In other words, the cable will experience damage if the bend radii encountered in the deflected configuration are smaller that the minimum allowable bending radius for the cable. The loop may open with the reapplication of tension under certain conditions. Otherwise, when the cable is retensioned, decreases in the loop diameter will occur which leads to kinking and this may cause severe damage to the cable structure. This is illustrated in Figure 1.4. An important point is that conditions for looping depend on the level of residual twist and the cable's flexural rigidity as well as the tension and the curvature. The latter two parameters are established from the global dynamic analysis of the cable which is the subject of this thesis.

This work is primarily concerned with the dynamic behaviour of low tension telecommunication marine cables during their deployment on the seabed. Nevertheless, owing to the fact that full scale measurements encountered in the literature are obtained from ocean trials of towed cables, the dynamic behaviour of towed cables is also studied. The main objective of the towed cable analysis is to validate the model formulated within this work.

SYSTEM	Year	SYSTEM	Year
Denmark-Sweden	1989	Denmark-Norway	1993
Guam-Philippines 2	1989	Guam-Japan	1993
Korea local	1989	Hawaii domestic	1993
Penbal 3	1989	Hong Kong-Philippines	1993
PTAT 1	1989	Hong Kong-Singapore	1993
UK-France 3	1989	Italy-Egypt	1993
UK-NSOS 1	1989	Japan-Taiwan	1993
Canaries 2	1990	Marocco-Senegal	1993
Denmark-Poland	1990	Netherlands-Denmark	1993
EMOS	1990	New Zealand-Canada	1993
GPT	1990	Pacrim East	1993
Greek Islands	1990	Philippines-Thailand	1993
Hong Kong-Taiwan	1990	SeaMeWe 2	1993
Italy-Sardinia	1990	South Africa-Europe	1993
Pencan 4	1990	Spain-Marocco	1993
APOCS (MTT)	1991	TAT 10	1993
Cyprus-Greece	1991	UK-Belgium	1993
Cyprus-Israel	1991	Hawaii-Japan	1994
Florico 2	1991	Japan-China	1994
HAW 4	1991	Japan-Hong Kong	1994
Italy-Greece	1991	Sicily-Tunisia	1994
Malaysia E-W	1991	Spain domestic	1994
Pencan 5	1991	Thailand-Singapore	1994
PTAT 2	1991	UK-France 5	1994
Singapore-Brunei	1991	UK-Spain 5	1994
Taiwan-China	1991	Argentina-Brazil	1995
Tasman 2	1991	Belgium-Spain 2	1995
TPC 3	1991	Brazil-USA	1995
UK-France 4	1991	Canaries-Venezuela	1995
UK-Germany 5	1991	Indonesia local	1995
UK-Spain 4	1991	Indonesia-Singapore	1995
Denmark-Norway	1992	UK-Scandinavia	1995
France south coast	1992	USA-Colombia	1995
France-Algeria	1992	USA-Honduras	1995
France-Marocco 2	1992	Australia-Guam	1996
HAW 5	1992	Brazil-Canaries	1996
HJK	1992	Norway-Iceland	1996
Hong Kong-Vietnam	1992	Pacrim West	1996
Japan-Korea	1992	Papua-New Guinea	1996
Philippines-Brunei	1992	UK-Netherlands 13	1996
Sicily-Libya	1992	Indonesia local	1997
Spain-Sicily	1992	Brazil domestic	1998
TPC 4	1992	Japan-Philippines	1998
Canaries 3	1993	TPC 5	1998
Denmark-Germany	1993	-	-

Table 1.1 - Existing and planned optical submarine cables (Source: British Telecom)

The remainder of this introductory chapter is divided into three sections. In the first section, a summary of the development of telecommunication systems based on submarine cables is given. Next, the main engineering problems concerning the installation of such cables are presented. The final section defines the scope of this work.

1.1 - A Brief Review of the History of Submarine Telecommunication Cables

In this section a brief review of the history of the development of submarine cable systems for telecommunication applications is presented. For a more detailed account of the remarkable events which have reduced the time for transatlantic communications from a month to less than a second the reader is referred to books by Clark (1958, 1992), Merret (1958) and Shimura (1984).

The history of the development of submarine cables is closely related to the development of the telecommunication industry. By the middle of the last century the telegraph was wide spread all over the world. However, these were land based telegraph systems and a message between Europe and North America, or vice-versa, would take a month to reach its destination and another month for the reply. Recognising the necessity need for a better communication system a group of far sighted men undertook the task of linking these land based telegraph systems across seas and oceans.

It was in 1851 when the first telegraph cable was successfully laid across the English Channel. Once the United Kingdom and continental Europe were connected, the more ambitious step of connecting Europe and North America was attempted. After several attempts, this was finally achieved in 1866 when a telegraph cable was successfully laid between Victoria Bay in Ireland and Newfoundland in Canada. This was a truly remarkable feat of engineering given the average depth of the Atlantic Ocean is approximately 3400 metres

(The Times Atlas of the Oceans, 1983). Thereafter a high level of activity in marine cable laying was maintained until the end of the last century where transoceanic cables were laid between France and the United States, between Singapore and Australia and between Brazil and Europe via Madeira. However, this initial high level of activity dropped substantially in the first half of this century. The reasons for this were Graham Bell's invention of the telephone and Marconi's work on communications by short-wave radio.

By the 1940's, the introduction of coaxial cable and the triode valve made the long distance telephonic communication feasible. As a result, the first submarine telephonic cable was installed between Cuba and the United States in 1950. The first transatlantic telephonic cable, TAT-1, was installed in 1956 between Scotland and Canada. Again, a high level of activity in cable laying followed the installation of the TAT-1 system. Table 1.2 shows the principal Atlantic and Pacific coaxial telephone cables.

NAME	YEAR	TERMINALS	CIRCUITS
TAT-1	1956	Scotland-Canada	36
TAT-2	1959	France-Canada	48
CANTAT-1	1961	Scotland-Canada	80
COMPAC	1963	Canada-Australia	80
TAT-3	1963	England-US	138
TRANSPAC	1964	Hawaii-Japan	138
TAT-4	1965	France-US	128
SEACOM	1965	Australia-Singapore	160
TAT-5	1970	Spain-US	845
CANTAT-2	1974	England-Canada	1840
TAT-6	1976	France-US	4000
TAT-7	1983	UK-US	4200

Table 1.2 - Principal Atlantic and Pacific telephone cables (Clarke,1992)

By the early 1960's, submarine telephonic cables came under strong competition from communication systems based on satellites. In fact, the first transatlantic television broadcast using satellites occurred in 1962. However, cable systems made a strong come back in the late 1980's. The reason for this was the introduction of optical fibre technology. Here signals are transmitted as pulses of light in a wave guide made of silica covered with a polymeric sheath. The losses in optical fibres are very low thus permitting large transmission distances before the attenuated signal requires amplification. As a consequence, optical fibre submarine cables became a viable alternative to celestial communication systems. In 1988, the first transatlantic optical fibre cable, TAT-8, commenced operating. Its capacity was equivalent to 40000 simultaneous conversations. Figure 1.5 summarises the principles of optical fibre technology and Figure 1.6 illustrates a typical optical fibre marine cable.

1.2 - Engineering Operations Related to Submarine Cable Systems

During the construction of a submarine cable system, a cable needs to be safely deployed on the seabed. Cable spans need to be avoided to ensure that they are not damaged as a consequence of hydrodynamic excitation by currents. In addition, in areas where the seabed is shared by other users of the sea, the cable has to be protected against the actions of these users. Furthermore, in the case of repair, the cable needs to be recovered from the seabed. Therefore, the three main engineering operations in a submarine cable system are installation, protection and recovery of the cable. These three operations are considered next.

1.2.1- Cable Installation

In order to install a submarine cable, a cable lay vessel is used. Figure 1.7 illustrates a typical cable lay vessel. Sufficient cable is stored in tanks to cover the projected route with a small amount of excess of cable. The vessel starts at the shore end where the water depth is often only a few metres. The vessel is moored in shallow water close to the shore and the cable is paid out along the surface to the shore supported by buoys. Once the cable shore end connection is made the buoys are progressively cut away from the shore end and the cable sinks to the seabed. Once all the buoys are released the vessel releases its mooring system apart from the bow anchors and starts to advance seawards pulling in the bow anchor lines and paying out cable using a linear engine or a drum at a rate governed by the vessel speed of advance along the route and the seabed topography.

The difference between the amount of cable actually paid out and the amount of cable necessary to cover the seabed for a given interval of time is called slack. Careful control of the slack is extremely important in order to avoid the extremes of running out of cable or causing cable suspensions on the seabed as well as avoiding the build up of excessive tension which can break the cable. For cases where the lay vessel is moving at a constant forward speed in still water with zero bottom tension, the cable assumes a straight line configuration (Zajac, 1957). The inclination of this straight line configuration to horizontal depends on the balance between the drag and the cable's weight. Along the route, the cable lay vessel's task will be complicated by adverse weather as well as having to lay cable between submarine mountains and valleys where water depths in excess of three kilometres are often encountered with the cable touching down on the seabed in the region of ten kilometres behind the lay vessel. Another complication is the launch of repeaters where the vessel has to

slow down in order to allow the repeater to pass through the cable laying equipment. Once the repeater is in suspension the vessel accelerates back to the laying speed. Figure 1.8 illustrates the launching of a repeater and Figure 1.9 illustrates a typical repeater. Representative weights of repeaters in water are in the range of 2.5 to 5 kN. This launching of a repeater introduces transient behaviour. In addition, the bottom of the oceans are shared by several users such as hydrocarbon pipelines and fishing nets. For this reason, the cable landing point on the seabed is not allowed to deviate substantially from the planned route.

1.2.2- Cable Protection

Once the cable has been deployed on the seabed, it is necessary to protect the cable from hazards such as ship anchors or beam trawls. In fact, soon after the very first underwater cable was installed across the English Channel it was cut as a result of a fishing incident Historically, more damage has been done to submarine cables by dragged anchors or trawls than by any other cause (Clarke,1992). To reduce the risk of damage in some locations cables are often buried. At one stage burial operations were only necessary for water depths of less than 100 metres. It has now become necessary to bury cables in water depths approaching 1000 metres owing to increased activities in deeper water.

The most effective way to protect a cable is by burying it at a safe depth where the risk of damage is minimised. This safe depth is a function of the depth of penetration of fishing gear and ship anchors and of the type of soil. Several alternative burial operations exist. The cable can be launched directly into a trench, it can be laid on the seabed and then buried at a later stage or it can be laid and buried at the same time. The burial of cables can be achieved through the use of jetting machines. In this method a high pressure jet is launched against the soil leading to an increase in the pore pressure. As a result the soil

loses strength and behaves like a liquid so that the cable self buries due to its weight. Because of this, this method can only be applied in cohesiveless soil bottoms. Alternatively, this burial can be achieved by ploughing. In this method, the cable is deposited into a trench opened by a plough. The trench is then backfilled by a plough mechanism. Ploughing operations are illustrated in Figure 1.10. Figure 1.11 shows a representative trenching machine and a plough.

The burial of cables by ploughing is more effective than trenching using a water jet because it can be applied to any type of soil and it allows better control of the depth of burial. However, the necessary tension to be applied in the towing cable in order to pull the plough is difficult to estimate. This is because of the complex phenomena involving the interaction between the plough and the soil. Although some work has been done using experiments and field experience such as Palmer et al, (1979), Hata (1979) and Shimura (1984), this problem lacks a consistent mechanical approach which can be attributed mainly to the uncertainty associated with the soil behaviour. Owing to the unpredictability of the tow wire rope tension during burial, there is a danger of destabilising the plough if the tow wire rope catenary is too steep at the seabed. As a consequence, it is extremely important to control the tow wire rope and cable catenaries. Fang and Witz (1993) describe in detail plough towing operations.

1.2.3 - Cable Recovery

There are situations in which the cable needs to be recovered from the sea bed. These situations occur when the cable needs to be repaired or when it can be reused elsewhere or scrapped. Cable recovery is a critical operation in that tensions can be significantly higher than those encountered during installation and therefore cable recovery operations need to be carefully controlled. The

cable vessel first has to grapple for the cable. In relatively shallow water where recovery tensions can be maintained within allowable limits for the cable, the cable can be lifted as shown in Figure 1.12. In deep water a cut and hold grapple is deployed such as the one shown in Figure 1.13 and the cable is lifted to the surface while carefully controlling the cable and grappling rig tensions. The cable can be recovered by the so called conventional procedure in which the ship pulls itself against the cable as shown in Figure 1.14. Alternatively the Shea procedure, which is shown in Figure 1.15, can be used (Zajac, 1957).

In the conventional procedure the straight line configuration no longer holds. This is because the normal drag force acts in the same sense as the normal component of the cable's self-weight. However the tangential drag force is proportional to the square of the magnitude of the vector difference between ship velocity and the haul in rate. As a consequence this force can generally be regarded as small and it is often neglected.

In contrast, in Shea's procedure, the equilibrium configuration is a straight line. This is because the angle between the cable and the seabed is allowed to be greater than 90 degrees and the normal drag force acts in the opposite sense to the normal component of the cable's weight. However the tangential drag force is a function of the vector addition between ship velocity and the haul in rate instead of the difference between these two quantities. As such, the tangential drag force can no longer be regarded as small and, therefore, it can not be neglected. In addition, another important disadvantage of this procedure is that the cable may experience very large curvature at the sea bottom. As a consequence, the flexural rigidity of the cable needs to be taken into account, at least in the region of the seabed.

1.3 - Scope of the Work

The previously described engineering operations related to submarine cable systems give rise to several questions which still need to be answered. These questions may be divided into three main categories. In the first category are those questions regarding the modelling of the global dynamic behaviour of the cable. In the second category are those questions that arise from the local instabilities of the cable and its interaction with the seabed. In the third category are those questions regarding the fluid loading. Obviously, it would be very ambitious to try to answer all these questions in a single work. In this context, this work is primarily concerned with the answers regarding the global dynamic response of the marine cable during installation as well as the dynamic response of towed cables.

In order to predict the dynamic response of a marine cable an original three dimensional model is introduced. This new model takes advantage of the geometric properties of a space curve to establish the equations of motion. The inclusion of the cable bending stiffness in the analysis is fundamental to guarantee continuity in slope as well as to avoid singularities.

With regard to the two other categories mentioned earlier, simplified models are adopted. In order to avoid complex formulae for the interaction between cable and seabed, it is assumed that the seabed is perfectly frictionless. In this case, the bottom tension is either zero or very close to zero. On the other hand the fluid loading on the cable is assumed to be given by the Morison equation (Sarpkaya and Isaacson, 1981). As a result of the cable's small diameter giving rise to high Keulegan-Carpenter numbers the fluid force is drag dominated.

This thesis is divided into a further six chapters. Chapter two presents a review of the previous work where static and stationary solutions are considered in some detail. This is because these solutions are well established and will not be considered elsewhere in this work. Chapter three presents the derivation of an original three dimensional dynamic model for marine cables based on the geometric properties of a space curve. The equations of motion are established by assuming that the cable undergoes large displacements and that the cable has flexural rigidity. Chapter four presents the two dimensional solution for the new model for marine cables. The solution is obtained by a finite element method which uses the Galerkin integral formulation for space integration and the Newmark scheme for time integration. The validation of the two dimensional model is considered in chapter five. This validation of the model is made by comparing full scale measurements of the transient response of a towed cable obtained by Hopland (1993) with the results obtained by the model. In addition, simulations for cable laying situations are made for both transient ship motions and wave induced ship motions. Chapter six presents a solution for the three dimensional equations of motion for marine cables. This solution is also obtained through a finite element method. However, it uses Euler rotations in combination with Frenet-Serret formulae instead of a displacement approach. The equations of motion are integrated in time by a finite difference scheme while the space integration uses again the Galerkin formulation. Results obtained for analysis carried out using the three dimensional model for illustrating the effects of sheared cross-current are also presented. These effects are very important in the prediction of the touchdown point of the cable and are assessed by carrying out a foot printing analysis. Finally, chapter seven presents the conclusions of this work and recommendations for further research.

2 - Previous Work

The use of cables as structural members for the construction of suspension bridges dates back from the early civilisations in the far East and Central and South America. However, the formulation of cable theory was only established in the seventeenth century. Galileo, in his work 'Discourse of Two Sciences' published in 1638, concluded that the shape of a hanging chain was parabolic. This view was proved to be wrong independently by the two Bernoulli brothers, James and John, Leibnitz and Huygens when they established the catenary shape. Huygens arrived at the catenary shape by using an approach based upon geometric principles while the Bernoullis and Leibnitz used an approach based on calculus. The vibrations of strings were studied in the eighteenth century when Daniel Bernoulli arrived at the solution for the natural frequencies of a hanging chain that hangs from one end and Lagrange used taut strings as an illustration of the application of his equations of motion. Irvine (1981) presents a useful review on this early work.

Marine cables differ from the cables used in the above analyses because they are subject to fluid forces such as quadratic drag and inertial forces. Figure 2.1 shows a two dimensional element of marine cable. The choice of the axes system is different from the usual one in order to maintain consistency with the notation used in this work. The differential equations of motion for this element in the tangent and normal directions are, respectively:

$$\frac{\partial T}{\partial s} + w\sin\theta - f_t - f_{at} - f_{mt} = 0 \tag{2.1}$$

and

$$T\frac{\partial \theta}{\partial s} + w\cos\theta - f_n - f_{an} - f_{mn} = 0 \tag{2.2}$$

where T is the effective axial force, θ is the slope, w is the submerged weight per unit length, f, f_a and f_m are the drag force, added mass force and D'Alembert force per unit length, respectively, and s is the arc length. The subscript t and n denote tangential and normal components of the appropriate force. The above equations were obtained through the assumption that the cable is inextensible. According to Faltinsen (1990) this assumption is a very good approximation except in the case of extreme conditions where the elasticity of the cable has to be taken into consideration.

The effective tension concept arises from the fact that the submerged weight can only be used to calculate the buoyancy force as long as Archimedes principle is valid. Archimedes principle is valid for freely floating bodies or for submerged bodies in which the fluid pressure acts over the entire body. As a result Archimedes principle cannot be used to calculate the buoyancy force which acts on an element of a continuous cable. This is because there is no fluid pressure acting on the cross-section of the element of cable. In order to use the submerged weight to calculate the buoyancy force, a tangential force which corresponds to the product of the fluid pressure and the cross-sectional area must be added to the element. This tangential force is usually added to the physical tension and the result is called effective tension. Seyed (1989) provides a comprehensive explanation of the concept of effective tension which also includes the effects of high curvature and internal pressure.

The differential equations of motion of a submarine cable are highly non-linear and in general, an explicit solution is not possible. This chapter presents a review of the principal solutions for these differential equations of motion. These solutions may be divided into groups. The first group corresponds to classical stationary solutions such as the solution for catenary cables and the stationary solution for cable laying. The second group of solution corresponds to numerical solutions. A literature review of the main numerical solutions for

both two and three dimensional dynamic analysis of marine cables with emphasis on cable laying applications is presented in the second part of this chapter.

2.1 - Stationary Solutions for Cables

This section presents some classical stationary solutions for the two dimensional differential equations of motion of a marine cable. The term stationary means that the solution is obtained either for the static case or for the case where the cable is moving at constant velocity in still water. The classical solutions for these two cases are presented bellow.

2.1.1 - Solution for the Catenary Cable

The static solution for the catenary cable presented here is based on the solution presented by Faltinsen (1990). Further to the assumption of static analysis, it is assumed that the drag force acting on the cable is negligible if compared with the submerged weight. This is a reasonable approximation for heavy cables or chains. Under these assumptions, the equations of motion of the cable become, respectively:

$$\frac{\partial T}{\partial s} + w \sin\theta = 0 \tag{2.3}$$

and

$$T\frac{\partial \theta}{\partial s} + w \cos\theta = 0 \tag{2.4}$$

Combining these two equations results in:

$$\frac{dT}{T} = \tan\theta \, d\theta \tag{2.5}$$

As result of the integration of the above equation, the tension may be written as:

$$T = T_0 \frac{\cos\theta_0}{\cos\theta} \tag{2.6}$$

where T_0 and θ_0 are integration constants.

The substitution of this equation into the differential equations of motion (2.3) and (2.4) leads the following expression for the arc length s, co-ordinate x and co-ordinate z:

$$s = s_0 + \frac{T_0 \cos\theta_0}{w}(\tan\theta - \tan\theta_0) \tag{2.7}$$

$$x = x_0 + \frac{T_0 \cos\theta_0}{w}\left[\log\left(\frac{1}{\cos\theta} + \tan\theta\right) - \log\left(\frac{1}{\cos\theta_0} + \tan\theta_0\right)\right] \tag{2.8}$$

$$y = y_0 + \frac{T_0 \cos\theta_0}{w}\left(\frac{1}{\cos\theta} - \frac{1}{\cos\theta_0}\right) \tag{2.9}$$

These equations together with the appropriate boundary conditions define completely the shape of the catenary. These catenary equations can be extended to include elasticity (Peyrot and Goulois, 1979, Faltinsen, 1990).

2.1.2 - Stationary Solution for Cable Laying with Zero Bottom Tension

Zajac (1957) solved the two dimensional differential equations of motion for stationary conditions during cable laying. In the stationary condition the cable is laid at constant pay out rate from a lay vessel moving at constant forward speed in still water. Zajac also assumes that the cable is inextensible and that the tangential component of the drag force is negligible. The former assumption is reasonable because the cable is under relatively low tension and very small changes in length due to the cable elasticity are expected. The latter assumption is a very good approximation because the tangential force is proportional to the square of the difference between the pay out rate and the tangential component of the vessel velocity which is small.

For cases where the bottom tension is zero, a solution similar to the catenary equation's presented in the previous section no longer holds since the governing equation becomes singular. Because of this, the only possible equilibrium position can be obtained when the curvature is zero in equation (2.2). That is, the cable configuration is a straight line. The angle of the straight line is given by:

$$\cos\theta = \frac{f_n}{w} = C_D \frac{\rho d (V \sin\theta)^2}{2w} \tag{2.10}$$

where C_D is the normal drag coefficient, ρ is the fluid density, d is the cable diameter and V is the vessel forward speed, and $w.$ is the submerged weight of the cable per unit length.

It may be concluded from the above derivation that the equilibrium position is achieved when the angle θ is such that the normal component of the drag force has exactly the same magnitude as the normal component of the submerged weight of cable. It also can be seen that the angle of equilibrium depends on the cable parameters and the fluid density which are constant. Because of this, it is usual to replace these constants by a single constant called the hydrodynamic constant H of the cable which is defined by:

$$H = \sqrt{\frac{2w}{C_D \rho d}} \tag{2.11}$$

Note that the hydrodynamic constant has the units of angle times the inverse units of the velocity. Table 2.1 gives some representative values of the hydrodynamic constant for different cables. These cables are illustrated in figure 2.2.

Property\Cable	A65F65	A65	C65	F65
Overall diameter (mm)	68	52	43	47
Weight in air (kg/m)	13.23	6.95	3.69	5.12
Weight in water (kg/m)	9.51	4.77	2.2	3.41
Ultimate Tensile Strength (kN)	1000	600	320	430
Maximum Service Tension (kN)	700	400	250	360
Normal Drag Coefficient	2.89	2.88	2.87	2.90
Hydrodynamic Constant (deg-knots)	107	87	65	77
Minimum Bending Diameter (m)	1.8	1.8	1.8	1.8

Table 2.1 - Properties of typical telecommunication marine cables

Zajac (1957) uses another constant defined as the ratio between the hydrodynamic constant and the vessel forward speed:

$$\alpha = \frac{H}{V} \tag{2.12}$$

As a result, the expression for the equilibrium angle becomes:

$$\cos\theta = \sqrt{1 + \frac{\alpha^4}{4}} - \frac{\alpha^2}{2} \tag{2.12}$$

It can be shown that for small angles the angle θ and the constant α are very close. This suggests that the constant α can be regarded as an approximate value for the angle θ. Zajac also shows that for small inclinations of the straight line configuration the cable sinking velocity can be approximated by the hydrodynamic constant.

2.1.3 - Kinematics of Stationary Cable Laying

For successful deployment of a telecommunication cable, cable suspensions on the seabed must be avoided. Therefore, the amount of cable paid out must be such that the whole seabed is covered. This amount of cable is a function of the vessel forward speed, pay out rate and the seabed topography. In practice, the amount of cable paid out is the amount of cable necessary to cover the seabed exactly plus a small amount of excess cable called slack. The slack has to be carefully controlled otherwise there is a risk of running out of cable.

As in Zajac (1957), Roden (1974) and Shimura (1984), this section considers the kinematics of three different cases regarding the seabed topography. These cases are the laying of a cable on a horizontal seabed, on a descending seabed and on ascending seabed.

Figure 1.1 shows a vessel laying a marine cable in a horizontal seabed. The amount of cable necessary to cover the seabed is the same as the horizontal displacement of the touchdown point. In the stationary analysis, the whole cable is moving at the same speed as the lay vessel. Therefore the displacement of the touchdown point is the same as the distance travelled by the lay vessel. Hence:

$$AA' = BB' \rightarrow V_{po}\Delta t = V\Delta t \rightarrow V_{po} = V \tag{2.13}$$

where V_{po} is the pay out rate, V is the lay vessel forward speed and Δt the time interval. The above equation shows that, for a horizontal seabed, the pay out rate should be at least the same as the vessel forward speed in order to cover the seabed without suspensions. As a consequence the definition of slack at the ship ε_s is:

$$\varepsilon_s = \frac{V_{po} - V}{V} \tag{2.14}$$

The same procedure can be adopted for the determination of the minimum pay out rate necessary to assure that the cable covers an ascending or a descending seabed as shown in figure 2.3. From simple geometry it can be readily shown that on a sloping seabed the bottom slack ε_b can be related to the ship slack ε_s by:

$$\varepsilon_s = f + \varepsilon_b \frac{\sin\theta}{\sin(\theta - \beta)} \tag{2.15}$$

where f is the just fill slack. This is given by:

$$f = \frac{\sin\theta - \sin\beta}{\sin(\theta - \beta)} - 1 \tag{2.16}$$

where β is the seabed slope which is positive for uphill slopes and negative for downhill slopes.

2.2 - Literature Review of Numerical Solutions for Marine Cables

This section is concerned with reviewing previous work carried out on numerical solutions for the dynamics of marine cables. Numerical solutions for marine cable laying analysis are seldom encountered in the literature. The few numerical models for marine cable laying that do appear in the literature are usually extensions of models originally developed for other analyses such as towed cables and mooring line analyses.

The dynamic analysis of towed cables and mooring lines has been the subject of considerable research effort. Reviews of the earlier work in this area can be

found in Choo and Casarella (1973) and Migliore and Webster (1979). With the increasing use of cable structures in the offshore environment for station keeping systems further research was carried out by Triantafyllou et al (1986a, b) where they reviewed the various techniques for solving the dynamics of cables as applied to mooring systems. The work was later extended to towed arrays (Triantafyllou and Chryssostomidis, 1989) and tethered underwater vehicles (Triantafyllou and Hover, 1990). Triantafyllou (1994) recently updated this work in the context of mooring systems.

Another area of extensive research related to these issues is the global dynamics of flexible risers. A recent excellent review by Seyed and Patel (1995) summarises the current state-of-the-art which is reasonable advanced. This is further demonstrated by Larsen (1992) who compared the result of different computer programs for the global dynamic analysis of flexible structures such as flexible risers and mooring lines. Many of these models first determine the large displacement non-linear static configuration and then treat the dynamic displacements as linear perturbations about the mean static configuration. An interesting feature of these models is that they were initially based on frequency domain approaches which linearises the quadratic drag and fixes the suspended length. A common linearisation approach for quadratic drag is to use equivalent energy dissipation over a loading cycle. These frequency domain methods have proved to be efficient engineering design tools. However, their accuracy is limited by the linearisations such as the assumption of constant suspended length which is inadequate in the context of cable laying. However, time domain approaches have now become established which avoid the simplifying linearisations and are able to deal with other sources of non-linearitiy such as the interaction with the seabed as in the case of mooring lines. It should be noted that time domain methods are significantly more expensive in terms of computational effort compared with the frequency domain method. Kwan and Bruen (1991) recently compared quasistatic frequency domain and

time domain method for mooring line dynamics and they conclude that the time domain approach is the best method. Further general reviews of slender marine structures can be found in the recent International Ship Offshore Structures Congress - Committee V7 reports (1994, 1991).

As this thesis is primarily concerned with marine cable laying analysis, this review focuses on the numerical models for the dynamics of cables which are relevant to those developed for marine cable laying analysis. The first consistent approach for the analysis of marine cable laying was presented by Zajac (1957) in his seminal work. This has been one of the cornerstones of cable laying operations. Here Zajac developed the stationary solutions for marine cable laying which were discussed in the previous section. Zajac also considered the solutions for some simple transient cases by means of perturbation techniques. However, these solutions are limited in their application.

The dynamics of marine cables has been addressed by a number of works which have mainly been developed for towed cable analysis. This is not surprising given the well defined terminal boundary conditions associated with towed cables. Walton and Polachek (1960) present the solution for the transient analysis of towed marine cables through a finite element model which assumes that the hydrodynamic forces on the cable comprise of quadratic drag and added mass forces. The model also takes into account the inertia of the cable. The finite element used by Walton and Polachek is rigid and the integration in time is performed by a central finite difference scheme. This analysis is also restricted to two dimensions. Choo and Casarella (1972) present a solution for a cable towing a submerged body from a vessel moving in a circular path. The cable is assumed to be inextensible and of zero flexural rigidity. The hydrodynamic forces acting on the cable include the side forces generated by stranded cables. The equations of motion are established for cylindrical co-

ordinates and are solved analytically in time. The space integration of the equations of motion is performed by a fourth order Runge-Kutta algorithm.

Finite element models have been developed for the analysis of cables without the action of fluid forces by Leonard and Recker (1972) and Peyrot and Goulois (1979) where the cable loading is only due to its submerged self-weight. Leonard and Recker use linear elements to model the geometric non-linearity of the cable while Peyrot and Goulois assume that the cable consists of several catenary elements and incorporates both physical and geometric non-linearities. The Peyrot and Goulois finite element model is widely used in quasi-static analysis of cable structures. The problem of concentrated loads is addressed by Irvine and Sinclair (1976). Breslin (1974) considers the formulation for the interaction between the components of a cable-buoy system. The two dimensional governing equations are linearised and then solved numerically. Sanders (1982) presents a simple model for the three dimensional analysis of a towed cable. The formulation is based on a rigid finite element model. The rotation from the local system of reference to the global system of reference is defined by two angles, namely, the azimuth and the elevation. The time integration of the equations is performed by a central finite difference method. Lo and Leonard (1982) derive the equations of motion for mooring cables using energy methods. The solution for the equations of motion is obtained by a finite element model which uses non-linear shape function in order to take into account of the curvature of the cable. Another finite element solution for towed nets is presented by Delmer et al (1983). Ablow and Schechter (1983) present a very useful formulation in which the equations of motion for a towed marine cable are written as functions of the components of the velocity vector and the Euler angles. The equations of motion are then solved by the finite difference method. Milinazzo et al (1987) present an improved finite difference algorithm for the solution of Ablow and Schechter's equations of motion.

The above works have in common the fact that in all of them the cable's length is known beforehand. The only changes in the cable length which may occur are those due to the cable's elasticity. This is not the situation for marine cable laying where the suspended length needs to be determined. In addition, the above models assume that the tension distribution in the cable is non-zero. In marine cable laying analysis, the bottom tension is zero for most of the time. Another difference associated with marine cable laying is that the cable has a pay out rate. As a result, in order to extend the above methods for marine cable laying analysis, it is necessary to adapt the model so that the above difficulties are overcome.

Kitazawa (1981) adapts the model developed by Walton and Polachek (1960) for the two dimensional analysis of marine cable laying. Later on, Kitazawa (1986) extends this method to three dimensions. The length of cable is found by adding or removing elements from the cable configuration so that the boundary condition which states that the vertical co-ordinate is the same as the water depth is satisfied. Since these models use rigid elements, they are unable to represent the effects of curvature in the cable.

Leonard and Karnoski (1990) present the simulation of steady state deployment of a marine cable from a lay vessel with controlled tension. The equations are solved by a shooting method in which the governing equations are solved by direct integration. The touchdown point of the cable is assumed to move with the same velocity and direction as the lay vessel. Sun et al (1994) extended the earlier work by Leonard and Karnoski to the unsteady simulation of marine cables during deployment. It is also assumed by Sun et al that the touchdown point moves with the same velocity as the lay vessel. This is a major disadvantage with these models because one of the aims of a good cable laying simulation is to determine the touchdown point.

Burgess (1991) adapted the Ablow and Schechter formulation and proposed a new finite difference scheme for the solution of the equations of motion. This finite difference scheme is centred in space and in time. Burgess introduces the pay out rate in the analysis and deals with the variable cable length by adding or removing nodes.

A different approach for cable laying is introduced by Gorban et al (1990). In this approach, the two dimensional equations of motion are expressed as function of the horizontal and vertical co-ordinates. These equations of motion are then solved using the Galerkin method with trigonometric shape functions. This model assumes that the pay out rate is known and that the cable may be excited by wave induced vessel motions.

There are two main problems with these models. The first problem is that, in cable laying analysis, zero tension conditions are very often encountered. None of the above models are able to deal with zero tension conditions. The second problem concerns the three dimensional models which use Euler angles as means of relating the local frame of reference to the inertial frame of reference. In this case, there are six differential equations of motion and seven unknowns. As a result, one of the Euler angles has to be specified arbitrarily. This leads to the break down of the transformation under certain conditions.

In order to overcome these problems two actions are necessary. The first is the introduction of the cable's flexural rigidity in the analysis as a means of ensuring continuity in slope. Therefore, the equation of geometric compatibility is satisfied even for zero tension conditions. The second action is concerned with the transformation from the local to the global co-ordinates. In this case an extra equation must be found so that none of the Euler angles need to be specified arbitrarily.

The introduction of the bending stiffness into the dynamic analysis of cables has been addressed by McCoy (1972), Howell (1992), Irvine (1992) and Burgess (1992a,b). Burgess (1992a) first presents a general formulation for the equations of motion with bending stiffness and Burgess (1992b) then presents the steady state solution for cable laying. However, this solution still does not fully overcome the problem of the instability in the transformation from the local to the global co-ordinates which uses Euler angles.

Despite the advances in the general area of cable dynamics, progress in the specific problem of marine cable laying has been limited since Zajac's monumental work published in 1957. This is primarily due to the difficulties associated with the seabed conditions. A general problem with cable laying is that conditions are only observed at the ship apart from the seabed topography. There is a need, therefore, for a general robust dynamic model for marine cable laying operations which includes the important effects such as cable curvature and is able to model transient phenomena such as vessel speed changes. This thesis presents such a model.

3 - A Three Dimensional Model for the Dynamic Analysis of Marine Cables

3.1 - Introduction

A good model for the global analysis of the dynamics of low tension marine cables should be able to simulate large displacements and, more importantly, it should be able to cope with singularities in the geometric stiffness matrix. These singularities in the geometric stiffness matrix occur whenever the tension becomes zero. Another important factor in the modelling of marine cables is the definition of the local co-ordinate system. An arbitrary choice of the local frame of reference usually leads to a situation where the number of unknowns become larger than the number of independent differential equations available. Because of this, an extra assumption has to be made. This extra assumption may introduce further singularities in the analysis.

This chapter introduces an original formulation which leads to a model capable of dealing with the problems described above. The new formulation presented here assumes that the marine cable may undergo large displacements and it takes into consideration the marine cable's flexural rigidity. Although the cable's flexural rigidity is not expected to affect significantly the global configuration of the marine cable, it enables the model to overcome the singularities in the geometric stiffness matrix. However, it also makes the dynamic analysis of the marine cable much more complex.

In order to make the number of unknowns the same as the number of independent differential equations in the analysis, the model used in the formulation assumes that the local frame of reference is the moving frame of a space curve. As a result, the relation between this local frame of reference and the inertial frame of reference may be established as a function of the curvature and the geometric torsion of a space curve. Here one should note that torsion is

a geometric scalar quantity and does not have the meaning as twist associated with a straight rod subject to torque (see appendix A). There are two main advantages in adopting such a frame for a local frame of reference. The first advantage is that the curvature, when defined in this frame of reference, is a scalar rather than a vector quantity. This facilitates the inclusion of the marine cable's flexural rigidity in the analysis. The second advantage is that in this approach it is not necessary to make an extra assumption in order to make the number of unknowns the same as the number of differential equations. The only disadvantage of adopting the moving frame of a space curve as the local frame of reference is that the principal normal direction can not be defined when the curvature is zero. Zero curvature occurs if a segment of the cable is a straight line or if the point being analysed on the cable is a point of inflection. Nevertheless, this disadvantage can be overcome as demonstrated later on in this work.

In order to present this new model for the dynamics of marine cables, this chapter is divided into four sections. The first section presents a discussion of the assumptions made in the model. The second section is concerned with the derivation of the kinematic relations for marine cables. The third section deals with the derivation of the kinetic relations and establishes the differential equations of motion for marine cables. The final section of this chapter presents an exercise in which the consistency and generality of the equations of motion obtained by the model are checked by obtaining the classical differential equations of motion for beams and cables as particular cases of the present model.

The concepts of the local theory of a space curve are extensively used throughout this chapter. In order to avoid lengthy mathematical developments during the derivation of the equations of motion for the marine cable, a brief review of these concepts is given in appendix A. More detailed information on

differential geometry can be found in Eisenhart (1947), Lipschutz (1969), do Carmo (1976), Milman and Parker (1977) and Burke (1985).

3.2 - Assumptions

In the derivation of the equations of motion of a marine cable the following assumptions are made:

(a) - The cable's is a long homogeneous linear elastic circular cylinder with small diameter compared with its length.

(b) - The configuration of the cable may be represented by a unit speed space curve, so that it can be parametrised by its arc length.

(c) - The cable flexural rigidity is taken into consideration.

(d) -The cable may undergo large displacements but only small deformations.

(e) - The rotatory inertia of the cable is negligible.

(f) - The kinetic energy due to axial deformation is small if compared with the kinetic energy due to rigid body motions.

(g) - There are no twisting moments acting on the cable.

(h) - The forces acting on the cable are the self-weight, buoyancy, tangential and normal drag forces, added mass force and D'Alembert force.

(i) - The fluid forces acting on a segment of cable due to the external hydrostatic pressure can be incorporated by the use of the concept of effective tension.

(j) - The Froude-Kriloff force is negligible.

Assumption (a) means that the coupled axial-torsional behaviour of armoured cables is not considered here. This is reasonable for cables which are designed with contra-helical armour layers so that there is torsional balance under tensile

load. For unbalanced cables the torque generated by the tension are relatively low owing to the small lay angles normally associated with the armour layers. Assumption (b) is made in order to allow the stretched arc length to be used as a parameter in the parametric form of the curve which defines the configuration of the cable. Assumption (c) is in order to introduce a more rigorous model and to overcome singularities in the geometric stiffness matrix. Assumption (d) is made in order to restrict the analysis to elastic regime. This is very reasonable for low tension marine cables. Assumptions (e) and (f) are a direct consequence of assumption (d). If the displacements are large and the deformations are small the kinetic energy due to the small deformations will be negligible if compared with the kinetic energy due to the large displacements. Since the main source of twisting moments in the dynamic analysis of marine cable comes from the coupled axial-torsional effects associated with armoured cables, assumption (g) is in line with assumption (a). Assumption (h) is made because the cable has a small diameter and, therefore, the fluid loading is drag dominated. As for assumption (i), the tangential and normal force acting on a curved segmentof submarine cable due to external hydrostatic pressure may be incorporated by subtracting from the axial force the preduct of the cable cross-sectional area and the external hydrostatic pressure. This introduces the concept of effective tension. Assumption (j) can be justified since there is no Froude-Kriloff force acting on the cable as it is assumed that the fluid medium is at constant velocity and the effects of wave kinematics on the cable configuration is negligible.

3.3 - Kinematics of Marine Cables

This section is concerned with the determination of expressions for the position, absolute velocity and absolute acceleration vectors for an element of the submarine cable as well as expressions for the geometrical compatibility of

deformation. Expressions for the relative velocity and relative acceleration between an element of cable and the fluid are also determined.

3.3.1 - Reference System

In order to obtain expressions for these kinematic quantities, a reference system consisting of two Lagrangean co-ordinates and three frames of reference is adopted. As shown in figure 3.1, the two Lagrangean co-ordinates are the unstretched arc length s and the stretched arc length p. The origin of these co-ordinates is placed exactly at the point where the cable leaves the vessel. The three frames of reference are the inertial frame of reference ($\mathbf{I},\mathbf{J},\mathbf{K}$), the vessel frame of reference ($\mathbf{i},\mathbf{j},\mathbf{k}$), and the local frame of reference ($\mathbf{t},\mathbf{n},\mathbf{b}$). This local frame is assumed to be the intrinsic frame of a space curve.

The origin of the inertial frame of reference is placed at some fixed point in space and time. The origin of the vessel frame of reference coincides with the origin of the Lagrangean co-ordinates s and p. The reason for this is that the vessel position with respect to the inertial frame of reference becomes independent of the Lagrangean co-ordinates. Finally, the origin of the local frame of reference is placed at the centre of gravity of the element in question.

The relationship between the two Lagrangean co-ordinates is given by the following expression:

$$\delta p = \delta s(1+\varepsilon) \tag{3.1}$$

which also may be written in the following differential form:

$$\frac{\partial p}{\partial s} = 1+\varepsilon \tag{3.2}$$

where ε is the cable axial strain. For an elastic cable the strain ε can be written as:

$$\varepsilon = \frac{T_{ph}}{EA} \tag{3.3}$$

where T_{ph} is the physical tension and EA is the cable's axial stiffness. For the case of a submerged marine cable with a free end Archimedes principle is valid so that there is no need to correct the buoyancy force. As a result the physical tension T_{ph} is the same as the effective tension T. However, when the marine cable touches the seabed Archimedes principle no longer holds and the physical tension is the effective tension minus the product of the fluid pressure times the cross-sectional area of the marine cable.

In order to establish the relationship between the three frames of reference, the relationship between the inertial and the vessel frames of reference is first considered. The vessel frame of reference has its origin placed at the point where the cable departs from the lay vessel. In addition the unit vector $\mathbf{j}$ is always point towards the centre of the earth. As shown in figure 3.2, the unit vector $\mathbf{i}$ has the opposite sense of the vessel's mean forward velocity vector. As a result, the relationship between the inertial and vessel frames can be expressed mathematically by the matrix form:

$$\begin{Bmatrix} \mathbf{I} \\ \mathbf{J} \\ \mathbf{K} \end{Bmatrix} = \begin{bmatrix} -\cos\beta & 0 & \sin\beta \\ 0 & 1 & 0 \\ -\sin\beta & 0 & -\cos\beta \end{bmatrix} \begin{Bmatrix} \mathbf{i} \\ \mathbf{j} \\ \mathbf{k} \end{Bmatrix} \tag{3.4}$$

The angle β is measured between the unit vectors $\mathbf{K}$ and $\mathbf{k}$ and is given by the expression:

$$\beta = \cos^{-1} \frac{\overline{V}_{vx}}{\sqrt{\overline{V}_{vx}^2 + \overline{V}_{vz}^2}} \tag{3.6}$$

where $\overline{V}_{vx}$ and $\overline{V}_{vz}$ are the components of the vessel's mean forward velocity vector with respect to the inertial frame of reference.

The relationship between the vessel frame of reference and local frame of reference is addressed next. The local frame of reference is the intrinsic frame of a space curve. The unit vector **t** is tangent to the curve while the unit vector **n** is always pointing towards the centre of curvature for the element of cable. Because of this, the direction of the unit vector **n** is called the principal normal direction. The unit vector **b** is obtained through the cross product of the unit vectors **t** and **n** so that the triad (**t**,**n**,**b**) forms a right-handed axis system. The unit vector **b** is called the binormal vector. According to Eisenhart (1947), the relationship between the vessel frame and the local frame of reference may be expressed as:

$$\begin{Bmatrix} \mathbf{i} \\ \mathbf{j} \\ \mathbf{k} \end{Bmatrix} = \begin{bmatrix} \frac{\partial x}{\partial p} & \frac{1}{\kappa}\frac{\partial^2 x}{\partial p^2} & \frac{1}{\kappa}\left(\frac{\partial y}{\partial p}\frac{\partial^2 z}{\partial p^2} - \frac{\partial^2 y}{\partial p^2}\frac{\partial z}{\partial p}\right) \\ \frac{\partial y}{\partial p} & \frac{1}{\kappa}\frac{\partial^2 y}{\partial p^2} & \frac{1}{\kappa}\left(\frac{\partial^2 x}{\partial p^2}\frac{\partial z}{\partial p} - \frac{\partial x}{\partial p}\frac{\partial^2 z}{\partial p^2}\right) \\ \frac{\partial z}{\partial p} & \frac{1}{\kappa}\frac{\partial^2 z}{\partial p^2} & \frac{1}{\kappa}\left(\frac{\partial x}{\partial p}\frac{\partial^2 y}{\partial p^2} - \frac{\partial^2 x}{\partial p^2}\frac{\partial y}{\partial p}\right) \end{bmatrix} \begin{Bmatrix} \mathbf{t} \\ \mathbf{n} \\ \mathbf{b} \end{Bmatrix} \tag{3.7}$$

where κ is the curvature of the cable. Since the rotation is an orthogonal transformation, the inverse relation of equation (3.7) can be obtained by transposing the rotation matrix. In addition, this rotation matrix can be expressed as function of the Lagrangean co-ordinate s through the application of the chain rule to equation (3.7). As a result, equation (3.7) may expressed as:

$$[\mathbf{t} \quad \mathbf{n} \quad \mathbf{b}] = [\mathbf{i} \quad \mathbf{j} \quad \mathbf{k}]\mathbf{C}^{\mathrm{T}} \tag{3.8}$$

where:

$$\mathbf{C}^{\mathrm{T}} = \begin{bmatrix} c_{11} & c_{21} & c_{31} \\ c_{12} & c_{22} & c_{32} \\ c_{13} & c_{23} & c_{33} \end{bmatrix} = \begin{bmatrix} \dfrac{1}{1+\varepsilon}\dfrac{\partial x}{\partial s} & \dfrac{1}{\kappa(1+\varepsilon)^2}\dfrac{\partial^2 x}{\partial s^2} & \dfrac{1}{\kappa(1+\varepsilon)^3}\left(\dfrac{\partial y}{\partial s}\dfrac{\partial^2 z}{\partial s^2} - \dfrac{\partial^2 y}{\partial s^2}\dfrac{\partial z}{\partial s}\right) \\ \dfrac{1}{1+\varepsilon}\dfrac{\partial y}{\partial s} & \dfrac{1}{\kappa(1+\varepsilon)^2}\dfrac{\partial^2 y}{\partial s^2} & \dfrac{1}{\kappa(1+\varepsilon)^3}\left(\dfrac{\partial^2 x}{\partial s^2}\dfrac{\partial z}{\partial s} - \dfrac{\partial x}{\partial s}\dfrac{\partial^2 z}{\partial s^2}\right) \\ \dfrac{1}{1+\varepsilon}\dfrac{\partial z}{\partial s} & \dfrac{1}{\kappa(1+\varepsilon)^2}\dfrac{\partial^2 z}{\partial s^2} & \dfrac{1}{\kappa(1+\varepsilon)^3}\left(\dfrac{\partial x}{\partial s}\dfrac{\partial^2 y}{\partial s^2} - \dfrac{\partial^2 x}{\partial s^2}\dfrac{\partial y}{\partial s}\right) \end{bmatrix} \tag{3.9}$$

3.3.2 - Position Vector

The position of an element of cable with respect to the inertial frame of reference $\mathbf{r_c}$ consists of the vector sum of the position of the vessel frame with respect to the inertial frame $\mathbf{r_v}$ plus the position of the local frame with respect to the vessel frame $\mathbf{r}$. That is:

$$\mathbf{r}_c(p,t) = \mathbf{r}_v(t) + \mathbf{r}(p,t) \tag{3.10}$$

The position of the vessel frame of reference with respect to the inertial frame may be written as:

$$\mathbf{r}_v = \overline{X}_v\mathbf{I} + \overline{Z}_v\mathbf{K} + x_w\mathbf{i} + y_w\mathbf{j} + z_w\mathbf{k} \tag{3.11}$$

where $\overline{X}_v$ and $\overline{Z}_v$ are the co-ordinates of the vessel mean path while x_w, y_w and z_w are the wave induced surge, heave and sway motions of the origin of the vessel frame of reference, respectively. By applying the transformation given by equation (3.4), the above equation becomes:

$$\mathbf{r}_v = x_v\mathbf{i} + y_v\mathbf{j} + z_v\mathbf{k} = \left(x_w - \overline{X}_v\cos\beta - \overline{Z}_v\sin\beta\right)\mathbf{i} + y_w\mathbf{j} + \left(z_w + \overline{X}_v\sin\beta - \overline{Z}_v\cos\beta\right)\mathbf{k} \tag{3.12}$$

The position of the element of cable with respect to the vessel frame of reference may be expressed as:

$$\mathbf{r} = x\mathbf{i} + y\mathbf{j} + z\mathbf{k} \tag{3.13}$$

As a result, the expression for the position of the element of cable with respect to the inertial frame becomes:

$$\mathbf{r}_e = (x + x_v)\mathbf{i} + (y + y_v)\mathbf{j} + (z + z_v)\mathbf{k} \tag{3.14}$$

3.3.3 - Absolute and Relative Velocity Vectors

In this section, derivations of the absolute and relative velocity vectors are presented.

Absolute Velocity Vector

The absolute velocity vector of an element of cable is the time derivative of the element position vector with respect to the inertial frame of reference. In the case of towed cable analysis, the velocity vector of the element of cable is the same as the velocity vector of the local frame of reference. However, for cable laying or cable recovery analyses, an observer placed at the local frame of reference sees cable passing with a velocity V_{po} which is tangent to the cable configuration. The magnitude of this velocity is equal to the pay out rate for cable laying analysis and equal to the haul in rate for cable recovery analysis. Therefore, in order to obtain the absolute velocity vector, the velocity V_{po} must be added to the local frame of reference velocity vector. Accordingly, the absolute velocity vector may be expressed as:

$$\mathbf{V} = \mathbf{V}_c + V_{po}\mathbf{t} \tag{3.15}$$

where $\mathbf{V}$ is the absolute velocity vector, $\mathbf{V}_c$ is the velocity vector of the local frame of reference and V_{po} is the pay out rate. The velocity vector of the local frame of reference is the time derivative of equation (3.14) which is given by:

$$\mathbf{V}_c = V_{cx}\mathbf{i} + V_{cy}\mathbf{j} + V_{cz}\mathbf{k} \tag{3.16}$$

or:

$$\mathbf{V}_c = \left[\frac{\partial x}{\partial t} + \frac{\partial x_v}{\partial t} + (z + z_v)\frac{\partial \beta}{\partial t}\right]\mathbf{i} + \left[\frac{\partial y}{\partial t} + \frac{\partial y_v}{\partial t}\right]\mathbf{j} + \left[\frac{\partial z}{\partial t} + \frac{\partial z_v}{\partial t} + (x + x_v)\frac{\partial \beta}{\partial t}\right]\mathbf{k} \tag{3.17}$$

As a result of the combination of equations (3.15) and (3.16) with the rotation matrix given by equation (3.8), the absolute velocity vector of an element of cable may expressed in the vessel frame of reference as:

$$\mathbf{V} = V_x\mathbf{i} + V_y\mathbf{j} + V_z\mathbf{k} = \left(V_{cx} + c_{11}V_{po}\right)\mathbf{i} + \left(V_{cy} + c_{12}V_{po}\right)\mathbf{j} + \left(V_{cz} + c_{13}V_{po}\right)\mathbf{k} \tag{3.18}$$

This same vector can be written in the local frame of reference as:

$$\mathbf{V} = \left(c_{11}V_x + c_{12}V_y + c_{13}V_z\right)\mathbf{t} + \left(c_{21}V_x + c_{22}V_y + c_{23}V_z\right)\mathbf{n} + \left(c_{31}V_x + c_{32}V_y + c_{33}V_z\right)\mathbf{b} \tag{3.19}$$

Relative Velocity Vector

The relative velocity vector is the difference between the absolute velocity vector and the fluid velocity vector which is assumed to be given by the following expression:

$$\mathbf{U} = U_X\mathbf{I} + U_Y\mathbf{J} + U_Z\mathbf{K} \tag{3.20}$$

where the components U_X, U_Y, and U_Z are known quantities.

Alternatively, the fluid velocity vector may be written in either the vessel frame of reference or the local frame of reference. For the vessel frame of reference the fluid velocity vector expression is:

$$\mathbf{U} = U_x\mathbf{i} + U_y\mathbf{j} + U_z\mathbf{k} = (-U_X\cos\beta + U_Z\sin\beta)\mathbf{i} + U_Y\mathbf{j} + (-U_X\sin\beta - U_Z\cos\beta)\mathbf{k} \tag{3.21}$$

while for the local frame of reference the expression of the fluid velocity vector becomes:

$$\mathbf{U} = U_t\mathbf{t} + U_n\mathbf{n} + U_b\mathbf{b} \tag{3.22}$$

The above equation may be expanded as:

$$\mathbf{U} = (c_{11}U_x + c_{12}U_y + c_{13}V_z)\mathbf{t} + (c_{21}U_x + c_{22}U_y + c_{23}U_z)\mathbf{n} + (c_{31}U_x + c_{32}U_y + c_{33}U_z)\mathbf{b} \tag{3.23}$$

As a result the relative velocity vector can either be written as:

$$\mathbf{V}_r = V_{rx}\mathbf{i} + V_{ry}\mathbf{j} + V_{rz}\mathbf{k} = (V_x - U_x)\mathbf{i} + (V_y - U_y)\mathbf{j} + (V_z - U_z)\mathbf{k} \tag{3.24}$$

or as:

$$\mathbf{V}_r = V_{rt}\mathbf{t} + V_{rn}\mathbf{n} + V_{rb}\mathbf{b} = (V_t - U_t)\mathbf{t} + (V_n - U_n)\mathbf{n} + (V_b - U_b)\mathbf{b} \tag{3.25}$$

3.3.4 - Absolute and Relative Acceleration Vectors

This section deals with the determination of expressions for the absolute and relative acceleration vectors.

Absolute Acceleration Vector

The absolute acceleration vector is the time derivative of the absolute velocity vector. Thus, the absolute acceleration vector may be expressed with respect to the vessel frame of reference as:

$$\mathbf{a} = a_x\mathbf{i} + a_y\mathbf{j} + a_z\mathbf{k} = \left(\frac{\partial V_x}{\partial t} + V_z\frac{\partial \beta}{\partial t}\right)\mathbf{i} + \frac{\partial V_y}{\partial t}\mathbf{j} + \left(\frac{\partial V_z}{\partial t} - V_x\frac{\partial \beta}{\partial t}\right)\mathbf{k} \tag{3.26}$$

Alternatively, the absolute acceleration vector can be written with respect to the local frame of reference as:

$$\mathbf{a} = a_t\mathbf{t} + a_n\mathbf{n} + a_b\mathbf{b} \tag{3.27}$$

or:

$$\mathbf{a} = \left(c_{11}a_x + c_{12}a_y + c_{13}a_z\right)\mathbf{t} + \left(c_{21}a_x + c_{22}a_y + c_{23}a_z\right)\mathbf{n} + \left(c_{31}a_x + c_{32}a_y + c_{33}a_z\right)\mathbf{b} \tag{3.28}$$

Relative Acceleration Vector

The relative acceleration vector is the time derivative of the absolute velocity vector. Thus, the relative acceleration vector may be expressed with respect to the vessel frame of reference as:

$$\mathbf{a}_r = a_{rx}\mathbf{i} + a_{ry}\mathbf{j} + a_{rz}\mathbf{k} = \left(\frac{\partial V_{rx}}{\partial t} + V_{rz}\frac{\partial \beta}{\partial t}\right)\mathbf{i} + \frac{\partial V_{ry}}{\partial t}\mathbf{j} + \left(\frac{\partial V_{rz}}{\partial t} - V_{rx}\frac{\partial \beta}{\partial t}\right)\mathbf{k} \tag{3.29}$$

Alternatively, the relative acceleration vector can be written with respect to the local frame of reference as:

$$\mathbf{a_r} = a_{rt}\mathbf{t} + a_{rn}\mathbf{n} + a_{rb}\mathbf{b} \tag{3.30}$$

or:

$$\mathbf{a_r} = \left(c_{11}a_{rx} + c_{12}a_{ry} + c_{13}a_{rz}\right)\mathbf{t} + \left(c_{21}a_{rx} + c_{22}a_{ry} + c_{23}a_{rz}\right)\mathbf{n} + \left(c_{31}a_{rx} + c_{32}a_{ry} + c_{33}a_{rz}\right)\mathbf{b} \tag{3.31}$$

3.3.5 - Equation of Geometric Compatibility

The geometric compatibility equation comes from the necessity of the following constraint to be satisfied:

$$\left(\frac{\partial x}{\partial p}\right)^2 + \left(\frac{\partial y}{\partial p}\right)^2 + \left(\frac{\partial z}{\partial p}\right)^2 = 1 \tag{3.32}$$

The constraint equation can be expressed as function of the unstretched arc length s by applying the chain rule to the above equation. Hence:

$$\left(\frac{\partial x}{\partial s}\right)^2 + \left(\frac{\partial y}{\partial s}\right)^2 + \left(\frac{\partial z}{\partial s}\right)^2 = (1+\varepsilon)^2 \tag{3.33}$$

3.4 - Kinetics of Marine Cables

Figure 3.3 shows an element of marine cable. The forces acting on the element are the external force vector per unit length $\mathbf{f_{ext}}$, the tension **T** and the shear force **Q**. The moments acting on the element are the bending moment vector **M** and the twisting moment $\mathbf{M_T}$. No external moments are present.

The external vector $\mathbf{f_{ext}}$ contains of terms due to the cable self-weight and buoyancy, drag and added mass forces. There is no Froude-Kriloff force acting

on the cable as it is assumed that the fluid medium is at constant velocity and the effects of wave kinematics on the cable's global configuration are negligible.

3.4.1 - Dynamic Equilibrium for an Element of Marine Cable

Following earlier assumptions, the dynamic balance of forces may be written in the following vector form:

$$\delta\mathbf{T} + \delta\mathbf{Q} + \mathbf{f}_{ext}\delta p - \frac{\partial \mathbf{L}}{\partial t}\delta p = \mathbf{0} \tag{3.34}$$

where $\mathbf{L}$ is the linear momentum per unit length. Likewise, the balance of moments may be expressed as:

$$\delta\mathbf{M} + \delta\mathbf{M}_T + \frac{\delta p}{2}\delta\mathbf{r} \times \mathbf{f}_{ext} + \delta\mathbf{r} \times (\mathbf{T} + \delta\mathbf{T} + \mathbf{Q} + \delta\mathbf{Q}) - \frac{\partial \mathbf{H}}{\partial t}\delta p = \mathbf{0} \tag{3.35}$$

where $\mathbf{H}$ is the angular momentum per unit length. Since it is assumed that there are no external moments and that the internal energy in comparison with the energy due to large displacements is negligible, equation (3.34) can be written as:

$$\frac{\partial \mathbf{T}}{\partial p} + \frac{\partial \mathbf{Q}}{\partial p} + \mathbf{f}_{ext} + \mathbf{f}_m = \mathbf{0} \tag{3.36}$$

while equation (3.35) becomes:

$$\frac{\partial \mathbf{M}}{\partial p} + \frac{\partial \mathbf{M}_T}{\partial p} + \mathbf{t} \times (\mathbf{T} + \mathbf{Q}) = \mathbf{0} \tag{3.37}$$

where the second order differentials have been neglected.

Since the local frame of reference is the intrinsic frame of a space curve, the cable's cross-section rotates about the binormal direction. As a result, the bending moment vector is parallel to the unit vector in the binormal direction. Thus:

$$\mathbf{M} = M\mathbf{b} \tag{3.38}$$

where M is the magnitude of the bending moment. Consequently, the shear force and the axial force vectors are parallel to the principal normal and tangent vectors, respectively. Hence:

$$\mathbf{Q} = Q\mathbf{n} \tag{3.39}$$

and

$$\mathbf{T} = T\mathbf{t} \tag{3.40}$$

where Q is the magnitude of the shear force and T is the magnitude of the axial force. Finally, the twisting moment vector is tangent to the cable and is expressed as:

$$\mathbf{M}_T = M_T\mathbf{t} \tag{3.41}$$

where $\mathbf{M}_T$ is the magnitude of the twisting moment.

Combining equations (3.36) and (3.39) and (3.40) gives:

$$\frac{\partial T}{\partial p}\mathbf{t} + T\frac{\partial \mathbf{t}}{\partial p} + \frac{\partial Q}{\partial p}\mathbf{n} + T\frac{\partial \mathbf{n}}{\partial p} + \mathbf{f}_{ext} + \mathbf{f}_m = \mathbf{0} \tag{3.42}$$

The space derivatives of the unit vectors (**t**,**n**,**b**) may be written as functions of the unit vectors themselves through the Frenet-Serret formulae (Eisenhart, 1947). These formulae are given by the following matrix form:

$$\frac{\partial}{\partial p}\begin{Bmatrix}\mathbf{t}\\ \mathbf{n}\\ \mathbf{b}\end{Bmatrix}=\begin{bmatrix}0 & \kappa & 0\\ -\kappa & 0 & \tau\\ 0 & -\tau & 0\end{bmatrix}\begin{Bmatrix}\mathbf{t}\\ \mathbf{n}\\ \mathbf{b}\end{Bmatrix} \tag{3.43}$$

Using the Frenet-Serret formulae, equation (3.42) becomes:

$$\left(\frac{\partial T}{\partial p}-\kappa Q\right)\mathbf{t}+\left(\kappa T+\frac{\partial Q}{\partial p}\right)\mathbf{n}+\tau Q\mathbf{b}+\mathbf{f}_{\text{ext}}+\mathbf{f}_{\text{m}}=\mathbf{0} \tag{3.44}$$

A similar expression can be obtained for the balance of moments by combining equations (3.37), (3.38) and (3.41). This gives:

$$\frac{\partial M_T}{\partial p}\mathbf{t}+M_T\frac{\partial \mathbf{t}}{\partial p}+\frac{\partial M}{\partial p}\mathbf{b}+M\frac{\partial \mathbf{b}}{\partial p}+Q\mathbf{b}=\mathbf{0} \tag{3.45}$$

which, combined with Frenet-Serret formulae, gives:

$$\frac{\partial M_T}{\partial p}\mathbf{t}+(\kappa M_T-\tau M)\mathbf{n}+\left(\frac{\partial M}{\partial p}+Q\right)\mathbf{b}=\mathbf{0} \tag{3.46}$$

The magnitude of the bending moment M may be obtained by the product of the curvature κ and the cable bending stiffness EI while the magnitude of the shear force Q can be obtained by multiplying the cable bending stiffness by the derivative of the curvature with respect to the stretched arc length p. These relations combined with equations (3.45) and (3.46) result in the following expression:

$$\left(\frac{\partial T}{\partial p}+EI\kappa\frac{\partial \kappa}{\partial p}\right)\mathbf{t}+\left(\kappa T-EI\frac{\partial^2\kappa}{\partial p^2}\right)\mathbf{n}+EI\tau\kappa\mathbf{b}+\mathbf{f}_{\text{ext}}-\frac{\partial \mathbf{L}}{\partial t}=\mathbf{0} \tag{3.47}$$

The above equation is the governing differential equation of equilibrium of moments and forces acting on an element of cable under the assumptions made

earlier in this work. This differential equation can also be written as function of the unstretched arc length s. In this case, the differential equation becomes:

$$\left(\frac{1}{1+\varepsilon}\right)\left(\frac{\partial T}{\partial s}+EI\kappa\frac{\partial \kappa}{\partial p}\right)\mathbf{t}+\left(\kappa T-\frac{EI}{(1+\varepsilon)^2}\frac{\partial^2\kappa}{\partial s^2}\right)\mathbf{n}+EI\tau\kappa\mathbf{b}+\mathbf{f}_{ext}-\frac{\partial \mathbf{L}}{\partial t}=\mathbf{0} \qquad (3.48)$$

3.4.2 - Vector Equation of Motion

The equations of motion of a marine cable are obtained by combining the above vector equation of equilibrium with the geometric constraint given by equation (3.33). The vector equation of equilibrium can be resolved in three scalar equations parallel to the tangent **t**, the principal normal **n** and the binormal **b** directions, respectively. Therefore, four independent equations can be written. In these four equations there are six unknown quantities. The unknowns are the three co-ordinates x, y and z, the tension T, the curvature κ and the torsion τ. Consequently, two more equations are needed to solve the problem. These two equations can be obtained by expressing the curvature and the torsion as functions of the co-ordinates x, y and z and their derivatives.

The curvature is defined as being the magnitude of the vector obtained through the derivative of the unit tangent vector with respect to the stretched arc length p. This magnitude is given by the expression:

$$\kappa=\sqrt{\left(\frac{\partial^2 x}{\partial p^2}\right)^2+\left(\frac{\partial^2 y}{\partial p^2}\right)^2+\left(\frac{\partial^2 z}{\partial p^2}\right)^2} \qquad (3.49)$$

Thus, the expression for the curvature as a function of the unstretched arc length s is:

$$\kappa=\frac{1}{(1+\varepsilon)^2}\sqrt{\left(\frac{\partial^2 x}{\partial s^2}\right)^2+\left(\frac{\partial^2 y}{\partial s^2}\right)^2+\left(\frac{\partial^2 z}{\partial s^2}\right)^2} \qquad (3.50)$$

Eisenhart (1947) shows that the torsion of a space curve can be expressed as a function of the global co-ordinates x, y and z:

$$\tau = \frac{1}{\kappa^2}\begin{vmatrix} \frac{\partial x}{\partial p} & \frac{\partial y}{\partial p} & \frac{\partial z}{\partial p} \\ \frac{\partial^2 x}{\partial p^2} & \frac{\partial^2 y}{\partial p^2} & \frac{\partial^2 z}{\partial p^2} \\ \frac{\partial^3 x}{\partial p^3} & \frac{\partial^3 y}{\partial p^3} & \frac{\partial^3 z}{\partial p^3} \end{vmatrix} \tag{3.51}$$

Alternatively, the torsion can be expressed as:

$$\tau = \frac{1}{\kappa^2}\begin{vmatrix} \frac{1}{1+\varepsilon}\frac{\partial x}{\partial s} & \frac{1}{1+\varepsilon}\frac{\partial y}{\partial s} & \frac{1}{1+\varepsilon}\frac{\partial z}{\partial s} \\ \frac{1}{(1+\varepsilon)^2}\frac{\partial^2 x}{\partial s^2} & \frac{1}{(1+\varepsilon)^2}\frac{\partial^2 y}{\partial s^2} & \frac{1}{(1+\varepsilon)^2}\frac{\partial^2 z}{\partial s^2} \\ \frac{1}{(1+\varepsilon)^3}\frac{\partial^3 x}{\partial s^3} & \frac{1}{(1+\varepsilon)^3}\frac{\partial^3 y}{\partial s^3} & \frac{1}{(1+\varepsilon)^3}\frac{\partial^3 z}{\partial s^3} \end{vmatrix} \tag{3.52}$$

Self-Weight and Buoyancy Forces

The self-weight and the buoyancy forces are approximated by the following expression:

$$\mathbf{w} = w\mathbf{j} = \frac{w}{1+\varepsilon}\frac{\partial y}{\partial s}\mathbf{t} + \frac{w}{\kappa(1+\varepsilon)^2}\frac{\partial^2 y}{\partial s^2}\mathbf{n} + \frac{w}{\kappa(1+\varepsilon)^3}\left(\frac{\partial^2 x}{\partial s^2}\frac{\partial z}{\partial s} - \frac{\partial x}{\partial s}\frac{\partial^2 z}{\partial s^2}\right)\mathbf{b} \tag{3.53}$$

where w is the cable's submerged weight of per unit length.

Drag Force

The drag force has two components, namely, the tangential drag force and the normal drag force. The tangential drag force is proportional to the square of the

tangential component of the relative velocity between fluid and cable and may be expressed as:

$$\mathbf{f_T} = -\frac{1}{2}\pi\rho d C_T |\mathbf{V_T}|\mathbf{V_T} \tag{3.54}$$

where ρ is the fluid density, d is the cable diameter, C_T is the tangential drag coefficient and $\mathbf{V_T}$ is the relative velocity vector in the tangent direction. On the other hand, the normal drag force is proportional to the square of the normal component of the relative velocity and it is given by:

$$\mathbf{f_N} = -\frac{1}{2}\rho d C_D |\mathbf{V_N}|\mathbf{V_N} \tag{3.55}$$

C_D is the normal drag coefficient and $\mathbf{V_N}$ is the relative velocity vector in the normal direction given by the vector sum of the components of the relative velocity vector in the principal normal and binormal directions multiplied by their respective unit vectors. Hence:

$$\mathbf{V_N} = V_{rn}\mathbf{n} + V_{rb}\mathbf{b} \tag{3.56}$$

As a result, the drag force vector may be written as:

$$\mathbf{f_D} = -\frac{1}{2}\pi\rho d C_T |V_n| V_n \mathbf{t} - \frac{1}{2}\rho d C_d V_{rn}\sqrt{V_{rn}^2 + V_{rb}^2}\,\mathbf{n} - \frac{1}{2}\rho d C_d V_{rb}\sqrt{V_{rn}^2 + V_{rb}^2}\,\mathbf{b} \tag{3.57}$$

Added Mass Force

The added mass force is proportional to the relative acceleration between the fluid and cable. However, in marine cable analysis the tangential component of the added mass force is very small in comparison with the normal component

of this force and it is, therefore, negligible. Thus, for a cylinder, the added mass force may be written as:

$$\mathbf{f}_A = -\rho A C_M \mathbf{a}_N \tag{3.58}$$

where C_M is the added mass coefficient and $\mathbf{a}_N$ is the normal component of the relative acceleration vector which is given by:

$$\mathbf{a}_N = a_m \mathbf{n} + a_{rb} \mathbf{b} \tag{3.59}$$

D'Alembert Force

The D'Alembert force is the time derivative of the linear momentum. The linear momentum per unit length is obtained by multiplying the cable's physical mass per unit length m by the absolute velocity vector $\mathbf{V}$. Since the cable's mass per unit length does not vary with the time, the D'Alembert force can be expressed as:

$$\mathbf{f}_m = -\frac{d}{dt}(m\mathbf{V}) = -m\mathbf{a} \tag{3.60}$$

where the acceleration vector $\mathbf{a}$ is the absolute acceleration vector of an element of cable.

3.4.3 - Scalar Equations of Motion

In order to obtain the scalar equations of motion, the expressions for cable self-weight and buoyancy, and the drag added mass and D'Alembert forces derived above are substituted into the vector equation of equilibrium (3.48). Then the

tangential, normal and binormal components of this vector equation are equated to zero. As a result, the scalar equations of motion are, respectively:

$$\frac{1}{1+\varepsilon}\frac{\partial T}{\partial s}+\frac{EI}{1+\varepsilon}\kappa\frac{\partial \kappa}{\partial s}+\frac{w}{1+\varepsilon}\frac{\partial y}{\partial s}-\frac{1}{2}\pi\rho dC_T|V_n|V_n-ma_t=0 \tag{3.61}$$

$$\kappa T-\frac{EI}{(1+\varepsilon)^2}\frac{\partial^2\kappa}{\partial s^2}+\frac{w}{\kappa(1+\varepsilon)^2}\frac{\partial^2 y}{\partial s^2}-\frac{1}{2}\rho dC_D V_{rn}\sqrt{V_{rn}^2+V_{rb}^2}-\rho Aa_{rn}-ma_n=0 \tag{3.62}$$

and

$$EI\tau\kappa+\frac{w}{\kappa(1+\varepsilon)^3}\left(\frac{\partial^2 x}{\partial s^2}\frac{\partial z}{\partial s}-\frac{\partial x}{\partial s}\frac{\partial^2 z}{\partial s^2}\right)-\frac{1}{2}\rho dC_D V_{rb}\sqrt{V_{rn}^2+V_{rb}^2}-\rho Aa_{rb}-ma_b=0 \tag{3.63}$$

The curvature κ and the torsion τ in the above equations can be replaced by their expression as functions of the derivatives of the co-ordinates x, y and z, given by equations (3.50) and (3.52), respectively. As a result, equations (3.61), (3.62) and (3.63) together with the equation of geometric compatibility (3.33) form a non-linear system of four differential equations. This non-linear system of differential equations may be applied to a number of problems such as the towing of a marine cable as well as marine cable laying. The specific solution is governed by the boundary conditions.

In the above system of differential equations, there are four dependent variables which are the three co-ordinates x, y and z and the tension T, and two independent variables which are the unstretched arc length s and the time t. In addition, the highest order derivatives for the co-ordinates are fourth order with respect to arc length and second order with respect to time while the highest order derivative for the tension with respect to arc length is first order. No time derivatives for the tension are present. As a result, four boundary conditions and two initial conditions must be specified for the co-ordinates while one boundary condition must be specified for the tension. As initial

conditions, it is assumed that both the marine cable's initial configuration and the initial velocity vector are known.

3.4.4 - Boundary Conditions

The boundary conditions for the co-ordinates are essentially the same as those used in beam theory. That is, either the linear displacement or the shear force are specified and either the angular displacement or the bending moment are specified at both ends of the cable. For instance, if the top end of the cable is considered to be pinned then in this case both linear displacement and bending moment are zero. In case of a towed marine cable the bottom end of the cable is free. As a result, the bottom boundary conditions consist of both shear force and bending moment being equal to zero. In contrast, for the case of cable laying, it can be assumed that the cable is parallel to the seabed at the touchdown point and, therefore, the angular displacement is known. Since the touchdown position is not known beforehand, it may be assumed that the shear force at the bottom end of the cable is zero.

The tension boundary condition depends on the slack and whether the cable is touching the seabed. If the cable is not touching the seabed then free bottom end boundary conditions may be assumed. In this case the bottom tension is zero. On the other hand, for cases where the cable touches the seabed but the cable is paid out with positive slack, the zero bottom tension condition can also be assumed. In contrast, for cases where the slack is negative the segment of cable lying on the seabed tends to be dragged along. Since there is friction between the cable and the seabed the bottom tension is no longer zero.

3.5 - Consistency and Generality of the Model

The consistency and generality of the model can be checked by reducing the three dimensional equations of motion to the two dimensional classical formulation for marine cables and beams. The two dimensional classical formulation assumes that the cable is inextensible and perfectly flexible. As a result, both the strain ε and the bending stiffness EI are zero. In addition, for the case where the cable lies in the vertical plane, the co-ordinate z and all its derivatives are assumed to be zero. As a result, the direction cosines of the unit tangent vector can be written in the following vector form:

$$\left[\frac{\partial x}{\partial s} \quad \frac{\partial y}{\partial s} \quad \frac{\partial z}{\partial s}\right] = [\cos\theta \quad \sin\theta \quad 0] \tag{3.64}$$

where θ is the angle between the unit tangent vector $\mathbf{t}$ and the unit vector in the x direction $\mathbf{i}$.

The substitution of the director cosines into the expression for the curvature given by equation (3.50) results in:

$$\kappa = \frac{\partial \theta}{\partial s} \tag{3.65}$$

Furthermore, the relation between the local unit vectors ($\mathbf{t}$,$\mathbf{n}$,$\mathbf{b}$) and the global unit vectors ($\mathbf{i}$,$\mathbf{j}$,$\mathbf{k}$) becomes:

$$\begin{Bmatrix} \mathbf{t} \\ \mathbf{n} \\ \mathbf{b} \end{Bmatrix} = \begin{bmatrix} \cos\theta & \sin\theta & 0 \\ -\sin\theta & \cos\theta & 0 \\ 0 & 0 & 1 \end{bmatrix} \begin{Bmatrix} \mathbf{i} \\ \mathbf{j} \\ \mathbf{k} \end{Bmatrix} \tag{3.66}$$

As a result of combining equations (3.64), (3.65) and (3.66) with the scalar equations of motion given by equations (3.61), (3.62) and (3.63), the two dimensional scalar equations of motion for a marine cable become, respectively:

$$\frac{\partial T}{\partial s} + w\sin\theta - \frac{1}{2}\pi\rho d C_T |V_n| V_n - m a_t = 0 \tag{3.67}$$

and

$$T\frac{\partial \theta}{\partial s} + w\cos\theta - \frac{1}{2}\rho d C_d |V_m| V_m - \rho A a_m - m a_n = 0 \tag{3.68}$$

Next, consider the following three steady state situations where the inertia terms zero. Firstly, if the drag terms in equations (3.67) and (3.68) are assumed negligible then these equations can be identified as the classical catenary equations. Secondly, if the bottom tension is assumed to be zero then this corresponds to Zajac's straight line solution where the angle θ is given by:

$$\theta = \cos^{-1}\left(\frac{\rho C_d |V_m| V_m}{2w}\right) \tag{3.69}$$

which is exactly the expression obtained by Zajac. Next, if the tangential drag term is assumed to be negligible then the quotient between equations (3.67) and (3.68) may be written as:

$$\frac{dT}{T} = \left(\frac{w\sin\theta}{w\cos\theta - \frac{1}{2}\rho C_d |V_m| V_m}\right) d\theta \tag{3.70}$$

which is Zajac's equation for cases where the bottom tension is not zero.

It is also possible to obtain the classical equation for the Bernoulli beam theory. This can be achieved by assuming that the angle θ is very small and that the

cable is subject to small displacements only. In this case, the expression for the curvature becomes:

$$\kappa = \frac{\partial^2 y}{\partial x^2} \tag{3.71}$$

Replacing the curvature into equation (3.62) by the above expression gives the following expression for the equation of motion in the normal direction:

$$T\frac{\partial^2 y}{\partial x^2} - EI\frac{\partial^4 y}{\partial x^4} - m\frac{\partial^2 y}{\partial t^2} = q \tag{3.72}$$

where q accounts for the distributed load on the beam and the damping forces have been neglected.

The above exercise shows that three classical equations can be obtained as particular cases of the model proposed here. It may be concluded, therefore, that the model is both consistent and general. This also demonstrates that, in addition to marine cable analysis, the formulation presented here can be applied to a number of applications such as pipelines and flexible risers.

4 - Two Dimensional Analysis of Low Tension Marine Cables

4.1 - Introduction

This chapter deals with the two dimensional solution of the equations of motion derived in chapter three and its applications. The motivation to study two dimensional solutions comes from the fact that many practical problems associated with the installation of marine cables are adequately represented by assuming that the cable configuration lies in the vertical plane. In addition, the two dimensional solution is less difficult to implement and, because of this, it offers greater opportunity to obtain an insight into the physical phenomena involved.

The analyses presented here can be applied to obtain the dynamic response of a marine cable when it is being laid or towed under low tension. There are two different situations that need to be taken into consideration. The first is when the towed cable does not touch the seabed. If the cable is not towing a submerged body, then the bottom end of the cable is free and therefore the boundary conditions are well defined. Furthermore, the suspended length of the cable does not change during the analysis. As a result, towed cables are often used in full scale experiments in order to establish the cable properties such as the hydrodynamic constant. Towed cables also allow insight into the dynamic response under transient excitation. For cases where the towed cable touches the seabed or for cable laying analysis, the bottom boundary condition is not well defined. This is because the bottom boundary condition depends on the complex interaction between the marine cable and the seabed. In addition, the suspended length of the cable is not fixed and it needs to be determined.

The two dimensional equations of motion are solved here by using a finite element model where the space integration is obtained by the application of a weighted residual formulation based on the Galerkin method and the time integration is obtained by the Newmark direct integration scheme. This procedure leads to a system of non-linear algebraic equations which is solved by the Newton-Raphson method. The solution presented in this chapter focuses on the effects of transient conditions associated with lay vessel speed changes and steady state conditions associated with wave induced motions of the lay vessel.

This chapter is divided into two main sections. The first section is concerned with the reduction of the two dimensional differential equations of motion. The second section presents the finite element model for the solution of the two dimensional equations of motion.

4.2 - Two Dimensional Equations of Motion

This section reduces the three dimensional dynamic model derived in chapter three to two dimensions. The additional assumptions for the two dimensional case are first considered. Then the general expressions for the differential equations of motion are established. Next, the expression for the curvature as well as the expressions for the forces acting on the cable are obtained. Finally, the boundary and initial conditions are considered.

4.2.1 - Two Dimensional Assumptions

In addition to the assumptions made in the last chapter, it is assumed here that the cable does not experience out of plane excitation and dynamic response. As a result, the cable configuration lies entirely in a vertical plane. The vertical plane used in this analysis is obtained by setting the co-ordinate

z equal to zero. It is further assumed that the cable is inextensible, the second order effect of the shear force on the tangential differential equation is negligible and there are no currents.

The assumption that the cable is inextensible can be justified by the fact that the cable is under low tension and has relatively high axial stiffness. According to Faltinsen (1990), the elasticity of the cable needs to be taken into consideration only in extreme conditions, which is clearly not the case being considered here. Therefore, the influence of the elasticity of the cable on the global configuration is very small.

The assumption that the second order effect of the shear force on the tangential equation of motion is negligible is very reasonable because both curvature and its derivative with respect to the arc length are small. This is because the flexural rigidity of the cable has little influence on the global configuration of the cable. The main reason why it is taken into consideration is to overcome singularities in the geometric stiffness matrix. Therefore, if the first order effect of the shear force on the global configuration of the cable is small, its second order effect is even smaller. Consequently, it is very reasonable to neglect the second order effect of the shear force.

Finally, in spite of the fact that the in plane currents do not change the two dimensional nature of the analysis, currents are essentially a three dimensional problem. Because of this, it is more appropriate to introduce currents in a three dimensional analysis such as the analysis presented in chapter six of this work.

4.2.2 - Two Dimensional Scalar Equations of Motion

The two dimensional equations of motion are obtained by applying the assumptions made earlier to the differential equations of motion of the model proposed in chapter three. As a result of the two dimensional assumption, the components of the velocity and acceleration vectors in the binormal direction are zero. In addition, the binormal direction does not change in either space or time. The assumption that the cable is inextensible makes the stretched arc length p the same as the unstretched arc length s. Following the assumption of no currents and the assumption made earlier that effects owing to wave kinematics are negligible, the relative velocity and acceleration vectors become equal to the absolute velocity and acceleration vectors respectively. It follows that the differential equation of motion in the tangent direction for an element of cable becomes:

$$\frac{\partial T}{\partial s} + w\frac{\partial y}{\partial s} - \frac{1}{2}\pi\rho d C_T |V_t| V_t - m a_t = 0 \tag{4.1}$$

where T is the tension, w is the submerged weight per unit length, d is the cable diameter, ρ is the fluid density, C_T is the tangential drag coefficient, V_t is the tangential component of the absolute velocity, m is the physical mass per unit length, and a_t is the tangential component of the absolute acceleration vector. In the above equation the term due to the second order effect of the shear force has been neglected in accordance with the assumption made earlier.

Similarly, the differential equation of motion in the normal direction for an element of cable becomes:

$$\kappa T - EI\frac{\partial^2 \kappa}{\partial s^2} + w\frac{\partial x}{\partial s} - \frac{1}{2}\rho d C_D V_n |V_n| - (m + \rho A) a_n = 0 \tag{4.2}$$

where EI is the cable bending stiffness, κ is the curvature, C_D is the normal drag coefficient, V_n in the normal component of the absolute velocity and a_n is the normal component of the absolute acceleration vector. The added mass coefficient C_M is assumed to be one.

Following the assumption that the co-ordinate z and, therefore, its derivatives are zero and that the cable is inextensible, the equation of geometric compatibility becomes:

$$\left(\frac{\partial x}{\partial s}\right)^2 + \left(\frac{\partial y}{\partial s}\right)^2 = 1 \tag{4.3}$$

The above equations form a non-linear system of three differential equations with three unknowns which are the tension T, and the co-ordinates x and y. In order to solve such a system, it is necessary to write the expressions for the curvature, velocities and accelerations as functions of the co-ordinates x and y and their derivatives. It is also necessary to establish the relationship between the different frames of reference used in the reference system.

4.2.3 - Two Dimensional Reference System and Curvature

The implications of the two dimensional assumptions on the reference system and curvature are considered next. The discussion which follows is based on figure 4.1 which shows an arbitrary two dimensional configuration together with the two dimensional version of the three frames of reference defined in chapter three. This discussion is divided into two parts. The first part is concerned with the relationship between the three frames of

reference while the second part deals with the derivation of the two dimensional expression for the curvature.

Relationship between the Reference Frames

As shown in figure 4.1, the inertial frame of reference defined by the triad $(\mathbf{I},\mathbf{J},\mathbf{K})$ is placed at the mean water level. There can be two classes of vessel motions. One class of motion is due to the forward speed. The forward speed is assumed to be either constant or to change at a constant rate with time. The other class of vessel motion consists of motion due to waves. In this work only regular waves are considered.

Since the vessel forward speed is parallel to the unit vector, $\mathbf{I}$ the angle β defined in chapter three becomes zero. Consequently, the transformation from the inertial frame of reference to the vessel frame of reference is given by the expression:

$$\begin{Bmatrix} \mathbf{i} \\ \mathbf{j} \\ \mathbf{k} \end{Bmatrix} = \begin{bmatrix} -1 & 0 & 0 \\ 0 & 1 & 0 \\ 0 & 0 & -1 \end{bmatrix} \begin{Bmatrix} \mathbf{I} \\ \mathbf{J} \\ \mathbf{K} \end{Bmatrix} \tag{4.4}$$

The two dimensional expression for the transformation from the vessel frame of reference to the local frame of reference can be obtained by setting the derivatives of the co-ordinates z to zero in the three dimensional transformation expression. As a result:

$$\begin{Bmatrix} \mathbf{t} \\ \mathbf{n} \\ \mathbf{b} \end{Bmatrix} = \begin{bmatrix} \dfrac{\partial x}{\partial s} & \dfrac{\partial y}{\partial s} & 0 \\ \dfrac{1}{\kappa}\dfrac{\partial^2 x}{\partial s^2} & \dfrac{1}{\kappa}\dfrac{\partial^2 y}{\partial s^2} & 0 \\ 0 & 0 & \dfrac{1}{\kappa}\left(\dfrac{\partial x}{\partial s}\dfrac{\partial^2 y}{\partial s^2} - \dfrac{\partial^2 x}{\partial s^2}\dfrac{\partial y}{\partial s}\right) \end{bmatrix} \begin{Bmatrix} \mathbf{i} \\ \mathbf{j} \\ \mathbf{k} \end{Bmatrix} \tag{4.5}$$

As mentioned earlier, for the two dimensional case, the direction of the binormal vector does not change in space or in time. As a result, the binormal direction is always parallel to both unit vectors **k** and **K**. However, the sense of the unit binormal vector depends on the position of the centre of curvature. In order to establish the sense of the unit binormal vector the two segments of the cable configuration shown in figure 4.1 are considered next.

In accordance with the definition presented in appendix A, the curvature is the magnitude of the second derivative of the position vector with respect the arc length s. In addition the unit principal normal vector always points to the centre of curvature. Consequently, for the concave segment AB, the centre of curvature is located bellow the curve. Therefore, the principal unit vector points downwards and the unit binormal vector has the same sense as the unit vector **k**. In contrast, for the convex segment BC, the centre of curvature is located above the curve. The unit principal normal vector points upwards and the unit binormal vector has the opposite sense to the unit vector **k**. Accordingly, the following expression can be written:

$$\mathbf{b} = \pm\mathbf{k} \rightarrow \frac{1}{\kappa}\left(\frac{\partial x}{\partial s}\frac{\partial^2 y}{\partial s^2} - \frac{\partial^2 x}{\partial s^2}\frac{\partial y}{\partial s}\right) = \pm 1 \tag{4.6}$$

where the positive sign is taken for concave segments and the negative sign is taken for convex segments of the cable configuration.

Determination of the Curvature

The expression for the curvature can be obtained by combining equation (4.5) with the derivative of the equation of geometric compatibility given by equation (4.3) with respect to the arc length s. Such a derivative can be expressed as:

$$\frac{\partial x}{\partial s}\frac{\partial^2 x}{\partial s^2}+\frac{\partial y}{\partial s}\frac{\partial^2 y}{\partial s^2}=0 \tag{4.7}$$

As a result, the expression for the curvature is:

$$\kappa=\pm\frac{\partial^2 y}{\partial s^2}\left(\frac{\partial x}{\partial s}\right)^{-1} \tag{4.8}$$

where again, the positive sign is taken for concave segments while the negative sign is taken for convex segments of the cable configuration.

There are two problems which arise from the use of the geometric definition of curvature in cable analysis. The first problem is concerned with the definition of the sign to be used during the analysis. The second problem comes from the fact that for inflection points such as the point B in figure 4.1 the curvature is zero. The centre of curvature is not defined for this point. Therefore, the principal normal direction cannot be defined. These problems can be overcome by the two main alternative procedures which are outlined next.

The first procedure consists of identifying whether the segment under investigation is concave or convex. Then the sign is chosen accordingly. In this procedure, inflection points are also identified and regarded as singular points. This can be achieved because the problem is non-linear and some

kind of initial approximation is necessary. Therefore, the concavity of the segment and the position of the inflection points can be determined from this initial approximation.

The second procedure to deal with the problem arising from the definition of curvature consists of the redefinition of curvature where the curvature is still a scalar quantity but not necessarily positive. That is, the curvature can assume negative values. Positive curvature represents concave segments and negative curvature represents a convex segments. A fourth reference frame defined by the triad $(\mathbf{e}_t, \mathbf{e}_n, \mathbf{e}_b)$ is now introduced. This reference frame is such that its unit vector $\mathbf{e}_t$ is equal to the unit tangent vector $\mathbf{t}$. The unit vector $\mathbf{e}_n$ is equal to the unit principal normal vector $\mathbf{n}$ for positive curvatures and is opposite to $\mathbf{n}$ for negative curvatures.

The second procedure has two main advantages over the first one. Firstly, there is no need to establish the concavity of the cable configuration and the position of inflection points beforehand. These are determined automatically by the sign of the curvature for the former and by the zero curvature condition for the latter. The second, and perhaps the more important advantage is that the second procedure allows the inclusion of straight line segments where the curvature is zero. For these reasons, the second procedure is adopted within this chapter. The relationship between the vessel frame of reference and the fourth frame of reference is considered next.

Assuming that the curvature is positive when the segment of cable is concave, the expression for the curvature becomes:

$$\kappa = \frac{\partial^2 y}{\partial s^2}\left(\frac{\partial x}{\partial s}\right)^{-1} \tag{4.9}$$

Substituting equation (4.9) into the transformation given by expression (4.6) and replacing the triad $(\mathbf{t},\mathbf{n},\mathbf{b})$ in that expression by the triad $(\mathbf{e}_t,\mathbf{e}_n,\mathbf{e}_b)$ results in:

$$\begin{Bmatrix}\mathbf{e}_t\\ \mathbf{e}_n\\ \mathbf{e}_b\end{Bmatrix}=\begin{bmatrix}\frac{\partial x}{\partial s} & \frac{\partial y}{\partial s} & 0\\ -\frac{\partial y}{\partial s} & \frac{\partial x}{\partial s} & 0\\ 0 & 0 & 1\end{bmatrix}\begin{Bmatrix}\mathbf{i}\\ \mathbf{j}\\ \mathbf{k}\end{Bmatrix} \tag{4.10}$$

4.2.4 - Determination of the Velocity and Acceleration Vectors

The expressions for the velocity and acceleration vectors are derived within this section. It is assumed throughout this chapter that the motions of the origin of the vessel frame of reference comprises of a straight line motion in head or following seas with constant acceleration combined with surge and heave motions of the cable departure point due to waves. Thus, the absolute velocity vector of an element of cable can be either written in the vessel frame of reference as:

$$\mathbf{V}_c = V_{cx}\mathbf{i}+V_{cy}\mathbf{j}=\left(\frac{\partial x}{\partial t}-V_0-at-\frac{\partial X_w}{\partial t}\right)\mathbf{i}+\left(\frac{\partial y}{\partial t}+\frac{\partial Y_w}{\partial t}\right)\mathbf{j} \tag{4.11}$$

where V_{cx} and V_{cy} are the components of the velocity vector in the x and y directions, respectively, V_0 is the lay vessel initial forward speed and a is the vessel's mean forward acceleration. X_w and Y_w are the surge and the heave motions of the cable departure point due to waves and t is time. This same vector may be written in the local frame of reference as:

$$\mathbf{V}_c = V_{ct}\mathbf{e}_t+V_{cn}\mathbf{e}_n=\left(V_{cx}\frac{\partial x}{\partial s}+V_{cy}\frac{\partial y}{\partial s}\right)\mathbf{e}_t+\left(V_{cy}\frac{\partial x}{\partial s}-V_{cx}\frac{\partial y}{\partial s}\right)\mathbf{e}_n \tag{4.12}$$

where V_{ct} and V_{cn} are the tangential and the normal components of the velocity vector respectively.

Similarly, the absolute acceleration vector can be written in the vessel frame of reference as:

$$\mathbf{a}_c = a_{cx}\mathbf{i} + a_{cy}\mathbf{j} = \left(\frac{\partial^2 x}{\partial t^2} - a - \frac{\partial^2 X_w}{\partial t^2}\right)\mathbf{i} + \left(\frac{\partial^2 y}{\partial t^2} + \frac{\partial^2 Y_w}{\partial t^2}\right)\mathbf{j} \tag{4.13}$$

where a_{cx} is the component of the acceleration vector in the x direction and a_{cy} is its component in the y direction.

The expression for the acceleration vector in the local frame of reference is:

$$\mathbf{a}_c = a_{ct}\mathbf{e}_t + a_{cn}\mathbf{e}_n = \left(a_{cx}\frac{\partial x}{\partial s} + a_{cy}\frac{\partial y}{\partial s}\right)\mathbf{e}_t + \left(a_{cy}\frac{\partial x}{\partial s} - a_{cx}\frac{\partial y}{\partial s}\right)\mathbf{e}_n \tag{4.14}$$

where a_{ct} and a_{cn} are the components of the acceleration in the tangential and normal directions, respectively.

For cable laying analysis, the pay out rate must be added to the tangential component of the velocity vector. Since the pay out rate is tangent to the cable, the additional velocity vector is:

$$\mathbf{V}_{po} = V_{po}\mathbf{t} = V_{po}\frac{\partial x}{\partial s}\mathbf{i} + V_{po}\frac{\partial y}{\partial s}\mathbf{j} \tag{4.15}$$

where V_{po} is the pay out rate.

Since the acceleration is the time derivative of the velocity vector, the following vector must be added to the acceleration vector as a result of the pay out rate:

$$\frac{\partial \mathbf{V}_{po}}{\partial t} = \frac{\partial V_{po}}{\partial t}\mathbf{t} + V_{po}\frac{\partial^2 y}{\partial s \partial t}\left(\frac{\partial x}{\partial s}\right)^{-1}\mathbf{n} = \left(\frac{\partial V_{po}}{\partial t}\frac{\partial x}{\partial s} + V_{po}\frac{\partial^2 x}{\partial s \partial t}\right)\mathbf{i} + \left(\frac{\partial V_{po}}{\partial t}\frac{\partial y}{\partial s} + V_{po}\frac{\partial^2 y}{\partial s \partial t}\right)\mathbf{j} \tag{4.16}$$

4.2.5 - Boundary Conditions and Final Expression for the Equations of Motion

The equations of motion given by equations (4.1) and (4.2) together with the equation of geometric compatibility given by equation (4.3) form a non-linear system of partial differential equations. In such a system, the dependent variables are the tension T and the co-ordinates x and y. The independent variables are the arc length s and the time t. In addition, as mentioned earlier in chapter three, the highest order derivatives for the co-ordinates are fourth order with respect to arc length s and second order with respect to time t. For the tension, the highest order derivative with respect to arc length s is first order while no time derivatives of the tension are present in the system of differential equations. As a result, there must be four boundary conditions and two initial conditions for the co-ordinates x and y and one boundary condition for the tension.

In the case of towed cable analysis in which the cable does not touch the seabed, the tension boundary conditions are well defined. That is, the tension, the shear force and the bending moment are all zero at the cable free end. In the case of cable laying analysis or towed cable analysis with the cable touching the seabed, the bottom boundary conditions depend on a complex interaction between the cable and the seabed. This complex

interaction can only be determined by a local analysis which is beyond the scope of this work. Under these circumstances, throughout this work it will be assumed that the bottom boundary conditions when the cable touches the seabed are the same as those adopted when the cable actually has a free end. The only difference is that when the cable touches the seabed the suspended length of the cable changes during the analysis.

If the bottom tension is assumed to be zero then the tension can be determined by performing the following integral of the tangential differential equation of motion:

$$T = w(h-y) + \int_s^l \left(\frac{1}{2}\pi\rho d C_T |V_n| V_n + m a_t \right) ds \tag{4.17}$$

where l is the total length of cable and h is the water depth.

Combining the equation of geometric compatibility with the differential equation of motion in the normal direction gives:

$$\frac{T\frac{\partial^2 y}{\partial s^2}}{\sqrt{1-\left(\frac{\partial y}{\partial s}\right)^2}} - \frac{\partial^2}{\partial s^2}\left[\frac{EI\frac{\partial^2 y}{\partial s^2}}{\sqrt{1-\left(\frac{\partial y}{\partial s}\right)^2}}\right] + w\sqrt{1-\left(\frac{\partial y}{\partial s}\right)^2} - \frac{1}{2}\rho d C_D V_n |V_n| - (m+\rho A)a_n = 0 \tag{4.18}$$

The solution of the above differential equation is considered next.

4.3 - Solution of the Differential Equation of Motion

The remainder of this chapter is concerned with the solution of the differential equation of motion given by equation (4.18) for cases where the

bottom tension is zero. The solution presented here consists of three main stages. The first step consists of the space integration of the differential equation of motion while the second step is concerned with the time integration of this equation. The third step is concerned with the solution of the non-linear system of algebraic equations which results from the integration described above. These three steps are considered in detail next. The computational implementation of such a solution is further discussed in Appendix E.

4.3.1 - Space Integration of the Equation of Motion

The space integration is performed by a finite element method based on the Galerkin weighted residual formulation. In this solution, the cable is first divided into a number of finite elements as shown in figure 4.2. The co-ordinate y is then approximated within each element by the following expression:

$$y \approx \tilde{y} = \sum_{j=1}^{n} u_j(t)\psi_j(s) = \mathbf{u}^{\mathrm{T}}\boldsymbol{\psi} \tag{4.19}$$

where u_j are unknown functions of time and ψ_j are the shape functions. The corresponding vectors are $\mathbf{u}$ and $\boldsymbol{\psi}$ respectively. Each element has n degrees of freedom.

Next, the co-ordinate y is replaced in differential equation (4.18) by its approximated value $\tilde{y}$. Owing to the fact that $\tilde{y}$ is not the exact solution of the differential equation (4.18), the right hand side of the new equation will take a residual value instead of zero. That is:

$$\frac{T\frac{\partial^2\tilde{y}}{\partial s^2}}{\sqrt{1-\left(\frac{\partial\tilde{y}}{\partial s}\right)^2}}-\frac{\partial^2}{\partial s^2}\left[\frac{EI\frac{\partial^2\tilde{y}}{\partial s^2}}{\sqrt{1-\left(\frac{\partial\tilde{y}}{\partial s}\right)^2}}\right]+w\sqrt{1-\left(\frac{\partial\tilde{y}}{\partial s}\right)^2}-\frac{1}{2}\rho dC_D V_n|V_n|-(m+\rho A)a_n=R_s \tag{4.20}$$

where R_s is the residual value.

In order to obtain an approximate solution which is sufficiently close to the exact solution, the residual value is minimised over each finite element. This minimisation can be performed by the weighted residual method. In this method the residual value given by equation (4.20) is multiplied by weighting functions. Then the result of this product is integrated over the element and the resulting integrals are equated to zero. The weighted residual expression for a generic finite element k in the present analysis is given by:

$$\int_{s_k}^{s_{k+1}}\{\frac{T\frac{\partial^2\tilde{y}}{\partial s^2}}{\sqrt{1-\left(\frac{\partial\tilde{y}}{\partial s}\right)^2}}-\frac{\partial^2}{\partial s^2}\left[\frac{EI\frac{\partial^2\tilde{y}}{\partial s^2}}{\sqrt{1-\left(\frac{\partial\tilde{y}}{\partial s}\right)^2}}\right]+w\sqrt{1-\left(\frac{\partial\tilde{y}}{\partial s}\right)^2}-\frac{1}{2}\rho dC_D V_n|V_n|$$

$$-(m+\rho A)a_n\}\overline{W}_i ds=0 \tag{4.21}$$

where s_k and s_{k+1} are the Lagrangean co-ordinates for the element nodes and $\overline{W}_i$ are the weighting functions.

The Galerkin method assumes that the weighting functions are the same as the shape functions. In addition, the highest order derivative which appears in equation (4.21) is the fourth order. Therefore, in order to model this derivative the shape function has to be of continuity C^3. In order to reduce this continuity requirement, the term of equation (4.21) which contains the

second derivative of the curvature with respect to the arc length can be twice integrated by parts. This gives:

$$\int_{s_k}^{s_{k+1}} \frac{\partial^2}{\partial s^2} \frac{EI\dfrac{\partial^2 \tilde{y}}{\partial s^2}}{\sqrt{1-\left(\dfrac{\partial \tilde{y}}{\partial s}\right)^2}} \psi_i ds = \int_{s_k}^{s_{k+1}} EI \frac{\dfrac{\partial^2 \tilde{y}}{\partial s^2}\dfrac{\partial^2 \psi_i}{\partial s^2}}{\sqrt{1-\left(\dfrac{\partial \tilde{y}}{\partial s}\right)^2}} ds - \left[EI\frac{\partial \tilde{\kappa}}{\partial s}\psi_i \right]_{s_k}^{s_{k+1}} + \left[EI\tilde{\kappa}\frac{\partial \psi_i}{\partial s} \right]_{s_k}^{s_{k+1}} \tag{4.22}$$

where the expressions in the square brackets correspond to the boundary terms and $\tilde{\kappa}$ is the expression for the curvature which is obtained with the approximation $\tilde{y}$ for the co-ordinate y.

For inter-element boundaries these terms vanish because it is assumed that there is continuity in slope. However, for the end points of the cable the boundary conditions must be applied. The first boundary condition can be obtained by expanding the expression in the first square brackets. That is:

$$\left[EI\frac{\partial \tilde{\kappa}}{\partial s}\psi_i \right]_{s_k}^{s_{k+1}} = EI\frac{\partial \tilde{\kappa}}{\partial s}\psi_i\Big|_{s=l} - EI\frac{\partial \tilde{\kappa}}{\partial s}\psi_i\Big|_{s=0} \tag{4.23}$$

where l is the marine cable length. The meaning of this expression is that, for both ends, either the shear force or the displacement must be specified.

Similarly, the expansion of the term in the second square brackets gives:

$$\left[EI\tilde{\kappa}\frac{\partial \psi_i}{\partial s} \right]_{s_k}^{s_{k+1}} = EI\tilde{\kappa}\frac{\partial \psi_i}{\partial s}\Big|_{s=l} - EI\tilde{\kappa}\frac{\partial \psi_i}{\partial s}\Big|_{s=0} \tag{4.24}$$

That is, either the bending moment or the slope must be specified at the end points.

Since the boundary terms vanish at the inter-element boundaries the boundary conditions are applied later on in the analysis. As a result, the Galerkin integral equation becomes:

$$\int_{s_k}^{s_{k+1}} \{ \frac{T\frac{\partial^2 \tilde{y}}{\partial s^2}}{\sqrt{1-\left(\frac{\partial \tilde{y}}{\partial s}\right)^2}} w\sqrt{1-\left(\frac{\partial \tilde{y}}{\partial s}\right)^2} - \frac{1}{2}\rho d C_D V_n |V_n| - (m+\rho A)a_n \} \psi_i ds$$

$$- \int_{s_k}^{s_{k+1}} EI \frac{\frac{\partial^2 \tilde{y}}{\partial s^2}\frac{\partial^2 \psi_i}{\partial s^2}}{\sqrt{1-\left(\frac{\partial \tilde{y}}{\partial s}\right)^2}} ds = 0 \qquad (4.25)$$

Once the shape functions are defined, the unknowns in the above integral equations are the functions of time **u** and their first and second derivatives with respect to time. Therefore, the result of the above integral equations is a system of second order ordinary differential equations in time. The integration of such a system is considered next.

4.3.2 - Time Integration of the Equation of Motion

This section is concerned with the solution of differential equation which results from the space integration of the differential equations of motion. The solution presented here is obtained in the time domain where the equations of motion are satisfied for discrete time intervals Δt apart. The direct integration method used in this work is the Newmark scheme which is briefly described next. For more information on the Newmark integration scheme see Bathe (1982), Burnett (1987), and Zienkiewicz and Taylor (1989, 1991).

The Newmark method is applied in order to obtain the solution of the following problem: given the position, velocity and acceleration of the cable

configuration at the time t, determine the new position, velocity and acceleration of the cable configuration at the time $t+\Delta t$. The Newmark scheme assumes that the acceleration varies linearly over the time interval Δt. The equations for the velocity and for the position are written as functions of the initial conditions and the acceleration of the cable at time $t+\Delta t$. The velocity for the time $t+\Delta t$ is given by:

$$ {}^{t+\Delta t}\frac{\partial \mathbf{u}}{\partial t} = {}^{t}\frac{\partial \mathbf{u}}{\partial t} + \left[{}^{t+\Delta t}\frac{\partial^2 \mathbf{u}}{\partial t^2}\delta + {}^{t}\frac{\partial^2 \mathbf{u}}{\partial t^2}(1-\delta) \right]\Delta t \tag{4.26} $$

where $\mathbf{u}$ is the unknown displacement vector. In the present analysis, the elements of the unknown vector are the nodal co-ordinate y and the nodal derivatives of the co-ordinate y with respect to the arc length s.

The position is obtained through the expression:

$$ {}^{t+\Delta t}\mathbf{u} = {}^{t}\mathbf{u} + {}^{t}\frac{\partial \mathbf{u}}{\partial t}\Delta t + \left[{}^{t+\Delta t}\frac{\partial^2 \mathbf{u}}{\partial t^2}\alpha + {}^{t}\frac{\partial^2 \mathbf{u}}{\partial t^2}\left(\frac{1}{2}-\alpha\right) \right]\Delta t^2 \tag{4.27} $$

where α and δ are parameters used to adjust the stability and accuracy of the method. If the parameter α is equated to 0.25 and the parameter δ is set equal to 0.50, the Newmark method is said to use the trapezoidal rule. For linear dynamic analysis these parameters make the Newmark integration scheme unconditionally stable. However, for non-linear analyses the stability of the method depends on the case being considered.

It follows from equations (4.26) and (4.27) that the new velocity and acceleration vector can be expressed as functions of the initial conditions and the position at the time $t+\Delta t$ itself. These expressions are, for velocity:

$$ {}^{t+\Delta t}\frac{\partial \mathbf{u}}{\partial t} = \left({}^{t+\Delta t}\mathbf{u} - {}^{t}\mathbf{u}\right)\beta_{v1} - {}^{t}\frac{\partial \mathbf{u}}{\partial t}\beta_{v2} - {}^{t}\frac{\partial^2 \mathbf{u}}{\partial t^2}\beta_{v3} \tag{4.28} $$

and, for acceleration:

$$ {}^{t+\Delta t}\frac{\partial^2 \mathbf{u}}{\partial t^2} = \left({}^{t+\Delta t}\mathbf{u} - {}^{t}\mathbf{u}\right)\beta_{a1} - {}^{t}\frac{\partial \mathbf{u}}{\partial t}\beta_{a2} - {}^{t}\frac{\partial^2 \mathbf{u}}{\partial t^2}\beta_{a3} \tag{4.29} $$

where the coefficients β_{ai} and β_{vi} are given in table 4.1.

i	β_{ai}	β_{vi}
1	$\frac{1}{\alpha \Delta t^2}$	$\frac{\delta}{\alpha \Delta t}$
2	$\frac{1}{\alpha \Delta t}$	$\left(\frac{\delta}{\alpha} - 1\right)$
3	$\frac{1}{2\alpha} - 1$	$\left(\frac{\delta}{2\alpha} - 1\right)\Delta t$

Table 4.1 - Newmark Coefficients

The substitution of the above expressions for the velocity and acceleration into the Galerkin integral equation leads to a non-linear system of algebraic equations whose unknowns are the temporal coefficients u_i at time $t + \Delta t$. For the very first time step, however, only two initial conditions are known. These initial conditions are the cable configuration and the cable velocity. Here, it is assumed that the initial condition is the stationary configuration throughout this work. Since the initial acceleration is not known, it is assumed that the acceleration is constant for the first time step. Then the expressions for the velocity and acceleration become, respectively:

$$ {}^{\Delta t}\frac{\partial \mathbf{u}}{\partial t} = \left({}^{\Delta t}\mathbf{u} - {}^{t}\mathbf{u}\right)\beta_{v1} - {}^{0}\frac{\partial \mathbf{u}}{\partial t}\beta_{v2} - \beta_{v3}\left[\frac{\beta_{a1}}{1+\beta_{a3}}\left({}^{\Delta t}\mathbf{u} - {}^{0}\mathbf{u}\right) - \frac{\beta_{a2}}{1+\beta_{a3}}{}^{0}\frac{\partial \mathbf{u}}{\partial t}\right] \tag{4.30} $$

and

$$ {}^{\Delta t}\frac{\partial^2 \mathbf{u}}{\partial t^2} = \frac{\beta_{a1}}{1+\beta_{a3}}\left({}^{\Delta t}\mathbf{u} - {}^{0}\mathbf{u}\right) - \frac{\beta_{a2}}{1+\beta_{a3}}\,{}^{0}\frac{\partial \mathbf{u}}{\partial t} \tag{4.31} $$

where the zero superscript denotes initial conditions for the time step.

For the k^{th} finite element, the Galerkin integral equation may be written in a more concise form as follows:

$$ \mathbf{f}^k = \mathbf{f}_g^k - \mathbf{f}_b^k + \mathbf{f}_w^k - \mathbf{f}_d^k - \mathbf{f}_m^k = 0 \tag{4.32} $$

where $\mathbf{f}^k$ is the vector which contains the nodal forces and moments for the element and $\mathbf{f}_g^k$, $\mathbf{f}_b^k$, $\mathbf{f}_w^k$, $\mathbf{f}_d^k$ and $\mathbf{f}_m^k$ are the nodal forces and moments of the terms associated with the cable's geometric stiffness, flexural rigidity, self-weight and buoyancy forces, drag forces and inertia forces, respectively.

The global forces and moments are obtained by adding the contribution of each element as well as applying the boundary conditions. That is:

$$ \mathbf{F}(\mathbf{U}) = \sum_{k=1}^{nel} \mathbf{f}^k = 0 \tag{4.33} $$

where $\mathbf{F}$ is the global vector of forces and moments, $\mathbf{U}$ is the global vector of displacements and *nel* is the total number of finite elements. The solution of the above system of non-linear algebraic equations is considered next.

4.3.3 - Solution of the Non-Linear System of Algebraic Equations

The solution of the non-linear set of algebraic equations given by the vector equation (4.32) is obtained through the Newton-Raphson method (Bathe,

1982, Buchanan and Turner, 1992). The Newton-Raphson method approximates the solution of a non-linear system of equations through an iterative procedure. It requires an initial estimation for the vector **U** which cannot be too far away from the solution otherwise convergence may not be achieved. However, when it does converge, the method presents quadratic convergence.

The idea of the method is very simple. Suppose that for an iteration q the unknown vector **U** is replaced in equation (4.33) by its approximated value $\mathbf{U}^q$. Then the right hand side of the equation is no longer zero but equal to a residual value **R**. Thus:

$$\mathbf{F}(\mathbf{U}^q) = \mathbf{R} \tag{4.34}$$

In order to estimate the value of the vector $\mathbf{U}^{q+1}$ for the iteration $q+1$ so that the residual value **R** is close enough to zero, the Newton-Raphson method considers the Taylor power series expansion of equation (4.33), which is:

$$\mathbf{F}(\mathbf{U}^{q+1}) = \mathbf{F}(\mathbf{U}^q) + \mathbf{H}(\mathbf{U}^q)\delta\mathbf{U} + \boldsymbol{\varepsilon}^2 \tag{4.35}$$

where $\delta\mathbf{U} = \mathbf{U}^{q+1} - \mathbf{U}^q$, $\boldsymbol{\varepsilon}^2$ is the vector sum of the terms with order higher than the first order and **H** is the Jacobian matrix whose elements are given by the expression:

$$H_{ij} = \frac{\partial F_i}{\partial U_j} \tag{4.36}$$

The terms higher than first order are neglected and the vector function $\mathbf{F}(\mathbf{U}^{q+1})$ given by equation (4.35) is set to zero. As a result, the vector $\mathbf{U}^{q+1}$ is given by:

$$\mathbf{U}^{q+1} = \mathbf{U}^{q} - \mathbf{H}^{-1}(\mathbf{U}^{q})\mathbf{F}(\mathbf{U}^{q}) \tag{4.37}$$

This procedure is repeated until convergence is achieved. Theoretically, the method should converge if the Jacobian matrix is positive definite. However, in practice the method also requires that the initial estimate of the vector $\mathbf{U}^{q+1}$ to be close to the actual solution.

The Newton-Raphson method can be summarised as following four steps:

(a) - estimate an initial value for the global displacement vector $\mathbf{U}^{q+1}$,
(b) - calculate the global forces vector $\mathbf{F}(\mathbf{U}^{q+1})$,
(c) - calculate the global Jacobian matrix $\mathbf{H}(\mathbf{U}^{q+1})$ and then
(d) - calculate the updated global displacement vector $\mathbf{U}^{q+1}$ by using equation (4.37).

These four steps are repeated until $\mathbf{U}^{q+1}$ converges to the solution for the global displacements. Next, the application of these four steps to the dynamic analysis of marine cables is considered.

Determination of the Global Force Vector

The global force vector is given by equation (4.33). Therefore, it is necessary to calculate the element force vector $\mathbf{f}^{k}$ for each element and then to add it to the global force vector. The element force vector is determined by performing the numerical integration of the Galerkin integral equation (4.25). The numerical integration method used here consists of a five point

Gauss quadrature. Therefore, it is necessary to evaluate the integrand for five points along the element. The evaluation of the Galerkin integral equation integrand requires knowledge of the co-ordinate y, the tension T, the tangential velocity V_t, the normal velocity V_n, the tangential acceleration a_t and the normal acceleration a_n.

Shape Functions

The co-ordinate y is approximated by a Hermite cubic polynomial within an finite element of cable. It is necessary to specify four boundary conditions in order to define a Hermite cubic polynomial. These boundary conditions come from the specification at both ends of the element of the co-ordinate y itself and the derivative of the co-ordinate y with respect to the arc length s which is the sine of the angle between the unit tangent vector **t** and the unit vector **i**. The expressions for the shape functions and their derivatives are given by table 4.2.

i	ψ_i	$\frac{\partial \psi_i}{\partial s}$	$\frac{\partial^2 \psi_i}{\partial s^2}$
1	$1-3\xi^2+2\xi^2$	$\frac{6\xi^2-6\xi}{l_k}$	$\frac{12\xi-6}{l_k^2}$
2	$l_k(\xi^3-2\xi^2+\xi)$	$3\xi^2-4\xi+1$	$\frac{6\xi-4}{l_k}$
3	$3\xi^2-2\xi^3$	$\frac{6\xi-6\xi^2}{l_k}$	$\frac{6-12\xi}{l_k^2}$
4	$l_k(\xi^3-\xi^2)$	$3\xi^2-2\xi$	$\frac{6\xi-2}{l_k}$

Table 4.2 - Shape functions and their derivatives

In table 4.2, l_k is the element length and the normalised co-ordinate ξ is given by the equation:

$$\xi = \frac{s - s_k}{l_k} \tag{4.38}$$

where s_k is the Lagrangean co-ordinate of the initial node of the element.

Vertical Co-ordinate and its Derivatives

The co-ordinate y is given by equation (4.19). As a result, its first and second derivatives with respect to the arc length s are given, respectively, by the following expressions:

$$\frac{\partial y}{\partial s} = \sum_{i=1}^{4} u_i \frac{\partial \psi_i}{\partial s} \tag{4.39}$$

and

$$\frac{\partial^2 y}{\partial s^2} = \sum_{i=1}^{4} u_i \frac{\partial^2 \psi_i}{\partial s^2} \tag{4.40}$$

Similarly, the first and second time derivatives of the co-ordinate y are:

$$\frac{\partial y}{\partial t} = \sum_{i=1}^{4} \frac{\partial u_i}{\partial t} \psi_i \tag{4.41}$$

and

$$\frac{\partial^2 y}{\partial t^2} = \sum_{i=1}^{4} \frac{\partial^2 u_i}{\partial t^2} \psi_i \tag{4.42}$$

Finally, the first and second time derivatives of the first derivatives of the co-ordinate y with respect to the arc length s are given by:

$$\frac{\partial^2 y}{\partial s \partial t} = \sum_{i=1}^{4} \frac{\partial u_i}{\partial t} \frac{\partial \psi_i}{\partial s} \tag{4.43}$$

and:

$$\frac{\partial^3 y}{\partial s \partial t^2} = \sum_{i=1}^{4} \frac{\partial^2 u_i}{\partial t^2} \frac{\partial \psi_i}{\partial s} \tag{4.44}$$

In the above expressions, the nodal coefficients of time $\frac{\partial u_i}{\partial t}$ and $\frac{\partial^2 u_i}{\partial t^2}$ are obtained by Newmark formulae given by equations (4.28) and (4.29), respectively.

Horizontal Co-ordinate and its Derivatives

In order to perform the integration of the Galerkin integral equations, it is necessary to determine expressions for the derivative of the co-ordinate x with respect to the arc length s and for the first and second derivatives of the co-ordinate x with respect to time t. In addition, the co-ordinate x itself needs to be determined so that the configuration of the cable can be established.

The first derivative of x with respect to s is given by the equation of geometric compatibility (4.3). That is:

$$\frac{\partial x}{\partial s} = \sqrt{1 - \left(\frac{\partial y}{\partial s}\right)^2} \tag{4.45}$$

The co-ordinate x for the k^{th} finite element is obtained through the integration of equation (4.45), which is given by:

$$x = x_k + \int_0^{\xi} l_k \sqrt{1 - \left(\frac{\partial y}{\partial s}\right)^2}\, \partial\xi \tag{4.46}$$

where x_k is the co-ordinate for the first node of the k^{th} finite element, l_k is the element length and ξ is the normalised arc length as defined by equation (4.38).

The time derivatives of the co-ordinate x are determined through the differentiation of the equation of geometric compatibility with respect to time. The first derivative of equation (4.3) with respect to time is:

$$\frac{\partial^2 x}{\partial s \partial t} = -\frac{\partial y}{\partial s}\frac{\partial^2 y}{\partial s \partial t}\left[1 - \left(\frac{\partial y}{\partial s}\right)^2\right]^{-\frac{1}{2}} \tag{4.47}$$

Consequently, the first derivative of the co-ordinate x with respect to time is obtained by the following integral:

$$\frac{\partial x}{\partial t} = \left.\frac{\partial x}{\partial t}\right|_k - \int_0^{\xi} l_k \frac{\partial y}{\partial s}\frac{\partial^2 y}{\partial s \partial t}\left[1 - \left(\frac{\partial y}{\partial s}\right)^2\right]^{-\frac{1}{2}} d\xi \tag{4.48}$$

where $\left.\frac{\partial x}{\partial t}\right|_k$ is the x component of the element velocity relative to the vessel frame of reference.

The second derivative of the equation of geometric compatibility with respect to time is given by:

$$\frac{\partial^3 x}{\partial s \partial t^2} = -\frac{\partial y}{\partial s}\frac{\partial^3 y}{\partial s \partial t^3}\left[1 - \left(\frac{\partial y}{\partial s}\right)^2\right]^{-\frac{1}{2}} - \left(\frac{\partial^2 y}{\partial s \partial t}\right)^2\left[1 - \left(\frac{\partial y}{\partial s}\right)^2\right]^{-\frac{3}{2}} \tag{4.49}$$

As a result, the second derivative of the co-ordinate x with respect to time may be expressed as:

$$\frac{\partial^2 x}{\partial t^2} = \left.\frac{\partial^2 x}{\partial t^2}\right|_k - \int_0^{\xi} l_k \left\{ \frac{\partial y}{\partial s}\frac{\partial^3 y}{\partial s \partial t^3}\left[1-\left(\frac{\partial y}{\partial s}\right)^2\right]^{-\frac{1}{2}} + \left(\frac{\partial^2 y}{\partial s \partial t}\right)^2 \left[1-\left(\frac{\partial y}{\partial s}\right)^2\right]^{-\frac{3}{2}} \right\} d\xi \qquad (4.50)$$

where $\left.\frac{\partial^2 x}{\partial t^2}\right|_k$ is the x component of the element velocity relative to the vessel frame of reference.

Tangent and Normal Components for the Velocity and Acceleration

The tangential and normal components for the velocity and acceleration are determined by combining equations (4.12), (4.14), (4.15) and (4.16). The resulting expressions are shown in table 4.3.

In table 4.3, V_{vx} is the x component while V_{vy} is the y component of the vessel's velocity vector. Similarly, a_{vx} and a_{vy} are the x and y components of the vessel's acceleration vector respectively.

V_t	$\left(V_{vx}+\frac{\partial x}{\partial t}\right)\frac{\partial x}{\partial s}+\left(V_{vy}+\frac{\partial y}{\partial t}\right)\frac{\partial y}{\partial s}+V_{po}$
V_n	$\left(V_{vy}+\frac{\partial y}{\partial t}\right)\frac{\partial x}{\partial s}-\left(V_{vx}+\frac{\partial x}{\partial t}\right)\frac{\partial y}{\partial s}$
a_t	$\left(a_{vx}+\frac{\partial^2 x}{\partial t^2}\right)\frac{\partial x}{\partial s}+\left(a_{vy}+\frac{\partial^2 y}{\partial t^2}\right)\frac{\partial y}{\partial s}+\frac{\partial V_{po}}{\partial t}$
a_n	$\left(a_{vy}+\frac{\partial^2 y}{\partial t^2}\right)\frac{\partial x}{\partial s}-\left(a_{vx}+\frac{\partial^2 x}{\partial t^2}\right)\frac{\partial y}{\partial s}+V_{po}\frac{\partial^2 y}{\partial s \partial t}\left(\frac{\partial x}{\partial s}\right)^{-1}$

Table 4.3 - Expressions for the Velocity and Acceleration

Tension

Unlikely the other quantities determined in this section, the tension must be integrated from the cable bottom end to the cable top end. This is because the boundary condition for the tension was applied at the bottom end. The tension for the k^{th} finite element is obtained by integrating the tangential equation of motion over the element. This gives:

$$T = T_{k+1} + w(y_{k+1} - y) - \int_{\xi}^{1} l_k \left(\frac{1}{2} \pi \rho d C_T V_t |V_t| + m a_t \right) d\xi \tag{4.51}$$

where T_{k+1} is the tension at node $k+1$ and y_{k+1} is the y co-ordinate for the same node.

Element Force Vector

The element force vector is obtained by the numerical integration of the Galerkin integral equation (4.25). These integral equations can be rewritten as:

$$f_i = \int_0^1 l_k T \kappa \psi_i d\xi - \int_0^1 l_k EI \kappa \frac{\partial^2 \psi_i}{\partial s^2} d\xi + \int_0^1 l_k w \frac{\partial x}{\partial s} \psi_i d\xi - \int_0^1 l_k \frac{1}{2} \rho d C_D V_n |V_n| \psi_i d\xi - \int_0^1 l_k (m + \rho A) a_n \psi_i d\xi \tag{4.52}$$

The element force vector is then added to the global force vector. The position in the global force vector at which the element force vector should be placed is given by the expression:

$$F_{2k-1+i} = F_{2k-1+i} + f_i \qquad \text{for } i = 1, 4 \tag{4.53}$$

4.4 - Determination of the Jacobian Matrix

The Jacobian matrix can be determined analytically by performing the derivatives of the Galerkin integral equation with respect to the coefficients U_i. Alternatively, it can be determined numerically. Since the analytical expressions for the Jacobian matrix are very complex, this work uses a numerical procedure to obtain the Jacobian matrix.

The elements of the Jacobian matrix are given by the expression:

$$H_{ij} = \frac{\partial F_i\left(U_1, U_2, ..., U_j, ..., U_n\right)}{\partial U_j} \tag{4.54}$$

where n is the total number of degrees of freedom.

In order to determine the derivative of the force vector for element i with respect to the displacement vector for the element j the following two expansions in power series are considered:

$$F_i\left(U_1 ..., U_j + \Delta U_j, ..., U_n\right) = F_i\left(U_1 ..., U_j, ..., U_n\right) + \frac{\partial F_i\left(U_1 ..., U_j, ..., U_n\right)}{\partial U_j} \Delta U_j + \varepsilon^2 \tag{4.55}$$

and

$$F_i\left(U_1 ..., U_j - \Delta U_j, ..., U_n\right) = F_i\left(U_1 ..., U_j, ..., U_n\right) - \frac{\partial F_i\left(U_1 ..., U_j, ..., U_n\right)}{\partial U_j} \Delta U_j + \varepsilon^2 \tag{4.56}$$

If the terms of second order or higher are neglected in equation (4.55) and (4.56) then the difference between these two equations gives the Jacobian matrix element H_{ij}. Hence:

$$H_{ij} = \frac{\partial F_i(U_1,...,U_j,...,U_n)}{\partial U_j} = \frac{F_i(U_1,...,U_j+\Delta U_j,...,U_n) - F_i(U_1,...,U_j-\Delta U_j,...,U_n)}{2\Delta U_j} \tag{4.57}$$

Equation (4.57) correspond to the central finite difference formula for differentiation. This is the formula used here to obtain the Jacobian matrix.

This chapter has presented the two dimensional equations of motion for the dynamic analysis of marine cables. The solution for these equations are obtained using a finite element approach based on the Galerkin weighted residual formulation. The time integration is performed by the Newmark scheme and the system of algebraic equations is solved by the Newton-Raphson method.

5 - Two Dimensional Results

5.1 - Introduction

This chapter is concerned with the application of the two dimensional finite element model developed in the last chapter to a number of marine cable analyses. The objectives of these analyses are, on the one hand, to validate the model and, on the other hand, to carry out a parametric study of the cable's dynamic response. In order to achieve these objectives the analyses are divided into two main groups. The first group deals with towed marine cables where the cable length is such that it does not touch the seabed. In this case, the suspended length is constant and the bottom boundary conditions are well defined. The simulations for the first group of analyses are used to validate the two dimensional finite element model by comparing its results with full scale measurements obtained by Hopland (1993). In addition, the same simulations are used to assess the influence of curvature on the cable's transient response by comparing the results with those obtained by a similar finite element formulation which uses linear shape functions. The second group of analyses is concerned with the dynamic response of marine cables during installation. In this case, the cable touches the seabed and, as a result, the cable's suspended length changes with time. Simulations for this case are carried out in order to assess the influence of several parameters such as the cable pay out rate, water depth and the wave induced motions of the cable lay vessel, amongst others.

The cases simulated throughout this chapter use two different types of cable. These cables consist of a heavy armoured cable (HA) and a light armoured cable (LA), whose properties are shown in table 5.1. These data are presented by Hopland (1993). Hopland (1993) performed full scale towing tests in order to obtain the hydrodynamic constants for both cables. These tests were carried out in a location near the Norwegian coast where the influence of waves and

currents is relatively small (Hopland and Klykken, 1992). The cables' hydrodynamic constants were obtained by towing lengths of cable at constant vessel speed. In addition, the transient response of the towed cables was investigated for both the speeding up and the slowing down of the cable lay vessel. The bending stiffness and the tangential drag coefficients are estimates since they were not given by Hopland. The values for the bending stiffnesses are slightly higher than representative values for the full slip bending stiffness of comparable marine cables. However, they are realistic under conditions of partial slip between the cables' component layers as a result of tension. This is not a critical issue as the bending stiffness has very little influence on the cables' global configuration. The value for the tangential drag coefficient is typical of that associated with marine cables.

Marine Cable	HA	LA
Diameter (mm)	33.2	26.4
Physical mass (kg/m)	2.70	1.64
Hydrodynamic constant (rad*m/s)	0.7974	0.6173
Bending stiffness ($N*m^2$)	1000	500
Weight in water (N/m)	17.80	10.96
Normal drag coefficient	1.64	2.12
Tangential drag coefficient	0.01	0.01

Table 5.1 - Properties of LA and HA marine cables

This chapter is divided into two parts. Firstly, constant length towed cable simulations are carried out. These simulations are then used to compare with full scale measurements and to assess the influence of curvature on the cable's transient response. Secondly, cable laying analyses are used to study the influence of pay out rate, water depth and wave induced motions of the lay vessel. In addition, the installation of a hydrophone is simulated.

5.2 - Towed Cable Simulations

This section deals with simulations of the transient response of a towed marine cable as a result of changes in the vessel's forward speed. The results are then compared with those obtained from full scale sea trials performed by Hopland (1993). Hopland presents transient trials for cases where the vessel speeds up and for cases where the vessel slows down for both cables. The heavy armoured cable used in the simulation is 300 metres long while the light armoured cable is 360 metres long. The changes in the vessel forward speed are shown in table 5.2. It should be noted that Hopland only measured the initial and final vessel velocities and the duration of the speed change. Unfortunately, the exact vessel speed change profile was not recorded. It is assumed here that this profile is linear. These trials are simulated by the two dimensional finite element model. The cable is divided into 20 elements and the integration time step is one second.

Cable and Case	Initial Speed (m/s)	Final Speed (m/s)	Time for Change in Speed (s)
HA-Speeding up	0.565	1.235	45
HA-Slowing down	1.286	0.514	45
LASpeeding up	0.462	1.286	45
LA-Slowing down	1.235	0.462	45

Table 5.2 - Vessel changes in speed for towed cable analyses

Next, the results obtained by the two dimensional finite element model are compared with the results obtained with a similar finite element formulation which uses linear elements rather than cubic ones. The linear elements have no

curvature and form the basis of many existing cable models reported in the literature (Kitazawa, 1986, Leonard and Karnoski, 1990).

5. 2 1 - Comparison with Full Scale Measurements

In order to validate the model for cable dynamics presented in this thesis, the results of full scale sea trials for towed marine cables presented by Hopland (1992) are used. During the sea trials, Hopland studied the transient response of both heavy armoured and light armoured cables to changes in the vessel's forward speed. It is assumed that there are no effects of marine currents on the cable global configuration. Measurements of the position of the cable were taken for four locations along the cable. The measurements were obtained by transponders attached to the cable whose weight in water and drag did not significantly affected the cable's global configuration. The comparison of these results with those obtained for the two dimensional finite element model are shown in figures 5.1 to 5.4. The configurations shown in these figures are labelled with the letter t followed by a number n. This indicates the configuration for the time corresponding to the number n in minutes, unless stated otherwise. This notation is adopted throughout this chapter.

Figure 5.1 shows the comparison of the transient response for the HA cable when the vessel forward speed increases from 0.565 m/s to 1.235 m/s in 45 seconds while figure 5.2 shows the similar comparison for the case where the vessel slows down from 1.286 m/s to 0.514 m/s also in 45 seconds. Figures 5.3 and 5.4 show the same comparisons for the LA cable. However, in the speeding up analysis the vessel accelerates from 0.462 m/s to 1.286 m/s while in the slowing down analysis the vessel forward speed decreases from 1.235 m/s to 0.462 m/s. Here, the time interval in which the vessel changes its forward speed is also 45 seconds.

Throughout this section, it is assumed that the vessel forward speed varies linearly with time during the change. Although during the sea trials the way in which the acceleration is applied is not recorded, the assumption that the acceleration is constant is reasonable. This is because the magnitude of the acceleration is very small. It also should be pointed out that the measured data plotted in figures 5.1 to 5.4 have been scanned from the graphs presented in Hopland's paper and therefore are subject to some inaccuracy associated with the resolution.

From figures 5.1 and 5.2, it can be seen that the two dimensional finite element (FE) model simulates very well the transient response when the vessel forward speed increases. In the case of the vessel slowing down there is also good agreement between results of the finite element model and the measured data as shown in figures 5.3 and 5.4. However, for the light cable the intermediate configurations show some differences which are relatively small. In spite of that, it can also be seen that the model predicts with very good accuracy the duration of the transient even for the light cable slowing down analysis. The elapsed times for the transients are shown in table 5.3. The times in the fourth column of the table are obtained using Zajac's formula based on the sinking velocity of the cable which is given by:

$$t_{\Delta v} = \frac{h}{H} \tag{5.1}$$

where $t_{\Delta v}$ is the time for the transient, h is the water depth and H is the cable hydrodynamic constant. Since the depth of the bottom end extremity of the cable varies with time, Hopland approximates the water depth with the cable length. This assumption is conservative because the average water depth is significantly lower than the cable length.

These results combined with the theoretical check in consistency presented in chapter three show that the formulation presented in this work is able to simulate the transient response of marine cables to changes in the lay vessel's forward speed with very good accuracy.

Cable/ Case	Measured Time (s)	FE Model Time (s)	$t_{\Delta v}$ (s)	FE Rigid Time (s)
HA-Speeding up	360	360	-	320
HA-Slowing down	480	495	360	380
LASpeeding up	420	420	-	390
LA-Slowing down	540	555	515	520

Table 5.3 - Transient times for vessel changes in speed for the towed cable with constant length

5.2.2 - Comparison with a Rigid Element Model

During the development of the two dimensional finite element model presented in chapter four, the same formulation was applied to a finite element model in which the shape functions were linear. Linear elements are widely used for modelling the dynamics of marine cables. The main problem with linear element models is that they cannot simulate the effects of the curvature. As a result, the two dimensional equation of motion in the normal direction (4.18) becomes independent of the tension. Furthermore, the linear model which uses linear shape functions for displacements is unable to model continuity in slope. Consequently, the model can be regarded as an assembly of rigid elements connected at the nodes by rings. The dynamic equation of motion in the normal direction depends on the self-weight and the buoyancy terms, the normal drag term and the inertia term.

Figures 5.5 to 5.8 show the results for the marine cable configuration obtained with the cubic and the linear finite element models with 20 elements. The time integration step is 0.15 seconds for the rigid element model and one second for the cubic element model. It can be seen from these figures that the influence of the curvature on the cable configuration is quite significant. It also can be seen from table 5.3 that the linear element formation underestimates the elapsed time for the transient. The calculated transient times for the linear or rigid element are more or less in line with those calculated from the sink velocity formula. This can be attributed to the fact that rigid elements do not take into account the cable's geometric stiffness.

The heavy cable slope for both linear and cubic finite element analyses is plotted against time in figures 5.9 and 5.10 for speeding up and slowing down analyses, respectively. For plots of slope against time the curves are labelled with the letter n for node followed by a number j that identifies the number of the node corresponding to that curve. The slope is defined as the angle that the cable makes to the horizontal. These figures show again that the linear finite element formulation underestimates the time in which the transient takes place. Furthermore, they show that for speeding up analyses, the slope first goes up and then starts descending to its final equilibrium position. In contrast, for slowing down analyses, the slope goes down in the first instance and then starts to ascend to its final equilibrium position. This behaviour does not occur with the cubic finite element formulation. Therefore, it may be concluded that this is consequence of the geometric constraint at the connections between elements introduced by the linear element formulation. That is, if one linear element is rotated in one direction then a joining element tends to rotate in the other direction.

These results demonstrated that linear finite element models may be only used as a first approximation and they are not reliable for rigorous analyses. This is particularly true for cases where the dynamic excitation is strong.

5.3 - Cable Laying Simulations

This section addresses the dynamic response of marine cables during installation where the cable touches the seabed and the suspended length of the cable needs to be determined. Following the assumption made during the development of the model in chapter four, the bottom tension is zero during cable laying. Therefore, the analyses considered within this section differ from the towed marine cable analyses studied in last section because of the changes in the cable's suspended length with time. This means that the suspended length of the cable needs to be regarded as an extra unknown in the problem. Consequently, an extra equation must be sought to make the solution of the problem possible. This extra equation is given by the continuity relation which states that the cable suspended length at time $t+\Delta t$ is the cable suspended length at time t plus the amount of cable paid out l_{po} minus the amount of cable deployed on the seabed l_{dp} for the time interval in question. Hence:

$$l(t+\Delta t) = l(t) + l_{po} - l_{dp} \tag{5.2}$$

The amount of cable paid out is obtained through the integration of the pay out rate. The pay out rate is assumed to be a known function of time. Thus:

$$l_{po} = \int_{t}^{t+\Delta t} V_{po}(t)dt \tag{5.3}$$

The amount of cable deployed on the seabed is the displacement of the touchdown point relative to its previous position. Such a displacement can be calculated by the following expression:

$$l_{dp} = \sum_{1}^{n} \left[\int_{0}^{1} \sqrt{1 - \left(\frac{\partial y}{\partial s} \right)^2} \, l_k \, d\xi \right] \tag{5.4}$$

where n is the number of finite elements, l_k is the element length and ξ is the normalised arc length. These equations are used as constraints in the two dimensional finite element model derived in chapter four.

The remainder of this chapter presents a parametric study of marine cables for laying situations. Firstly, the cable transient response to changes in the vessel forward speed is considered. Then the influence of wave induced vessel motions is investigated. Finally, the simulation of an installation of hydrophone attached to the cable is performed.

5.3.1 - Parametric Study of the Transient Response of Marine Cables During Deployment due to Vessel Speed Changes

The parametric study presented in this section consists of the simulation of a cable's transient response to changes in the vessel's forward speed. The parameters studied are the vessel acceleration, the cable's weight in water, the cable pay out rate and the water depth. All simulations use a mesh with 30 elements and a integration time step of one second.

Two cases are considered in order to investigate the influence of the acceleration on the cable's transient response. The first simulation considers the case where the vessel speeds up from 0.5 m/s to 1.5 m/s in 30 seconds. The second simulation is concerned with the case where the vessel slows down

from 1.5 m/s to 0.5 m/s, also in 30 seconds. Regarding the study of the influence of the cable's weight in water the two cables whose properties are presented in table 5.1 are considered. The influence of the pay out rate is assessed by comparing the cases where the pay out rate is the same as the vessel's forward speed with the cases where there is no pay out of cable. The latter case means that the cable is effectively being dragged along the seabed which is assumed to be frictionless. Because of this, the simulations for zero pay out rate are labelled as towed cable analyses. Finally, the influence of the water depth is investigated by simulating the cable's response in both shallow and deep water. Shallow water is assumed to be 200 metres deep and deep water is taken as 1000 metres deep.

The results plotted for each simulation are the configuration, the slope against time and the top tension against time. In addition, the variation of the suspended length with time is plotted for the HA cable for the shallow water simulations. The results for all these combinations of parameters under investigation are shown in figures 5.11 to 5.60. In these figures, the simulations are labelled with four characters. The first character is either "L" for light or "H" for heavy armoured cable. The second character is either "A" for an accelerating or "D" for a decelerating analysis. The third character is either "S" for shallow or "D" for deep water. The final character is either "L" for cable laying or "T" for towed cable analysis.

The cable configuration is mostly affected by the vessel acceleration. The cable assumes the convex configuration when the vessel speeds up as seen in figures 5.11, 5.19, 5.25, 5.31, 5.37, 5.43, 5.49 and 5.55 in which the configurations are one minute apart. In contrast, the cable assumes the concave configuration when the vessel slows down. This can be seen in figures 5.15, 5.22, 5.28, 5.34, 5.40, 5.46, 5.52 and 5.58. In addition, it should be noted that the curvature wave is shorter and it has larger amplitude for a speeding up vessel whilst the

curvature wave is longer with smaller amplitude for the case where the vessel slows down.

By comparing the laying configurations with the corresponding towed configurations one may conclude that the pay out rate does not affect the cable configuration significantly. This is because the top tension has little influence on the configuration.

The slope variation with time for the nodes 1, 8, 16, 23 and 31. Not surprisingly, the slope is also mainly affected by the vessel acceleration. As shown in figures 5.12, 5.20, 5.26, 5.32, 5.38, 5.44, 5.50 and 5.56, when the vessel speeds up, the slope decreases, and the transient for the slope is shorter and sharper. It can also be seen that the transient times increase for the nodes placed further along the cable. When the vessel slows down, the slope increases, and the changes in slope are less abrupt and larger. Nevertheless, transient times also increase for nodes further along the cable. This is shown in figures 5.16, 5.23, 5.29, 5.35, 5.41, 5.47, 5.53 and 5.59.

Figures 5.13, 5.17, 5.21, 5.24, 5.30, 5.33, 5.36, 5.39, 5.42, 5.45, 5.48, 5.51, 5.54, 5.57 and 5.60 show the variation of the top tension with time. The figures show that the top tension is affected by the vessel acceleration, by the pay out rate, by the water depth and by the submerged weight. The top tension changes very quickly while the vessel acceleration is applied. In addition when the cable is towed, the tension is more affected by the tangential friction compared with cable laying. This is because the tangential relative velocity is higher since there is no pay out rate. The opposite occurs for cable laying situations. Another interesting fact arises from the assumption that the pay out rate is the same as the vessel forward speed. Under this assumption the top tension increases when the vessel slows down and decreases when the vessel speeds up. The top tension is higher for deeper water and it is also higher for the heavier cable.

The key points arising from figures 5.11 to 5.60 are discussed below. These figures readily demonstrate the influence of curvature on the cable laying configuration. The configuration figures show the propagation of the curvature wave along the cable with time. The figures showing corresponding slope changes with time indicate a more gradual slope change for the positions further along the cable. The top tension variations are constrained to the period of application of vessel acceleration with a more gradual variation thereafter. This indicates that the dynamic tension is an acceleration driven process. This is reasonable since the tangential drag is low. This is particularly true for cable laying because the tangential drag is even smaller owing to the low relative tangential velocity. An interesting difference between the top tension variation with time between towed and laid cables is that for laid cables the tension falls during the positive acceleration period whereas the opposite holds for towed cables during the same period. This is a result of assuming that the pay out rate follows the instantaneous vessel velocity. For cable laying the non-linear variation of the suspended length with time is clearly evident in the figures thus indicating that the a linear approximation for the suspended length is inadequate.

Figure 5.61 shows a three dimensional plot comparing the curvature for the heavy armoured cable for speeding up laying analysis in shallow water (HASL) with the curvature of the same cable for slowing down laying analysis in shallow water (HDSL). This figure show that the curvature wave is more significant for accelerating conditions compared with decelerating conditions.

The duration of the transient for each simulation is presented in table 5.4. This table shows that the transients responses are considerable longer than the duration of the vessel speed change. In addition, the transient response times increase with water depth. For the deep water accelerating simulations the

vessels will have advanced approximately 3.6 km before the response transient has elapsed.

Simulation	Time (min)	Simulation	Time (min)
HASL	9.75	LASL	11.50
HDSL	13.25	LDSL	14.75
HAST	10.00	LAST	11.50
HDST	13.25	LDST	14.50
HADL	38.00	LADL	43.00
HDDL	43.00	LDDL	51.0
HADT	38.00	LADT	43.00
HDDT	43.00	LDDT	51.00

Table 5.4 - Transient times for vessel changes in speed simulations

Influence of the Vessel Acceleration

This discussion of the influence of the vessel acceleration assumes that the vessel is either speeding up or slowing down in still water. It is also assumed that the pay out rate of the cable is the same as the vessel forward speed. Under these circumstances, if the vessel is speeding up, the curvature of the cable configuration is concave or positive and the cable suspended length increases with time. If the vessel is slowing down, the curvature of the cable configuration is convex or negative. In this case, the cable suspended length decreases with time. The curvature magnitude is larger for cases where the vessel forward speed increases. However, the transient takes longer for cases where the vessel forward speed decreases. The effect of the acceleration on the tension occurs only during the application of the acceleration. In this case, there is a pulse change in the tension. For cable laying analysis, if the vessel speeds

up, the component of the tension due to the acceleration is compressive while this component is tensile for the case where the vessel slows down.

Influence of the Cable Weight in Water

The cable weight in water affects the cable's transient response in two different ways. Firstly, the top tension is higher for heavy cables than it is for light cables. Therefore, the heavy cable has higher geometric stiffness. Secondly, the duration of the transient is shorter for the heavy cable. This is because the heavy cable has a higher hydrodynamic constant and, therefore, it experiences smaller slope changes during the transient compared with the light cable for the same change in speed.

Influence of the Pay Out Rate

In order to assess the influence of the pay out rate two cases are considered. Firstly, the case of cable laying analysis where the pay out rate is the same as the vessel forward speed is investigated. Secondly, the case of cable laying analysis with no pay out rate is considered. It is noticed that the mechanism of the application of the tension changes completely for these two cases. For the zero pay out rate the tension rises as the vessel has positive forward acceleration and it goes down when the vessel's forward acceleration is negative. This is the opposite of what occurs for cable laying situations. However, for the cases simulated in this section, the influence of the pay out rate does not affect significantly the global configuration of the cable or the duration of the transient.

Influence of the Water Depth

The water depth affects mainly the tension and the duration of the transient. The top tension increases with the water depth. In addition, the duration of the transient is larger for deeper water. This is due to the fact that the cable needs to travel a larger distance to reach the seabed.

5.3.2 - Analysis of Vessel Wave Induced Motion

This section considers the dynamic response of a marine cable being laid from a vessel which experiences motions induced by regular waves. The wave and vessel response amplitude operator (RAO) data used to define the displacements, velocities and accelerations of the point where the cable leaves the lay vessel are given in table 5.5. The simulations performed here use again a 30 element mesh with the time integration step equal to half a second.

Encounter Period (s)	10.0	Surge Phase (deg)	-45.9
Wave Height (m)	3.0	Heave RAO	1.619
Surge RAO	0.708	Heave Phase (deg)	0.0

Table 5.5 - Wave and vessel data for head seas simulations

The results of cable dynamic analyses for both the heavy and the light cable are shown in figures from 5.62 to 5.73 where the letter "W" in the labels refer to vessel wave induced motions analysis. Figures 5.62 and 5.69 show the configuration envelope while figures 5.63 and 5.70 show three dimensional plots of the co-ordinate against time for the first few nodes of the two cables in question. Figures 5.64 and 5.71 show the plot of the slope against time for the first two nodes. The top tension is plotted against time in figures 5.65 and 5.72 and it is plotted against the water depth in figures 5.66 and 5.73 for the heavy and light armoured cable respectively. The water depth used in these

simulations was 300 metres and the vessel mean forward speed was 1.5 m/s which was the same as the pay out rate.

It may be concluded from these results that the tension rises quite sharply for vessel motions even for zero bottom tension conditions. In spite of that, the change in configuration is constrained to the first few elements. This can be seen in the plots of the slope against time. The magnitude of the slope of the second node is very small if compared with the magnitude of the slope of the first node. It can be also seen that the tension variation with the water depth is very close to a straight line.

The presence of higher harmonics can be clearly seen in the tension time histories due to the non-linearity of the problem. In order to assess the variation of the top tension with the period, two more simulations with periods of 8 seconds and 15 seconds were carried out for the heavy cable. Figures 5.67 and 5.68 show that tension variations are higher for shorter wave periods. These tension variations are consistent with full scaled data recorded by Curtis (1992). Note that for waves with small periods and relatively shallow water the analysis indicates that the top tension can go negative one part of the cycle. This large tension variation for shorter period waves in shallow water has significant implications will regard to the stability of the cable.

5.4 - Hydrophone Installation

Launching of hydrophones and repeaters is a common cable laying operation. Often it is necessary to slow down for a short duration in order to pass the bight of cable with the attached hydrophone or repeater through the laying equipment. A widely used approach is to rapidly slow down the lay vessel, launch the hydrophone and rapidly accelerated the vessel back to its laying speed. The cable pay out rate follows the vessel forward speed during this

operation. The question is how does this operation affect the cable configuration. A hydrophone launch is considered here where it is assumed that the properties of the hydrophone are equal to the cable's properties.

In order to simulate the installation of a hydrophone, the following manoeuvre is considered. The vessel initially travels at the constant forward speed of 3 m/s. Then, the vessel retards to 0.25 m/s and stays there for another 30 seconds to launch the hydrophone. Next, the vessel speeds up again to 3 m/s in 30 seconds and travels at 3 m/s thereafter. This is a typical operation for hydrophone and repeater installation. The hydrophone is considered here because it can be assumed to be an extension of the cable.

Figures 5.74 to 5.82 show the configuration, slope against time and top tension against time for the heavy and light armoured cables. It can be seen that cable motions relative to the vessel are relatively small. It also can be seen that variations in slope are limited to a small number of elements from the top. This means that the cable curvature is not very large. This is illustrated in figures 5.79 and 5.82 which show a three dimensional plot of the curvature as a function of time and arc length. Figure 5.83 shows the variation of the cable's suspended length during the manoeuvre.

5.5 - Concluding Remarks

The two dimensional finite element model developed in chapter four has been successfully applied to a large number of marine cable analyses. The model's performance is consistent throughout the simulations. It also demonstrated that the model accurately replicates measurements presented by Hopland (1993) for towed cables. In addition, the model has shown that linear element models are not very good at modelling cases where the curvature is important. The two

dimensional analyses presented in this chapter has allowed a very good insight of the physical phenomena involved in complex marine cable laying situations.

6 - Solution of the Three Dimensional Equations of Motion for Marine Cables

6.1 - Introduction

This chapter is concerned with the solution of the three dimensional differential equations of motion derived in chapter three. This solution presented here differs from the two dimensional one presented in chapter four as it uses Euler angles to transform the local co-ordinates to the global co-ordinates and vice-versa.

As it was seen earlier, two problems arise from the use of the moving frame of a space curve as the local frame of reference for the dynamic analysis of marine cables. The first problem concerns the definition of the unit vector in the principal normal direction. This vector is defined as being the quotient between the first derivative of the unit tangent vector with respect to the arc length and the curvature. Therefore, the unit vector in the principal normal direction is not defined whenever the curvature is zero. The second problem arises from the fact that the integration of the differential equations of motion require establishing the concavity of the curve which defines the cable configuration. This is because the unit principal normal vector and the unit binormal vector rotate through 180 degrees when the curve changes concavity.

In the two dimensional solution presented in chapter four, the first problem is overcome by the redefinition of curvature as a scalar that can assume negative as well as positive values. In addition, it is possible to eliminate the square root in the expression for the curvature by combining this expression and the equation of geometric compatibility. In this case, the sign for the curvature is obtained automatically during the analysis. The second problem is overcome by adopting a fourth frame of reference defined by the triad $(\mathbf{e}_t, \mathbf{e}_n, \mathbf{e}_b)$ whose

unit vectors do not change with the concavity of the cable configuration. These vectors can be regarded as the tangent, principal normal and binormal vectors affected by the sign of the curvature. Therefore, the unit vector $\mathbf{e}_t$ is the same as the unit tangent vector $\mathbf{t}$ while the unit vectors $\mathbf{e}_n$ and $\mathbf{e}_b$ are the same as the unit vectors $\mathbf{n}$ and $\mathbf{b}$ if the curvature is positive and are their opposite vectors if the curvature is negative. This allows the modelling of not only points of inflection but also the modelling of straight line segments of the cable configuration.

For three dimensional analysis, the second problem can be overcome in the same manner as it was overcome in the two dimensional analysis. However, the first problem can not be overcome through the redefinition of curvature for a displacement formulation. This is because it is very difficult to eliminate the square root in the expression for the curvature. This elimination requires further research. Nevertheless, the curvature can be redefined as an scalar which can assume either positive or negative values if an angular displacement formulation is adopted.

In this angular displacement formulation, three Euler angles are used instead of the three co-ordinates. These angles can then be related to the components of the velocity vector through the equation of geometric compatibility. They can also be related to curvature and geometric torsion of the cable configuration through the Frenet-Serret formulae. As result, the differential equations of motion are rewritten as system of nine differential equations with nine unknowns. These unknowns are the three Euler angles, the three components of the velocity vector, curvature, geometric torsion and tension. This system of differential equations is of fourth order in space and first order in time.

Here, the solution of this system of differential equations is obtained through a finite difference procedure for the time domain. The equations of geometric

compatibility are integrated in space by a Runge-Kutta fourth order algorithm. The tension is determined by solving the integral of the tangential equation of motion. Next, a finite element formulation based on the Galerkin weighted residual method for the space integration of the kinetic equations of motion in the normal and binormal directions. This results in a non-linear system of algebraic equations whose solution is obtained through the Newton-Raphson method.

The first part of this chapter is concerned with establishing the differential equations as functions of the Euler angles. The second part is concerned with the solution of these differential equations of motion. The model for the solution of the three dimensional equations of motion is demonstrated by a simulation of the response of a marine cable subject to out of plane sheared currents.

6.2 - Equations of Motion for the Angular Displacements Formulation

In this section, the differential equations of motion derived in chapter three are functions of the co-ordinates x, y and z and their derivatives are re-expressed as functions of three Euler angles and three velocities. The derivations for the Euler angles are detailed in appendix B in order to keep the formulation presented here more concise. The Euler angles used here are denoted by θ_1, θ_2 and θ_3. They are defined such that θ_1 is the rotation about unit vector $\mathbf{i}$ in order to bring the unit vector $\mathbf{j}$ to the plane formed by $\mathbf{e}_n$ and $\mathbf{e}_b$, θ_2 is the rotation about the new unit vector $\mathbf{j}$ in order to bring the unit vector $\mathbf{k}$ coincident with $\mathbf{e}_b$ and θ_3 is the rotation about the new unit vector $\mathbf{k}$ in order to bring both frames together.

The solution obtained here assumes that the cable is inextensible and that the second order effect of the shear force on the tension is negligible. These assumptions can be justified by the same reasons as those given in chapter four. Under these circumstances, the differential equations of motion for an element of marine cable given by equations (3.61) to (3.63) can be written as:

$$\frac{\partial T}{\partial s} + w(\mathbf{j}\cdot\mathbf{t}) - \frac{1}{2}\pi\rho d C_T V_n |V_n| - m a_t = 0 \tag{6.1}$$

$$\kappa T - EI\frac{\partial^2 \kappa}{\partial s^2} + w(\mathbf{j}\cdot\mathbf{n}) - \frac{1}{2}\rho d C_N V_m V_{RN} - (m+\rho A)a_n = 0 \tag{6.2}$$

$$EI\tau\kappa + w(\mathbf{j}\cdot\mathbf{b}) - \frac{1}{2}\rho d C_N V_{rb} V_{RN} - (m+\rho A)a_b = 0 \tag{6.3}$$

where the normal added mass coefficient is assumed to be one and the added mass force in the tangent direction is neglected, V_n, V_m and V_{rb} are the components of the relative velocity vector in the tangential, normal and binormal directions, respectively. The velocity magnitude V_{RN} is given by:

$$V_{RN} = \sqrt{V_m^2 + V_{rb}^2} \tag{6.4}$$

Equation (6.1) is the equation of motion in the tangential direction, equation (6.2) is the equation of motion in the principal normal direction and equation (6.3) is the equation of motion in the binormal direction.

The kinematic relations are obtained by stating the equation of geometric compatibility in the following form:

$$\frac{\partial^2 \mathbf{r}_c}{\partial s \partial t} = \frac{\partial}{\partial s}\left(\frac{\partial \mathbf{r}_c}{\partial t}\right) = \frac{\partial}{\partial t}\left(\frac{\partial \mathbf{r}_c}{\partial s}\right) = \frac{\partial \mathbf{V}_c}{\partial s} = \frac{\partial \mathbf{e}_t}{\partial t} \tag{6.5}$$

where $\mathbf{r}_c$ and $\mathbf{V}_c$ are, respectively, the position and velocity vectors of an element of cable and $\mathbf{e}_t$ is the unit tangent vector of the fourth reference frame.

The derivative of the velocity vector $\mathbf{V}_c$ with respect to the arc length s is given by:

$$\frac{\partial \mathbf{V}_c}{\partial s} = \frac{\partial V_{ct}}{\partial s}\mathbf{e}_t + V_{ct}\frac{\partial \mathbf{e}_t}{\partial s} + \frac{\partial V_{cn}}{\partial s}\mathbf{e}_n + V_{cn}\frac{\partial \mathbf{e}_n}{\partial s} + \frac{\partial V_{cb}}{\partial s}\mathbf{e}_b + V_{cb}\frac{\partial \mathbf{e}_b}{\partial s} \tag{6.6}$$

Combining the above expression with the Frenet-Serret formulae gives:

$$\frac{\partial \mathbf{V}_c}{\partial s} = \left(\frac{\partial V_{ct}}{\partial s} - \kappa V_{cn}\right)\mathbf{e}_t + \left(\frac{\partial V_{cn}}{\partial s} + \kappa V_{ct} - \tau V_{cb}\right)\mathbf{e}_n + \left(\frac{\partial V_{cb}}{\partial s} + \tau V_{cn}\right)\mathbf{e}_b \tag{6.7}$$

An equivalent expression can be obtained by using Euler angles. This is demonstrated in appendix C.

The time derivative of the unit vectors $(\mathbf{e}_t, \mathbf{e}_n, \mathbf{e}_b)$ can be expressed as functions of the unit vectors $(\mathbf{e}_t, \mathbf{e}_n, \mathbf{e}_b)$ themselves, as shown in appendix D. It follows that the time derivative of the unit tangent vector $\mathbf{e}_t$ may be written as:

$$\frac{\partial \mathbf{e}_t}{\partial t} = \left(\sin\theta_2\frac{\partial \theta_1}{\partial t} + \frac{\partial \theta_3}{\partial t} - \sin\theta_1\cos\theta_2\frac{\partial \beta}{\partial t}\right)\mathbf{e}_n + \left[\cos\theta_2\sin\theta_3\frac{\partial \theta_1}{\partial t} - \cos\theta_3\frac{\partial \theta_2}{\partial t} + \left(\sin\theta_1\sin\theta_2\sin\theta_3 - \cos\theta_1\cos\theta_3\right)\frac{\partial \beta}{\partial t}\right]\mathbf{e}_b \tag{6.8}$$

Combining vector equations (6.7) and (6.8) gives the following scalar equations of geometric compatibility:

$$\frac{\partial V_{ct}}{\partial s} - \kappa V_{cn} = 0 \tag{6.9}$$

$$\frac{\partial V_{cn}}{\partial s} + \kappa V_{ct} - \tau V_{cb} - \sin\theta_2\frac{\partial \theta_1}{\partial t} - \frac{\partial \theta_3}{\partial t} + \sin\theta_1\cos\theta_2\frac{\partial \beta}{\partial t} = 0 \tag{6.10}$$

$$\frac{\partial V_{cb}}{\partial s} + \tau V_{cn} - \cos\theta_2 \sin\theta_3 \frac{\partial \theta_1}{\partial t} + \cos\theta_3 \frac{\partial \theta_2}{\partial t} - (\sin\theta_1 \sin\theta_2 \sin\theta_3 - \cos\theta_1 \cos\theta_3)\frac{\partial \beta}{\partial t} = 0 \tag{6.11}$$

The equations of dynamic equilibrium (6.1), (6.2), and (6.3) together with the equations of kinematic compatibility (6.9), (6.10) and (6.11) form a system of six differential equations with nine unknowns. These unknowns are the three components of the element velocity vector, V_{ct} , V_{cn} and V_{cb}, the three Euler angles, θ_1, θ_2 and θ_3, the tension T, the curvature κ and the geometric torsion τ. Therefore, in order to solve such a system of differential equations three more equations are need to be established. These equations may be obtained by expressing the derivatives of the unit vectors ($\mathbf{e}_t, \mathbf{e}_n, \mathbf{e}_b$) with respect to the arc length s as functions of the Euler angles θ_1, θ_2 and θ_3, and the vectors ($\mathbf{e}_t, \mathbf{e}_n, \mathbf{e}_b$) themselves, as shown in appendix C. Then these expressions are compared with the Frenet-Serret formulae derived in appendix A. As a result, it may be written that:

$$\kappa = \sin\theta_2 \frac{\partial \theta_1}{\partial s} + \frac{\partial \theta_3}{\partial s} \tag{6.12}$$

$$\tau = \cos\theta_2 \cos\theta_3 \frac{\partial \theta_1}{\partial s} + \sin\theta_3 \frac{\partial \theta_2}{\partial s} \tag{6.13}$$

and

$$\cos\theta_2 \sin\theta_3 \frac{\partial \theta_1}{\partial s} - \cos\theta_3 \frac{\partial \theta_2}{\partial s} = 0 \tag{6.14}$$

6.2.1 - Relative Velocity Vector

The relative velocity vector is the difference between the absolute velocity vector for an element of marine cable and the fluid velocity. In the case of marine cable analysis, the pay out rate must be added to the tangent

component of the velocity vector. As a result, the relative velocity vector may be expressed as:

$$\mathbf{V}_r = \left(V_{ct} + V_{po} - U_{ft}\right)\mathbf{e}_t + \left(V_{cn} - U_{fn}\right)\mathbf{e}_n + \left(V_{cb} - U_{fb}\right)\mathbf{e}_b \tag{6.15}$$

where V_{po} is the pay out rate and U_{ft}, U_{fn} and U_{fb} are the tangent, the principal normal and the binormal components of the fluid velocity respectively.

Since the effects of wave kinematics are neglected, the fluid velocity comes entirely from currents. The current velocity is usually given in the inertial frame of reference. In addition, the fluid velocity vector due to currents is horizontal and, therefore, the component of the fluid velocity vector in the **J** direction is zero. As a result, the components of the fluid velocity in the tangent direction may be expressed as:

$$U_{ft} = U_{fX}\cos\theta_2\cos\theta_3 + U_{fZ}\sin\theta_2 \tag{6.16}$$

while its component in the principal normal direction is given by:

$$U_{fn} = U_{fX}\left(\cos\theta_1\sin\theta_3 + \sin\theta_1\sin\theta_2\cos\theta_3\right) - U_{fZ}\sin\theta_1\cos\theta_2 \tag{6.17}$$

The component of the fluid velocity in the binormal direction is:

$$U_{fb} = U_{fX}\sin\theta_2 + U_{fZ}\cos\theta_1\cos\theta_2 \tag{6.18}$$

In the above equations U_{fX} is the component of the fluid velocity in the **I** direction and U_{fZ} is its component in the **K** direction of the inertial frame of reference.

6.2.2 - Acceleration Vector

The acceleration vector is needed in order to determine the D'Alambert and added mass forces. The D'Alambert force uses the absolute acceleration while the added mass force requires the use of the relative acceleration vector. However, throughout this work, it is assumed that the fluid acceleration is zero. Therefore, the added mass force is also calculated by using the absolute acceleration. The acceleration vector is determined by performing the time derivative of the absolute velocity vector. That is:

$$\mathbf{a} = \frac{\partial \mathbf{V_c}}{\partial t} = \left(\frac{\partial V_{ct}}{\partial t} + \frac{\partial V_{po}}{\partial t} \right) \mathbf{e_t} + \left(V_{ct} + V_{po} \right) \frac{\partial \mathbf{e_t}}{\partial t} + \frac{\partial V_{cn}}{\partial t} \mathbf{e_n} + V_{cn} \frac{\partial \mathbf{e_n}}{\partial t} + \frac{\partial V_{cb}}{\partial t} \mathbf{e_b} + V_{cb} \frac{\partial \mathbf{e_b}}{\partial t} \tag{6.19}$$

The time derivatives of the unit vectors ($\mathbf{e_t}, \mathbf{e_n}, \mathbf{e_b}$) are given in appendix D. Substituting these expressions into equation (6.19) gives:

$$\mathbf{a} = \left(\frac{\partial V_{ct}}{\partial t} + \frac{\partial V_{po}}{\partial t} - V_{cn} D_{T_{12}} - V_{cb} D_{T_{13}} \right) \mathbf{e_t} + \left[\frac{\partial V_{cn}}{\partial t} + \left(V_{ct} + V_{po} \right) D_{T_{12}} - V_{cb} D_{T_{23}} \right] \mathbf{e_n} + \left[\frac{\partial V_{cb}}{\partial t} + \left(V_{ct} + V_{po} \right) D_{T_{13}} + V_{cb} D_{T_{23}} \right] \mathbf{e_b} \tag{6.20}$$

where $D_{T_{12}}$, $D_{T_{13}}$ and $D_{T_{23}}$ are defined in appendix D by equations (D.4), (D.5) and (D.6), respectively.

6.3 - Solution for the Three Dimensional Equations of Motion

In order to solve the differential equations of motion the curvature and the geometric tension are replaced in the equations of motion by the expressions (6.12) and (6.13) respectively. This eliminates two variables. The time integration is performed using a finite difference method. As a result, the

equations of motion may be written as functions of the variables at time t and time $t+\Delta t$. The variables corresponding to time t are determined by the initial conditions. The space integration of the equations of motion is performed according to the following steps. First, the values for the Euler angles θ_2 and θ_3 are estimated. Then the three equations of geometric compatibility, the kinetic equation of motion in the tangential direction and the constraint equation (6.14) can be directly integrated. Finally, the kinetic equations in the normal and binormal directions are minimised in order to determine the approximated solution for the angles θ_2 and θ_3. This minimisation is obtained by a finite element Galerkin formulation. These steps are detailed next.

6.3.1 - Time Integration of the Differential Equations of Motion

In order to calculate the time integrals the unknowns are stored in the vector $\mathbf{u}$. Then the vector $\mathbf{u}$ for the time $t+\Delta t$ is determined by a finite difference method. The expression for this vector is established by considering the following Taylor power series expansion:

$$\mathbf{u}(t+\Delta t)=\mathbf{u}(t)+\frac{\partial \mathbf{u}(t)}{\partial t}\Delta t+\frac{1}{2}\frac{\partial^2 \mathbf{u}(t)}{\partial t^2}\Delta t^2+... \tag{6.21}$$

If only the linear terms of the series are considered then:

$$\frac{\partial \mathbf{u}(t)}{\partial t}=\frac{\mathbf{u}(t+\Delta t)-\mathbf{u}(t)}{\Delta t}=\frac{\mathbf{u}-\mathbf{u}_0}{\Delta t} \tag{6.22}$$

where the vector $\mathbf{u}_0$ corresponds to the initial conditions.

This procedure corresponds to a finite difference scheme for the time integration of the non-linear system of differential equations. The stability and accuracy of the scheme is controlled by the integration time step and the instant

for which the vector $\mathbf{u}$ is written. A non-dimensional variable of time ζ which defines introduced this instant is now introduced:

$$\zeta = \frac{t - t_0}{\Delta t} \tag{6.23}$$

where t_0 is the initial time for the interval, t is the time in consideration and Δt is the time interval. Then the vector $\mathbf{u}$ at time t is given by:

$$\mathbf{u}(t) = \mathbf{u}(t_0)(1-\zeta) + \mathbf{u}(t+\Delta t)\zeta \tag{6.24}$$

The non-dimensional parameter ζ defines the type of algorithm. Typical values of ζ for the most used algorithms are shown in table 6.1.

ζ	Algorithm
0	Explicit
1/2	Crank-Nicholson
2/3	Galerkin
1	Standard Implicit

Table 6.1 - Typical finite difference algorithms

In the solution presented here, the standard implicit algorithm is adopted.

6.3.2 - Space Integration of the Differential Equations of Motion

The space integration of the equations of motion is performed through a finite element formulation for the Euler angles θ_2 and θ_3. The cable is divided into a number of finite elements where the nodal values for θ_2 and θ_3. are approximated along the element by linear shape functions. The nodal values for θ_2 and θ_3 are stored in vector $\mathbf{v}$ such that the first and third elements of $\mathbf{v}$

are the nodal values of θ_2 and the second and fourth elements of $\mathbf{v}$ are the nodal values of θ_3. The vector $\mathbf{v}$ is approximated over the element by the expression:

$$u_j = v_j(1-\xi) + v_{j+2}\xi = v_j\psi_1 + v_{j+2}\psi_2 \tag{6.25}$$

where u_1 and u_2 are the angles θ_2 and θ_3 for the position ξ and ξ is the normalised Lagrangean co-ordinate for the element domain. This co-ordinate is defined by:

$$\xi = \frac{s - s_k}{l_k} \tag{6.25}$$

where s_k is the arc length for node k and l_k is the element length.

Since the problem is non-linear, the solution starts with an estimate for the values of the angles θ_2 and θ_3. Then the value of the Euler angle θ_1 can be obtained by integrating equation (6.14) which gives:

$$\theta_1 = \ln\sqrt{\frac{1+\sin\theta_2}{1-\sin\theta_2}} + C_\theta \tag{6.26}$$

where C_θ is an integration constant which is determined through the application of boundary conditions. After this integration, the estimated values for the three Euler angles are known. As a result, the three equations of geometric compatibility form a system of first order differential equations with respect to the arc length s. This system can be readily integrated by a Runge-Kutta algorithm. Once the velocities are obtained, the equation of motion in the tangent direction can be integrated in order to determine the tension. At this stage the values of all variables are known. However, the above calculations started with the estimated values for the Euler angles θ_2 and θ_3. In order to

determine the values of these estimated variables that minimise the problem, the equations of motion in the normal and binormal directions (6.2) and (6.3) are minimised by the Galerkin weighted residual integral method. The Galerkin integrals are:

$$\int_{s_1}^{s_2}\left[\kappa T - EI\frac{\partial^2\kappa}{\partial s^2} + w(\mathbf{j}\cdot\mathbf{n}) - \frac{1}{2}\rho d C_N V_m V_{RN} - (m+\rho A)a_n\right]\psi_i ds = 0 \tag{6.26}$$

$$\int_{s_1}^{s_2}\left[EI\tau\kappa + w(\mathbf{j}\cdot\mathbf{b}) - \frac{1}{2}\rho d C_N V_{rb} V_{RN} - (m+\rho A)a_b\right]\psi_i ds = 0 \tag{6.27}$$

Then, the term involving the second derivative of the curvature with respect to arc length s is integrated by parts once. This allows the representation of curvature and bending stiffness with the linear shape functions for the angles.

This procedure is repeated for each finite element of marine cable. This leads to a local forces vector which is then added to global force vector. The global force vector corresponds to a system of algebraic equations which is solved by the Newton-Raphson method. This procedure is very similar to the one adopted to solve the two dimensional equations of motion presented in chapter four and therefore is not repeated here.

6.3.3 - Determination of the Cable Configuration

The solution of the non-linear differential equations of motion established in the previous section gives the nodal values for the three components of the velocity vector, for the three Euler angles and for the tension. However, in order to determine the cable configuration, it is necessary to determine the nodal co-ordinates x, y and z. The expressions for these co-ordinates are obtained by relating the transformation matrix given by the differential

geometry approach with the transformation matrix given by the Euler rotations approach. This relationship is established in appendix B. As a result, the co-ordinate x is calculated by the following integral:

$$x = x_k + \int_0^{\xi} l_k \cos\theta_2 \cos\theta_3 d\xi \tag{6.28}$$

while the co-ordinate y is given by:

$$y = y_k + \int_0^{\xi} l_k (\cos\theta_1 \sin\theta_3 + \sin\theta_1 \sin\theta_2 \cos\theta_3) d\xi \tag{6.29}$$

Finally, the co-ordinate z is expressed as:

$$z = z_k + \int_0^{\xi} l_k (\sin\theta_1 \sin\theta_3 - \cos\theta_1 \sin\theta_2 \cos\theta_3) d\xi \tag{6.30}$$

Therefore the cable configuration is completely defined.

6.4 - Cable Configuration during Laying in the Presence of Sheared Currents

In order to illustrate the application of the three dimensional model presented earlier in this chapter the influence of sheared oceanic currents on the cable configuration during steady state laying conditions is addressed. With the increasing requirement to position the cable accurately on the seabed there is a need to predict where it will land. The greatest operational uncertainty is the variation in the strength and direction of oceanic currents with depth during installation (Burgess, 1994). At this point in time accurate real time measurement of currents with depth during installation is not practically possible. The alternative approach is to adopt a foot print analysis which assumes a range of current profiles which are, in general, not in the same plane as the vessel's heading. The foot print analysis needs to determine the cable suspended length with the presence of these spatially varying current and to

determine the cable touchdown position relative to the position predicted by the stationary straight line solution.

The first approach for foot print analysis was introduced by Zajac (1957) who applied uniform transverse currents. After several approximations a redirected straight line solution was obtained. This analysis has proved to be limited in application. Only recently has this issue been the subject of further attention by Burgess (1994). Unfortunately, present cable laying models only approximate the suspended length of the cable. This may introduce inaccuracies in the determination of the touchdown point leading to an inaccurate foot print analysis.

In order to assess the influence of sheared currents on the cable configuration a three dimensional transient analysis is required. Here attention is focused on the final equilibrium position of the cable in the presence of sheared currents. The starting point is invariably the straight line solution and the sheared current profile with its spatially varying strength and direction is applied gradually in time to it final steady state current profile. Next, a foot print analysis is presented using the three dimensional model presented earlier.

For this footprint analysis it is assumed that the vessel is laying cable at speed of 2 m/s and the current profile with depth is linear with a surface velocity of 1 m/s and a seabed velocity of 0.1 m/s. The current direction with respect to the vessel heading is allowed to vary. Analysis are carried out for head, bow quartering beam, stern quartering and following currents. The results of this analysis are presented here.

Figure 6.1 shows the cable configuration in head and following sheared currents compared with the straight line solution. The curvature is clearly evident in these figures. In a head sea current the suspended length is 30%

greater that the straight line solution with the touchdown point trailing by 100% of the water depth. In the case of following currents the situation is reversed with the suspended length being 22% lower that the straight line solution and with the touchdown point leading by 25% of the water depth. Figure 6.1 can also be regarded as the projection envelope in the vertical plane of the vessel heading. Figure 6.2 shows the out of plane projection for beam sheared currents. In this case the touchdown point is deviated by 85% of the water depth and the suspended length is 10% larger than the length for the straight line solution. This figure can be regarded as the out of plane projection envelope for all current directions.

Figure 6.3 shows the three dimensional plots for several headings. This figure can be regarded as the three dimensional configuration envelope. The foot print of the cable touchdown position can be seen in this figure. Figures 6.4 and 6.5 show the curvature envelopes in two orthogonal directions with the presence of sheared current. The maximum in plane and out of plane curvatures in these figures correspond to a radii of 1000 m and 1500 m. Finally, figure 6.6 shows the foot print diagram for the case under investigation. The centre of the foot print on the layback axis corresponds to the touchdown position predicted by the straight line solution. It can be seen from this figure that the radius of the foot print is approximately the water depth.

6.5 - Concluding Remarks

In this chapter a solution for the three dimensional equations of motion given in chapter three was presented which includes the cable's flexural rigidity. The model is demonstrated for the three dimensional case of cable laying in sheared currents.

7 - Conclusions

This thesis has been concerned with the global dynamic analysis of marine cables. An original three dimensional formulation for the problem has been presented. This formulation takes advantage of the simplicity of the Frenet-Serret formulae to establish the differential equations of motion for a marine cable. The formulation can also be applied to other slender marine structures such as flexible risers and mooring lines. The equations of motion have been solved for both two and three dimensions. The two dimensional solution the has been obtained by a new time domain finite element displacement analysis based on the Galerkin weighted residual formulation for space integration and on the Newmark method for time integration. The three dimensional solution has been obtained by using an angular displacement approach based on Euler angles. The space integration was also performed by a finite element weighted residual formulation based on the Galerkin method but the time integration used a finite difference scheme.

The main advantages introduced by the formulation of the dynamic analysis of marine cables are as follows:

(a) The formulation introduces a relatively straightforward way of taking into consideration the cable's flexural rigidity in the dynamic analysis of marine cables. This is achieved by the adoption of the intrinsic frame of a space curve as the local frame of reference and the use of the Galerkin integral formulation for space integration which reduces the continuity requirements for the shape functions to be able to model bending moments and shear forces.

(b) The model is able to determine the instantaneous suspended length of the cable for marine cable laying analysis. This aspect is very important since

one of the main objectives of cable laying analysis is to determine the point where the cable lands in the seabed.

(c) The model is robust as it avoids singularities owing to zero tension situations. This is achieved by the introduction of bending stiffness and

(d) The model overcomes numerical instability in the transformation matrix from the local co-ordinates to the global co-ordinates.

It is concluded that the new model presented in this thesis includes a number of significant advances making it suitable for cable laying analysis under transient conditions.

The formulation has been used to investigate a range of practical problems such as the response of marine cables to changes in the lay vessel forward speed, wave induced vessel motions, hydrophone installation and sheared cross-currents. The latter used the three dimensional model.

The two dimensional model performed very well and consistently throughout the simulations. The results obtained with the model show good agreement with full scale measured data. The main conclusions from the simulations are:

(a) For changes in the lay vessel forward speed, the curvature affects significantly the position of the cable configuration and the time for the transient.

(b) The dynamic tension does not affect the configuration of the cable with changes in the lay vessel forward speed.

(c) The variation of the cable's suspended length with time is non-linear.

(d) For wave induced vessel motions simulation, the curvature is constrained to a small numbers of elements near the surface.

(e) For wave induced vessel motions, the dynamic tension can be significant and it can lead to local instability in the marine cable configuration.

(f) For the hydrophone installation simulation, the time for the transient is shorter than the time for the cable settle down when the vessel slows down.

The three dimensional simulation shows that sheared ocean currents introduce curvature in the cable configuration. This curvature affects significantly the suspended length of cable and the touchdown position.

The model can be improved by including the following features to the analysis:

(a) a model for the bottom tension which takes into consideration the effects of seabed friction and reflections of axial wave,

(b) the effects of the elasticity,

(c) the implementation of the two dimensional displacement formulation into three dimensions, and,

(d) the introduction of finite elements with different properties to allow the simulation of repeater installation and multiple cable laying.

A significant improvement in the model would be the introduction of local stability analysis so that the model would be able to predict instabilities such as

loop formation. This will provide a direct link between the local mechanical behaviour of cables with their global dynamic response.

Another area for further work is the application of the original formulation presented here to the analysis of other slender marine structures such as mooring systems, towed pipelines and flexible risers.

References

Ablow C. M. and Schechter, S. (1983) - "Numerical Simulation of Undersea Cable Dynamics", Ocean Engineering, Vol. 10, No. 6, pp. 443-457.

Bathe, K-J (1982) - Finite Element Procedures in Engineering Analysis, Prentice-Hall, Englewood Cliffs, New Jersey, 735p.

Breslin, J. P. (1974) - "Dynamic forces exerted by oscillating cables", J. Hydronautics, Vol. 8, No. 1, pp.19-31.

Buchnan,J.L. and Turner, P. R. (1992) - Numerical Methods and Analysis, McGRAW-HILL International edition,Singapore.

Burgess, J. J. (1991) - "Modelling of undersea cable installation with a finite difference method", Proc. of the First Int. Offshore and Polar Eng. Conf., Vol. III, Edinburgh, pp. 222-227.

Burgess, J. J. (1992a) - "Equations of motion of a submerged cable with bending stiffness", OMAE, Vol. I-A, pp. 283-288.

Burgess, J. J. (1992b) - "Bending stiffness in a simulation of undersea cable deployment", Proc. of the Second Int. Offshore and Polar Eng. Conf., Vol. III, San Francisco, pp. 308-315.

Burgess, J. J. (1994) - "The deployment of an undersea cable system in sheared current", BOSS'94, Vol 2, pp. 327-334

Burke, W. L. (1985) - Applied Differential Geometry, Cambridge University Press, 414p.

Burnett, D. S. (1987) - Finite Element Analysis: from concepts to applications, Addison-Wesley, Reading, Mass, 843p.

do Carmo, M. P. (1976) - Differential Geometry of Curves and Surfaces, Prentice-Hall, Englewood Cliffs, New Jersey, 503p.

Choo, Y-I. and Casarella, M. J. (1972) - "Configuration of a towline attached to a vehicle moving in a circular path", J. Hydronautics, Vol. 6. No. 1, pp. 51-57.

Choo, Y-I. and Casarella, M. J. (1973) - "A survey of analytical methods for dynamic simulation of cable-body system", J. Hydronautics, Vol. 7. No. 4, pp. 137-144.

Clarke, A. C. (1958) - Voice Across the Sea, Harper & Brothers, New York, 208p.

Clarke, A. C. (1992) - How the world was one: the turbulent history of world Communication, Victor Gollantz,London, 289p.

Committee VII- Slender Marine Structures report, C M Larsen, Chairman, Proceedings of the 11th ISSC, Vol.2, p275-315, Elsevier Applied Science, 1991.

Committee VII- Slender Marine Structures report, C M Larsen, Chairman, Proceedings of the 12th ISSC, Vol.2, p297-338, 1994.

Costello, G. A. (1990) - Theory of Wire Rope, Springer-Verlag, New York, 106 p.

Coyne, J. (1990) - "Analysis of the formation and elimination of loops in twisted cable", IEEE Journal of Ocean Engineering, Vol. 15, No 2, pp. 72-83.

Curtis, D.I. (1992) - "Design, manufacture and deep water deployment of submarine cables", Marinflex 92, London.

Delmer, T.N. and Stephens, T. C. (1983) - "Numerical simulation of towed cables", Ocean Engineering, Vol. 10, No. 2, pp. 119-132.

Eisenhart, L. P. (1947) - An Introduction to Differential Geometry, Princeton University Press, Princeton, 303p.

Faltinsen, O. M. (1990) - Sea loading on ships and offshore structures, Cambridge University Press, Cambridge, 328p.

Fang, J. and Witz, J. A. (1993) - "Plough - towing analysis in submarine cable laying", Proc. of Int. Wire & Cables Symposium., pp. 740-748.

Feld G., Owen D. G., Reuben R. L. and Crockett A. E. (1992) - "Mechanical behaviour of the metallic elements of submarine cables as a function of cable loading", Marinflex 92, Proc. of the First European Conference on Flexible Pipes., Umbilicals & Marine Cables, London.

Gorban, V. A., Pol'shin, M.E. and Leonidov, I. D. (1991) - "Investigation of the dynamics of laying a cable on the sea floor", Translated from Problemy Prochinosti, No 1, pp. 27-31.

Hata, S. (1979) - " Submarine Cable: Multi-blade Plough", Géotechnique,Vol. 29, No. 1, pp. 73-90.

Hopland, S. and Klykken, A. (1992) - "Installation of submarine fiberoptic cables in rugged coastal terrain", Proc. of Int. Wire & Cables Symposium., pp. 492-496.

Hopland, S. (1993) - "Investigation of cable behaviour in water during laying of fiberoptic submarine cables", Proc. of Int. Wire & Cables Symposium., pp. 734-739.

Howell, C. T. (1992) - "Investigation of Large Amplitude Nonlinear Dynamics of Hanging Chains", Proc. of the Second Int. Offshore and Polar Eng. Conf., Vol. III, San Francisco, pp. 316-320.

Irvine, H. M. and Sinclair, G. B. (1976) - "The suspended elastic cable under the action of concentrated vertical loads", Int. J. Solids Structures, Vol. 12, pp. 309-317.

Irvine, H. M. (1981) - Cable Structure, The MIT Press, Cambridge, Massachusetts.

Irvine, M. (1992) - "Local bending stress in cables", Proc. of the Second International Offshore and Polar Engineering Conference, San Francisco, USA, p342-345.

Jolicoeur, C and Cardou, A. (1991) - "A numerical comparison of current mathematical models of twisted wire cables under axisymmetric loads", Journal of Energy Resources Technology, Vol. 113, p241-149.

Kitazawa, I. (1981) - "Submarine cable dynamics and laying design", Review of the Electrical Communications Laboratories, Vol. 29, No. 5, pp. 557-570.

Kitazawa, I. (1986) - "Three-dimensional dynamic analysis for submarine cables", OMAE, pp. 492-498.

Knapp R. H., Le T. T. and Cruickshank M. J. (1991) - "Design methodology for undersea umbilical cables", Ocean's 91, Ocean Technology & Opportunities in the Pacific for the '90s, Proc. IEEE., Vol. 3, October, Honolulu, Hawaii.

Kwan, C. T. and Bruen, F. J.. (1991) - "Mooring line dynamics: comparison of time domain, frequency domain and quasi-static analyses", Proc. of the 23rd Annual Offshore Technology Conference , Houston, pp. 95-108.

Larsen, C. M. (1992) - "Flexible riser analysis - comparison of results from computer program", Journal of Marine Structures, Vol. 5, Nos 2 and 3, p2103-119.

Leonard, J. W. and Recker, W. W. (1972) - "Nonlinear dynamics of cables with low initial tension", Journal of the Engineering Mechanics Division, Proc. of the American Society of Civil Engineers, p293-309.

Leonard, J. W. and Karnoski, S. R. (1990) - "Simulation of tension controlled cable deployment", Applied Ocean Research, Vol. 12, No. 1, pp. 34-42.

Lipschutz, M. M. (1969) - Theory and Problems of Differential Geometry, McGRAW-HILL.

Lo, A. and Leonard, M. (1982) - "Dynamic analysis of underwater cables", J. of the Engng. Mech. Division, Proc. ASCE., Vol. 108, No. EM4., pp. 605-621

McCoy, J. J. (1972) - "Effects of bending Stiffness in tow and salvage cables", J. Hydronautics, Vol. 6, No. 2, pp.77-82.

Merret, J. (1958) - Three Miles Deep: the story of the transatlantic cables, Hamish Hamilton, London, pp. 191.

Migliore, H. J. and Webster, R. L. (1979) - "Current methods for analysing dynamics cable response", Shock & Vibration Digest, Vol. 11, No 6.

Milinazzo, F., Wilkie, M. and Latchman, S. A. (1987) - "An efficient algorithm for simulating the dynamics of towed cable systems", Ocean Engineering, Vol. 14, No. 6, pp. 513-526.

Millman, S. R. and Parker, G. D. (1977) - Elements of Differential Geometry, Prentice-Hall, Englewood Cliffs, New Jersey, 265p.

Palmer, A. C., Kenny, J. P., Perera, M. R. and Reece, A. R. (1979) - "Design and operation of an underwater pipeline trenching plough", Géotechnique,Vol. 29, No. 3, pp. 305-322.

Patel, M. H. (1989) - Dynamics of Offshore Structures, Butterworths, London, 402p.

Peyrot, A. H. and Goulois, A. M. (1979) - "Analysis of cable structures", Computers & Structures, Vol. 10, pp. 805-813.

Roden, C. E. (1974) - Submarine Cable Mechanics and Recommended Laying Procedures, AT&T Bell Laboratories Technical Publication.

Sanders, J. V. (1982) - "A three-dimensional dynamic analysis of a towed system", Ocean Engineering, Vol. 9, No. 5, pp. 483-489.

Sarpkaya, T. and Isaacson, M. (1981) - Mechanics of Wave Forces on Offshore Structures, Van Nostrand Reinhold, New York.

Seyed, F. B. and Patel, M. H. (1995) - "Review of flexible risers modelling and analysis techniques", Journal of Engineering Structures, in press.

Shimura, S. (1984) - International Submarine Cable Systems, KDD Engineering and Consulting, Tokyo.

Sun Y., Leonard J. W. and Chiou R. B. (1994) - "Simulation of unsteady oceanic cable deployment by direct integration with suppression", Ocean Engineering, Vol. 21, No. 3, pp. 243-256.

The Times Atlas of the Oceans, Edited by Alistair Couper, Times Books, London.

Triantafyllou M. S., Bliek A., Burgess J. and Shin H. (1986a) - "Mooring dynamics for offshore applications, part I", Technical Report, MITSG 86-1, Index No. NA 81AA-DO-00069, Project No. R/O-5.

Triantafyllou M. S., Bliek A., Burgess J. and Shin H. (1986b) - "Mooring dynamics for offshore applications, part II", Technical Report, MITSG 86-2, Index No. NA 81AA-DO-00069, Project No. R/O-5.

Triantafyllou M. S., Hover F. (1990) - "Cable dynamics for tethered underwater vehicles", Technical Report, MITSG 90-4, Grant No. NA 86AA-D-SG089, Project No. RU-21.

Triantafyllou, G. S. and Chryssostomidis, C. (1989) - "The dynamics of towed arrays", Transactions of the ASME, Journal of Offshore Mechanics and Artic Engineering, Vol. 111, pp. 208-213.

Triantafyllou, M. S. (1994) - "Cable mechanics for moored floating systems", BOSS'94, Vol 2, pp. 57-78.

Walton, T. S. and Polacheck, H.. (1960) - "Calculation of transient motion of submerged cables", Mathematics of Computation, 14, pp. 27-46.

Witz, J. A. and Tan, Z. (1992a) - "On the Axial-Torsional Structural Behaviour of Flexible Pipes, Umbilicals and Marine Cables", Journal of Marine Structures, Vol. 5.

Witz, J. A. and Tan, Z. (1992b) - "On the flexural structural behaviour of flexible pipes, umbilicals and marine cables", Journal of Marine Structures, Vol. 5, Nos 2 & 3, p229-249.

Zajac, E. E. (1957) - "Dynamics and kinematics of the laying and recovery of submarine cable", Bell System Technical Journal, Vol. 35, No 5, pp. 1129-1207.

Zienkiewicz, O. C. and Taylor, R. L. (1989) - The Finite Element Methods, 4th ed. Vol.1: Basic formulations and linear problems, McGraw-Hill, London, 648p.

Zienkiewicz, O. C. and Taylor, R. L. (1991) - The Finite Element Methods, 4th ed. Vol.2: Solid and fluid mechanics dynamics and non-linearity, McGraw-Hill, London, 807p.

Appendix A - Review of the Theory of Space Curves

A brief review of the theory of space curves is presented here. The review covers those aspects of the theory which are relevant to the derivation of the model for simulating the dynamics of marine cables presented in this work. More detailed studies of the theory of space curves can be found in texts on differential geometry such as Einsenhart (1947), Lipschultz (1969), do Carmo (1976), Milman and Parker (1977) and Burke (1985).

As far as the model for the dynamics of marine cables is concerned, there are three main aspects of the theory of space curves which have to be understood. The first aspect is the definition of a local frame of reference which is the intrinsic or moving frame of the curve. The second aspect is the establishment of the Frenet-Serret formulas in which the derivatives of the unit vectors of the intrinsic frame are written as functions of the unit vectors themselves. Finally, the last important aspect is the establishment of a relationship between the intrinsic frame of reference and a Cartesian frame of reference. These three aspects of the theory of space curves are discussed below.

A.1 - Intrinsic Basis of a Space Curve

Let C be a unit speed space curve parametrised by its arc length p and defined by the vector function **r** such that:

$$\mathbf{r} = \mathbf{r}(p) \tag{A.1}$$

Since the curve C is a unit speed curve, it is straightforward to show that the unit tangent vector to the curve C is the derivative of **r** with respect to p. Hence:

$$\mathbf{t} = \frac{\partial \mathbf{r}}{\partial p} \tag{A.2}$$

In addition, the derivative of the unit tangent vector **t** with respect to the arc length p gives the rate of change of the tangent direction with p. This rate of change in the tangent direction is also a vector and its magnitude is called curvature. The curvature κ should be regarded as a measure of the bending of the curve. Accordingly, the curvature may be defined as:

$$\kappa = \left|\frac{\partial \mathbf{t}}{\partial p}\right| = \left|\frac{\partial^2 \mathbf{r}}{\partial p^2}\right| \tag{A.3}$$

Furthermore, the direction of the rate of change in the tangent direction can be determined by considering the following steps. Firstly, since the tangent vector defined in equation (A.2) is a unit vector, the dot product between **t** and itself is given by:

$$\mathbf{t} \cdot \mathbf{t} = 1 \tag{A.4}$$

Secondly, the derivative of (A.4) with respect to the arc length p gives:

$$2\mathbf{t} \cdot \frac{\partial \mathbf{t}}{\partial p} = 0 \tag{A.5}$$

From equation (A.5) it may be concluded that the unit tangent vector and the vector given by the derivative of the unit tangent vector with respect to the arc length p are normal to each other. For this reason the direction of the vector derivative of the unit tangent vector with respect to the arc length is called the principal normal direction. Furthermore, the unit vector in the principal normal direction, denoted by **n**, is given by the following expression:

$$\mathbf{n} = \frac{\dfrac{\partial \mathbf{t}}{\partial p}}{\left|\dfrac{\partial \mathbf{t}}{\partial p}\right|} = \frac{1}{\kappa}\frac{\partial \mathbf{t}}{\partial p} \tag{A.6}$$

As a consequence of the unit tangent vector **t** and the principal normal vector **n** being unit vectors and normal to each other, a third unit vector may be obtained by taking the result of the cross product **t**×**n**. This third unit vector is normal to both **t** and **n** and it is called the binormal vector, denoted by **b**. The direction of the binormal vector is called the binormal direction. Hence:

$$\mathbf{b} = \mathbf{t} \times \mathbf{n} \tag{A.7}$$

As a result the unit tangent vector, **t**, the principal normal unit vector, **n**, and the binormal vector, **b**, are linearly independent and normal to each other. Therefore, these vectors form an orthonormal basis of the Euclidean space of dimension three. This basis is called the intrinsic basis of a curve. This intrinsic basis is always right-handed oriented. This is because the curvature is always positive as it is the magnitude of the rate of change in the tangent direction. This frame is also sometimes called the moving frame.

A.2 - Frenet-Serret Formulae and Torsion of a Curve

In spite of **t**,**n** and **b** being unit vectors, their directions change as the moving frame moves along the curve C. As a consequence, derivatives of vector quantities expressed in the intrinsic basis involve derivatives of the unit vectors as well. Because of this, it is useful to express the derivatives of

the unit vectors with respect to the arc length p as function of the unit vectors themselves. The derivation of such expressions is considered next.

Firstly, the scalar product between **t** and **b** is zero, because **t** and **b** are orthogonal vectors. Hence:

$$\mathbf{b}\cdot\mathbf{t}=0 \tag{A.8}$$

The derivative of (A.8) with respect to the arc length p is:

$$\frac{\partial}{\partial p}(\mathbf{b}\cdot\mathbf{t})=\frac{\partial \mathbf{b}}{\partial p}\cdot\mathbf{t}+\mathbf{b}\cdot\frac{\partial \mathbf{t}}{\partial p}=\frac{\partial \mathbf{b}}{\partial p}\cdot\mathbf{t}+\kappa(\mathbf{b}\cdot\mathbf{n})=\frac{\partial \mathbf{b}}{\partial p}\cdot\mathbf{t}=0 \tag{A.9}$$

It follows that the vector derivative of the binormal vector with respect to the arc length p is normal to the tangent vector, **t**. This vector gives the rate of change in the binormal direction with the arc length p. Secondly, the scalar product between the binormal vector **b** and itself is equal to one. That is:

$$\mathbf{b}\cdot\mathbf{b}=1 \tag{A.10}$$

The derivative of equation (A.10) with respect to the arc length p gives:

$$\frac{\partial}{\partial p}(\mathbf{b}\cdot\mathbf{b})=\frac{\partial \mathbf{b}}{\partial p}\cdot\mathbf{b}+\mathbf{b}\cdot\frac{\partial \mathbf{b}}{\partial p}=2\frac{\partial \mathbf{b}}{\partial p}\cdot\mathbf{b}=0 \tag{A.11}$$

It follows that the vector rate of change in the binormal direction with the arc length p is also normal to the binormal vector **b**. Therefore, this vector must be parallel to the principal normal direction **n**. The derivative of the binormal vector **b** with respect to the arc length p, can be written as the product of the unit principal normal vector **n** and a scalar quantity. That is:

$$\frac{\partial \mathbf{b}}{\partial p} = -\tau \mathbf{n} \tag{A.12}$$

where the negative sign follows common convention.

In order to understand the geometric meaning of the scalar τ it is necessary to obtain the scalar products between both sides of equation (A.12) and the unit principal normal vector **n**. As a result:

$$\frac{\partial \mathbf{b}}{\partial p} \cdot \mathbf{n} = -\tau(\mathbf{n} \cdot \mathbf{n}) \rightarrow \tau = -\left|\frac{\partial \mathbf{b}}{\partial p}\right| \cos\theta \tag{A.13}$$

where θ is the angle between both vectors. Since these vectors are parallel, the angle between them is either zero or π. As a result, the scalar quantity τ assumes the expression:

$$\tau = \mp\left|\frac{\partial \mathbf{b}}{\partial p}\right| \tag{A.14}$$

As a consequence, this scalar quantity should be regarded as the magnitude of the rate of change in the binormal direction affected by the sign. This rate of change in the binormal direction can be interpreted geometrically as a measure of the torsion of the curve. For this reason the scalar τ is called the torsion of a space curve. Torsion of a curve is purely geometric scalar quantity and does not have the meaning of twist of a rod.

Finally, the normal vector **n** may be written as the vector product of the binormal vector **b** and the tangent vector **t**:

$$\mathbf{n} = \mathbf{b} \times \mathbf{t} \tag{A.15}$$

The derivative of equation (A.15) with respect to the arc length p gives:

$$\frac{\partial \mathbf{n}}{\partial p} = \frac{\partial}{\partial p}(\mathbf{b} \times \mathbf{t}) = \frac{\partial \mathbf{b}}{\partial p} \times \mathbf{t} + \mathbf{b} \times \frac{\partial \mathbf{t}}{\partial p} = -\tau(\mathbf{n} \times \mathbf{t}) + \kappa(\mathbf{b} \times \mathbf{n}) = -\kappa \mathbf{t} + \tau \mathbf{b} \qquad \text{(A.16)}$$

From the combination of equations (A.6), (A.12) and (A.16), the derivatives of the unit vectors **t**, **n** and **b** with reference to the arc length p, may be written in the following matrix form:

$$\frac{\partial}{\partial p}\begin{Bmatrix}\mathbf{t}\\ \mathbf{n}\\ \mathbf{b}\end{Bmatrix} = \begin{bmatrix}0 & \kappa & 0\\ -\kappa & 0 & \tau\\ 0 & -\tau & 0\end{bmatrix}\begin{Bmatrix}\mathbf{t}\\ \mathbf{n}\\ \mathbf{b}\end{Bmatrix} \qquad \text{(A.17)}$$

The formulae in the above matrix form (A.17) are called Frenet-Serret formulas.

The local behaviour of a space curve is completely defined by its curvature and its torsion. In order to show how the curvature and the torsion affect the local behaviour of a space curve, consider the three orthogonal planes defined by the intrinsic frame of the curve. These three planes are the osculating plane, defined by the tangent and the principal normal vectors; the normal plane, defined by the principal normal and the binormal vectors; and the rectifying plane, defined by the tangent and binormal vectors.

Following the definition of curvature, it is straightforward to show that the principal normal vector is always pointing towards the centre of curvature. The distance between the centre of curvature and the point under consideration in the curve is called the radius of curvature. Therefore, for constant non-zero curvature, the radius of curvature is constant and the

curve behaves either as circle if the torsion is zero or as a helix if the torsion is constant. For a zero curvature, the radius of curvature is infinite and the curve becomes a straight line. As a result, the curvature is a measure of the bending of the curve.

On the other hand, the torsion is a measure of the rate of change in the binormal direction. Zero torsion means that the binormal direction does not change with the arc length p and, therefore, the curve lies entirely in the osculating plane. However, for cases in which the torsion is not zero, the curve tends to pull away from the osculating plane. As a result, the torsion can be regarded as a measure of the ability of a curve to move away from the osculating plane.

A.3- Representation of the Frenet-Serret Formulas in a Inertial Frame of Reference

In the foregoing sections the intrinsic basis of a space curve has been defined in terms of the tangent, normal and binormal vectors. In addition, the derivatives of these vectors with respect to the arc length have been expressed as functions of the vectors themselves. However, this frame of reference alone is not suitable for the dynamic analysis of the motion of a structure. This is because the equations of motion of the structure must be referred to an inertial frame of reference which, clearly, is not the case of the intrinsic basis.

In practice, the equations of motion of the structure are written in the local frame of reference such as the intrinsic basis. These equations of motion are then transformed to a global reference system which is inertial. Therefore, the transformation from one system to another must be established. This section is concerned with the derivation of this transformation.

Let **i, j** and **k** be the unit vectors of an orthonormal basis of the Euclidean space of dimension three. In addition, the unit vectors **i, j** and **k** do not depend on the arc length p. Under these circumstances, the parametric equation of a space curve may be written in the global inertial system as:

$$\mathbf{r} = x(p)\mathbf{i} + y(p)\mathbf{j} + z(p)\mathbf{k} \tag{A.18}$$

Following the definition of the unit tangent vector, it may be written that:

$$\mathbf{t} = \frac{\partial \mathbf{r}}{\partial p} = \frac{\partial x}{\partial p}\mathbf{i} + \frac{\partial y}{\partial p}\mathbf{j} + \frac{\partial z}{\partial p}\mathbf{k} \tag{A.19}$$

The principal normal vector is given by:

$$\mathbf{n} = \frac{1}{\kappa}\left(\frac{\partial^2 x}{\partial p^2}\mathbf{i} + \frac{\partial^2 y}{\partial p^2}\mathbf{j} + \frac{\partial^2 z}{\partial p^2}\mathbf{k}\right) \tag{A.20}$$

where the expression for the curvature κ is:

$$\kappa = \sqrt{\left(\frac{\partial^2 x}{\partial p^2}\right)^2 + \left(\frac{\partial^2 y}{\partial p^2}\right)^2 + \left(\frac{\partial^2 z}{\partial p^2}\right)^2} \tag{A.21}$$

Finally, the binormal vector is obtained through the vector product of the unit tangent and unit normal vectors. Thus:

$$\mathbf{b} = \mathbf{t} \times \mathbf{n} = \begin{vmatrix} \mathbf{i} & \mathbf{j} & \mathbf{k} \\ \dfrac{\partial x}{\partial p} & \dfrac{\partial y}{\partial p} & \dfrac{\partial z}{\partial p} \\ \dfrac{1}{\kappa}\dfrac{\partial^2 x}{\partial p^2} & \dfrac{1}{\kappa}\dfrac{\partial^2 y}{\partial p^2} & \dfrac{1}{\kappa}\dfrac{\partial^2 z}{\partial p^2} \end{vmatrix} \tag{A.22}$$

In order to obtain the transformation matrix from the global reference system, (**i**,**j**,**k**), to the local reference system, (**t**,**n**,**b**), equations (A.19), (A,20) and (A.22) are combined. As a result:

$$\begin{Bmatrix}\mathbf{t}\\ \mathbf{n}\\ \mathbf{b}\end{Bmatrix}^{T} = \begin{Bmatrix}\mathbf{i}\\ \mathbf{j}\\ \mathbf{k}\end{Bmatrix}^{T}\begin{bmatrix}\frac{\partial x}{\partial p} & \frac{1}{\kappa}\frac{\partial^2 x}{\partial p^2} & \frac{1}{\kappa}\left(\frac{\partial y}{\partial p}\frac{\partial^2 z}{\partial p^2}-\frac{\partial^2 y}{\partial p^2}\frac{\partial z}{\partial p}\right)\\ \frac{\partial y}{\partial p} & \frac{1}{\kappa}\frac{\partial^2 y}{\partial p^2} & \frac{1}{\kappa}\left(\frac{\partial^2 x}{\partial p^2}\frac{\partial z}{\partial p}-\frac{\partial x}{\partial p}\frac{\partial^2 z}{\partial p^2}\right)\\ \frac{\partial z}{\partial p} & \frac{1}{\kappa}\frac{\partial^2 z}{\partial p^2} & \frac{1}{\kappa}\left(\frac{\partial x}{\partial p}\frac{\partial^2 y}{\partial p^2}-\frac{\partial^2 x}{\partial p^2}\frac{\partial y}{\partial p}\right)\end{bmatrix} \tag{A.23}$$

One should note that the transformation matrix from the intrinsic frame of a space curve to the global co-ordinates does not depend on the torsion. However, in order to establish the global configuration of a space curve, it is necessary to express the torsion as a function of the global co-ordinates and their derivatives with respect to the arc length p. This derivation is considered next.

A.4 - Expression for the Torsion in the Inertial Frame of Reference

Eisenhart (1947) shows that the torsion of a unit speed curve is given by the expression:

$$\tau = \frac{\left(\frac{\partial \mathbf{r}}{\partial p}\times\frac{\partial^2 \mathbf{r}}{\partial p^2}\right)\cdot\frac{\partial^3 \mathbf{r}}{\partial p^3}}{\left|\frac{\partial \mathbf{r}}{\partial p}\times\frac{\partial^2 \mathbf{r}}{\partial p^2}\right|^2} \tag{A.24}$$

Following equations (A.2) and (A.6), it may be written that:

$$\frac{\partial \mathbf{r}}{\partial p}\times\frac{\partial^2 \mathbf{r}}{\partial p^2} = (\mathbf{t})\times(\kappa\mathbf{n}) = \kappa(\mathbf{t}\times\mathbf{n}) = \kappa\mathbf{b} \tag{A.25}$$

Hence, equation (A.23) may be rewritten as:

$$\tau = \frac{1}{\kappa^2}\left(\frac{\partial \mathbf{r}}{\partial p} \times \frac{\partial^2 \mathbf{r}}{\partial p^2}\right) \cdot \frac{\partial^3 \mathbf{r}}{\partial p^3} \tag{A.26}$$

Equation (A.26) may be expanded as the determinant:

$$\tau = \frac{1}{\kappa^2}\begin{vmatrix} \frac{\partial x}{\partial p} & \frac{\partial y}{\partial p} & \frac{\partial z}{\partial p} \\ \frac{\partial^2 x}{\partial p^2} & \frac{\partial^2 y}{\partial p^2} & \frac{\partial^2 z}{\partial p^2} \\ \frac{\partial^3 x}{\partial p^3} & \frac{\partial^3 y}{\partial p^3} & \frac{\partial^3 z}{\partial p^3} \end{vmatrix} \tag{A.27}$$

The above equation gives the torsion as a function of co-ordinates x, y and z and their first, second and third derivatives with respect to the arc length p. It should be pointed out that for curves whose parametric functions for the co-ordinates x, y and z, respectively, present continuity no higher than C^2 are plane curves.

Appendix B - Rotational Transformation of Co-ordinates

The transformation matrix which relates two three dimensional axes systems which are rotated from each other can be obtained through three partial rotations. These rotations are called Euler rotations and the angles corresponding to the rotations are called Euler angles. The total transformation matrix is the matrix product of the matrices which correspond to the partial rotations. Owing to the fact that the matrix product is not commutative, once a particular sequence of rotations is chosen it cannot be changed throughout the analysis.

The axes systems are $\mathbf{x}(x_1,x_2,x_2)$ and $\mathbf{x}_L(x_t,x_n,x_b)$. The following sequence of rotations is adopted throughout this work in order to bring these two axes systems together. Firstly, a rotation through θ_1 about the axis x_1 is performed in order to bring x_2 to the plane formed by the axes x_t and x_n. This rotation leads to a new axes system $\xi(\xi_1,\xi_2,\xi_3)$. Then a rotation through θ_2 about the new axis ξ_2 is performed leading to the axes system $\eta(\eta_1,\eta_2,\eta_3)$. This rotation brings the axis ξ_3 coincident with the axis x_b. Finally, the axes systems $\mathbf{x}_L(x_t,x_n,x_b)$ and $\eta(\eta_1,\eta_2,\eta_3)$ are brought together by performing a rotation through θ_3 about η_3.

The transformation matrix for the first rotation is given by:

$$\begin{Bmatrix}\xi_1\\ \xi_2\\ \xi_3\end{Bmatrix}=\begin{bmatrix}1 & 0 & 0\\ 0 & \cos\theta_1 & \sin\theta_1\\ 0 & -\sin\theta_1 & \cos\theta_1\end{bmatrix}\begin{Bmatrix}x_1\\ x_2\\ x_3\end{Bmatrix}\rightarrow \boldsymbol{\xi}=\mathbf{C}_1\mathbf{x} \qquad \text{(B.1)}$$

while the transformation matrix for the second rotation corresponds to the expression:

$$\begin{Bmatrix}\eta_1\\ \eta_2\\ \eta_3\end{Bmatrix}=\begin{bmatrix}\cos\theta_2 & 0 & -\sin\theta_2\\ 0 & 1 & 0\\ \sin\theta_2 & 0_1 & \cos\theta_2\end{bmatrix}\begin{Bmatrix}\xi_1\\ \xi_2\\ \xi_3\end{Bmatrix}\rightarrow \boldsymbol{\eta}=\mathbf{C}_2\boldsymbol{\xi} \tag{B.2}$$

Finally, the transformation matrix for the third rotation may be written as:

$$\begin{Bmatrix}x_t\\ x_n\\ x_b\end{Bmatrix}=\begin{bmatrix}\cos\theta_3 & -\sin\theta_3 & 0\\ \sin\theta_3 & \cos\theta_3 & 0\\ 0 & 0 & 1\end{bmatrix}\begin{Bmatrix}\eta_1\\ \eta_2\\ \eta_3\end{Bmatrix}\rightarrow \mathbf{x}_L=\mathbf{C}_3\boldsymbol{\eta} \tag{B.3}$$

The total transformation matrix is obtained by performing the following matrix product:

$$\mathbf{x}_L=\mathbf{C}_3\boldsymbol{\eta}=\mathbf{C}_3\mathbf{C}_2\boldsymbol{\xi}=\mathbf{C}_3\mathbf{C}_2\mathbf{C}_1\mathbf{x}=\mathbf{C}\mathbf{x} \tag{B.4}$$

where:

$$\mathbf{C}=\begin{bmatrix}\cos\theta_2\cos\theta_3 & \cos\theta_1\sin\theta_3+\sin\theta_1\sin\theta_2\cos\theta_3 & \sin\theta_1\sin\theta_3-\cos\theta_1\sin\theta_2\cos\theta_3\\ -\cos\theta_2\sin\theta_3 & \cos\theta_1\cos\theta_3-\sin\theta_1\sin\theta_2\sin\theta_3 & \sin\theta_1\cos\theta_3+\cos\theta_1\sin\theta_2\sin\theta_3\\ \sin\theta_2 & -\sin\theta_1\cos\theta_2 & \cos\theta_1\cos\theta_2\end{bmatrix}$$

Appendix C - Relationship between Differential Geometry and Euler Rotations Approaches

Assume that the axes system $\mathbf{x}_L$ defined in appendix B is the intrinsic frame of a space curve. Therefore, the unit vectors $\mathbf{t}$, $\mathbf{n}$ and $\mathbf{b}$ are the unit tangent vector, the unit principal normal vector and the unit binormal vector, respectively. The transformation matrix which relates these vectors with the unit vectors $\mathbf{i}$, $\mathbf{j}$ and $\mathbf{k}$ is given by:

$$\begin{Bmatrix} \mathbf{t} \\ \mathbf{n} \\ \mathbf{b} \end{Bmatrix} = \mathbf{C} \begin{Bmatrix} \mathbf{i} \\ \mathbf{j} \\ \mathbf{k} \end{Bmatrix} \tag{C.1}$$

where $\mathbf{C}$ is the rotation matrix as defined in equation (B.4). Obviously, this rotation matrix has to be the same as the matrix given by the expression (A.23) from appendix A which was obtained through the differential geometry approach. As a result, the elements of the matrix $\mathbf{C}$ can be given either by the second column or by the third column of the table C.1.

In addition the derivatives of the unit vectors $\mathbf{t}$, $\mathbf{n}$ and $\mathbf{b}$ with respect to the arc length p can be expressed as functions of the unit vectors themselves. In the differential geometry approach these functions are the Frenet-Serret formulae. In the approach using Euler rotations, similar expressions can be obtained by differentiating expression (C.1) with respect to the arc length, which gives:

$$\frac{\partial}{\partial p} \begin{Bmatrix} \mathbf{t} \\ \mathbf{n} \\ \mathbf{b} \end{Bmatrix} = \frac{\partial \mathbf{C}}{\partial p} \begin{Bmatrix} \mathbf{i} \\ \mathbf{j} \\ \mathbf{k} \end{Bmatrix} \tag{C.2}$$

and then replacing the unit vectors $\mathbf{i}$, $\mathbf{j}$ and $\mathbf{k}$ in the above expression by the inverse relation of equation (C.1). Since the rotation is an orthogonal

transformation, the inverse of the matrix $\mathbf{C}$ is the same as the matrix $\mathbf{C}$ transposed. As a result:

$$\frac{\partial}{\partial p}\begin{Bmatrix}\mathbf{t}\\ \mathbf{n}\\ \mathbf{b}\end{Bmatrix}=\frac{\partial \mathbf{C}}{\partial p}\mathbf{C}^{\mathrm{T}}\begin{Bmatrix}\mathbf{t}\\ \mathbf{n}\\ \mathbf{b}\end{Bmatrix}=\left(\frac{\partial \mathbf{C}_3}{\partial p}\mathbf{C}_2\mathbf{C}_1+\mathbf{C}_3\frac{\partial \mathbf{C}_2}{\partial p}\mathbf{C}_1+\mathbf{C}_3\mathbf{C}_2\frac{\partial \mathbf{C}_1}{\partial p}\right)\mathbf{C}^{\mathrm{T}}\begin{Bmatrix}\mathbf{t}\\ \mathbf{n}\\ \mathbf{b}\end{Bmatrix}=\mathbf{D}\begin{Bmatrix}\mathbf{t}\\ \mathbf{n}\\ \mathbf{b}\end{Bmatrix} \quad \text{(C.3)}$$

where $\mathbf{C}_1$, $\mathbf{C}_2$ and $\mathbf{C}_3$ are the first, second and third rotation matrices corresponding to Euler rotations θ_1 $\theta_2$and θ_3. These rotations matrices are given by equations (B.1), (B.2) and (B.3), respectively, in appendix B.

$$\mathbf{D}=\begin{bmatrix} 0 & \sin\theta_2\dfrac{\partial\theta_1}{\partial p}+\dfrac{\partial\theta_3}{\partial p} & \cos\theta_2\sin\theta_3\dfrac{\partial\theta_1}{\partial p}-\cos\theta_3\dfrac{\partial\theta_2}{\partial p}\\ -D_{12} & 0 & \cos\theta_2\cos\theta_3\dfrac{\partial\theta_1}{\partial p}+\sin\theta_3\dfrac{\partial\theta_2}{\partial p}\\ -D_{13} & -D_{23} & 0\end{bmatrix} \quad \text{(C.4)}$$

The following expressions can be written from the comparison of the above matrix with the Frenet-Serret formulae (A.17):

$$\kappa=\sin\theta_2\frac{\partial\theta_1}{\partial p}+\frac{\partial\theta_3}{\partial p} \quad \text{(C.5)}$$

$$\tau=\cos\theta_2\cos\theta_3\frac{\partial\theta_1}{\partial p}+\sin\theta_3\frac{\partial\theta_2}{\partial p} \quad \text{(C.6)}$$

and

$$\cos\theta_2\sin\theta_3\frac{\partial\theta_1}{\partial p}-\cos\theta_3\frac{\partial\theta_2}{\partial p}=0 \quad \text{(C.7)}$$

where κ is the curvature and τ is the geometric torsion of a space curve.

The above expressions are only true for the particular sequence of rotations adopted in appendix B. Similar expressions can be obtained for any other sequence of rotations. However, once the sequence of rotations is chosen it must be observed throughout the analysis.

Element	Differential Geometry	Euler Angles
C_{11}	$\frac{\partial x}{\partial p}$	$\cos\theta_2 \cos\theta_3$
C_{12}	$\frac{\partial y}{\partial p}$	$\cos\theta_1 \sin\theta_3 + \sin\theta_1 \sin\theta_2 \cos\theta_3$
C_{13}	$\frac{\partial z}{\partial p}$	$\sin\theta_1 \sin\theta_3 - \cos\theta_1 \sin\theta_2 \cos\theta_3$
C_{21}	$\frac{1}{\kappa}\frac{\partial^2 x}{\partial p^2}$	$-\cos\theta_2 \sin\theta_3$
C_{22}	$\frac{1}{\kappa}\frac{\partial^2 y}{\partial p^2}$	$\cos\theta_1 \cos\theta_3 - \sin\theta_1 \sin\theta_2 \sin\theta_3$
C_{23}	$\frac{1}{\kappa}\frac{\partial^2 z}{\partial p^2}$	$\sin\theta_1 \cos\theta_3 + \cos\theta_1 \sin\theta_2 \sin\theta_3$
C_{31}	$\frac{1}{\kappa}\left(\frac{\partial y}{\partial p}\frac{\partial^2 z}{\partial p^2} - \frac{\partial^2 y}{\partial p^2}\frac{\partial z}{\partial p}\right)$	$\sin\theta_2$
C_{32}	$\frac{1}{\kappa}\left(\frac{\partial^2 x}{\partial p^2}\frac{\partial z}{\partial p} - \frac{\partial x}{\partial p}\frac{\partial^2 z}{\partial p^2}\right)$	$-\sin\theta_1 \cos\theta_2$
C_{33}	$\frac{1}{\kappa}\left(\frac{\partial x}{\partial p}\frac{\partial^2 y}{\partial p^2} - \frac{\partial^2 x}{\partial p^2}\frac{\partial y}{\partial p}\right)$	$\cos\theta_1 \cos\theta_2$

Table C.1 - Elements for the Rotation Matrix

Appendix D - Time Derivatives of the Local Unit Vectors

In accordance with the definition of the reference system given in chapter three, the local frame of reference used in this work is the intrinsic frame of a space curve. This frame of reference is defined by the unit vectors **t**, **n** and **b**. This appendix is concerned with the expressions for the time derivative of these unit vectors as functions of the unit vectors themselves.

The reference system used in chapter three adopts two more frames of reference in addition to the intrinsic frame. These frames are the vessel frame of reference and the inertial frame of reference. The local frame of reference can be related to the vessel frame of reference by the expression:

$$\frac{\partial}{\partial t}\begin{Bmatrix}\mathbf{t}\\ \mathbf{n}\\ \mathbf{b}\end{Bmatrix} = \frac{\partial}{\partial t}\left(\mathbf{C}\begin{Bmatrix}\mathbf{i}\\ \mathbf{j}\\ \mathbf{k}\end{Bmatrix}\right) \tag{D.1}$$

where **C** is the rotation matrix defined in appendix B and **i**, **j** and **k** are the unit vectors of the vessel frame of reference. The unit vectors of the vessel frame of reference may also change direction with time. Because of this frame is not inertial. However, the relation of the vessel frame of reference with the inertial frame of reference is given by equation (3.4) in chapter three. According to that expression the time derivatives of the unit vectors **i**, **j** and **k** may be written as:

$$\frac{\partial}{\partial t}\begin{Bmatrix}\mathbf{i}\\ \mathbf{j}\\ \mathbf{k}\end{Bmatrix} = \frac{\partial\beta}{\partial t}\begin{bmatrix}\sin\beta & 0 & -\cos\beta\\ 0 & 0 & 0\\ \cos\beta & 0 & \sin\beta\end{bmatrix}\begin{Bmatrix}\mathbf{I}\\ \mathbf{J}\\ \mathbf{K}\end{Bmatrix} = \frac{\partial\beta}{\partial t}\begin{bmatrix}0 & 0 & 1\\ 0 & 0 & 0\\ -1 & 0 & 0\end{bmatrix}\begin{Bmatrix}\mathbf{i}\\ \mathbf{j}\\ \mathbf{k}\end{Bmatrix} \tag{D.2}$$

where **I**, **J** and **K** are the unit vectors of the inertial frame of reference and β is the angle between the vessel mean forward velocity and the unit vector **I** of the inertial frame of reference.

Substituting equation (D.2) into equation (D.1) and replacing the unit vectors **i**, **j** and **k** by the inverse relation of equation (C.1) gives:

$$\frac{\partial}{\partial t}\begin{Bmatrix}\mathbf{t}\\ \mathbf{n}\\ \mathbf{b}\end{Bmatrix} = \left(\frac{\partial \mathbf{C}}{\partial t}\mathbf{C}^{\mathrm{T}} + \mathbf{C}\begin{bmatrix} 0 & 0 & \frac{\partial \beta}{\partial t} \\ 0 & 0 & 0 \\ -\frac{\partial \beta}{\partial t} & 0 & 0 \end{bmatrix}\mathbf{C}^{\mathrm{T}}\right)\begin{Bmatrix}\mathbf{t}\\ \mathbf{n}\\ \mathbf{b}\end{Bmatrix} = \begin{bmatrix} 0 & D_{12} & D_{13} \\ -D_{12} & 0 & D_{23} \\ -D_{13} & -D_{23} & 0 \end{bmatrix}\begin{Bmatrix}\mathbf{t}\\ \mathbf{n}\\ \mathbf{b}\end{Bmatrix} \qquad \text{(D.3)}$$

where:

$$D_{12} = \mathrm{s}\theta_2 \frac{\partial \theta_1}{\partial t} + \frac{\partial \theta_3}{\partial t} + \mathrm{s}\theta_1 \mathrm{c}\theta_2 \frac{\partial \beta}{\partial t} \qquad \text{(D.4)}$$

$$D_{13} = \mathrm{c}\theta_2 \mathrm{s}\theta_3 \frac{\partial \theta_1}{\partial t} - \mathrm{c}\theta_3 \frac{\partial \theta_2}{\partial t} - (\mathrm{s}\theta_1 \mathrm{s}\theta_2 \mathrm{s}\theta_3 - \mathrm{c}\theta_1 \mathrm{c}\theta_3)\frac{\partial \beta}{\partial t} \qquad \text{(D.5)}$$

and

$$D_{23} = \mathrm{c}\theta_2 \mathrm{c}\theta_3 \frac{\partial \theta_1}{\partial t} + \mathrm{s}\theta_3 \frac{\partial \theta_2}{\partial t} - (\mathrm{c}\theta_1 \mathrm{s}\theta_3 + \mathrm{s}\theta_1 \mathrm{s}\theta_2 \mathrm{c}\theta_3)\frac{\partial \beta}{\partial t} \qquad \text{(D.6)}$$

where c and s stand for cosine and sine respectively.

Appendix E - Description of the program CATIA

E.1 - Introduction

A mathematical description of the two dimensional equations of motion was presented in chapter four. A general description on the numerical solution and procedures used in the implementation of the solution of the differential equations of motion is presented within this appendix.

The solution of the two dimensional equations of motion is obtained through a computer program called CATIA (CAble Towing and Installation Analysis of marine cables). The program uses a FORTRAN77 code which has not yet been optimised. The reason for this is that the main objective of the program was to show that the numerical solution of the differential equations of motion as presented in this thesis through a finite element method was feasible. Because of this the program's efficiency can be greatly improved from a computational point of view. In addition, the program's performance can be further improved by a study to find the optimal balance between the time step and the number of iterations performed by the Newton-Raphson method within one time step. That is, if a larger time step is chosen, the number of integrations in time will be lower. However, in this case, the number of Newton-Raphson iterations necessary to achieve convergence will be larger.

In spite of not being optimised, the program CATIA exhibited a reasonable performance during the simulations used in this thesis. Typical runs using time steps of between 0.5 and 2.0 seconds and up to 900 integration steps in time took about 2 to 4 hours on a 70 specmark DEC-ALPHA workstation.

The program CATIA is divided into three main procedures. The first procedure consists of the pre-processor. This procedure reads the input data, the initial

and boundary conditions and prepares the data for the main processor. The second procedure is the main processor which calculates the unbalanced forces, the associated tangent matrix and solves the resulting set of non-linear algebraic equations by the Newton-Raphson method. Finally, the third procedure is the post-processor where the results are placed in files and prepared tin a format suitable for graphic presentation.

Table E.1 shows the program's main routines. Next, a description of the three main procedures of CATIA is made. All quantities are input in SI units.

E.2 - Pre-processor

The pre-processor is the procedure responsible for the data input and for the preparation of this data for the main processor. The pre-processor uses the subroutines DATIN, CAB_PRP, C_BETA, MESH0, MESH1 and TOP_INFO.

Subroutine DATIN

The subroutine DATIN reads the input data from the keyboard, The input data is structured in three main types of data, namely, numerical and control data, cable data and kinematic data.

The numerical and control data consist of the following data:

Type of analysis: (1) LAYING, (2) TOWING.
Number of elements.
Number of steps in time.
Number of steps to print the results.
Switch for wave analysis: (0) OFF, (1) ON.

```
Program Catia

begin

call datin
call cab_prp
call c_beta
call mesh0
call mesh1

do itime = 1, nstp

        time = itime * nspt
        call top_info

        while convergence is not achieved

                call jglob
                call fglob
                call fnorm
                call unorm
                call solve_sys
                call update_u

        end while

        call update_u0t
        call mesht
        print result

  end do

end
```

Table E.1 - Main routines of CATIA

The cable data are:

Tangential drag coefficient.

Diameter (m).

Bending stiffness (Nm^2).

Hydrodynamic constant $(rad * m/s)$.

Length (hanging cable analysis) (m).

Physical mass (kg/m).

The kinematic data are:

Vessel initial forward speed (m/s).

Vessel final forward speed (m/s).

Vessel acceleration (m/s^2).

Water depth (cable touching the seabed) (m).

Wave data (wave analysis ON)

Wave period (s).

Wave height (m).

Surge RAO (m/m).

Surge phase (rad).

Heave RAO (m/m).

Heave phase (rad).

Subroutine CAB_PRP

This subroutine prepares the data for entering into the main processor. It calculates the weight in air per unit length, the submerged weight per unit length normal drag coefficient and the added mass per unit length.

The weight in air is given by the expression:

$$w_{air} = mg \tag{E.1}$$

where m is the cable physical mass per unit length and g is the gravitational acceleration. The submerged weight is obtained by subtracting the weight of the displaced fluid from the weight in air. Hence:

$$w = (m - \rho A)g \tag{E.2}$$

where ρ is the fluid density and A is the cable's cross-sectional area. The added mass is the mass of fluid affected by the cable's acceleration which is given by:

$$m_a = C_M \rho A \tag{E.3}$$

where the added mass coefficient C_M is assumed to be one. Finally, the normal drag coefficient is calculated from the definition of the hydrodynamic constant. That is:

$$C_D = \frac{2w}{\rho d H^2} \tag{E.4}$$

where w is the submerged weight, ρ is the fluid density, d is the diameter and H is the hydrodynamic constant.

Subroutine MESH0

This subroutine generates the initial mesh from the initial condition for the very first time step. The initial condition consists of the stationary straight line solution.

Subroutine MESH1

The subroutine MESH1 gives the initial estimate for the position which satisfies the dynamic equilibrium of the equations of motion.

Subroutine TOP_INFO

This routine applies the boundary conditions at the top end of the cable. The boundary conditions are the position, velocity and acceleration for the top point. The tension boundary condition is defined by the zero bottom tension condition.

E.3 - Main Processor

The main processor is responsible for the implementation of the numerical solution of the differential equations of motion. The numerical solution consists of the time integration through the Newmark method which uses the trapezoidal rule. That is it assumes the values 0.25 and 0.50 for the coefficients α and δ, respectively. The space integration is performed by a finite element method based on the Galerkin weighted residual method. This procedure leads to a set of non-linear algebraic equations that is then solved by the Newton-Raphson method. The Newton-Raphson method is an iterative procedure that approximates the zeroes of a multivariable vector function which in this case is the gradient. The method starts with an initial estimate that should be close to the true solution otherwise the method may not converge. Values for the gradient and for the Jacobian matrix are calculated. The new position is calculated by adding the initial position to the product of the inverse Jacobian matrix times the gradient. This process is repeated until convergence is achieved. Convergence is achieved when the norms of the gradient and the

norm of the difference of the displacement vectors for two successive iterations is also less than a specified tolerance. In this work such tolerances were taken as 0.001 and 0.0001 respectively.

The main processor uses the following routines:

Subroutine JGLOB

The subroutine JGLOB determines the global Jacobian matrix. It uses the central finite difference method to determine the matrix numerically.

Subroutine FGLOB

The subroutine FGLOB calculates the global gradient vector which is the vector of the global forces. In order to obtain this vector the local forces for each element are calculated. These forces are calculated by applying the Newmark method and then performing the Galerkin integral numerically. The numerical integration in this work uses a five point Gauss quadrature algorithm.

Subroutine SOLVE_SIS

This subroutine solves a linear set of algebraic equations using Gaussian elimination. The subroutine takes advantage of the concentration of non-zero terms near the matrix diagonal.

Subroutine UPDATE_U

This subroutine updates the displacement vector for next iteration. The expression for the new displacement vector is:

$$\mathbf{U} = \mathbf{U}_0 + \mathbf{J}^{-1}\mathbf{F} \tag{E.5}$$

where $\mathbf{U}_0$ is the displacement vector at the beginning of the step, $\mathbf{J}$ is the global Jacobian matrix and $\mathbf{F}$ is the global unbalanced force vector.

E.4 - Post-Processor

Once the Newton-Raphson method converges for a given time step, results are processed for the next time step as well as for plotting the required graphs. The post-processing routines are UPDATE_U0T, MESHT and RESULT. The subroutine UPDATE_U0T gives the initial condition for the next time step. This initial condition corresponds to the displacement vector for which convergence was achieved. The subroutine MESHT gives the initial estimate for the next time step while the subroutine RESULT prepares data for plotting. There are four types of plotting in CATIA. These plots are the cable configuration, the slope against time, the top tension against time and the suspended length against time. The latter graph is plotted for cases where the cable touches the seabed.

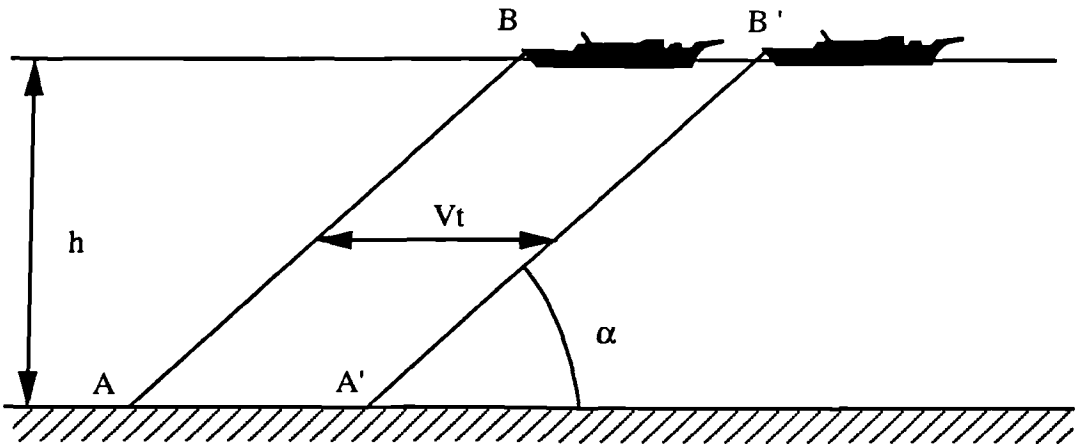

Figure 1.1 - Cable laying.

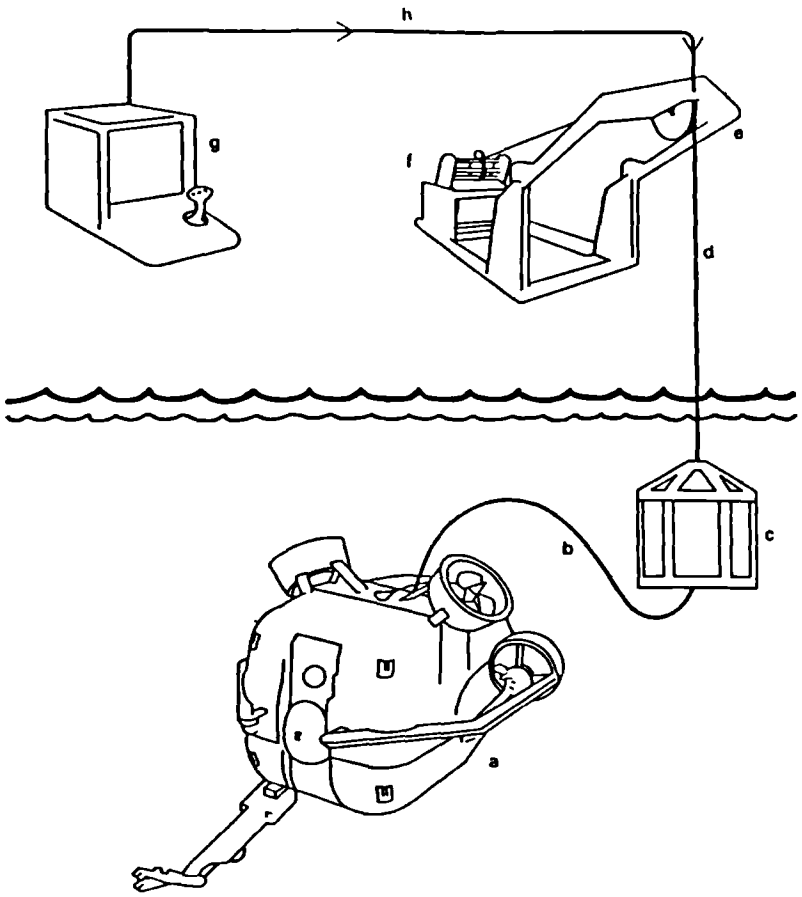

Figure 1.2 - Unmanned underwater operations. Key: a-remotely operated vehicle; b-umbilical; c-launching restraint;d- lifting and control cable; e-launching A frame; f-winch; g-control station;h-control signals (After Patel,1989).

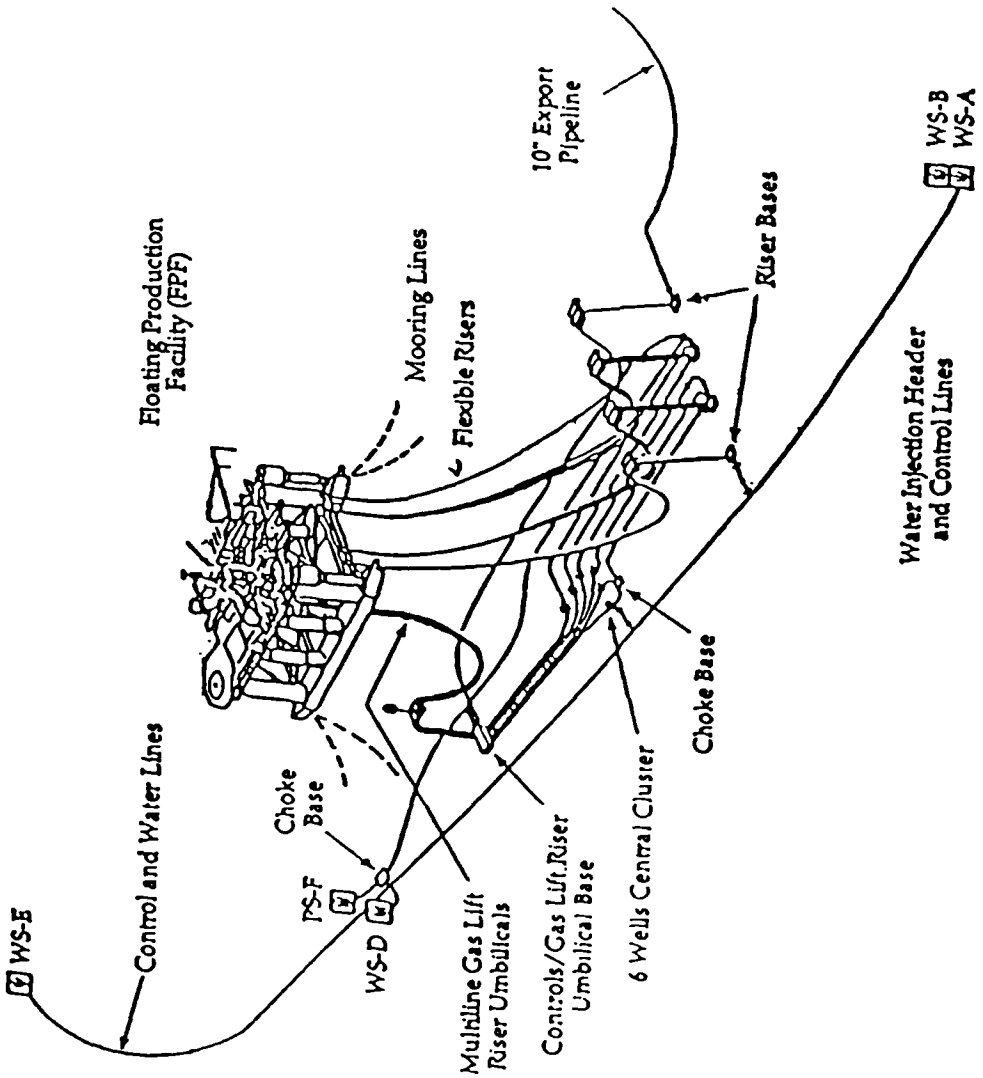

Figure 1.3 - Field development scheme at Emerald.

Figure 1.4 - Loop formation.

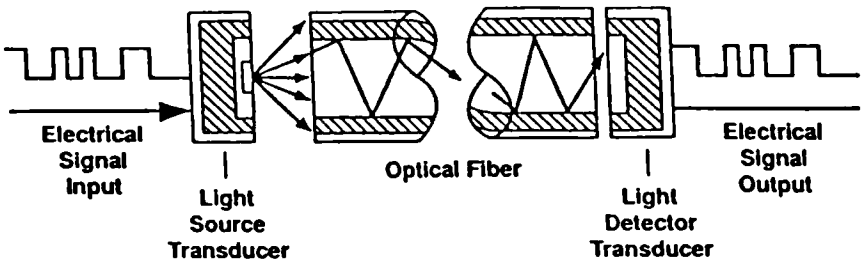

optical fiber link

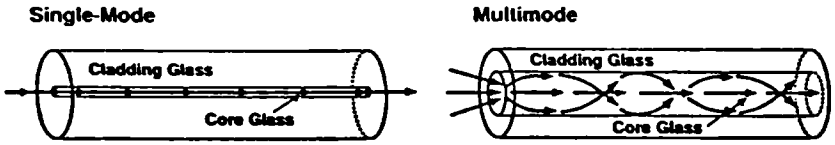

two basic types of optical fiber

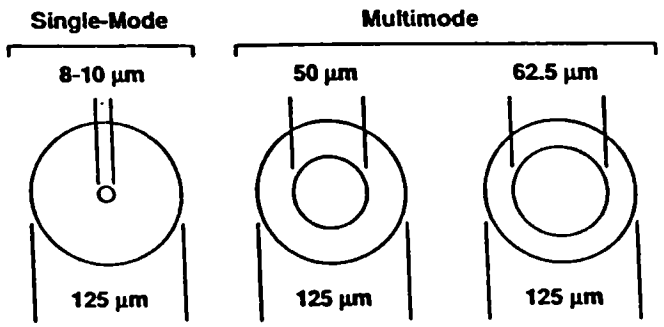

optical fiber sizes

Figure 1.5 - Optical fibre technology.

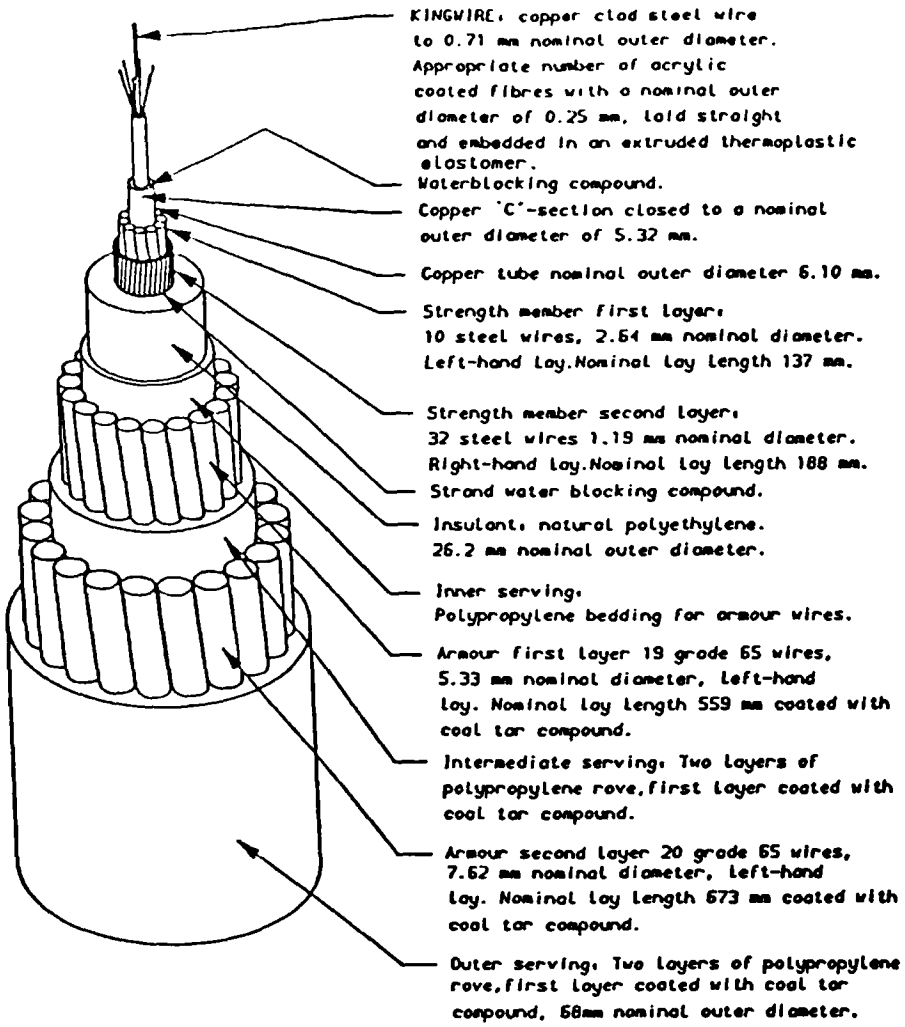

NOMINAL PHYSICAL CHARACTERISTICS OF CABLE

Doubled Armoured Type A65F65, 19/5.33mm and 20/7.62mm Grade 65 GSW

Inner serving diameter	30 mm
First pass amouring diameter	40 mm
Intermediate serving diameter	47 mm
Second pass armouring diameter	61 mm
Outer serving diameter	68 mm
Total cable weight in air	13.23 tonnes km^{-1}
Total cable weight in water	9.51 tonnes km^{-1}
Stowage factor	5.42 m^3 km^{-1}
Minimum load at 1% strain	900 kN
Maximum load for residual 0.1% strain	700 kN
Minimum bend dia. (Finished Cable)	1.8 m
Minimum storage diameter	2.0 m
Composite Power Feed Conductor Resistance	<0.70ohm km^{-1}@10°c
Insulation Resistance	>2 x 10^{11} ohm km^{-1}
Composite Power Feed Conductor Capacitance	0.192µf km^{-1}
King Wire Resistance	140 ohm Km^{-1}@10°c

Figure 1.6 - Typical optical fibre marine cable (STC).

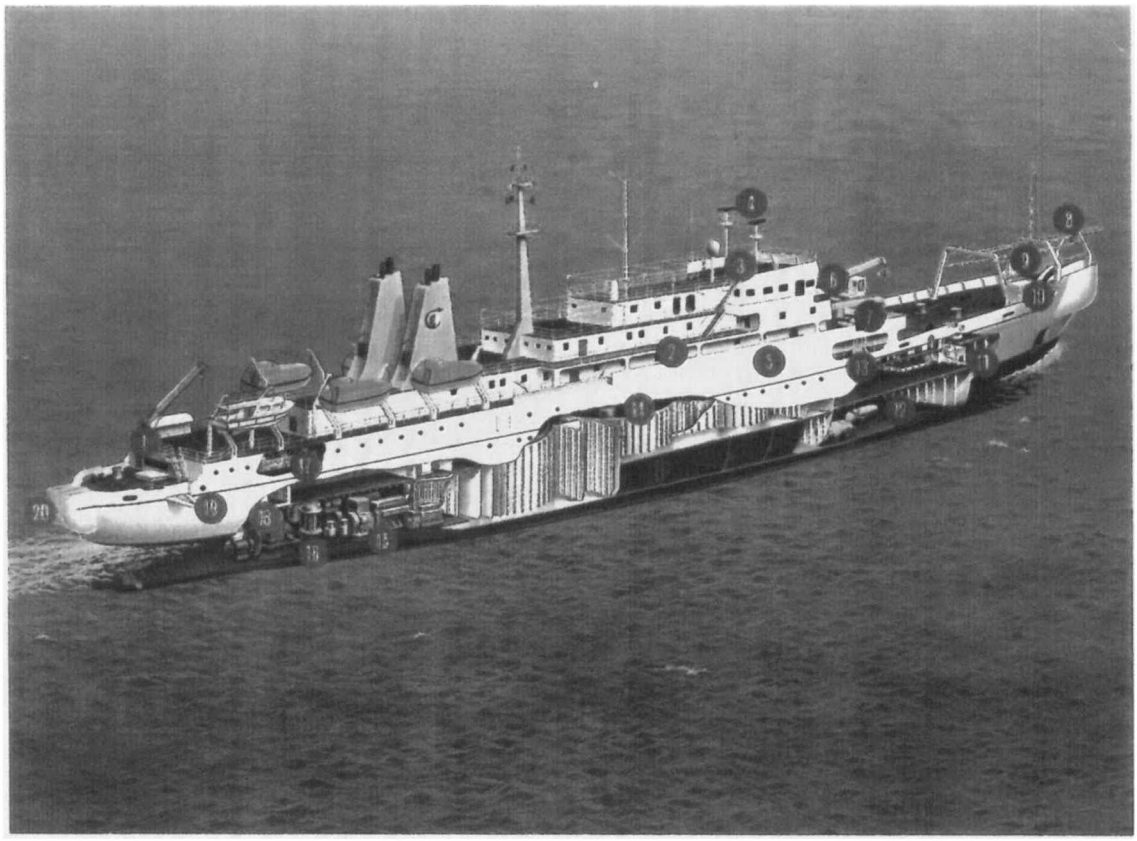

1. Taut Wire Room
2. Officers' and Cable Representatives' Accommodation
3. Wheelhouse, Chartroom and ROV Control Room
4. Radar (P & S)
5. Cable Working Deck
6. Electro-Hydraulic Telescopic Crane for ROV Deployment
7. Remotely Operated Vehicle
8. Bow Monorail Hoist
9. Bow Cable Sheaves
10. Bow Control Room
11. Bow Thruster
12. Cable Equipment Store
13. Buoy Cradle (P & S)
14. Cable Storage Tanks (Main Deck Removed)
15. Main Engine (P & S)
16. Stern Thruster
17. Linear Cable Engine
18. Propulsion Motor
19. Bumkin (P & S)
20. Cable Stern Sheave

Figure 1.7 - Typical cable lay vessel.

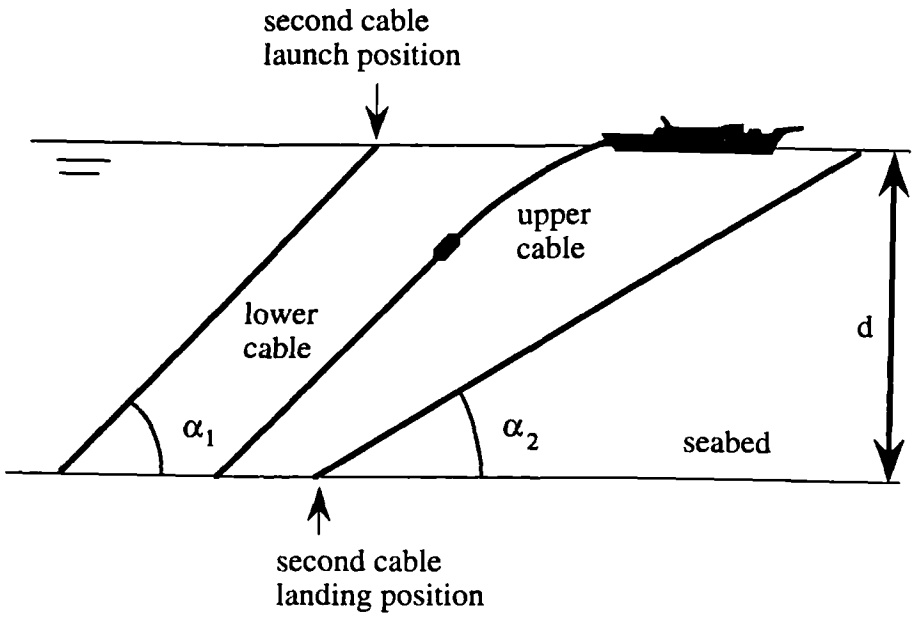

Figure 1.8 - Repeater launch.

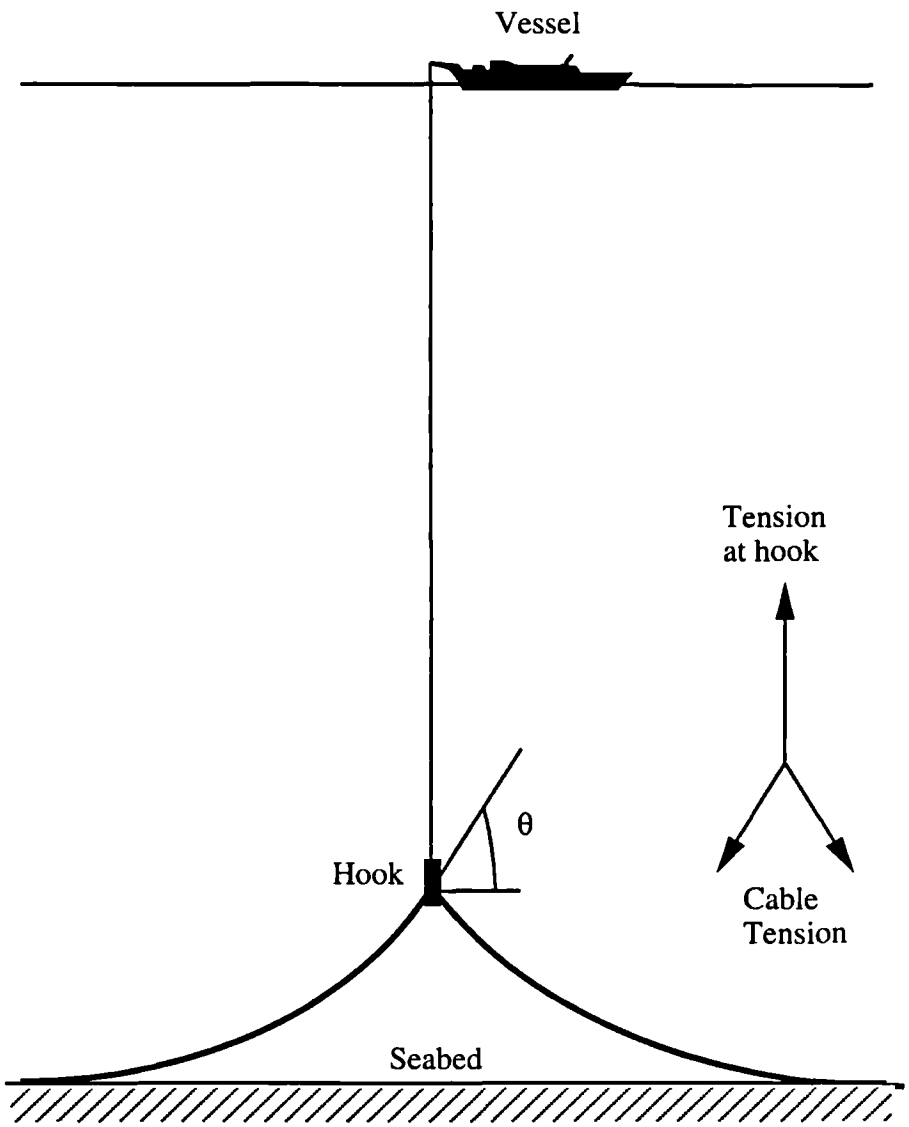

Figure 1.12 - Bight raising.

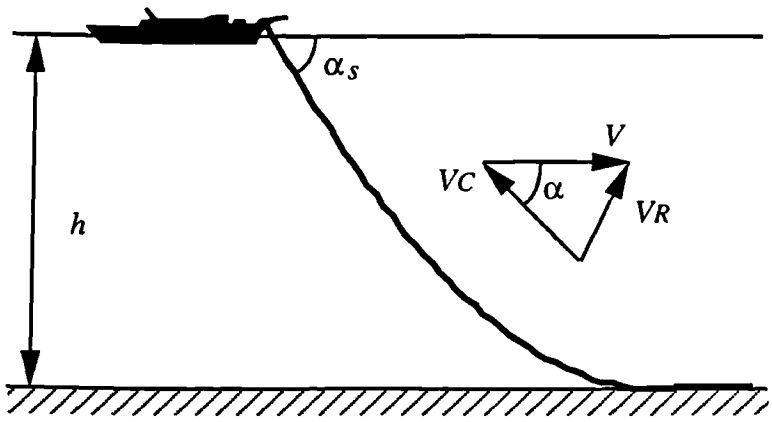

Figure 1.14 - Conventional procedure for cable recovery.

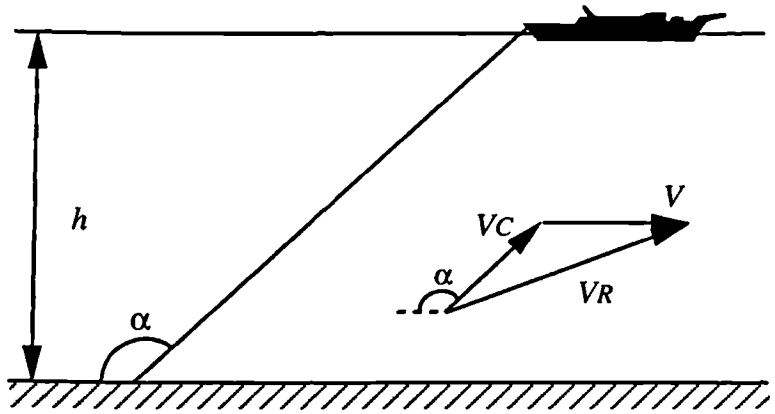

Figure 1.15 - Shea's procedure for cable recovery.

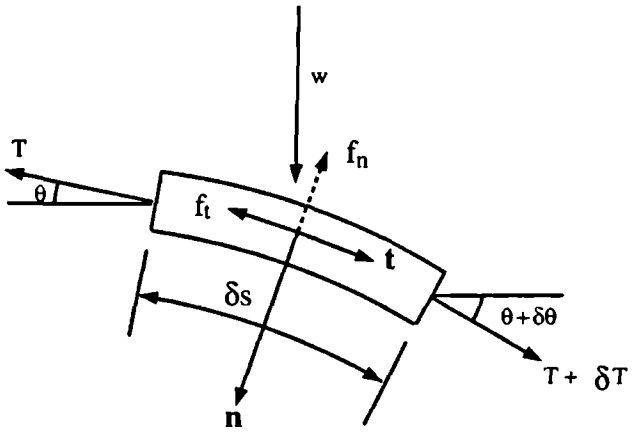

Figure 2.1 - Two dimensional element of cable.

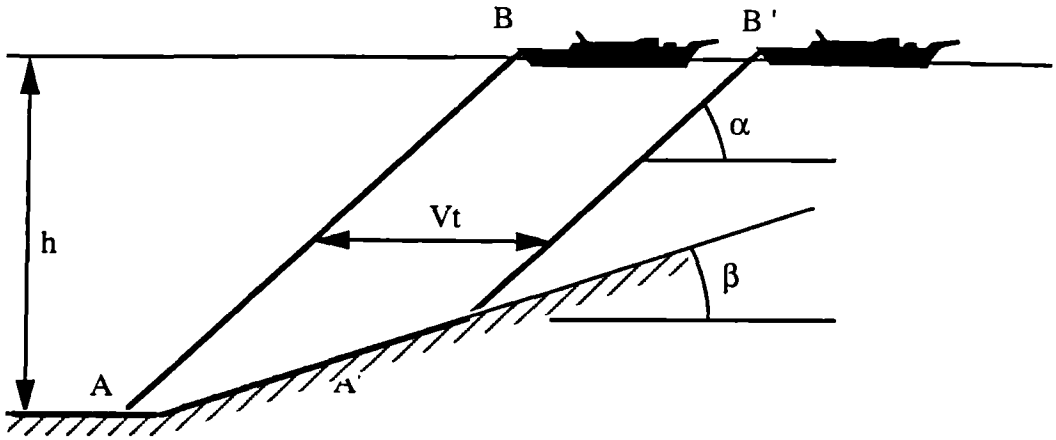

Figure 2.3 - Cable laying in a sloping seabed.

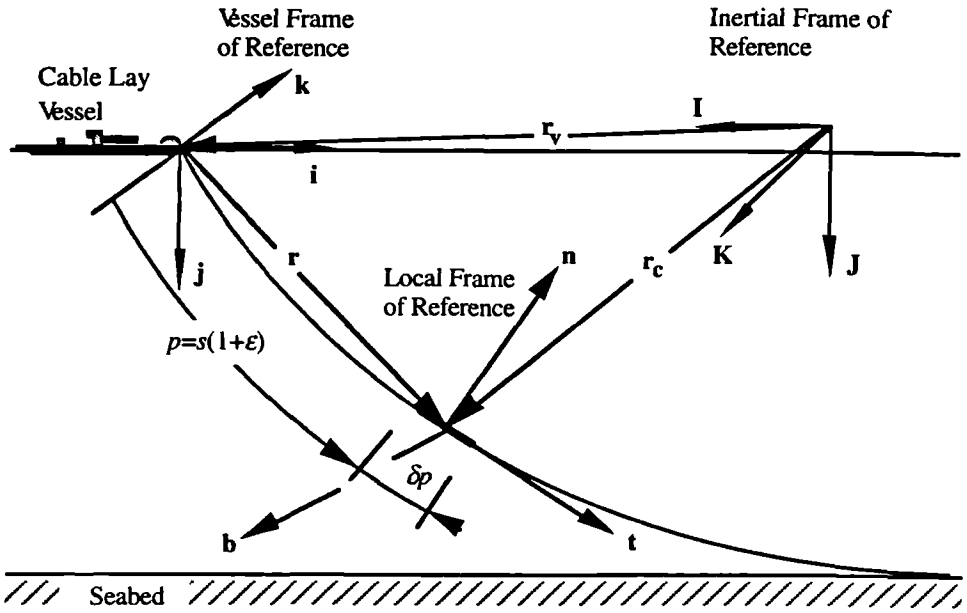

Figure 3.1 - Three dimensional reference system.

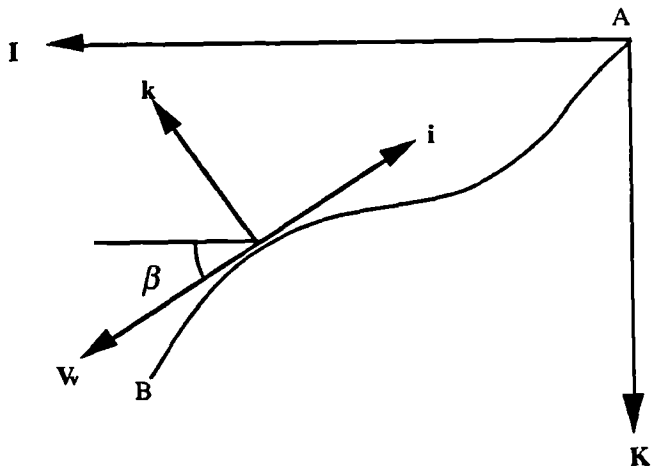

Figure 3.2 - Generic vessel path.

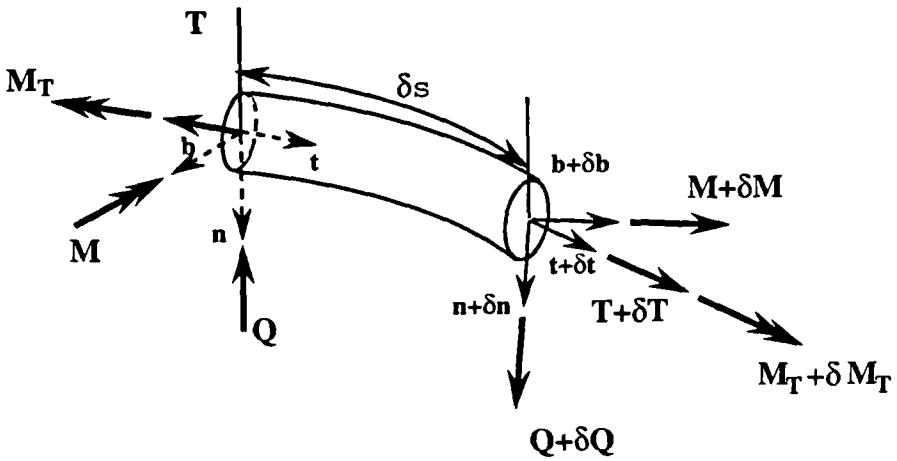

Figure 3.3 - Three dimensional element of cable.

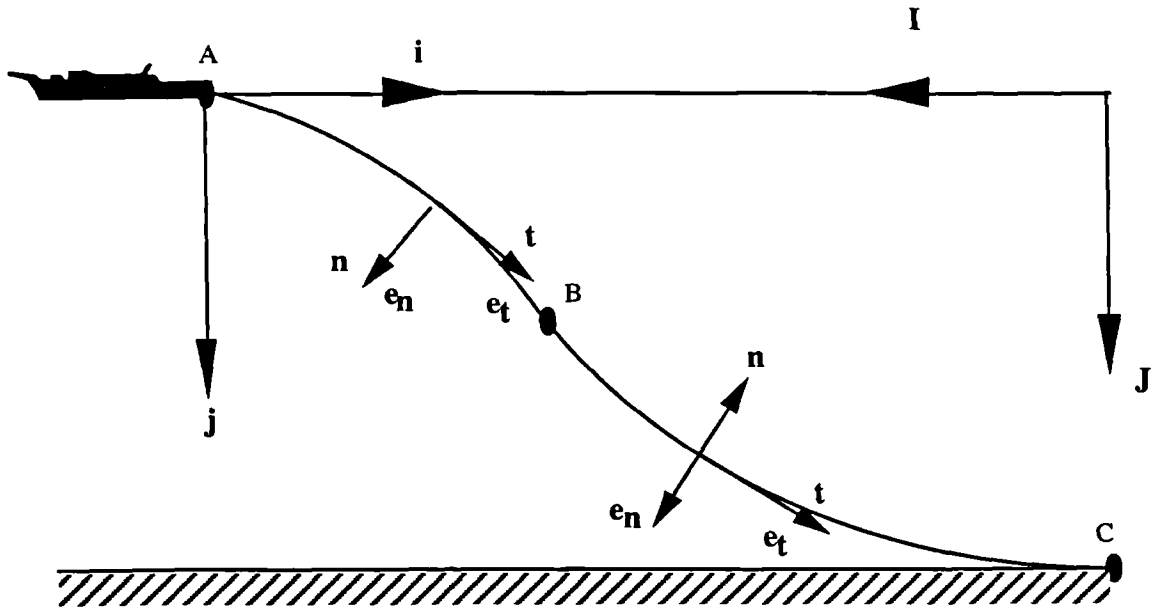

Figure 4.1 - Two dimensional reference system.

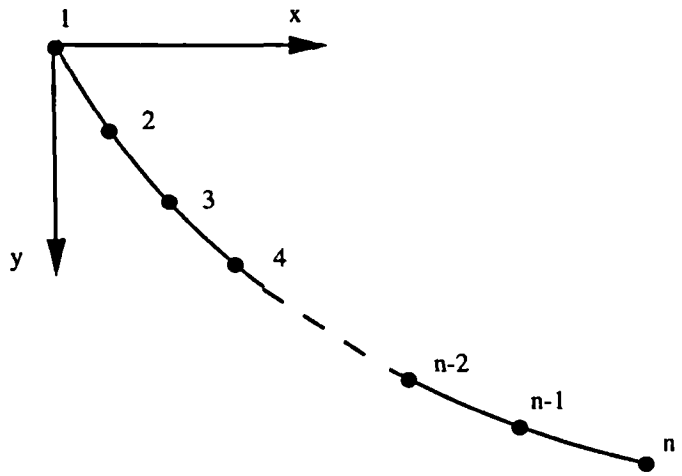

Figure 4.2 - Cable's finite element mesh.

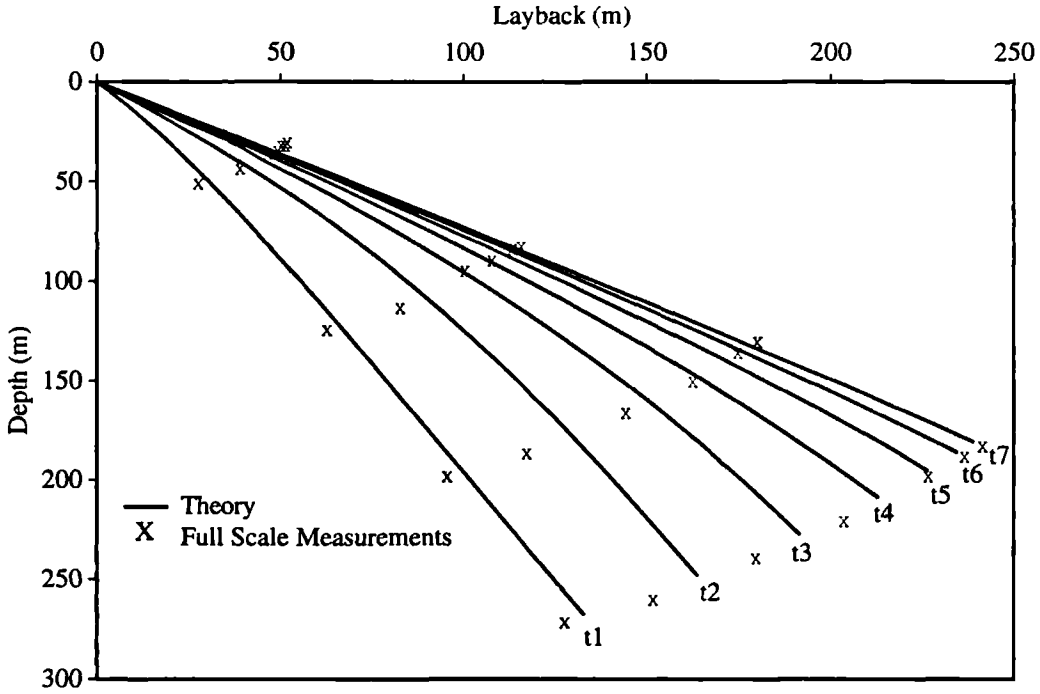

Figure 5.1 - Configuration for towed heavy cable; speeding up.

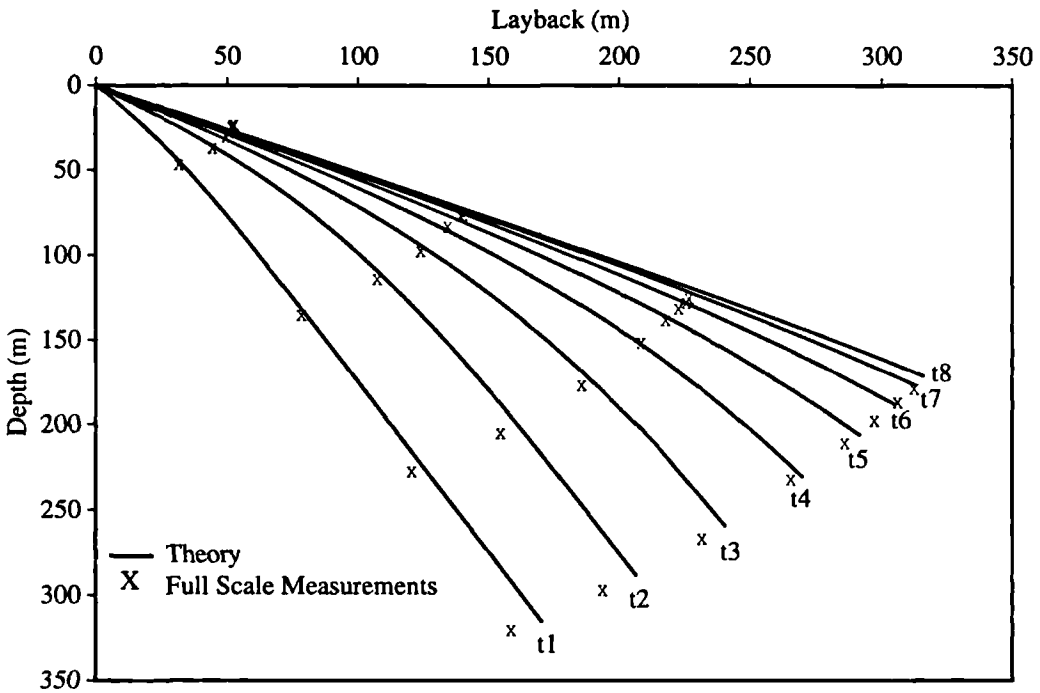

Figure 5.2 - Configuration for towed light cable; speeding up.

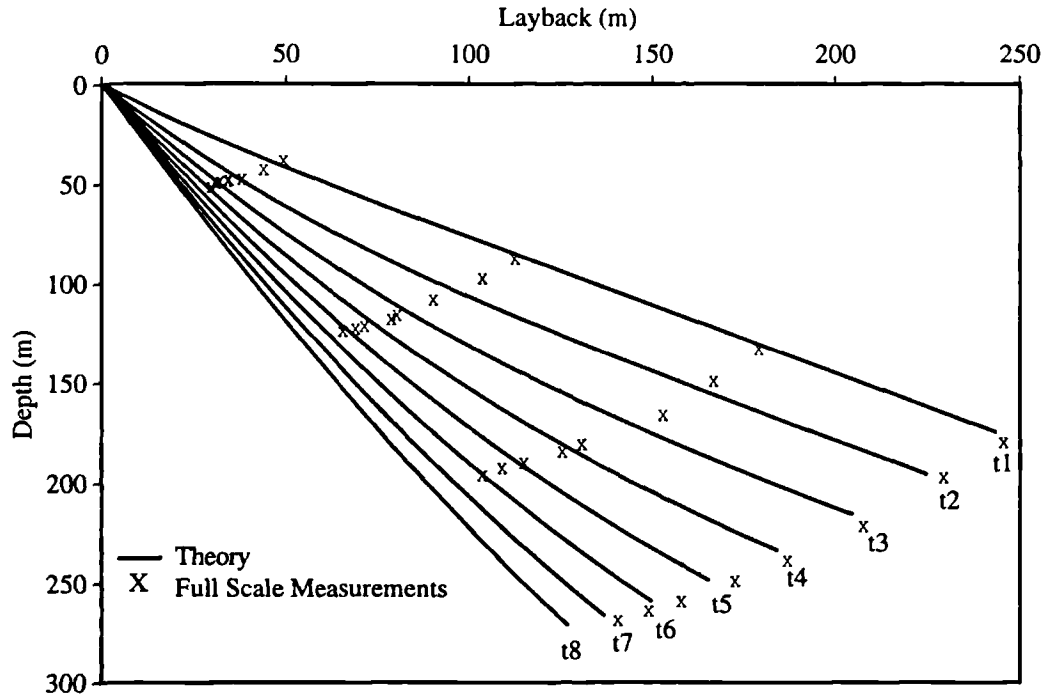

Figure 5.3 - Configuration for towed heavy cable; slowing down.

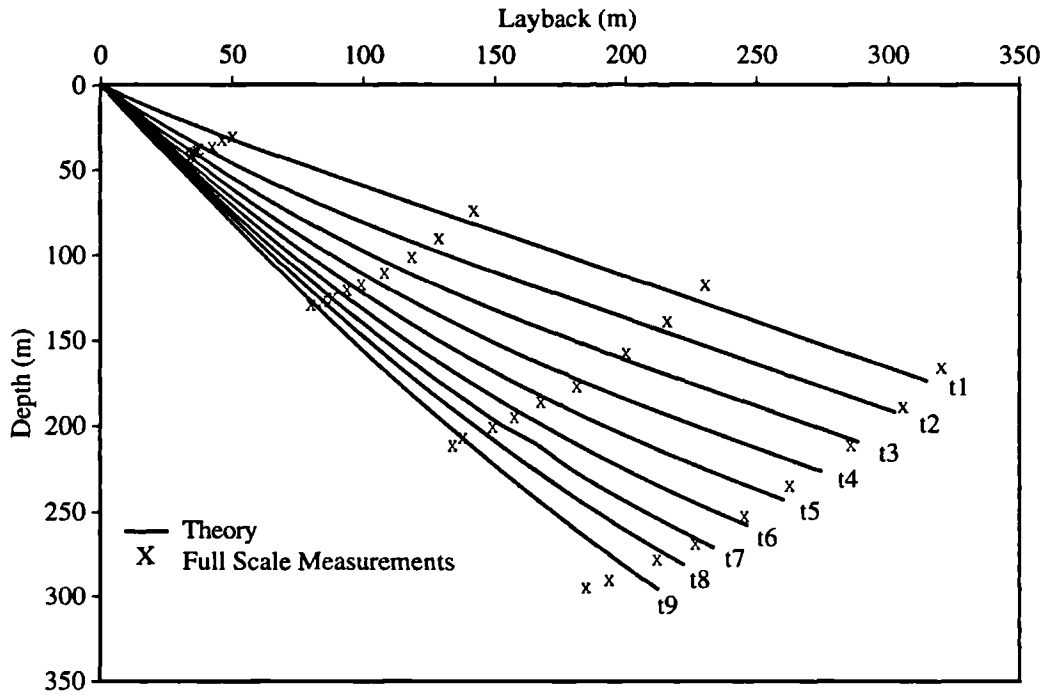

Figure 5.4 - Configuration for towed light cable; slowing down.

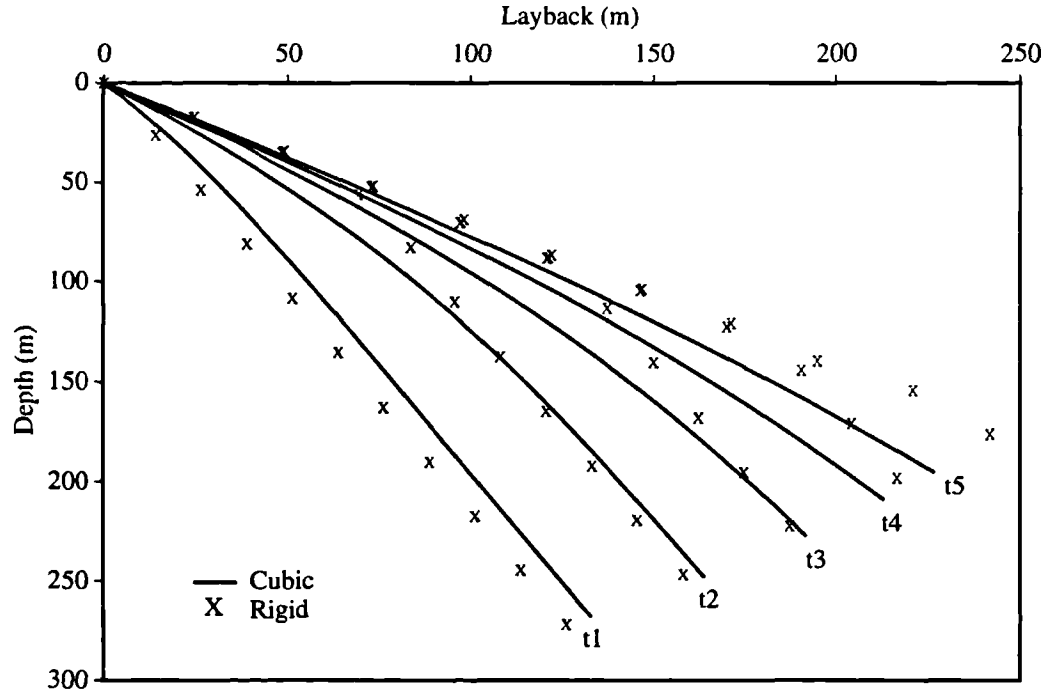

Figure 5.5 - Configuration for towed heavy cable; speeding up.

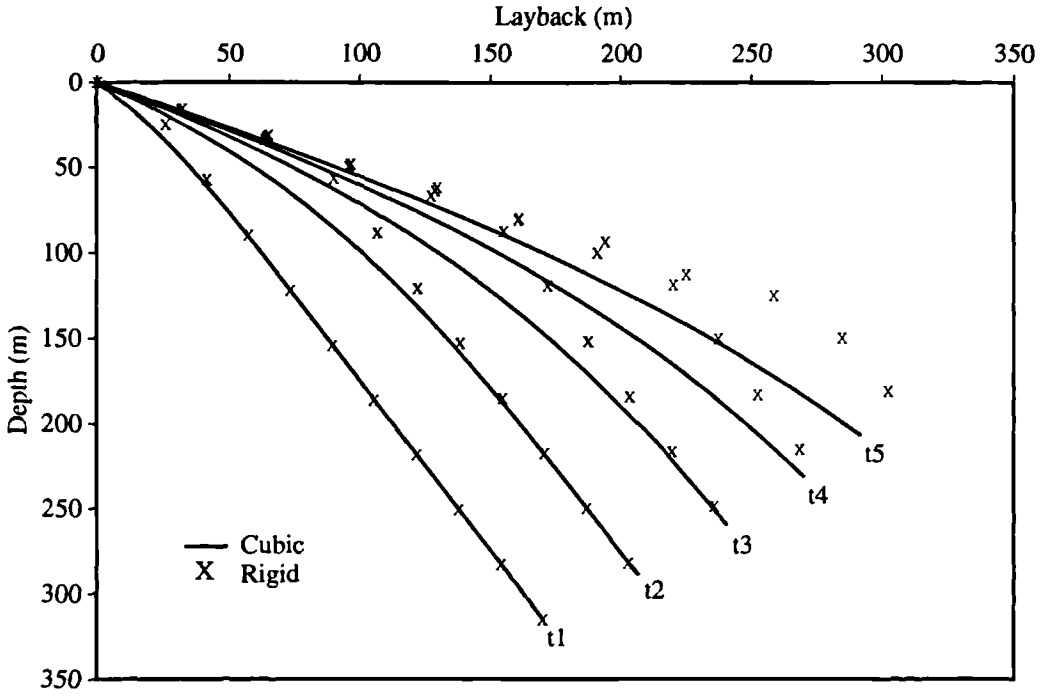

Figure 5.6 - Configuration for towed light cable; speeding up.

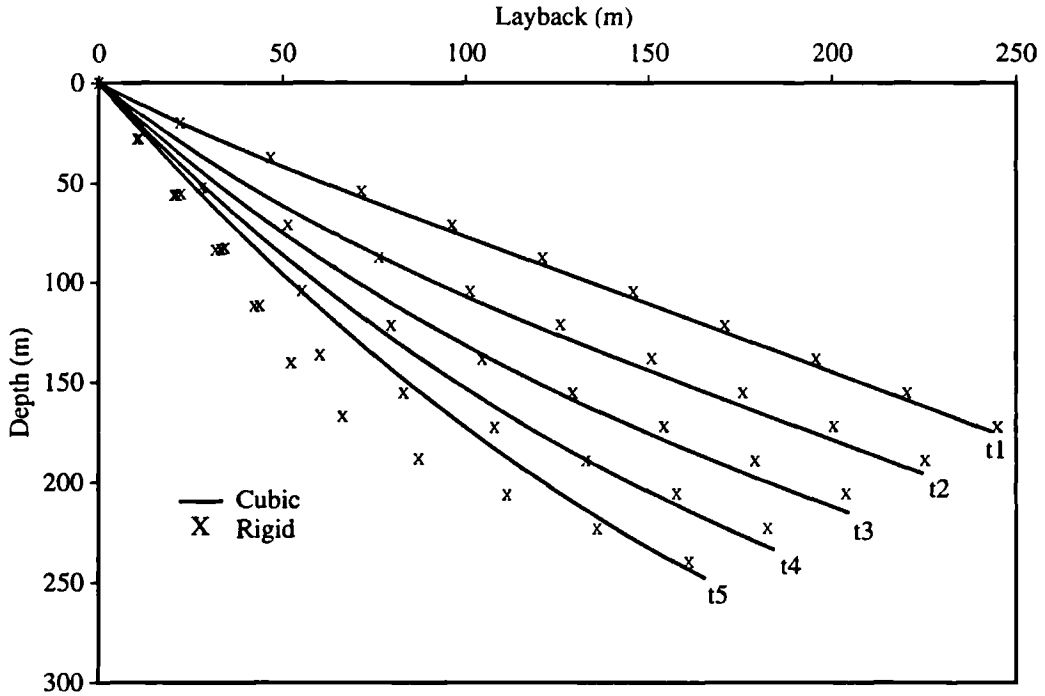

Figure 5.7 - Configuration for towed heavy cable; slowing down.

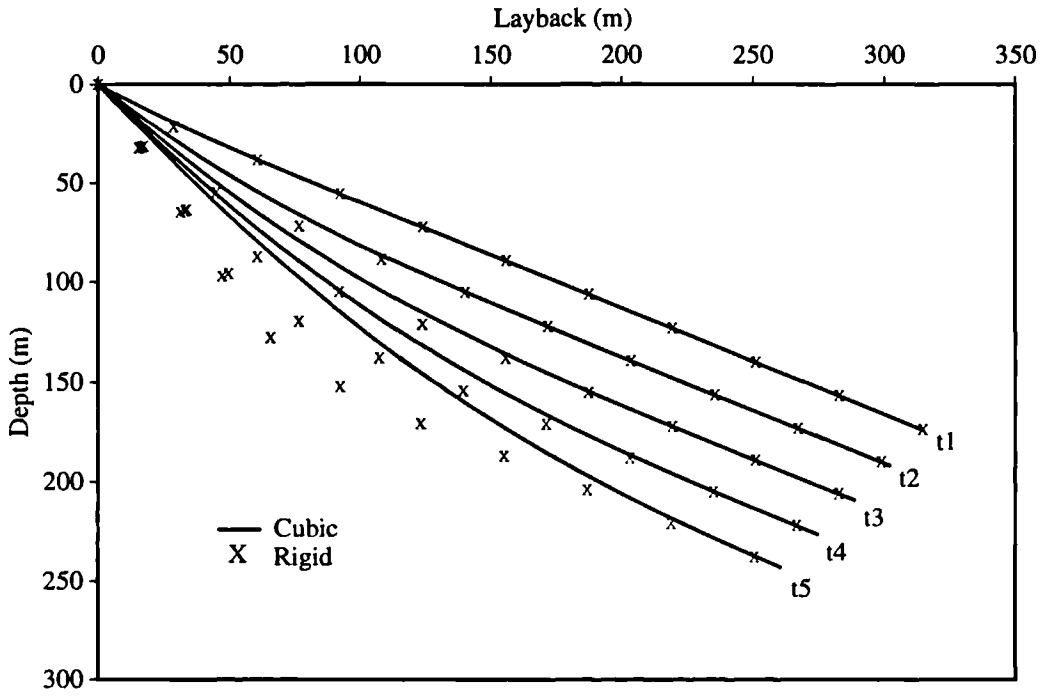

Figure 5.8 - Configuration for towed light cable; slowing down.

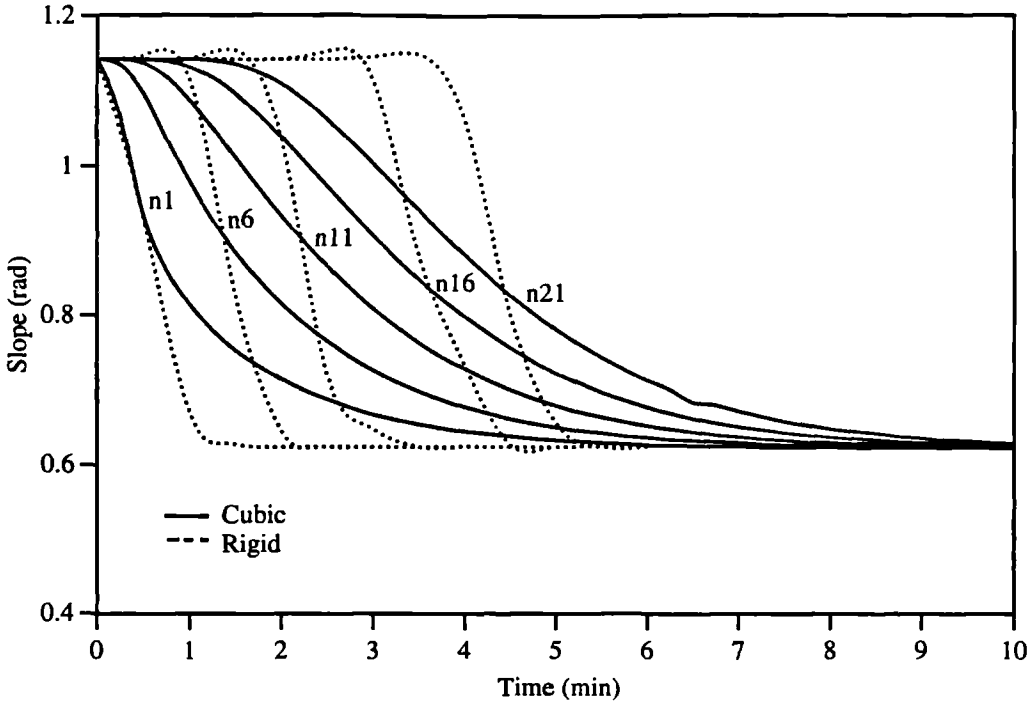

Figure 5.9 - Slope for towed heavy cable; speeding up.

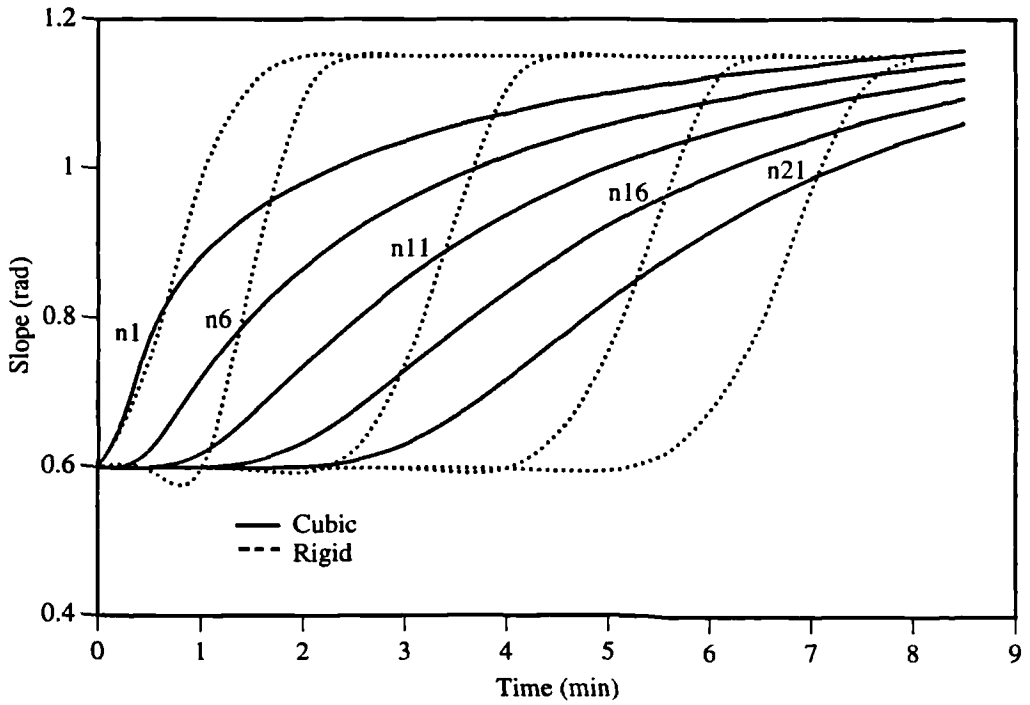

Figure 5.10 -Slope for towed heavy cable; slowing down.

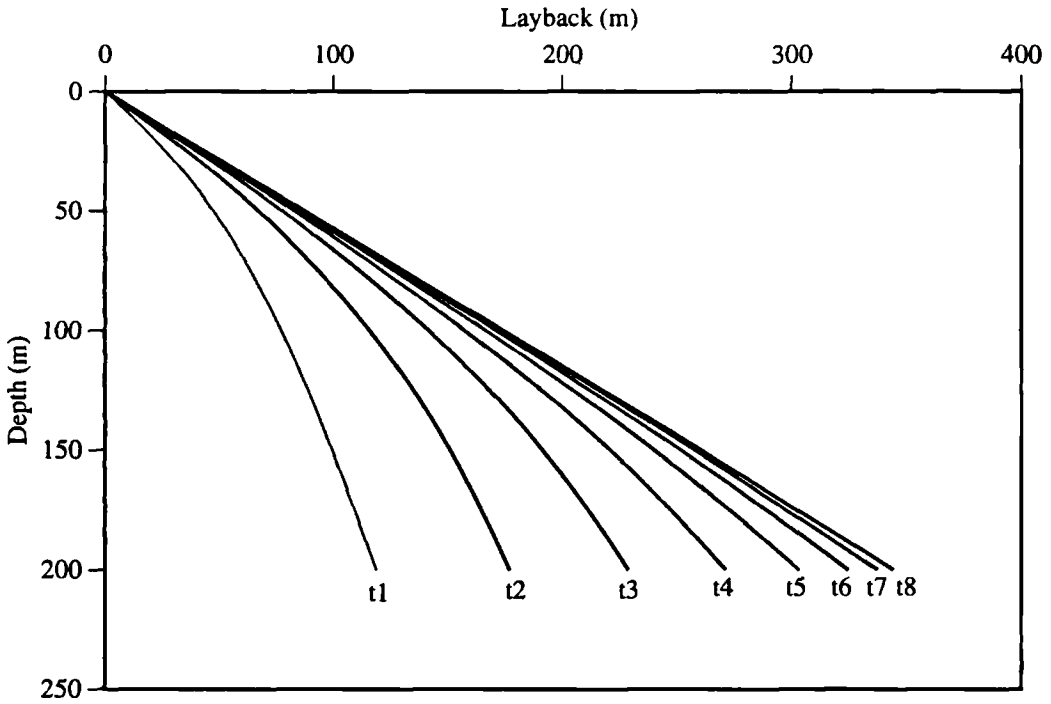

Figure 5.11 - Configuration for simulation HASL.

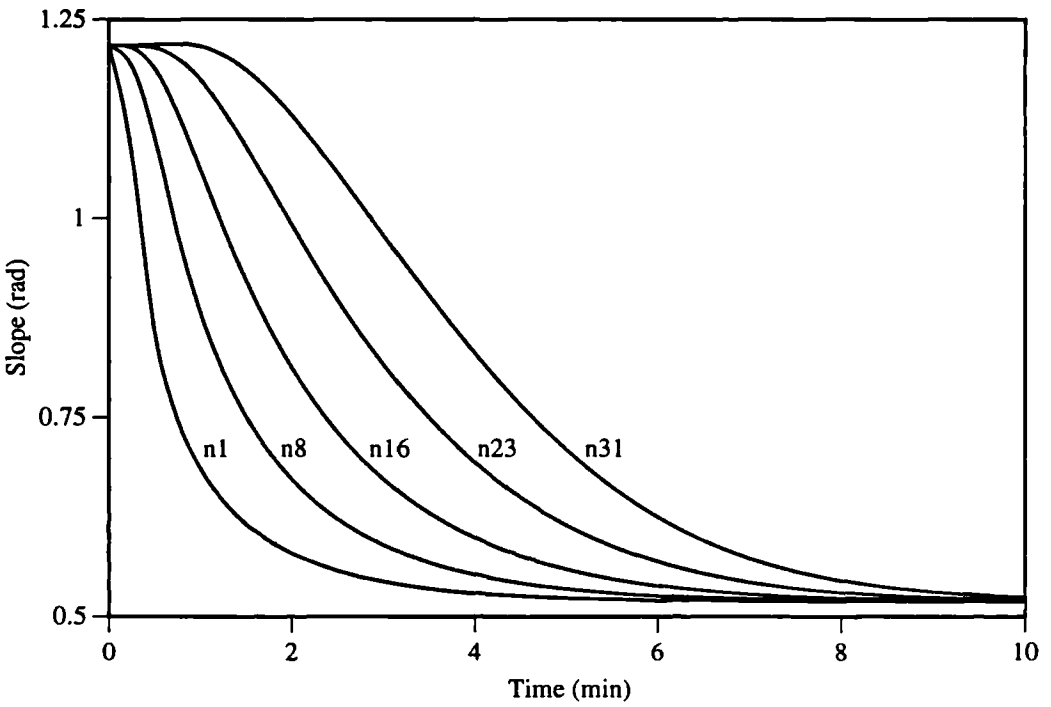

Figure 5.12 - Slope versus time for simulation HASL.

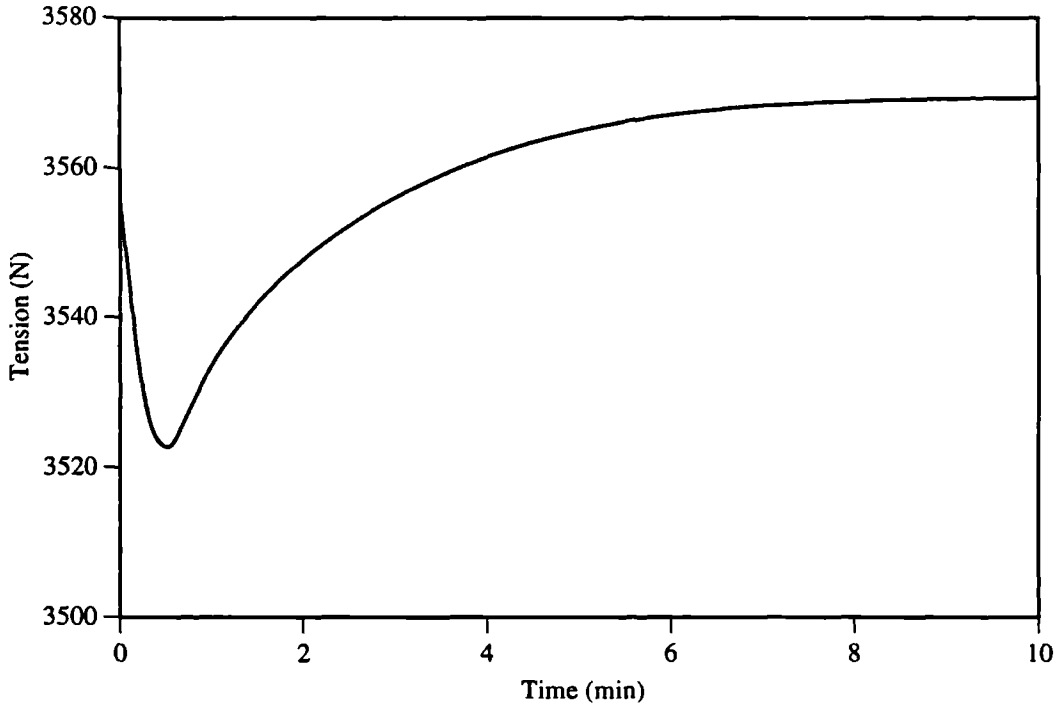

Figure 5.13 - Top tension versus time for simulation HASL.

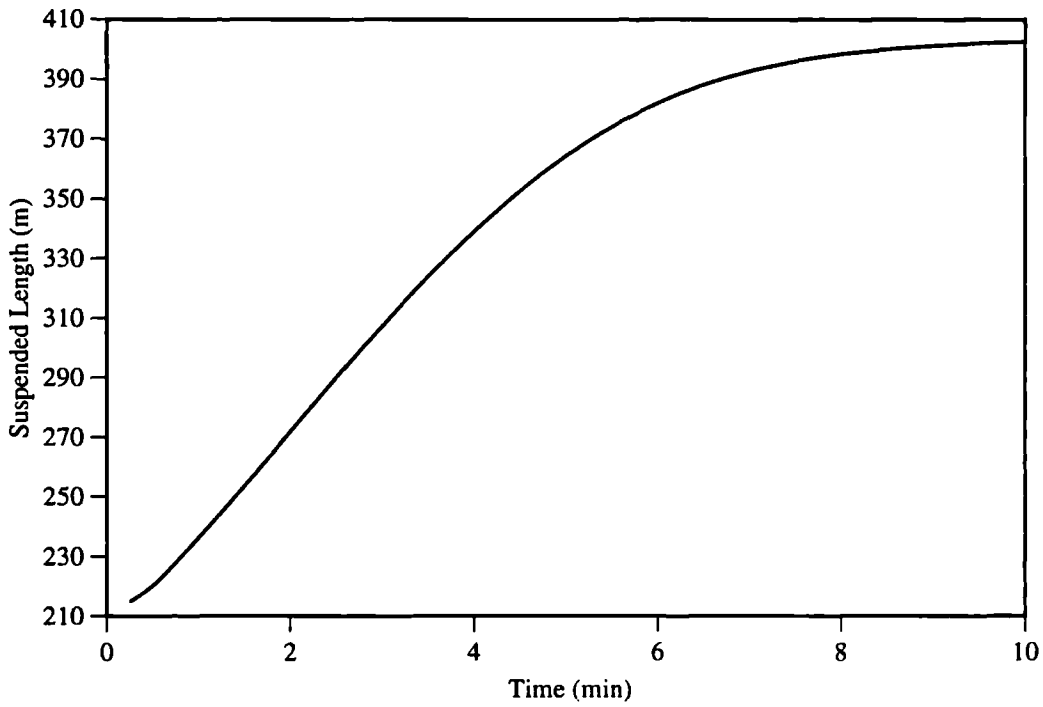

Figure 5.14 - Suspended length versus time for simulation HASL.

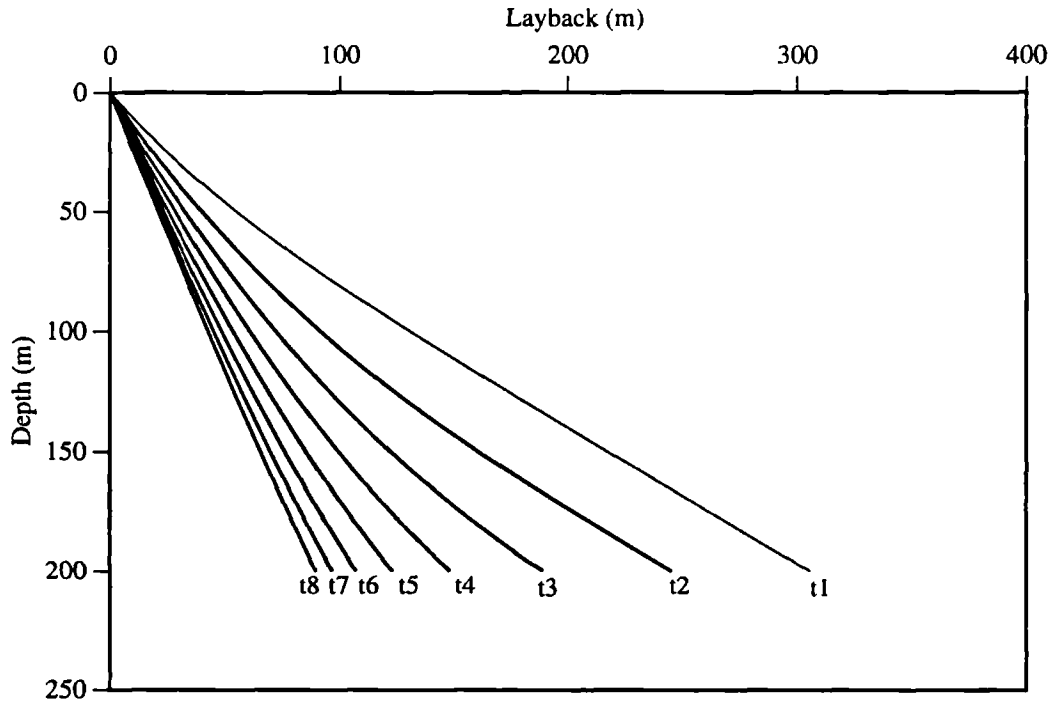

Figure 5.15 - Configuration for simulation HDSL.

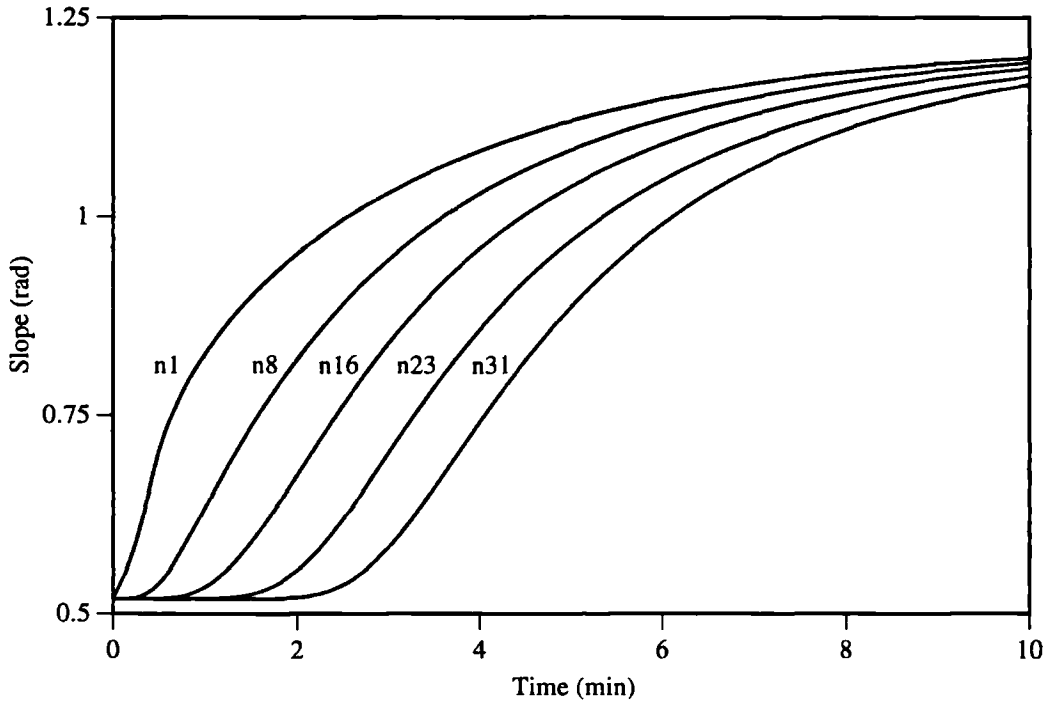

Figure 5.16 - Slope versus time for simulation HDSL.

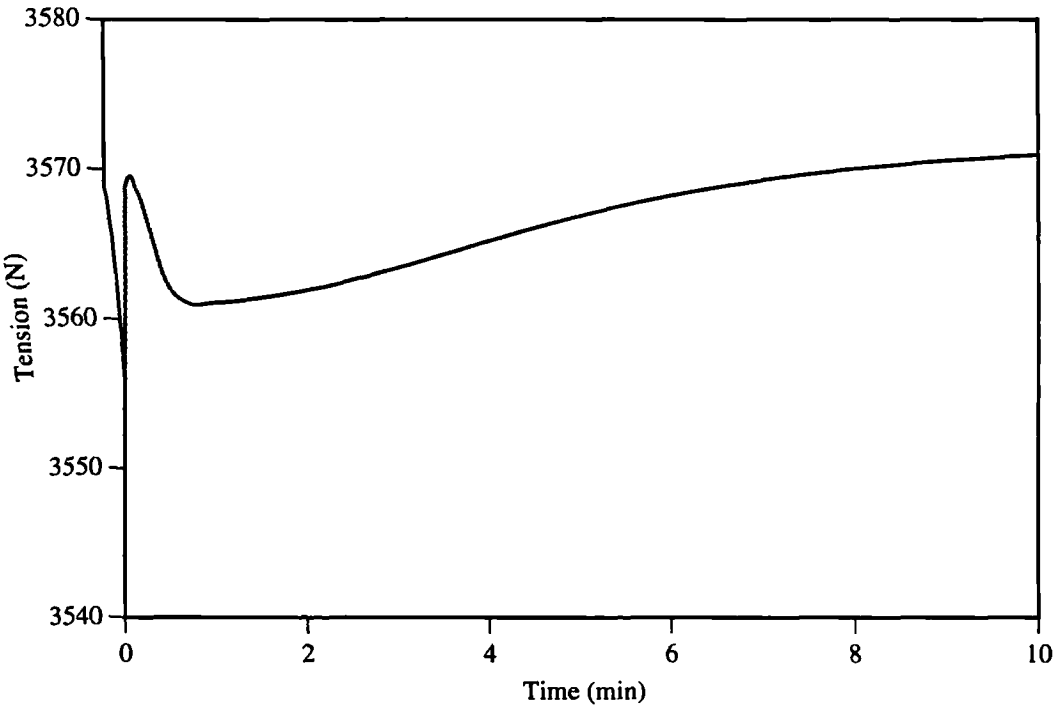

Figure 5.17 - Top tension versus time for simulation HDSL.

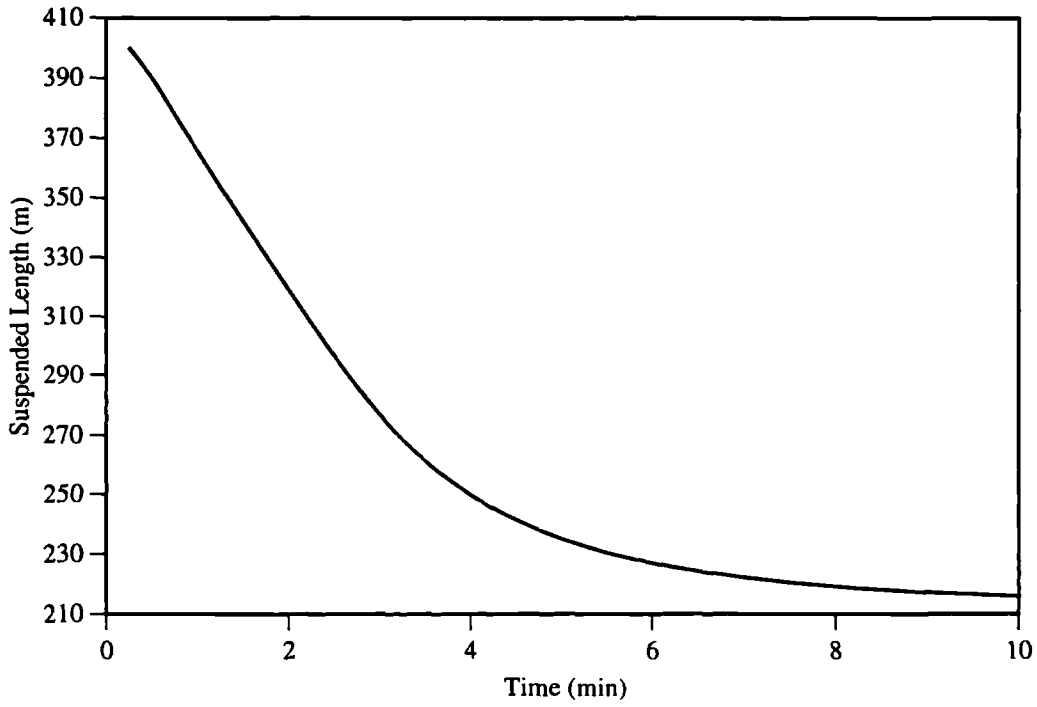

Figure 5.18 - Suspended length versus time for simulation HDSL.

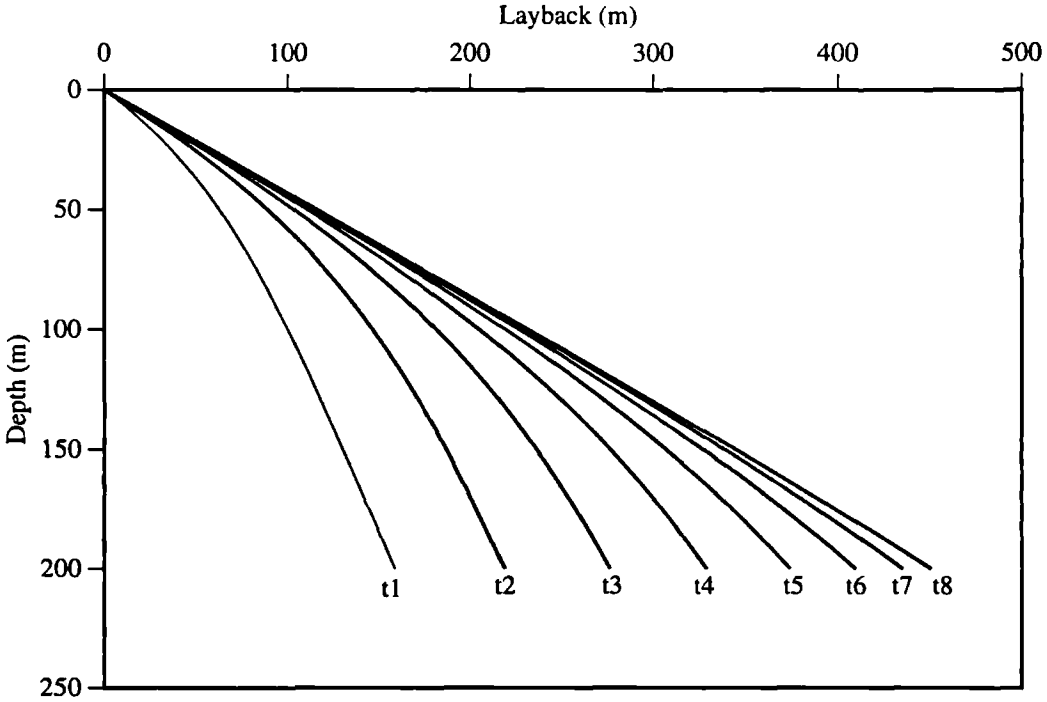

Figure 5.19 - Configuration for simulation LASL.

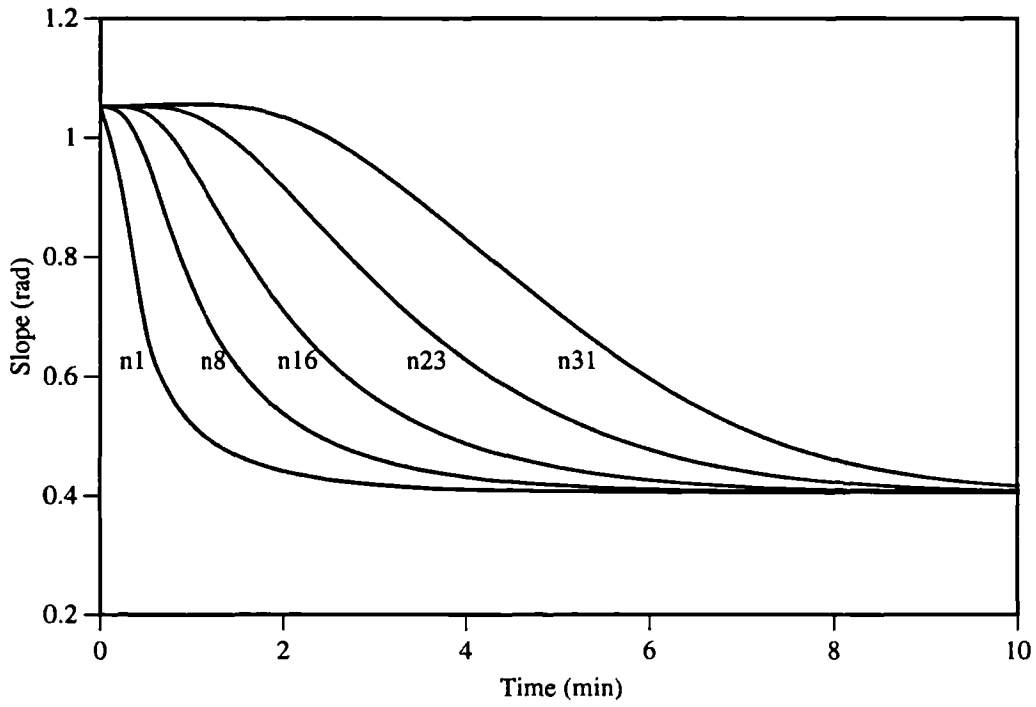

Figure 5.20 - Slope versus time for simulation LASL.

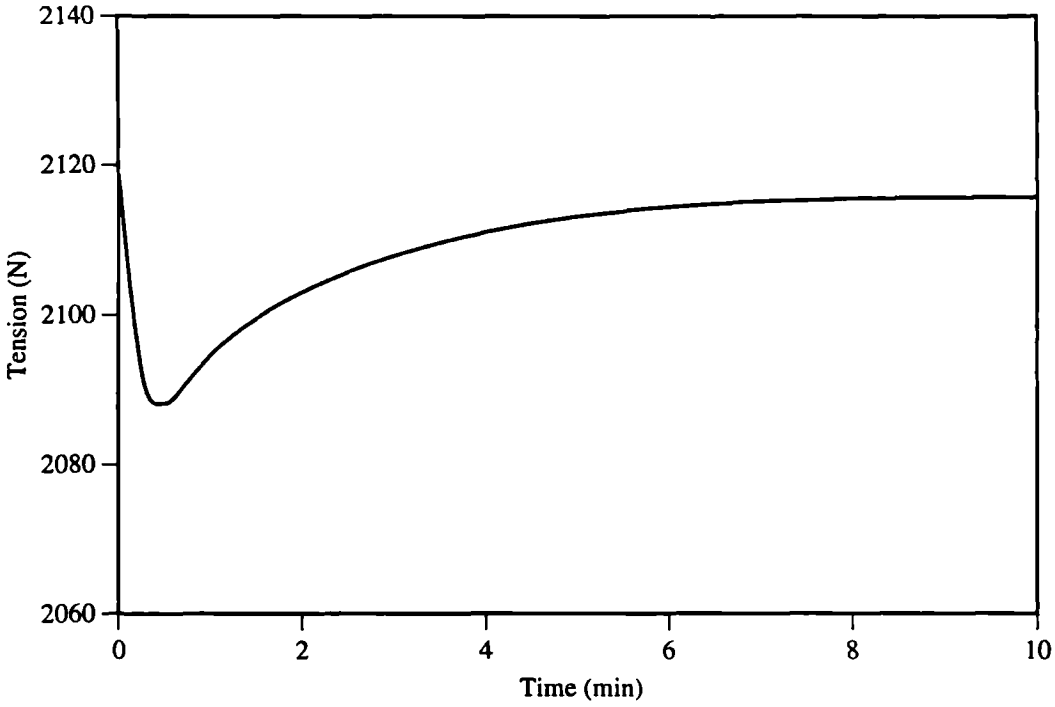

Figure 5.21 - Top tension versus time for simulation LASL.

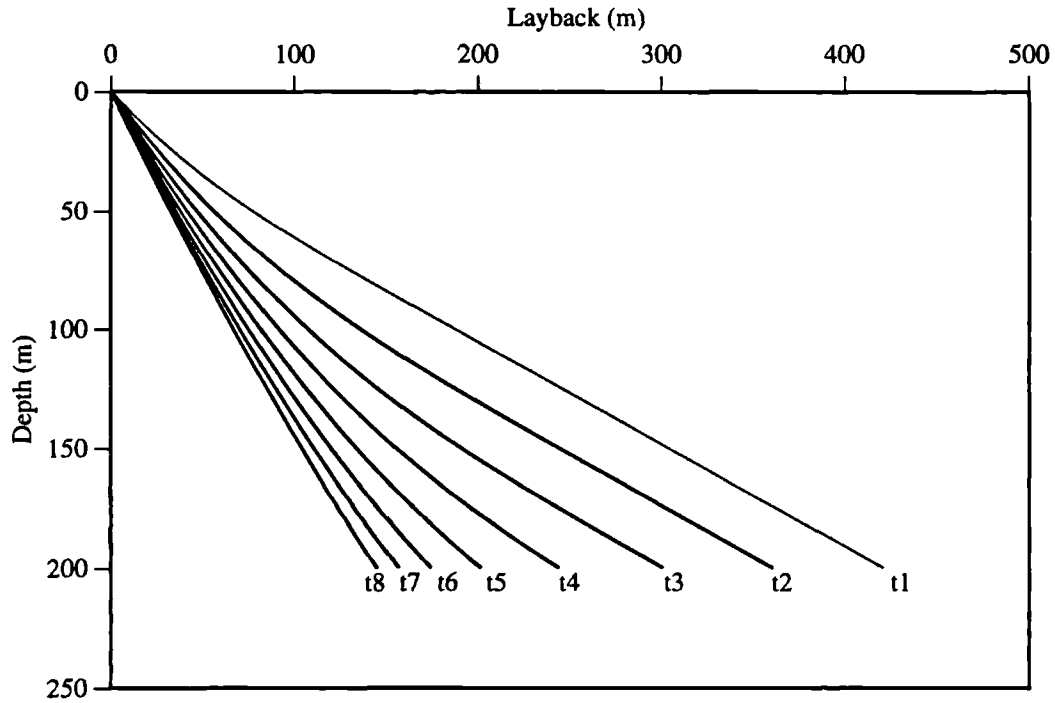

Figure 5.22 - Configuration for simulation LDSL.

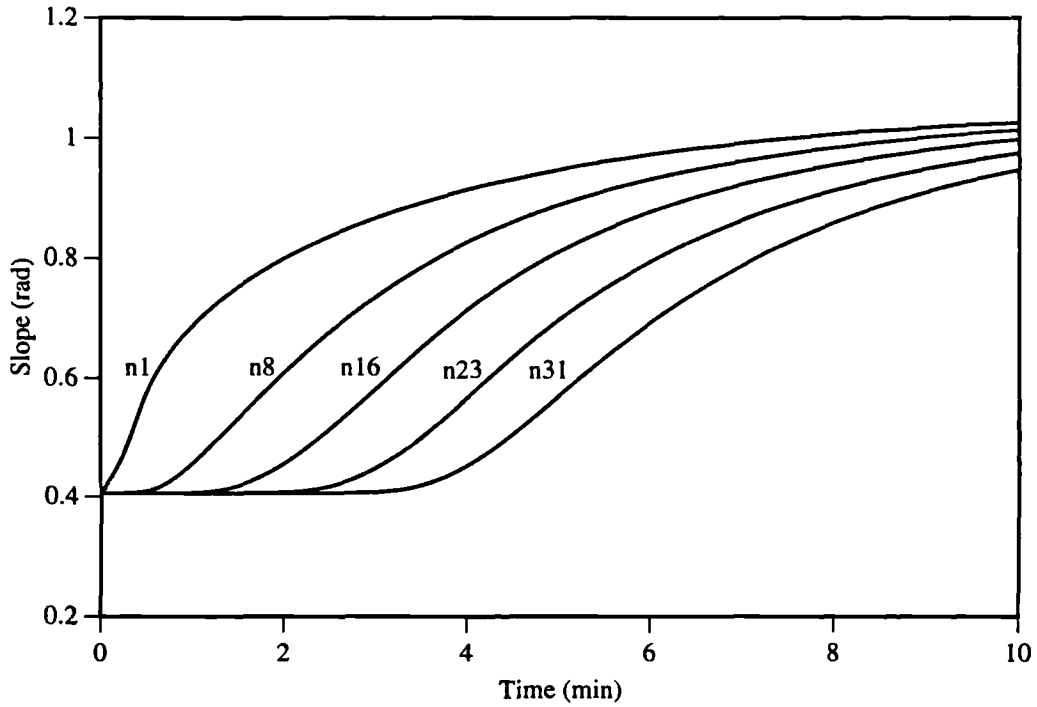

Figure 5.23 - Slope versus time for simulation LDSL.

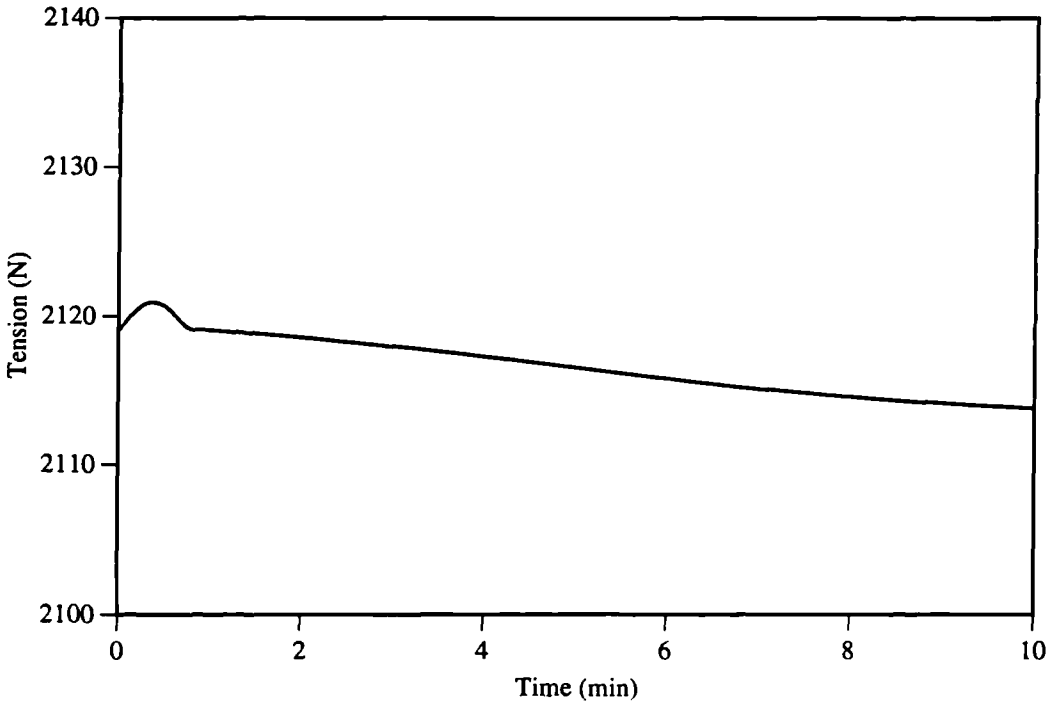

Figure 5.24 - Top tension versus time for simulation LDSL.

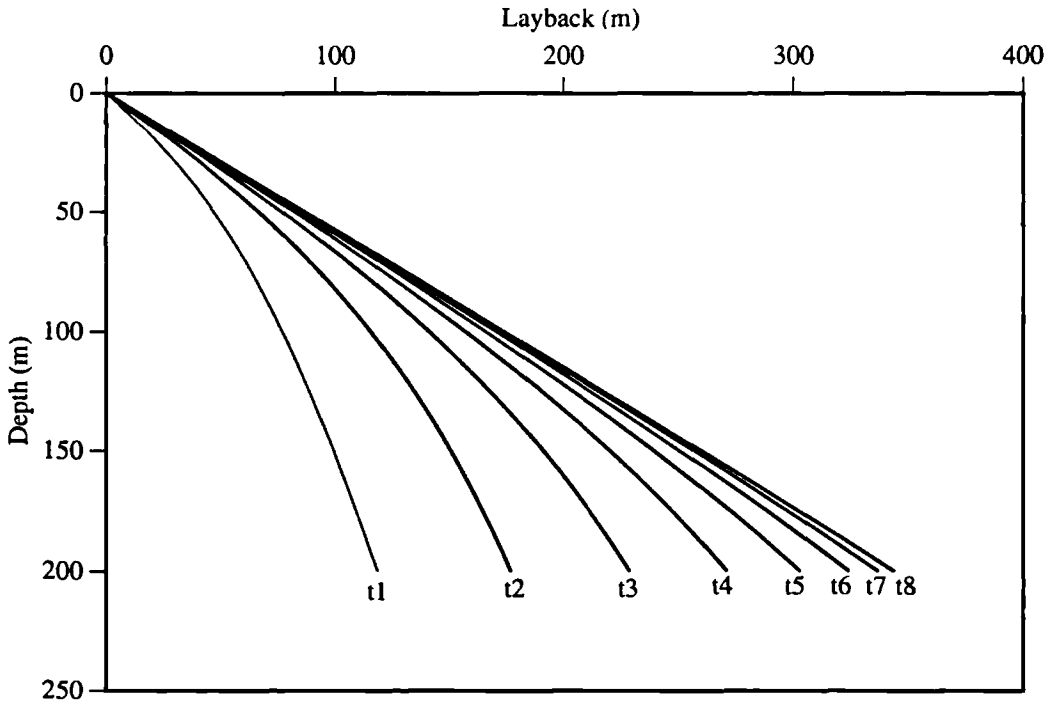

Figure 5.25 - Configuration for simulation HAST.

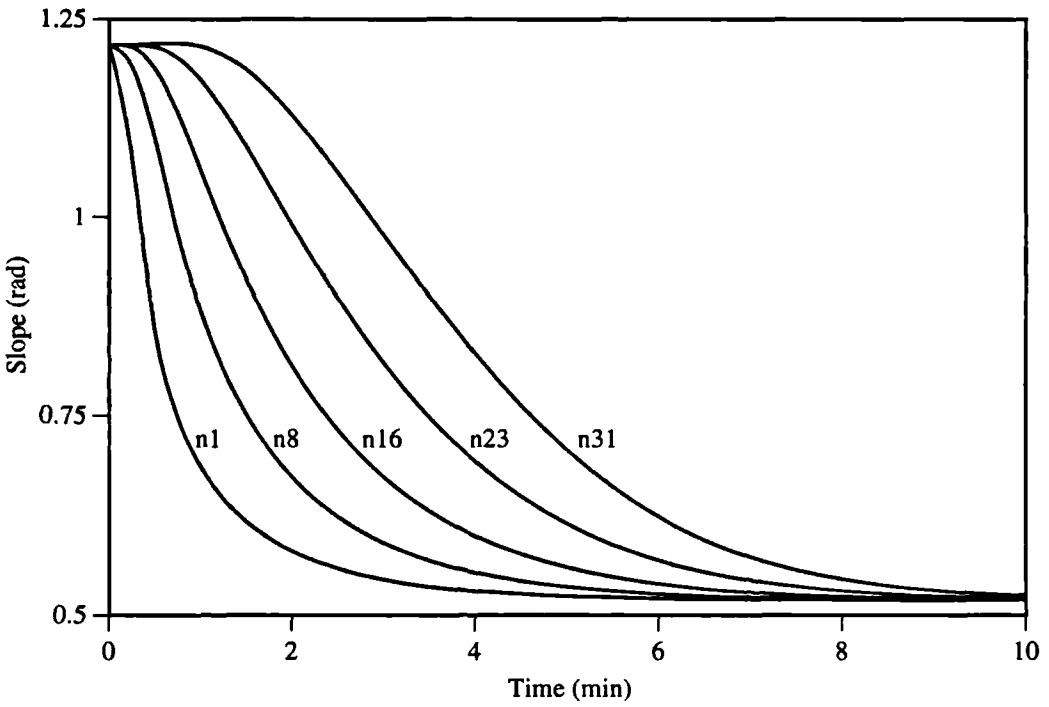

Figure 5.26 - Slope versus time for simulation HAST.

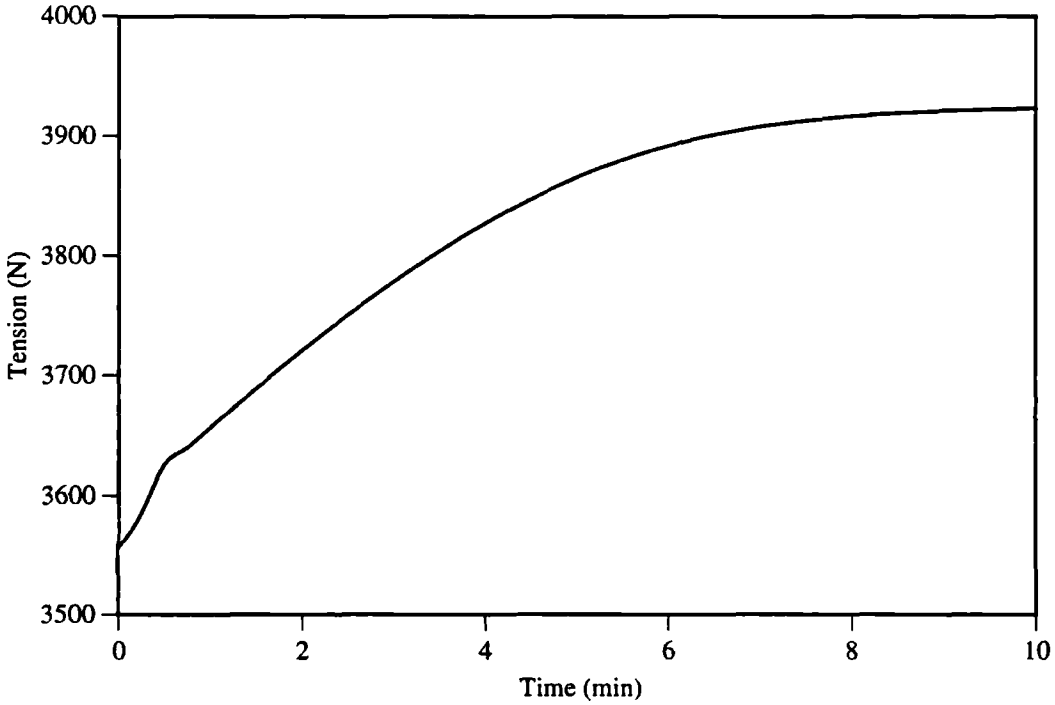

Figure 5.27 - Top tension versus time for simulation HAST.

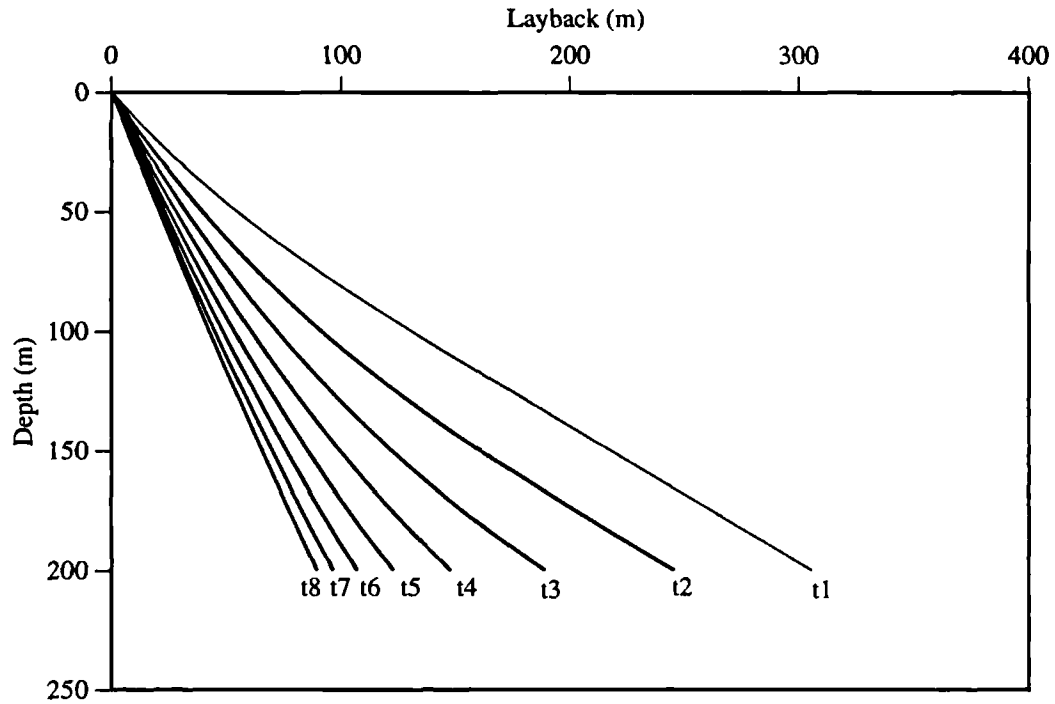

Figure 5.28 - Configuration for simulation HDST.

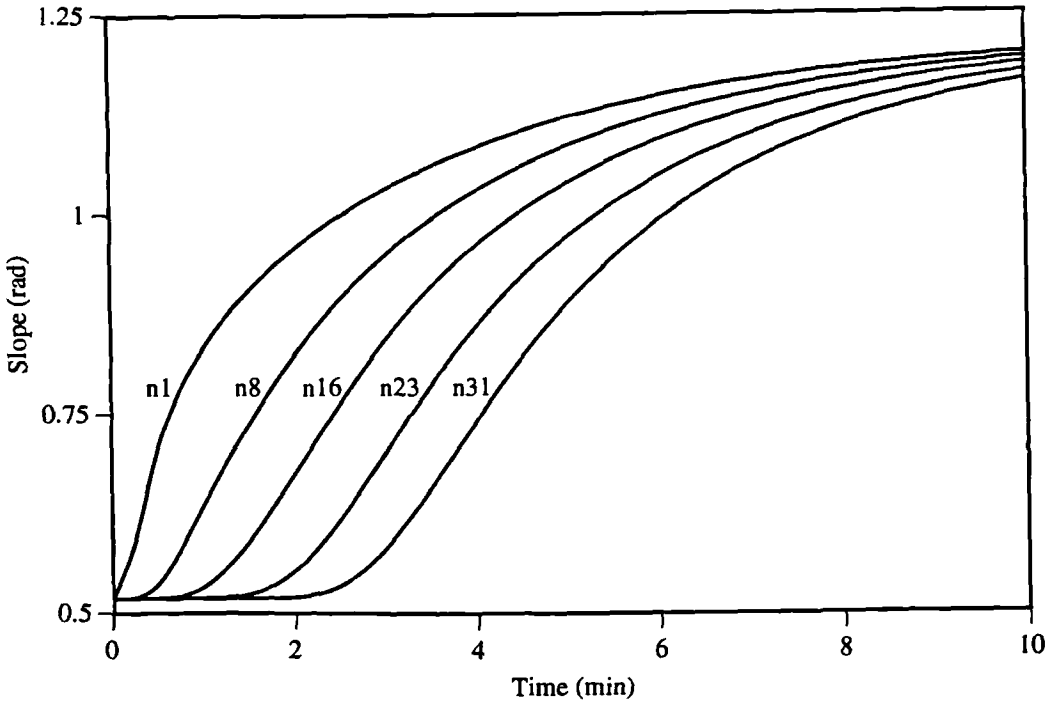

Figure 5.29 - Slope versus time for simulation HDST.

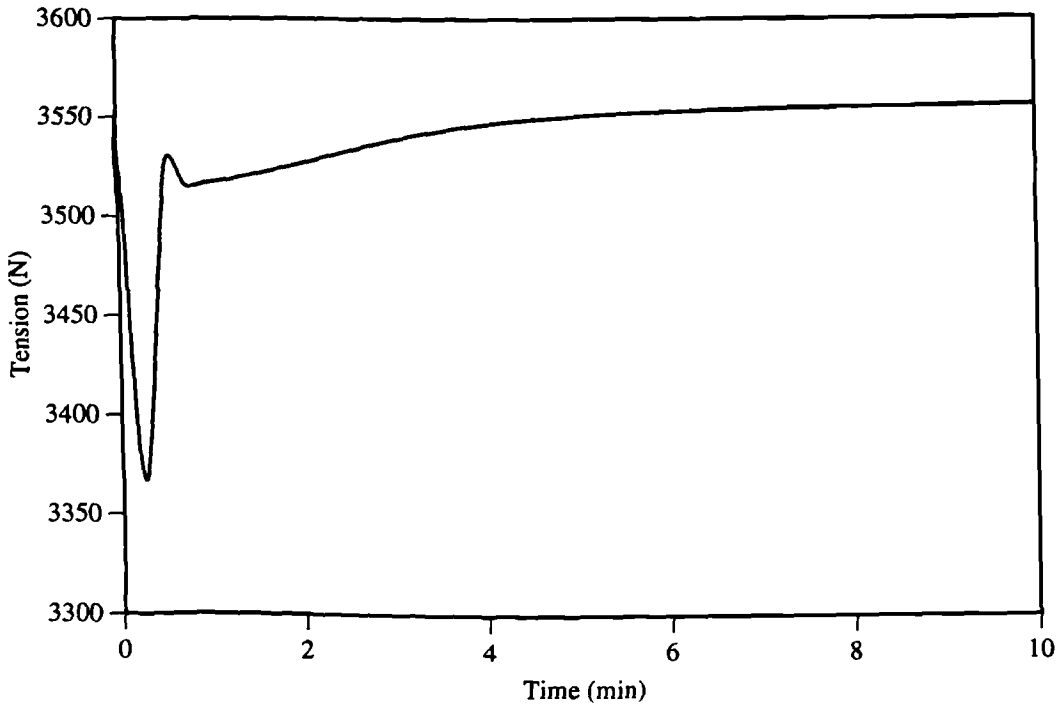

Figure 5.30 - Top tension versus time for simulation HDST.

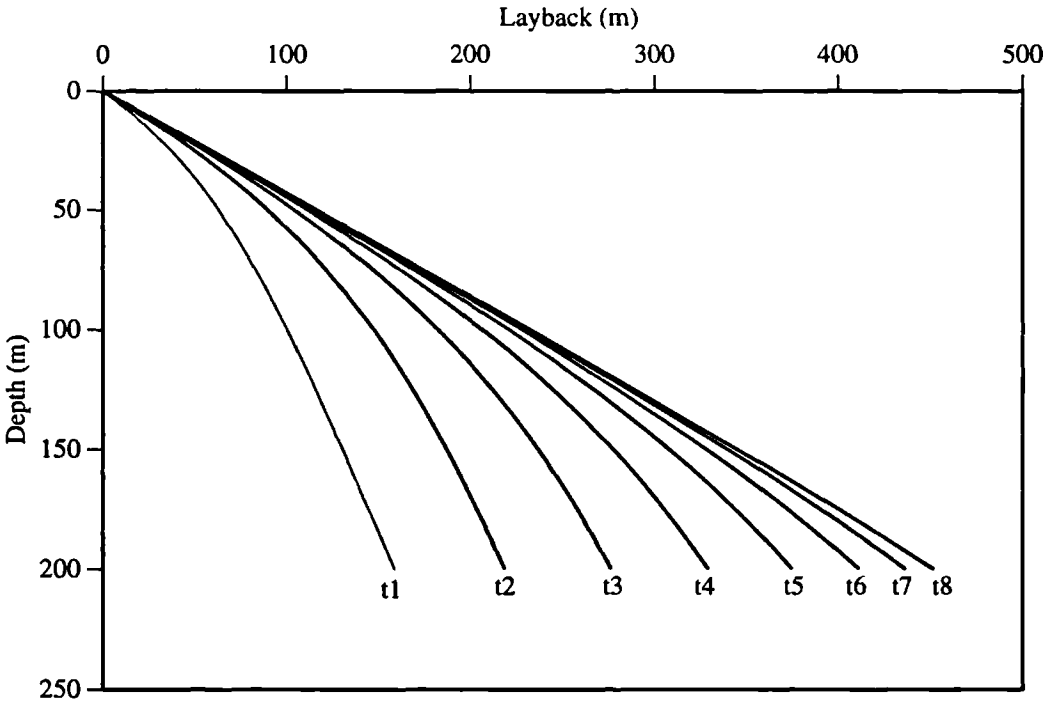

Figure 5.31 - Configuration for simulation LAST.

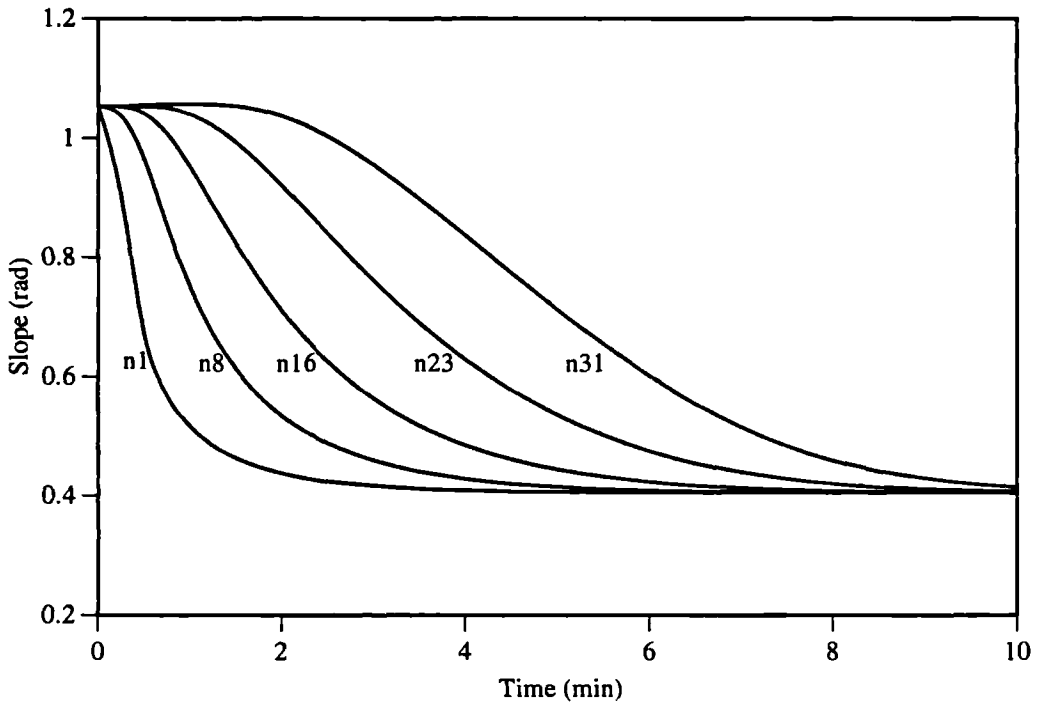

Figure 5.32 - Slope versus time for simulation LAST.

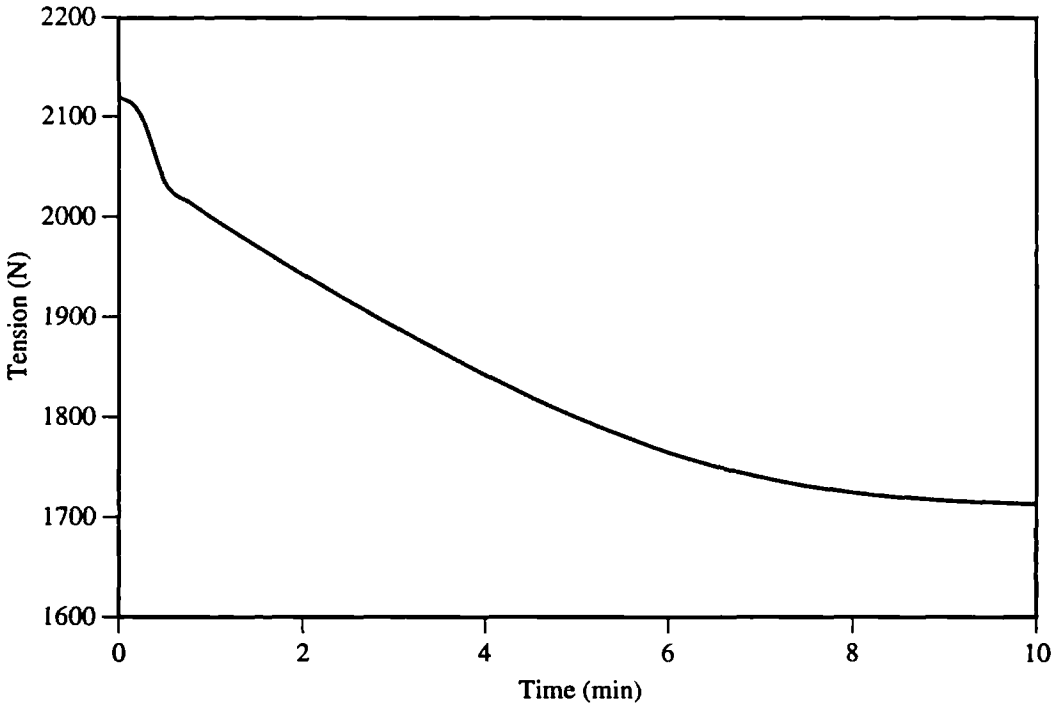

Figure 5.33 - Top tension versus time for simulation LAST.

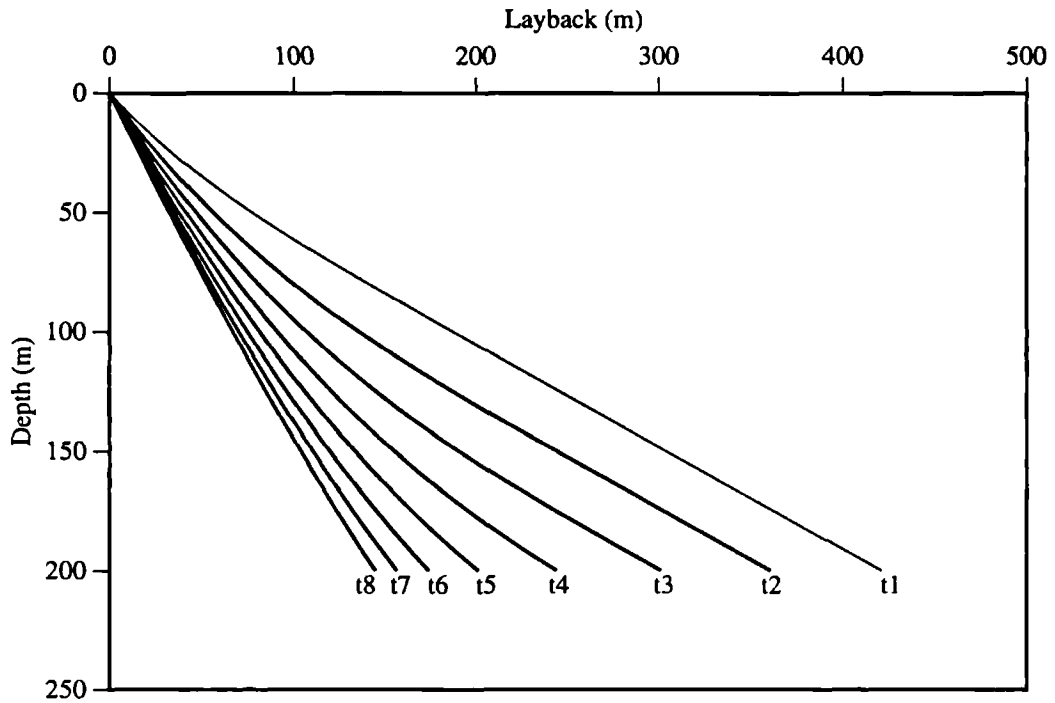

Figure 5.34 - Configuration for simulation LDST.

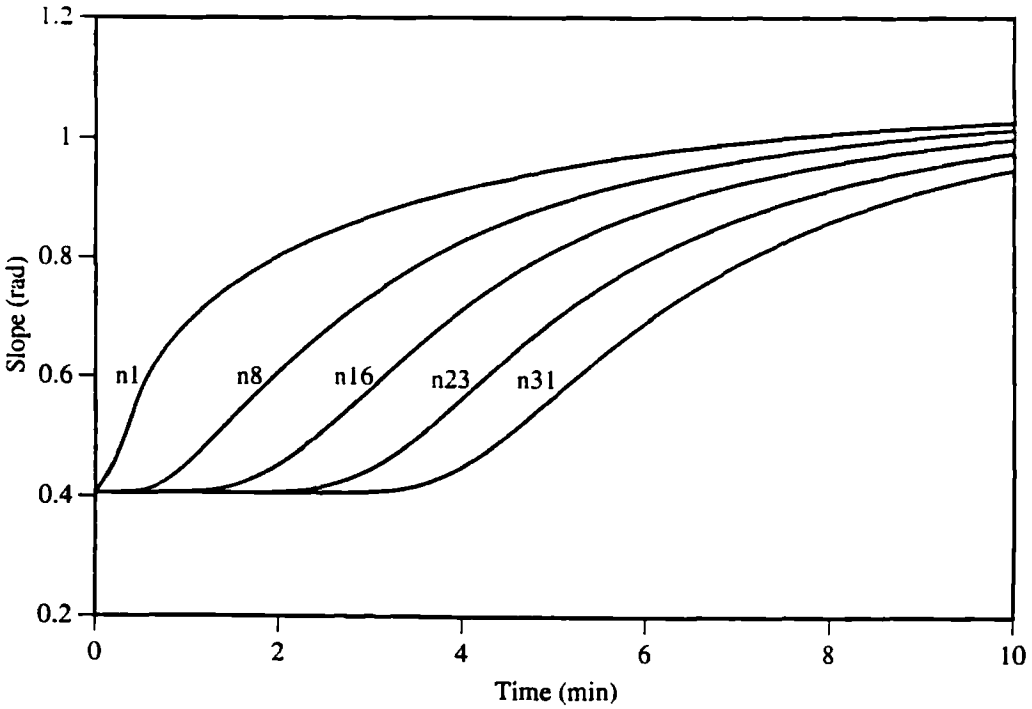

Figure 5.35 - Slope versus time for simulation LDST.

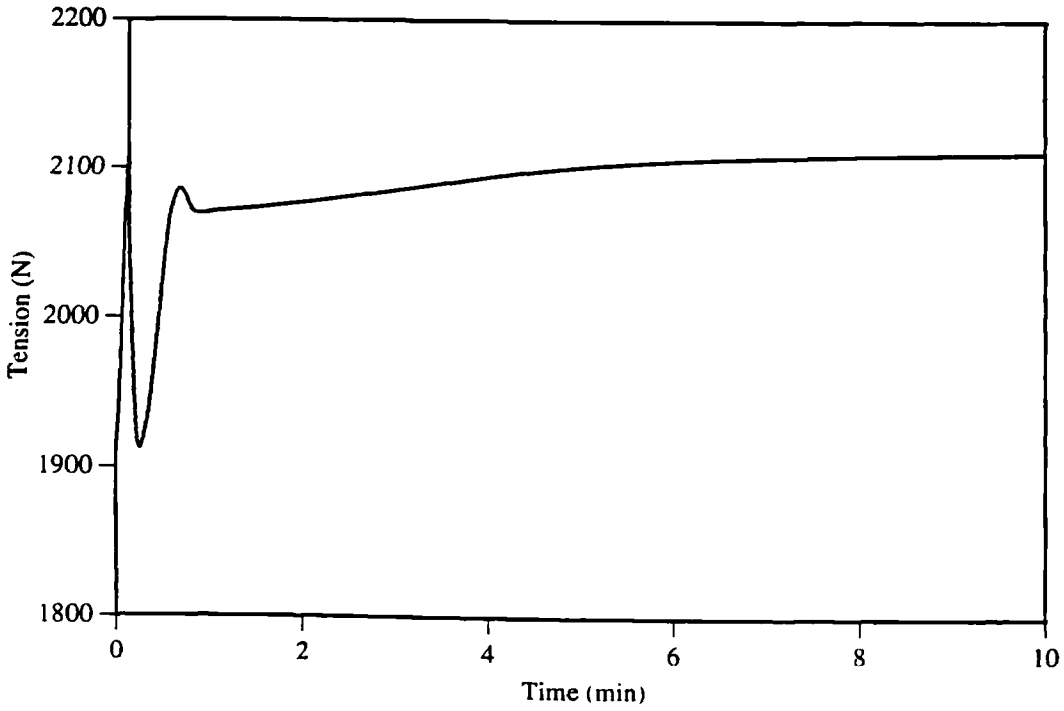

Figure 5.36 - Top tension versus time for simulation LDST.

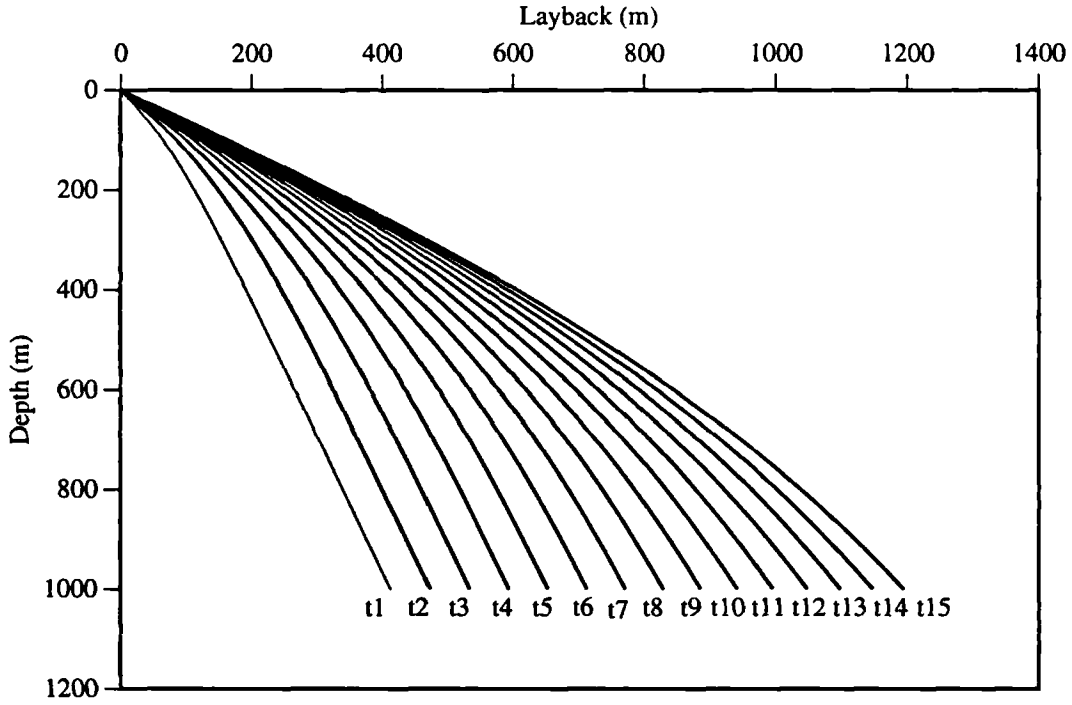

Figure 5.37 - Configuration for simulation HADL.

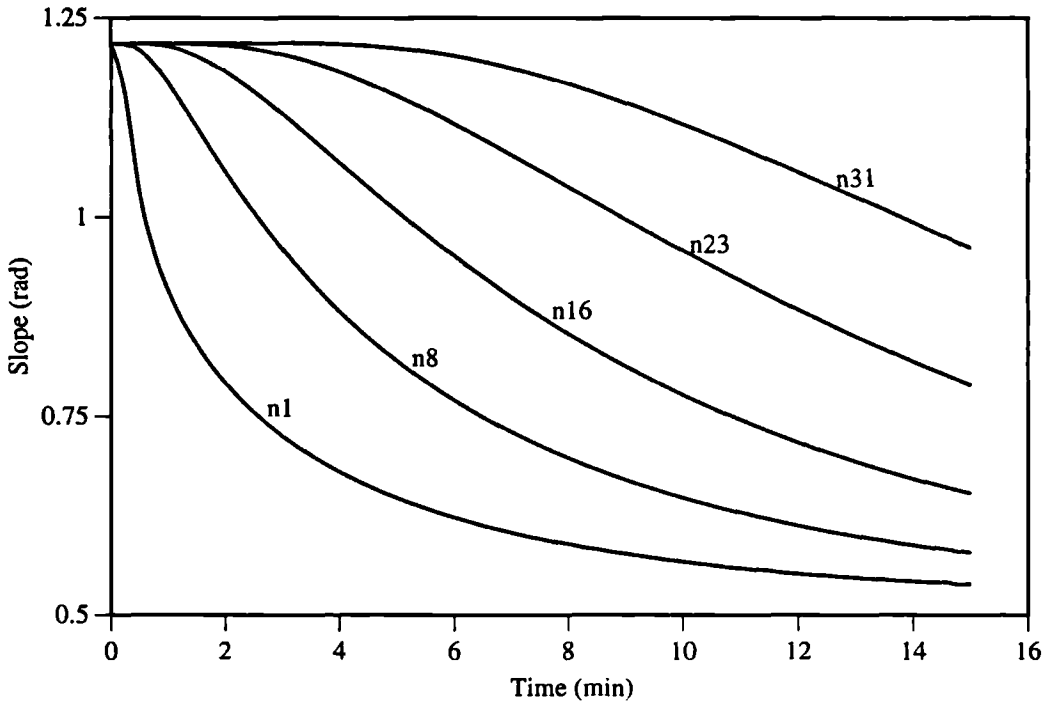

Figure 5.38 - Slope versus time for simulation HADL.

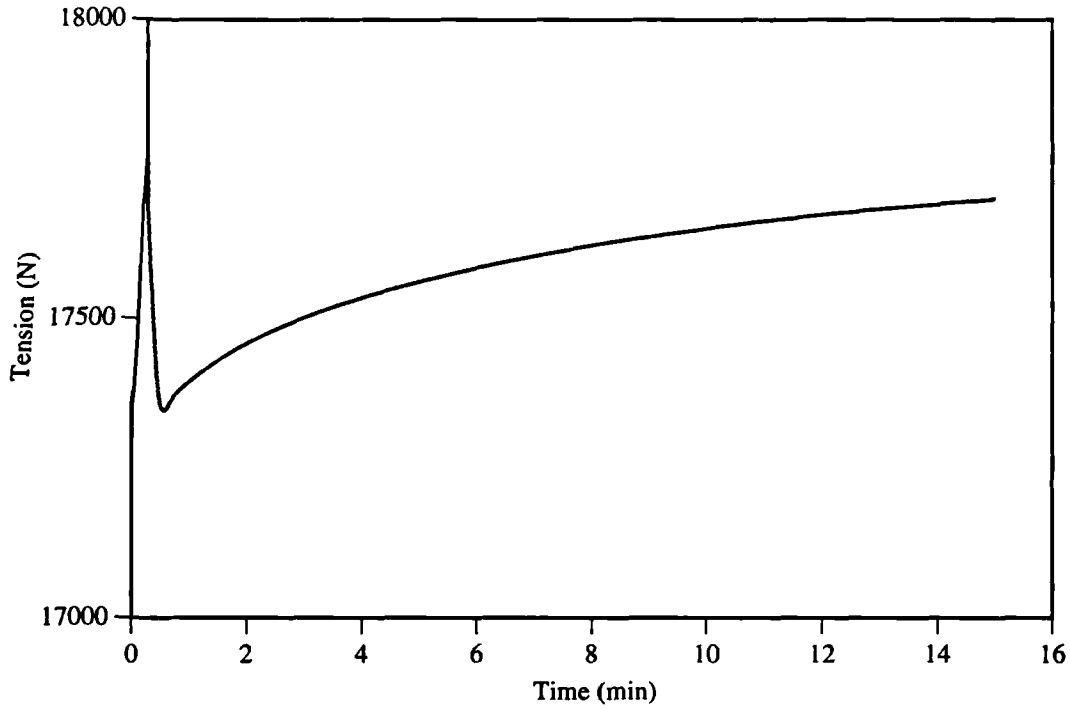

Figure 5.39 - Top tension versus time for simulation HADL.

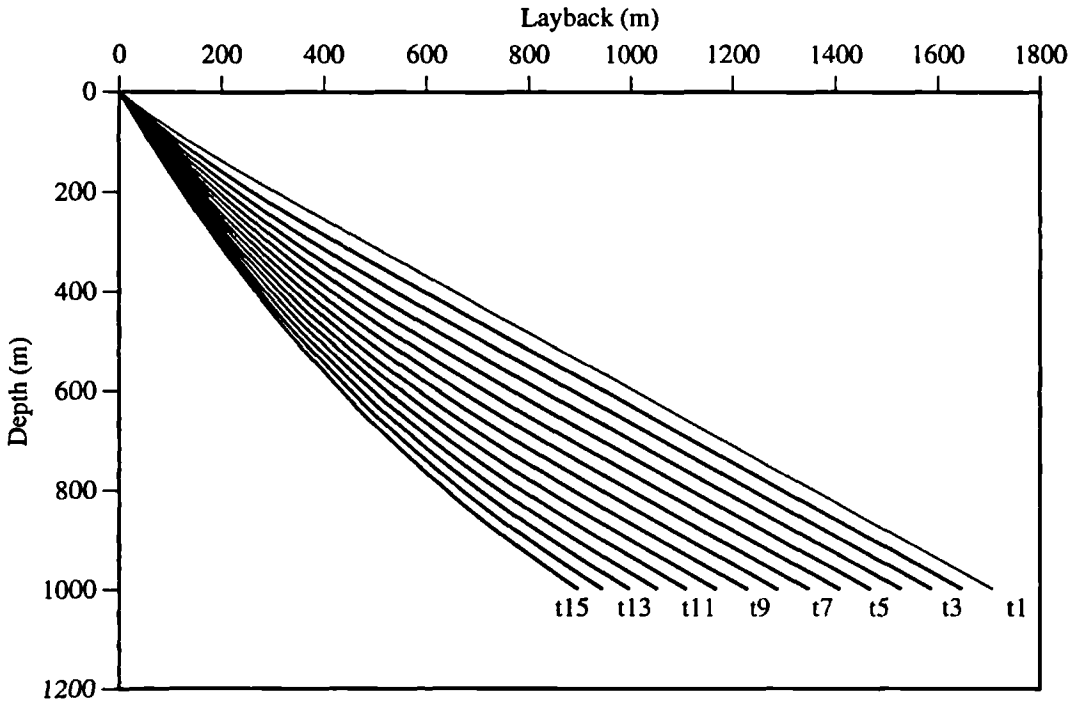

Figure 5.40 - Configuration for simulation HDDL.

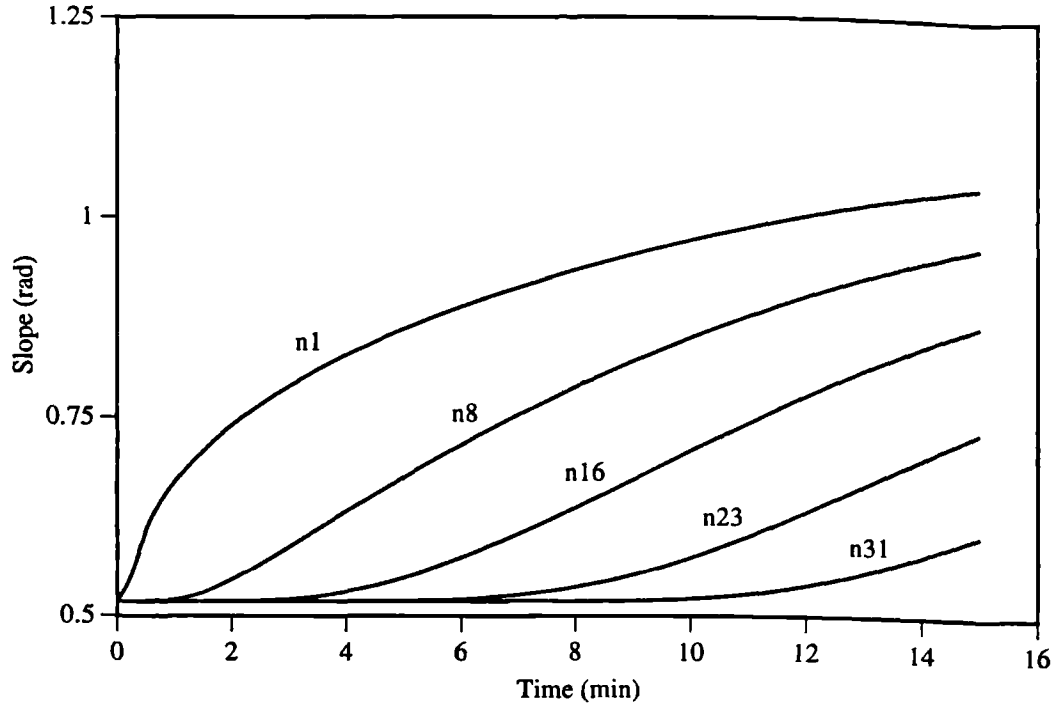

Figure 5.41 - Slope versus time for simulation HDDL.

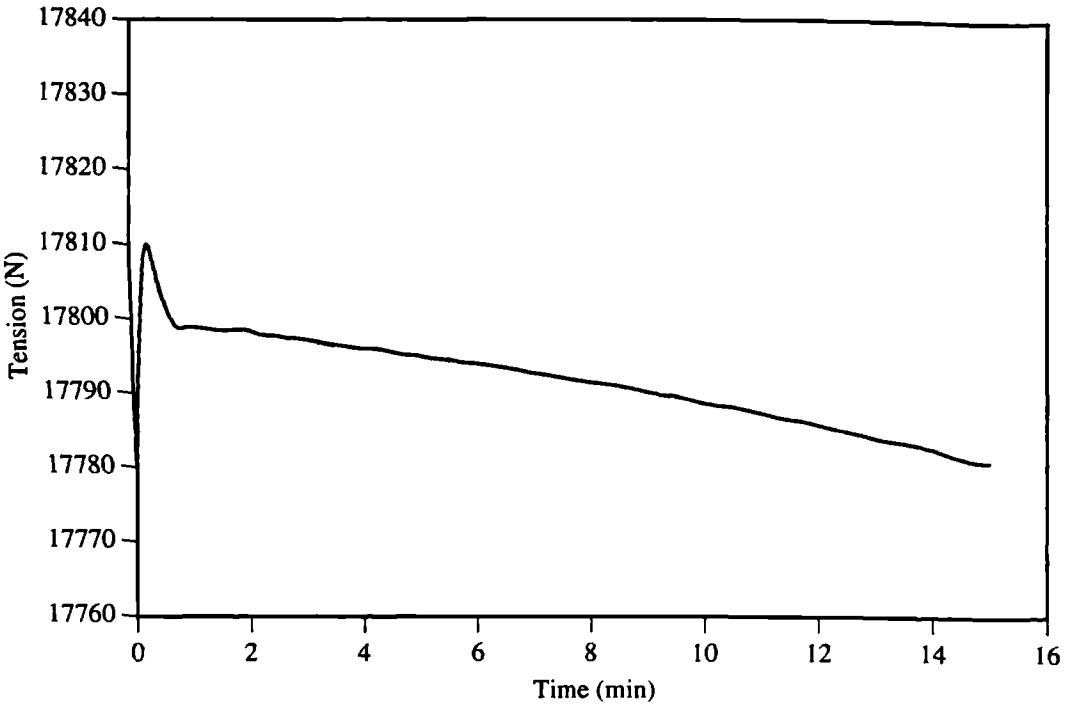

Figure 5.42 - Top tension versus time for simulation HDDL.

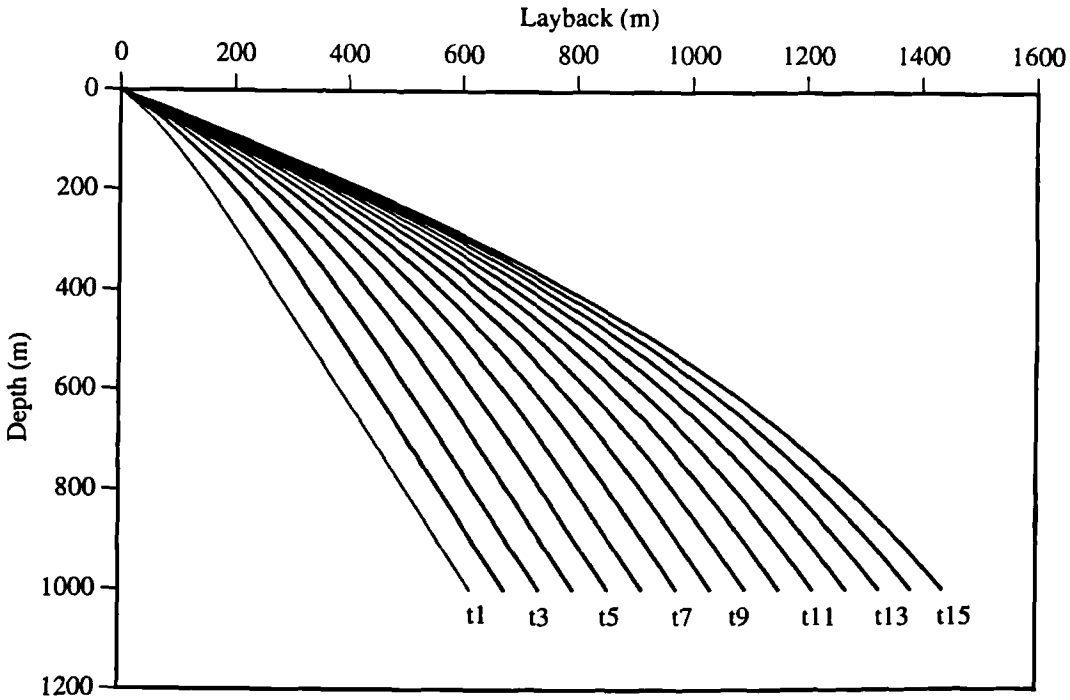

Figure 5.43 - Configuration for simulation LADL.

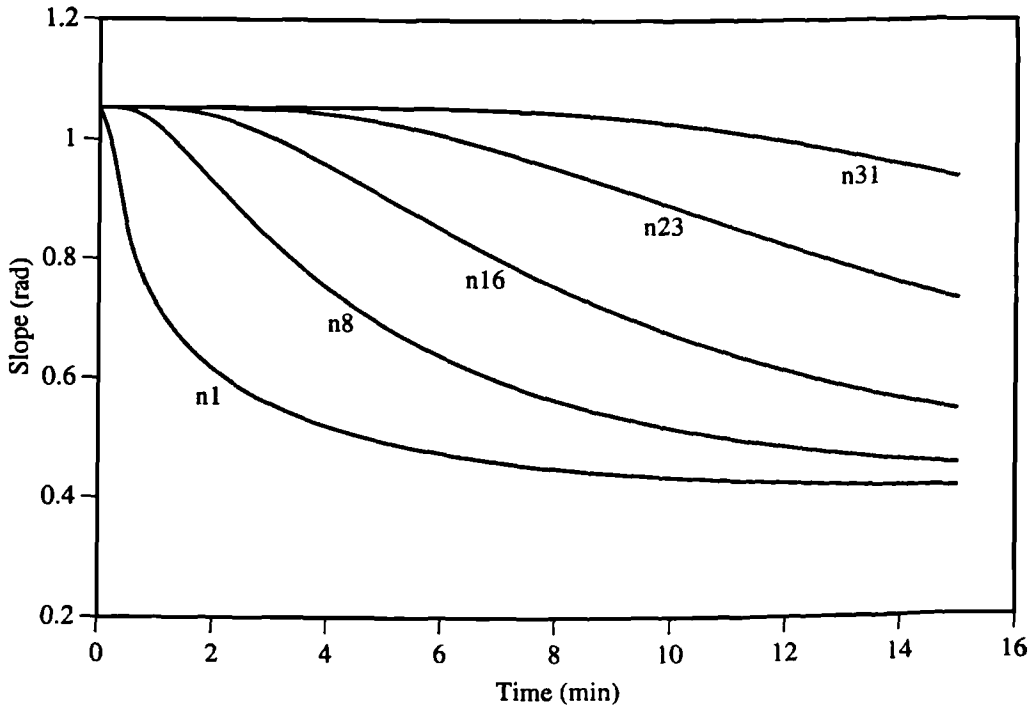

Figure 5.44 - Slope versus time for simulation LADL.

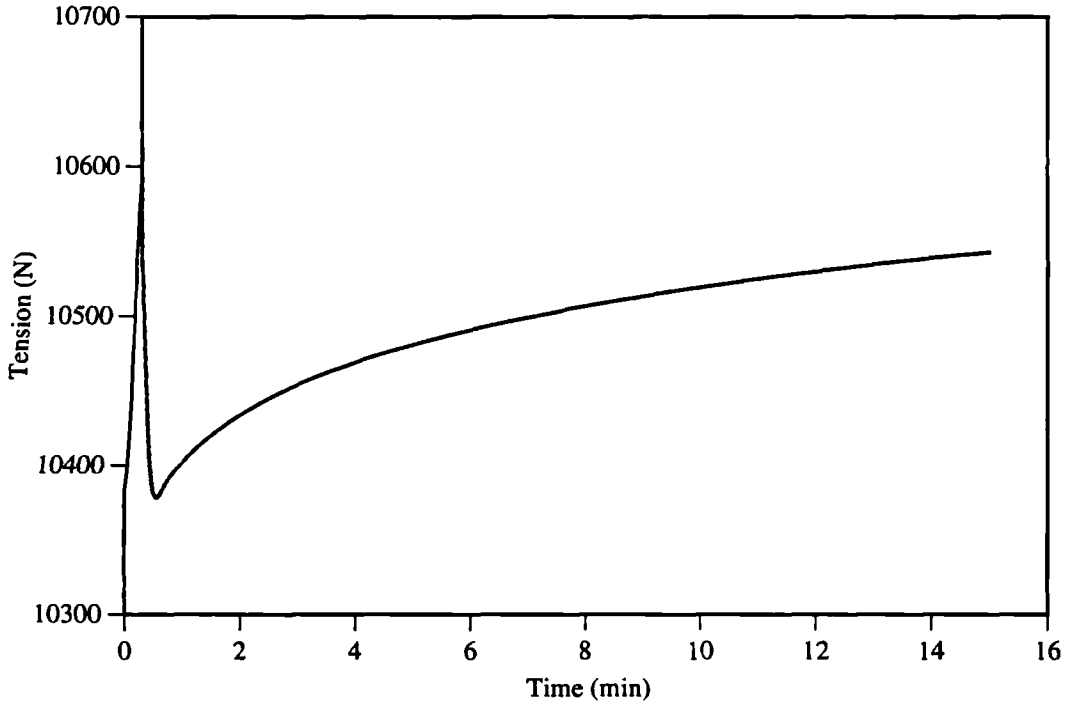

Figure 5.45 - Top tension versus time for simulation LADL.

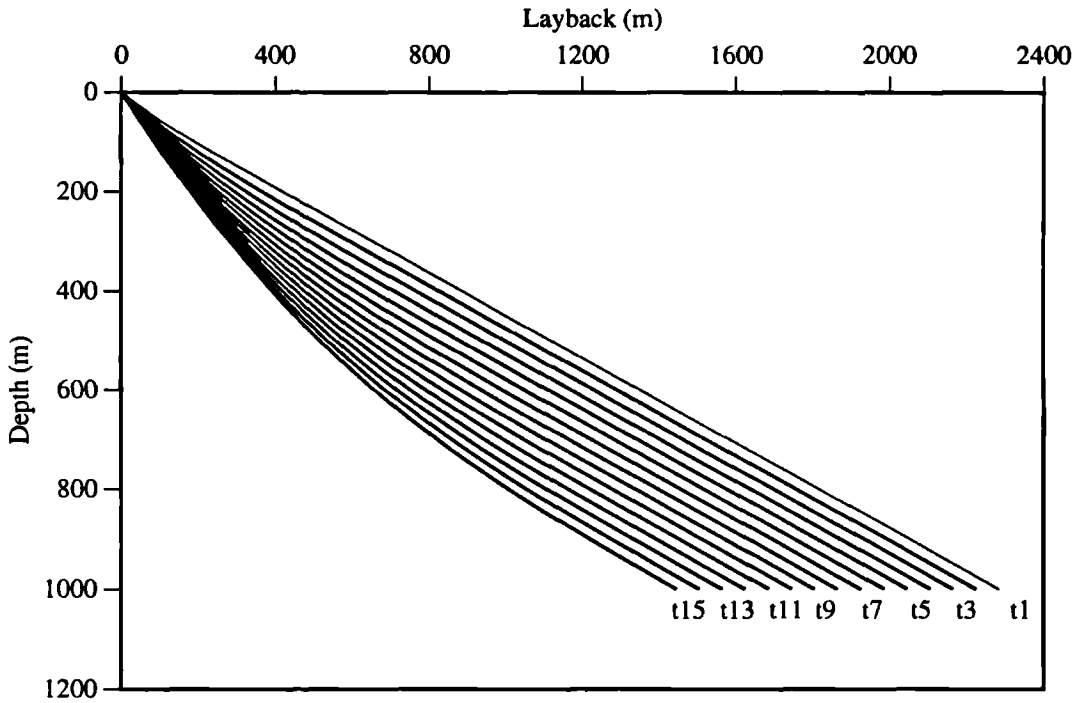

Figure 5.46 - Configuration for simulation LDDL.

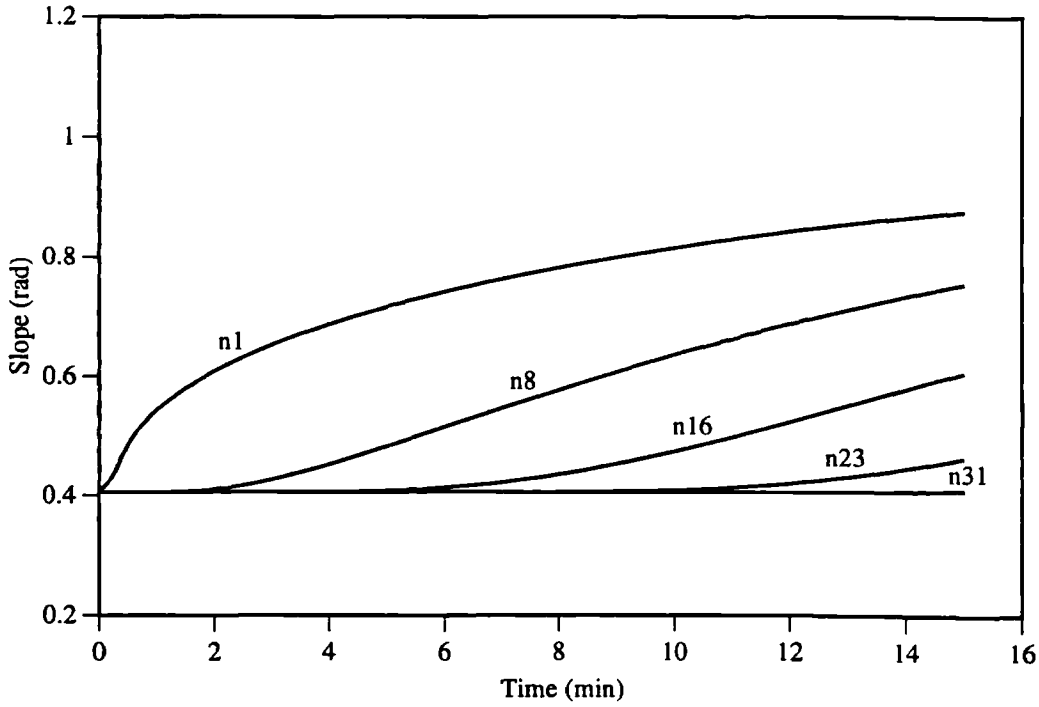

Figure 5.47 - Slope versus time for simulation LDDL.

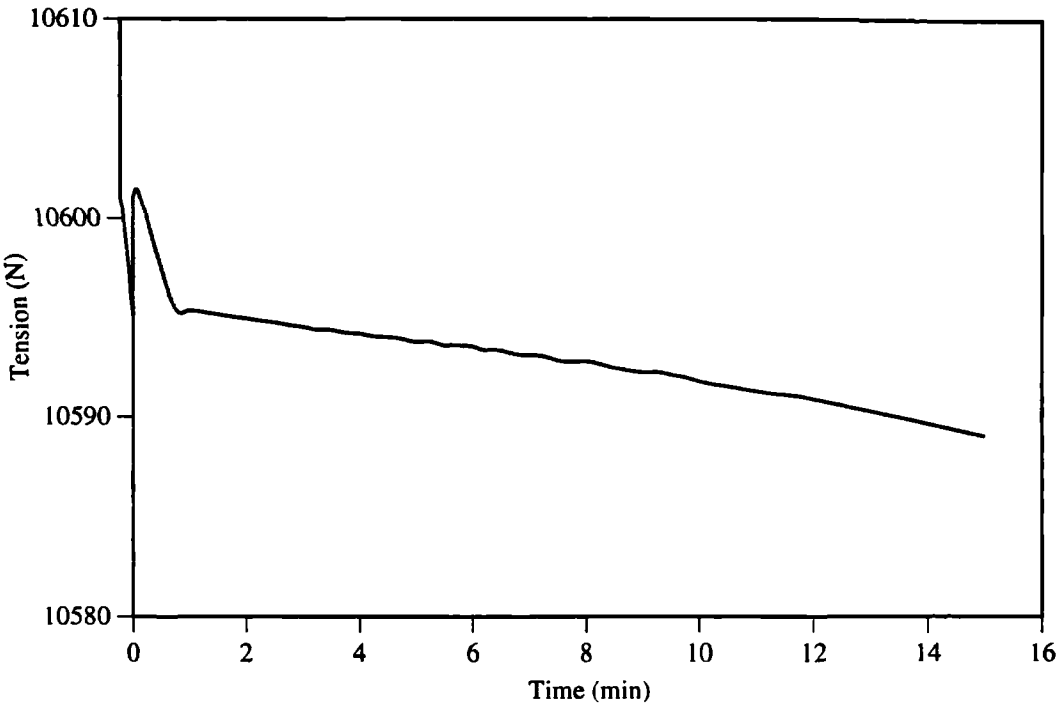

Figure 5.48 - Top tension versus time for simulation LDDL.

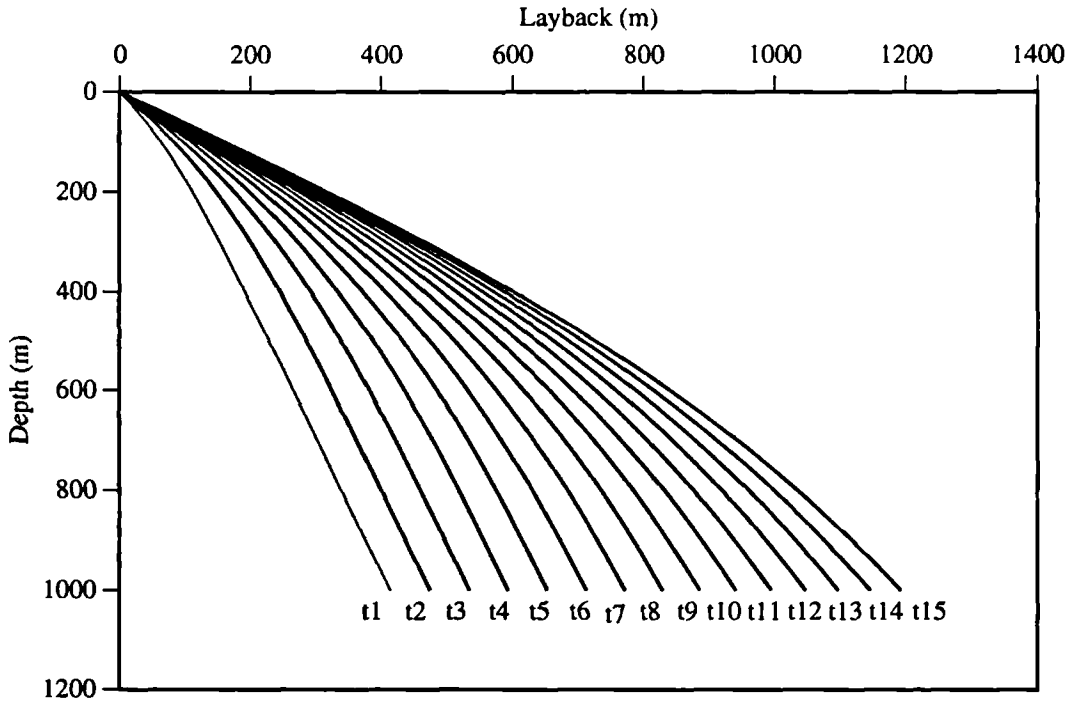

Figure 5.49 - Configuration for simulation HADT.

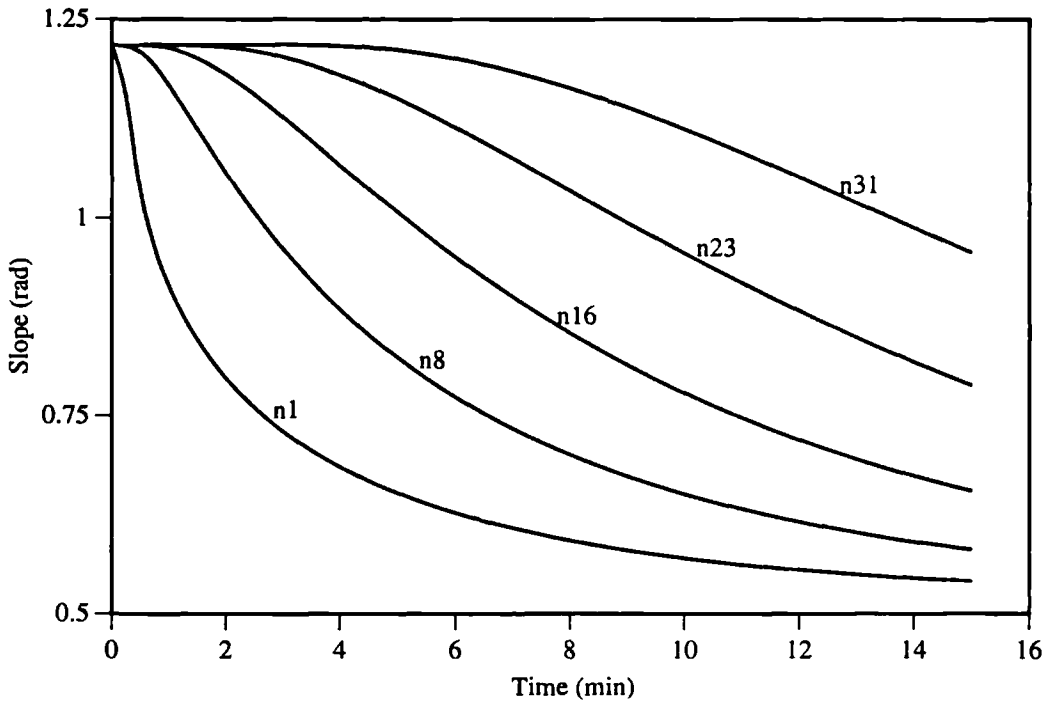

Figure 5.50 - Slope versus time for simulation HADT.

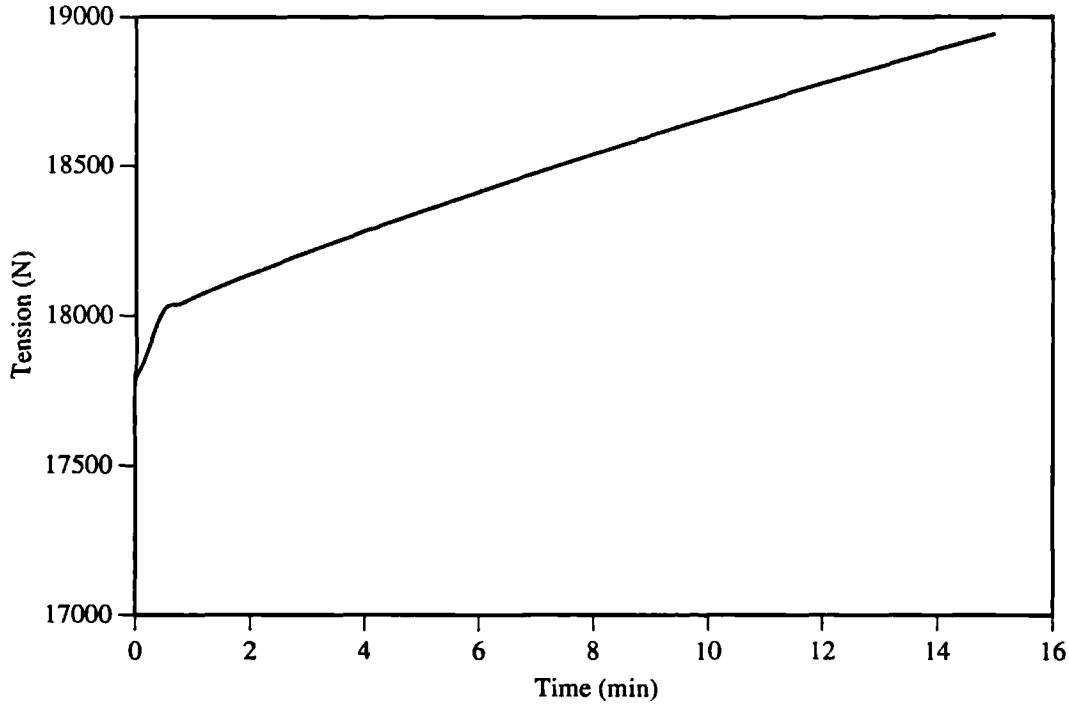

Figure 5.51 - Top tension versus time for simulation HADT.

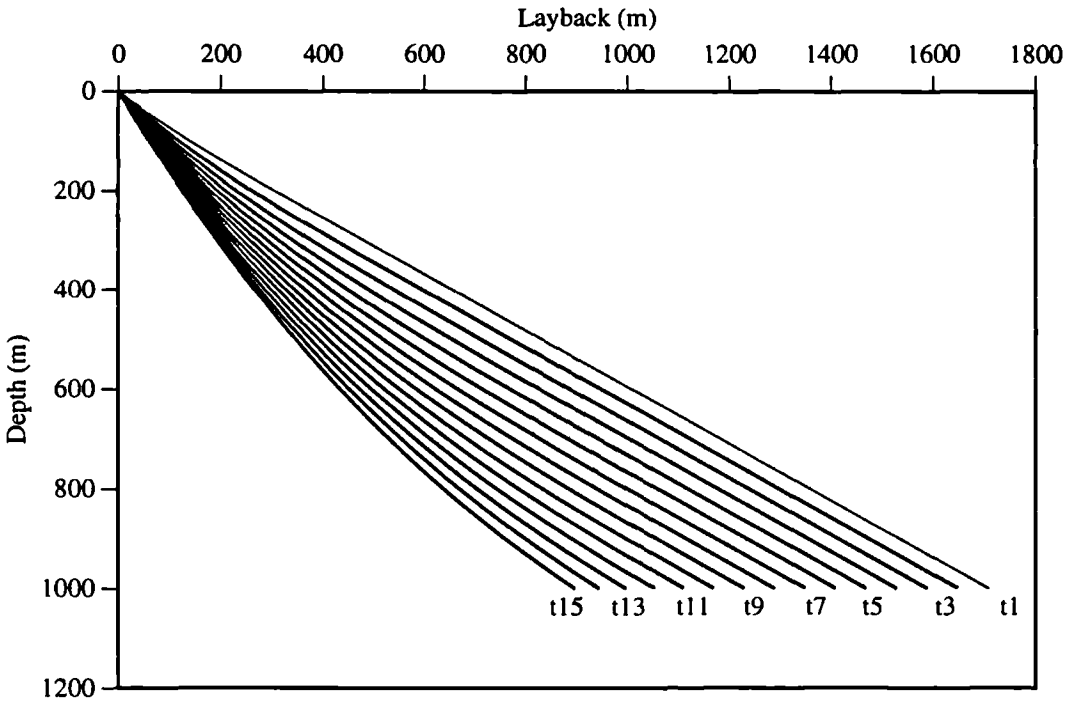

Figure 5.52 - Configuration for simulation HDDT.

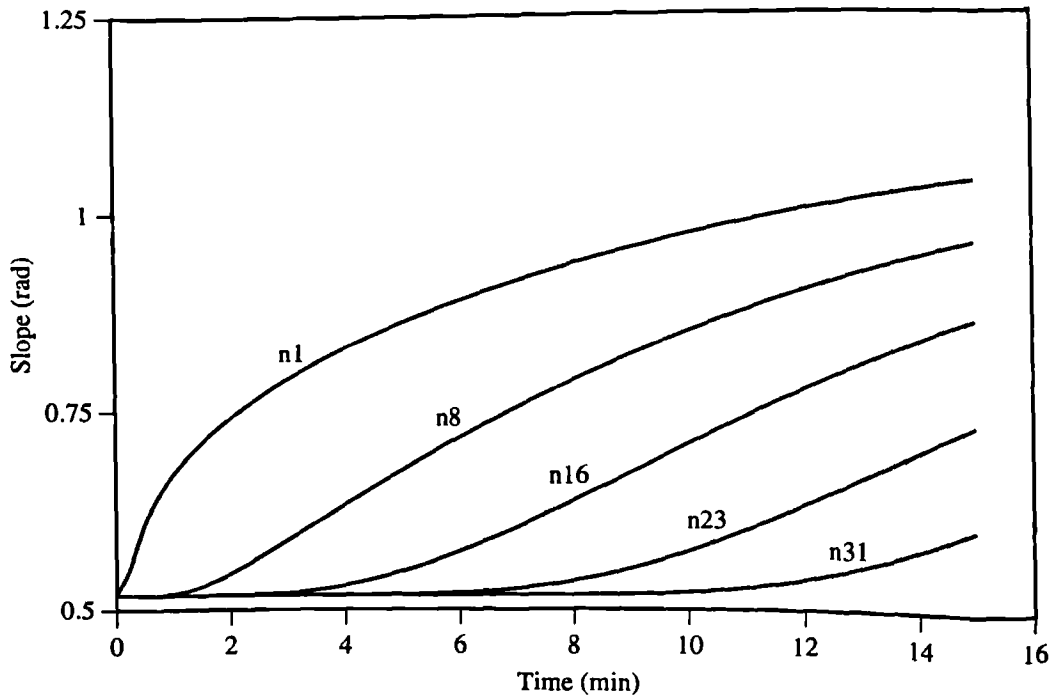

Figure 5.53 - Slope versus time for simulation HDDT.

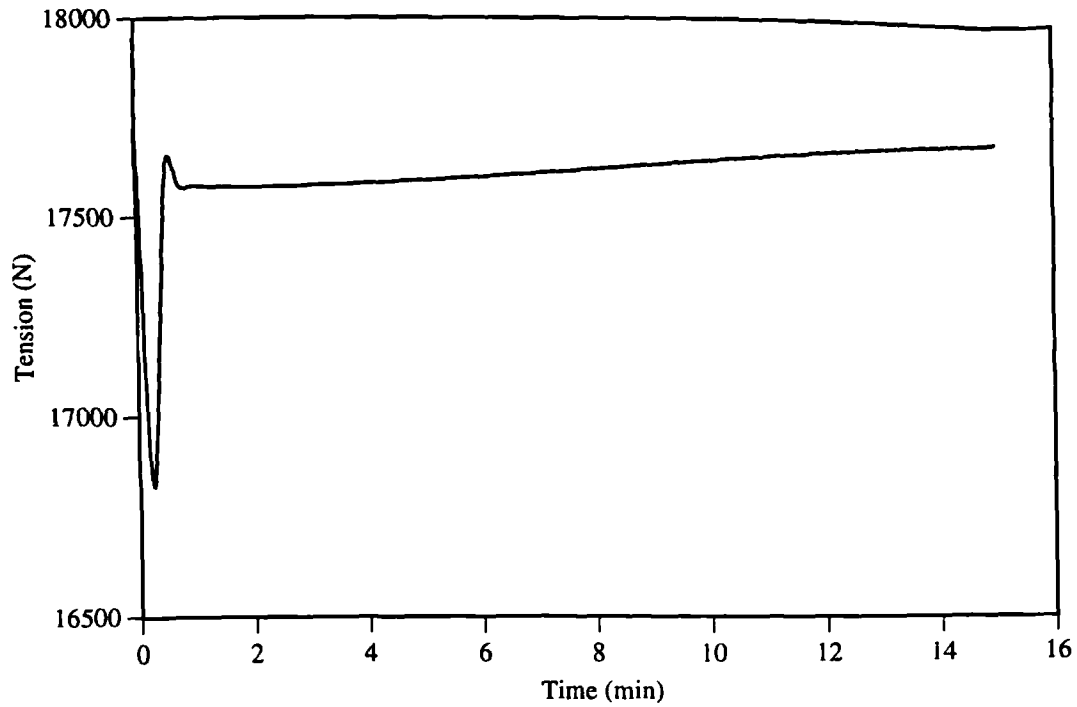

Figure 5.54 - Top tension versus time for simulation HDDT.

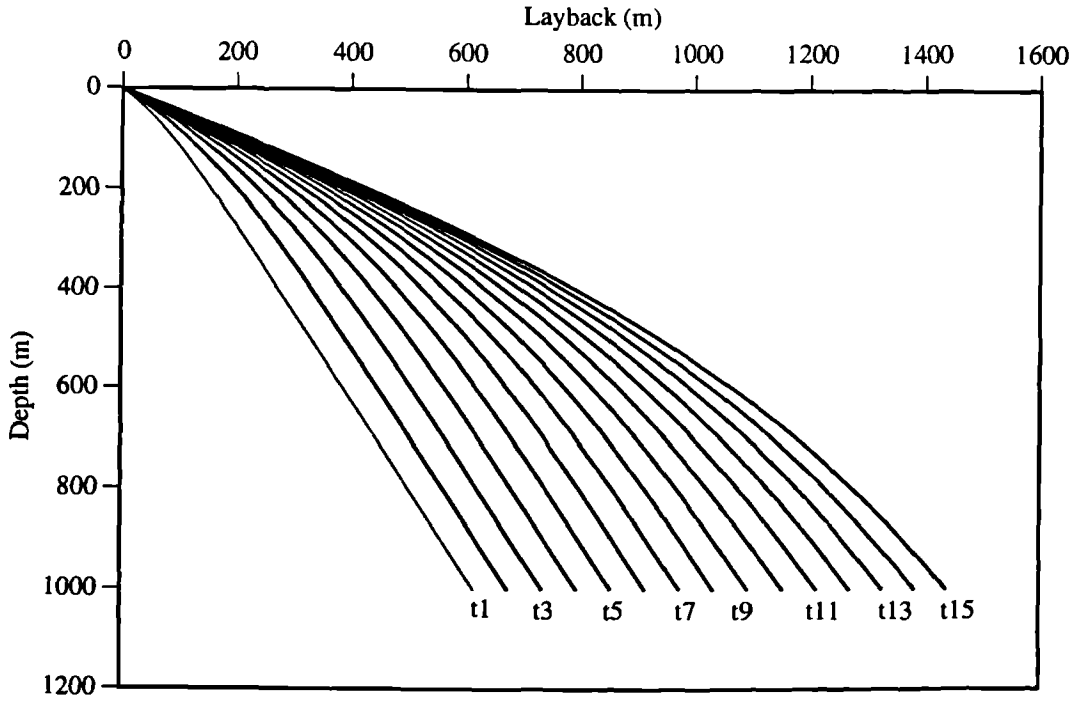

Figure 5.55 - Configuration for simulation LADT.

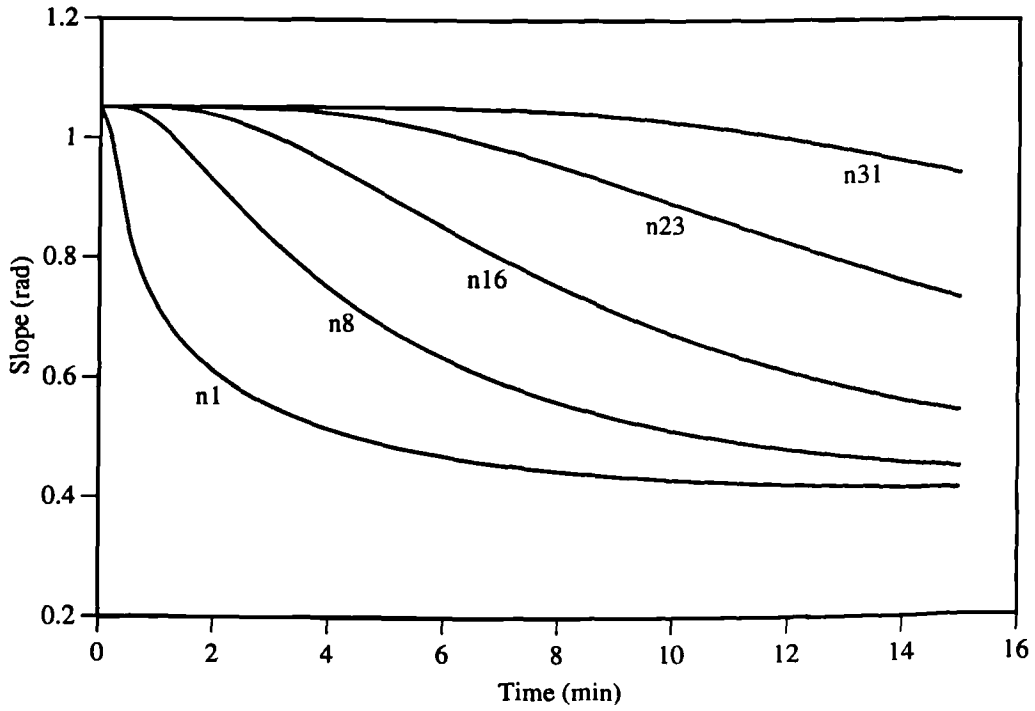

Figure 5.56 - Slope versus time for simulation LADT.

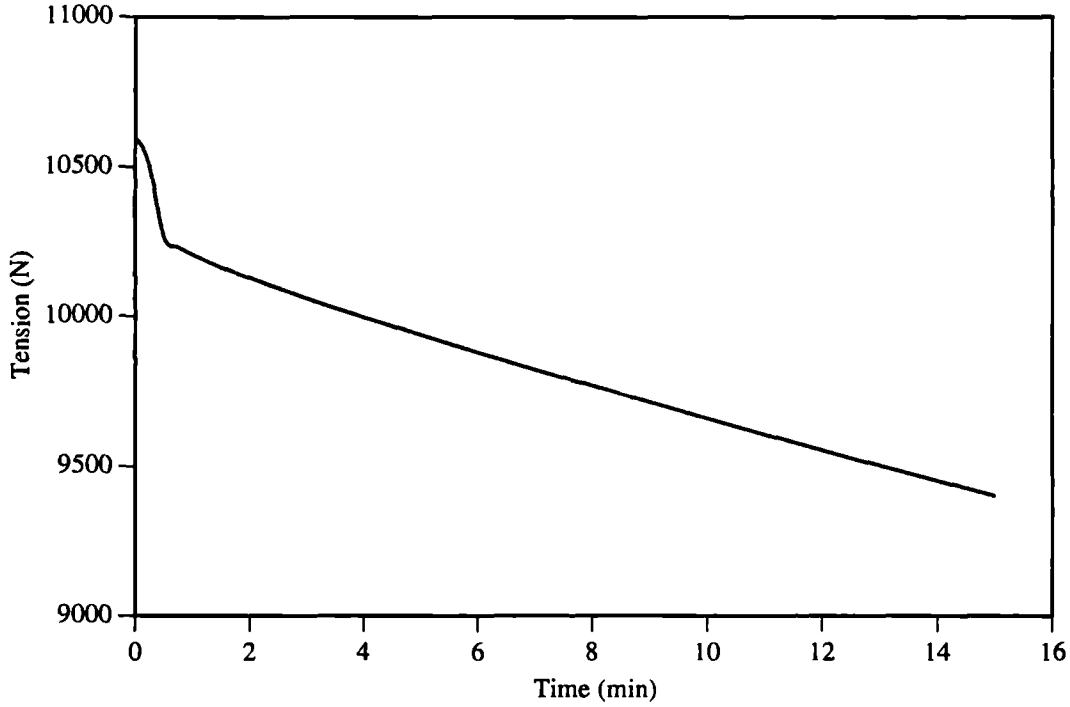

Figure 5.57 - Top tension versus time for simulation LADT.

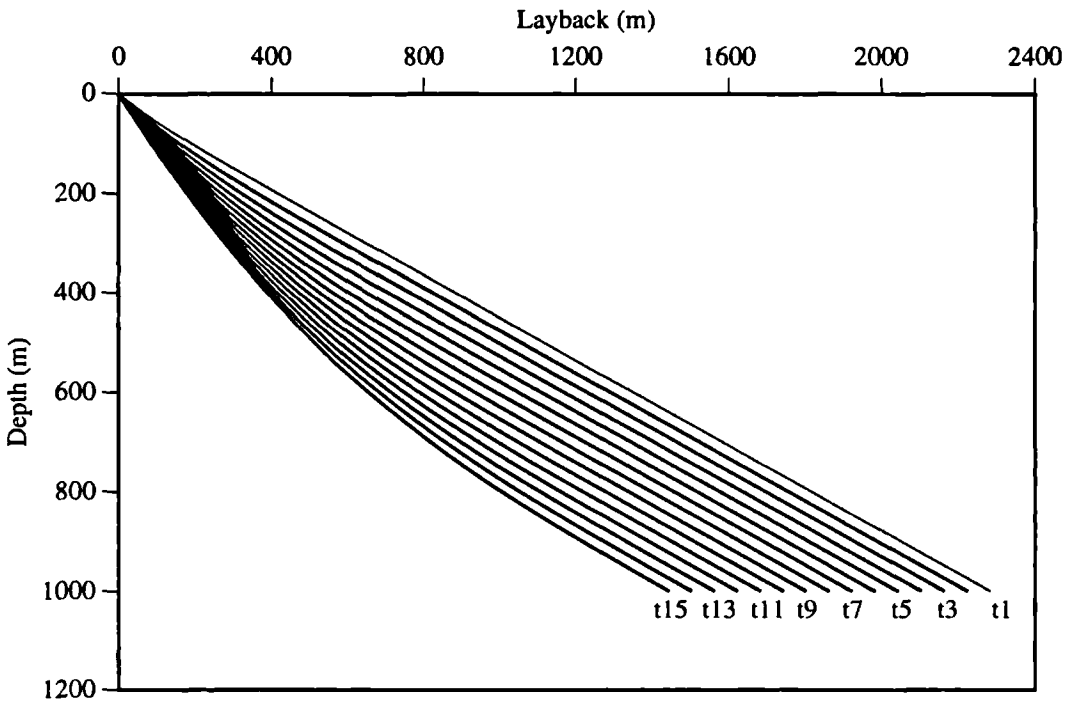

Figure 5.58 - Configuration for simulation LDDT.

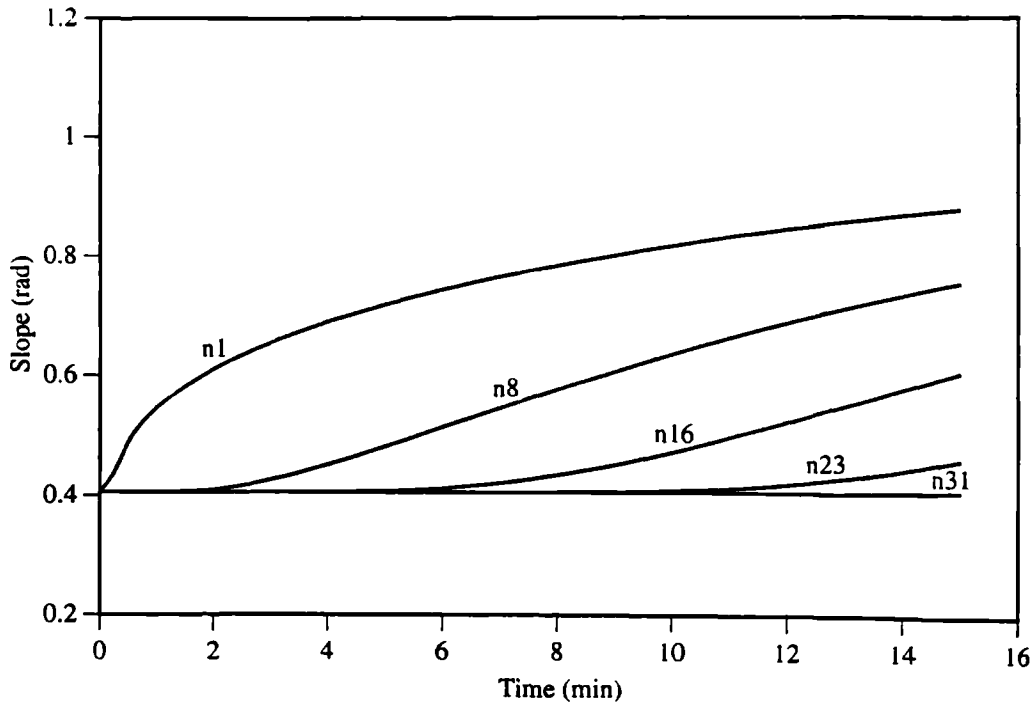

Figure 5.59 - Slope versus time for simulation LDDT.

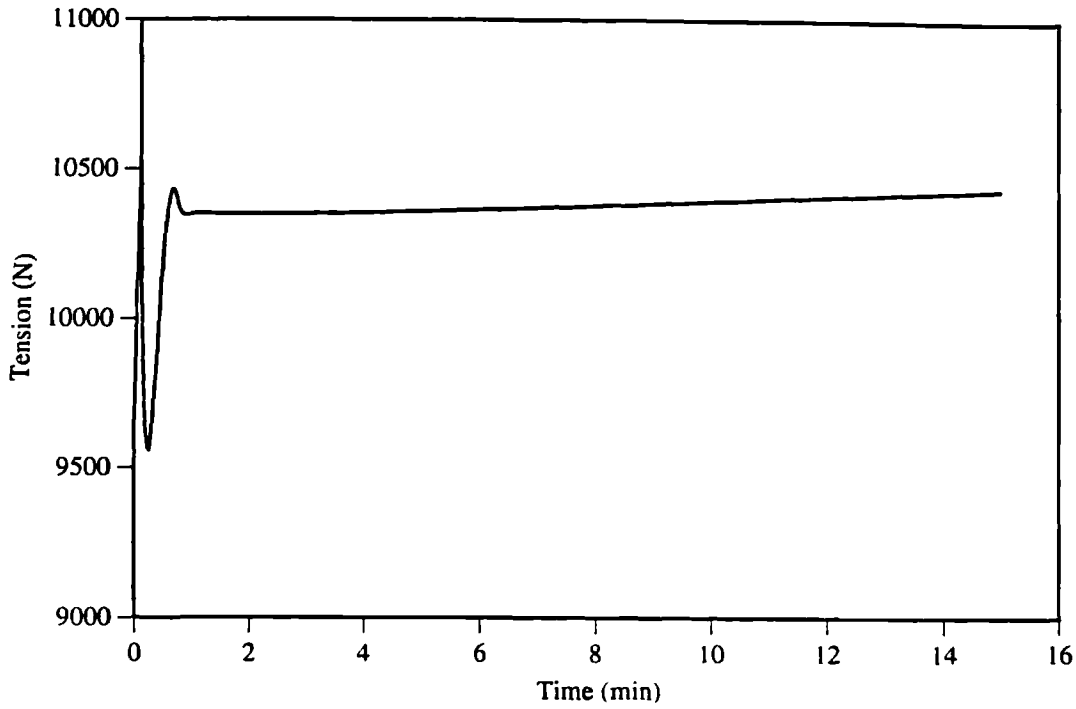

Figure 5.60 - Top tension versus time for simulation LDDT.

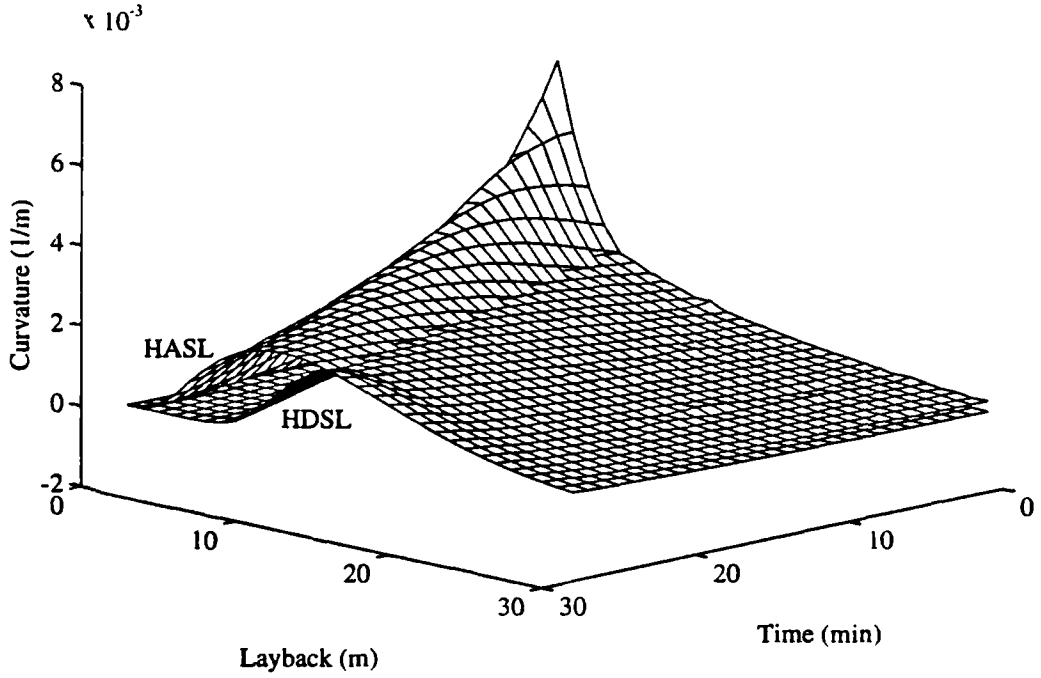

Figure 5.61 - Magnitude of curvature for HASL and HDSL.

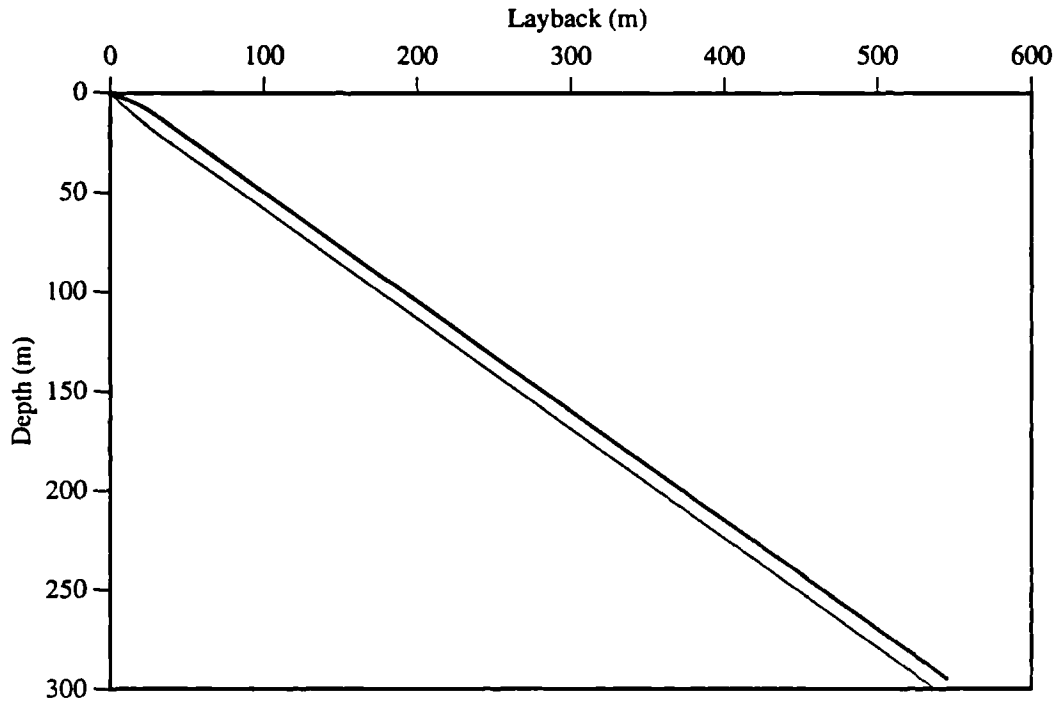

Figure 5.62 - Configuration envelope for simulation HWSL.

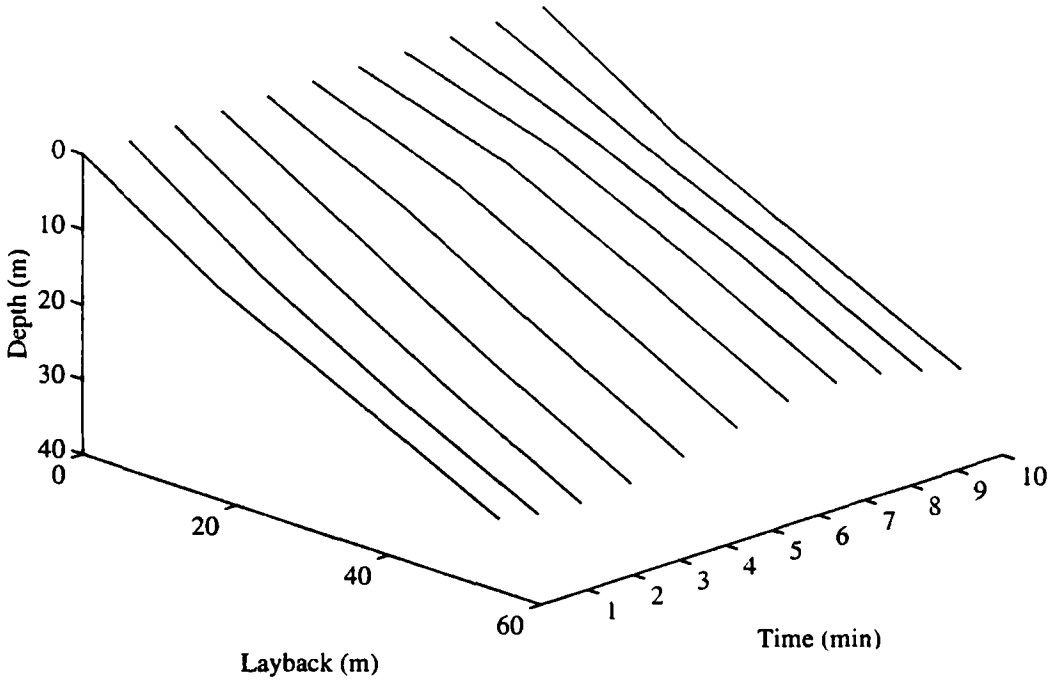

Figure 5.63 - Waterfall zoom configuration for simulation HWSL.

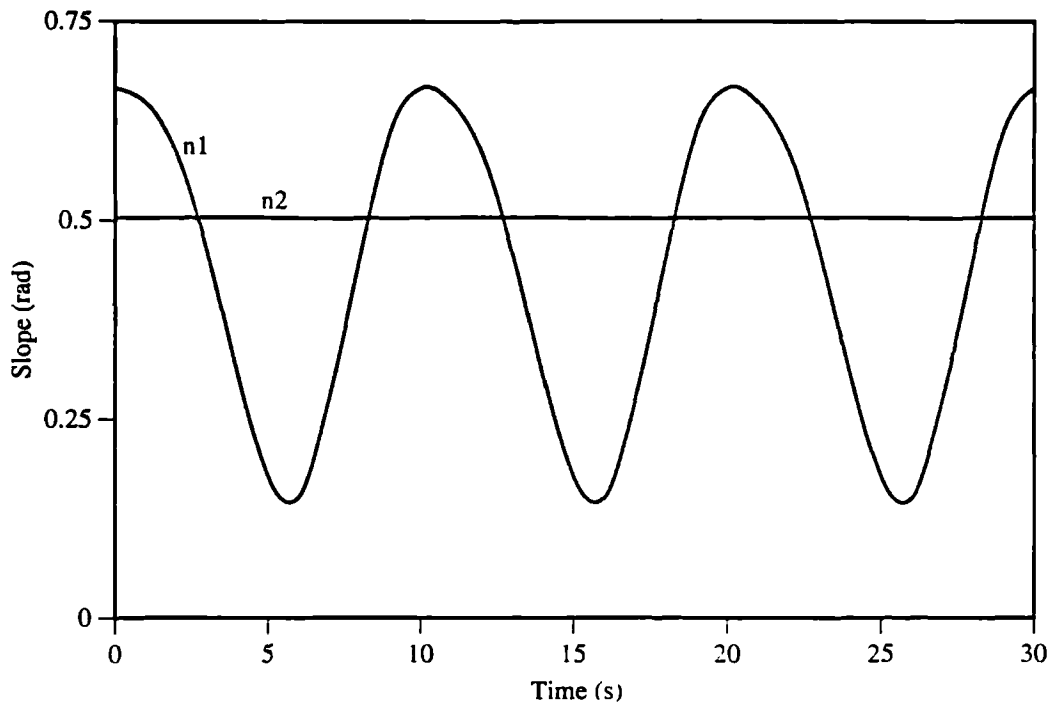

Figure 5.64 - Slope versus time for simulation HWSL.

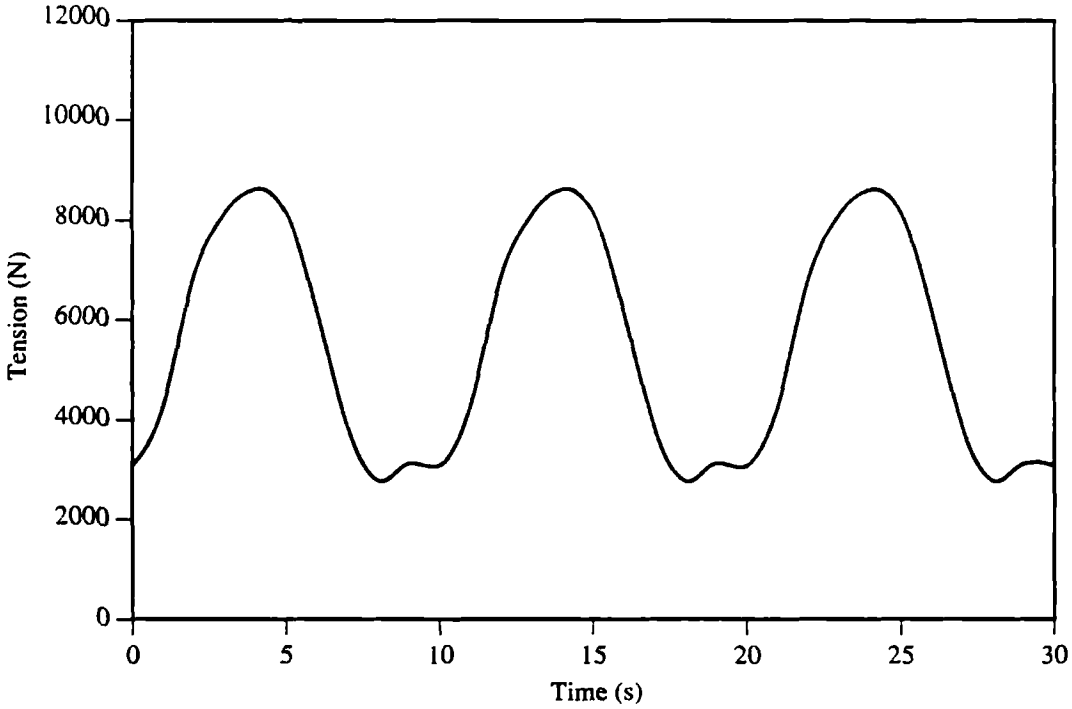

Figure 5.65 - Top tension versus time for simulation HWSL.

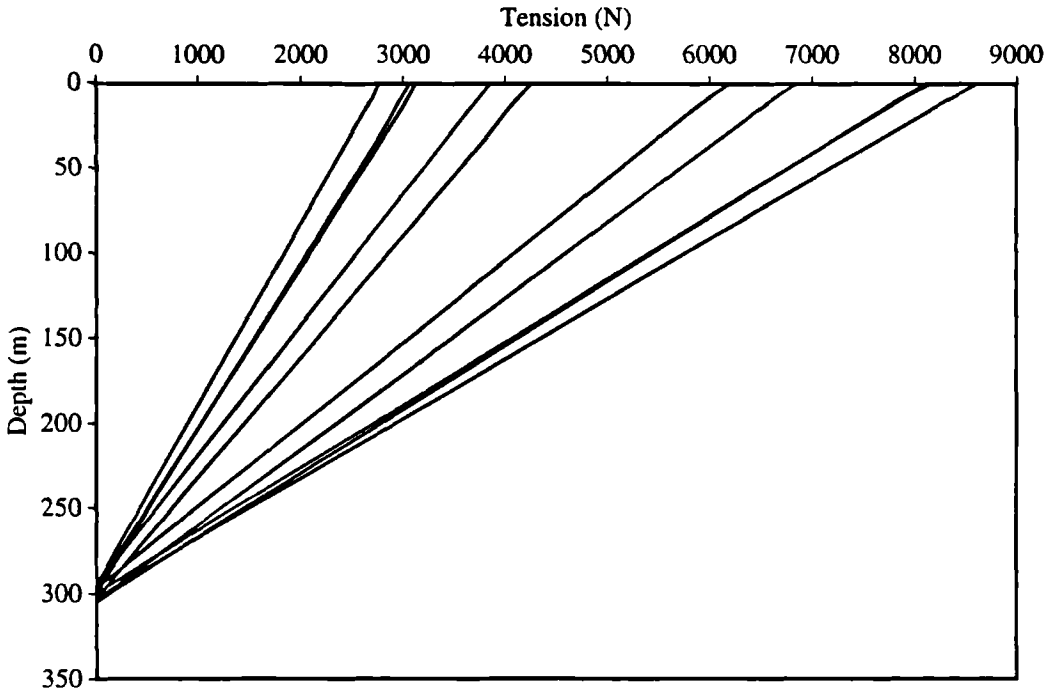

Figure 5.66 - Tension versus depth for simulation HWSL.

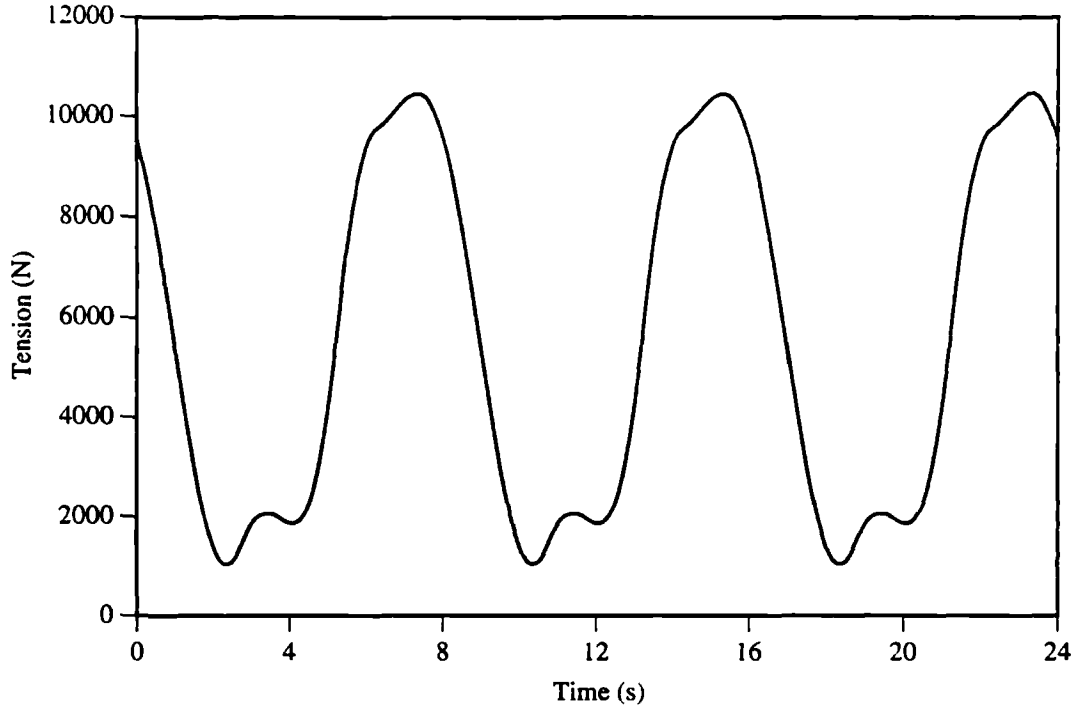

Figure 5.67 - Top tension versus time for simulation HWSL.

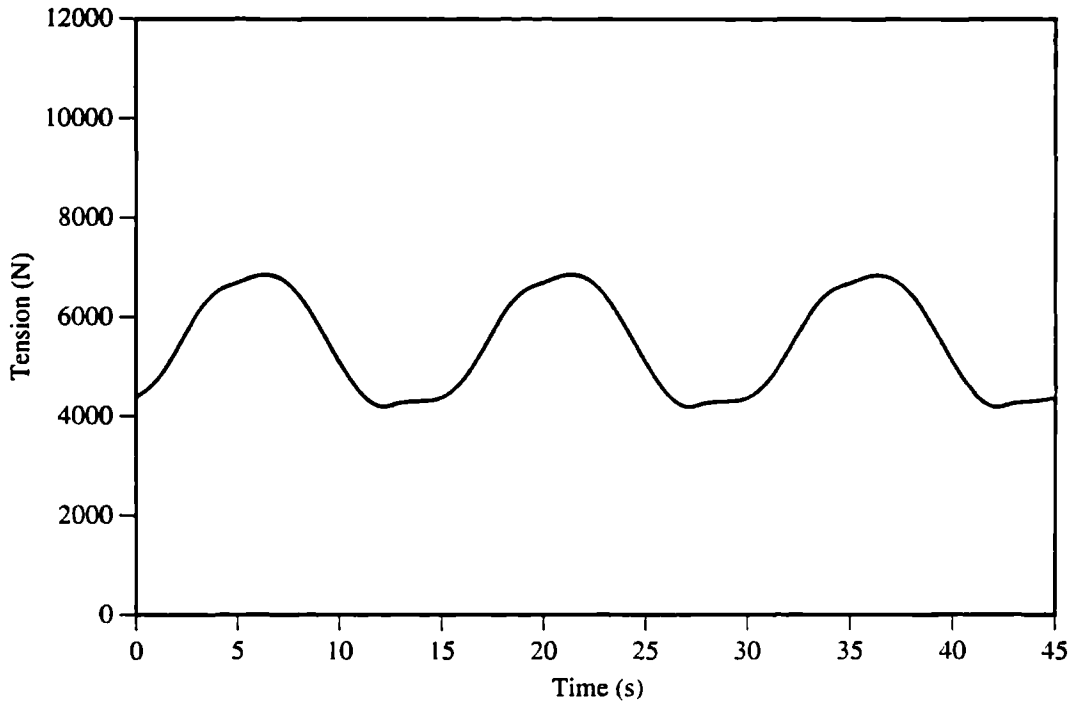

Figure 5.68 - Top tension versus time for simulation HWSL.

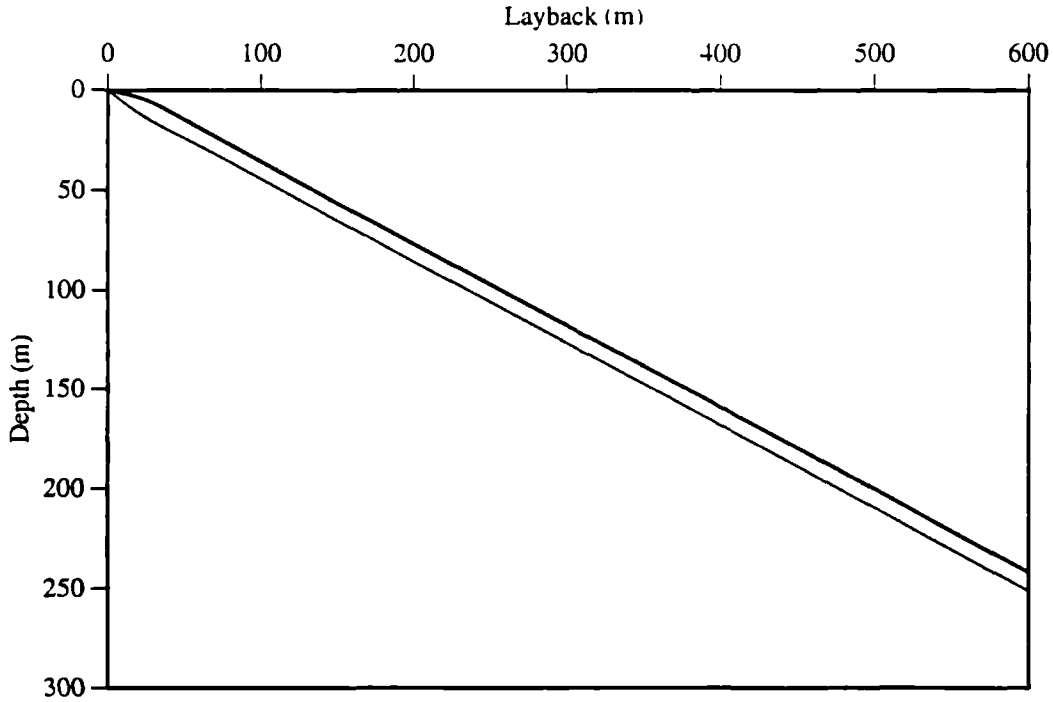

Figure 5.69 - Configuration envelope for simulation LWSL.

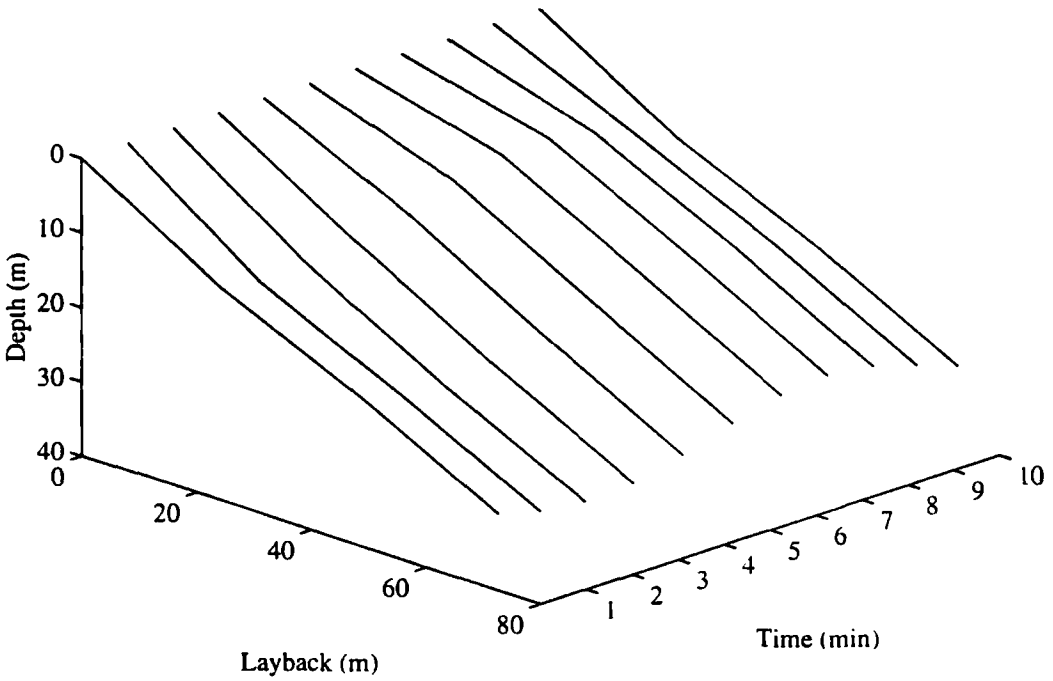

Figure 5.70 - Waterfall zoom configuration for simulation LWSL.

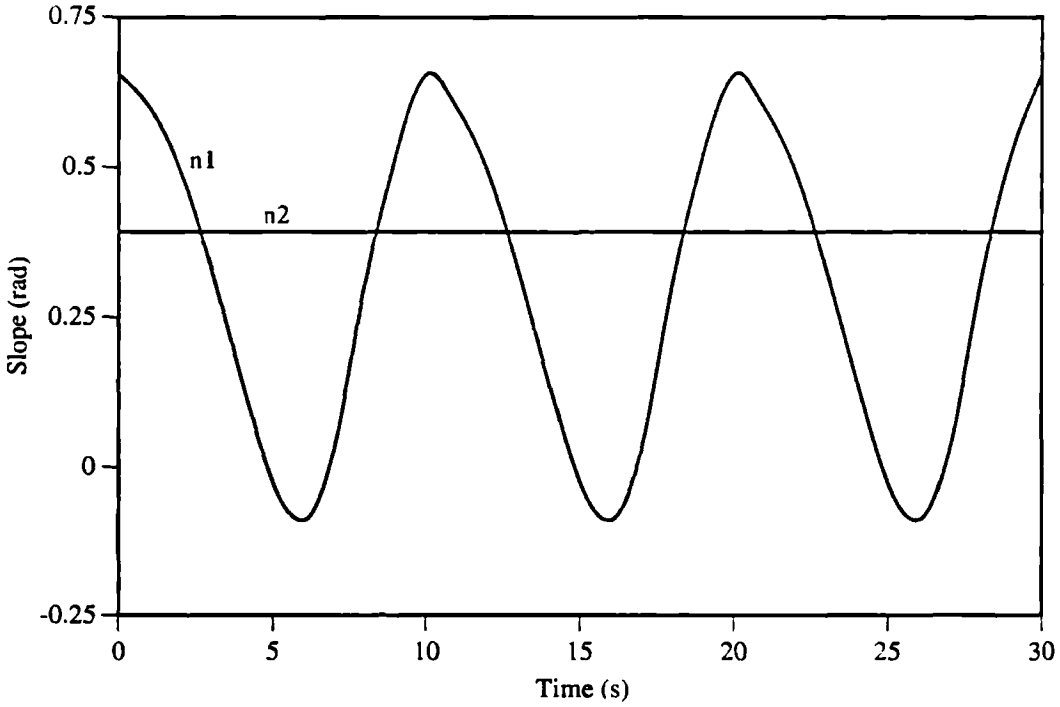

Figure 5.71 - Slope versus time for simulation LWSL.

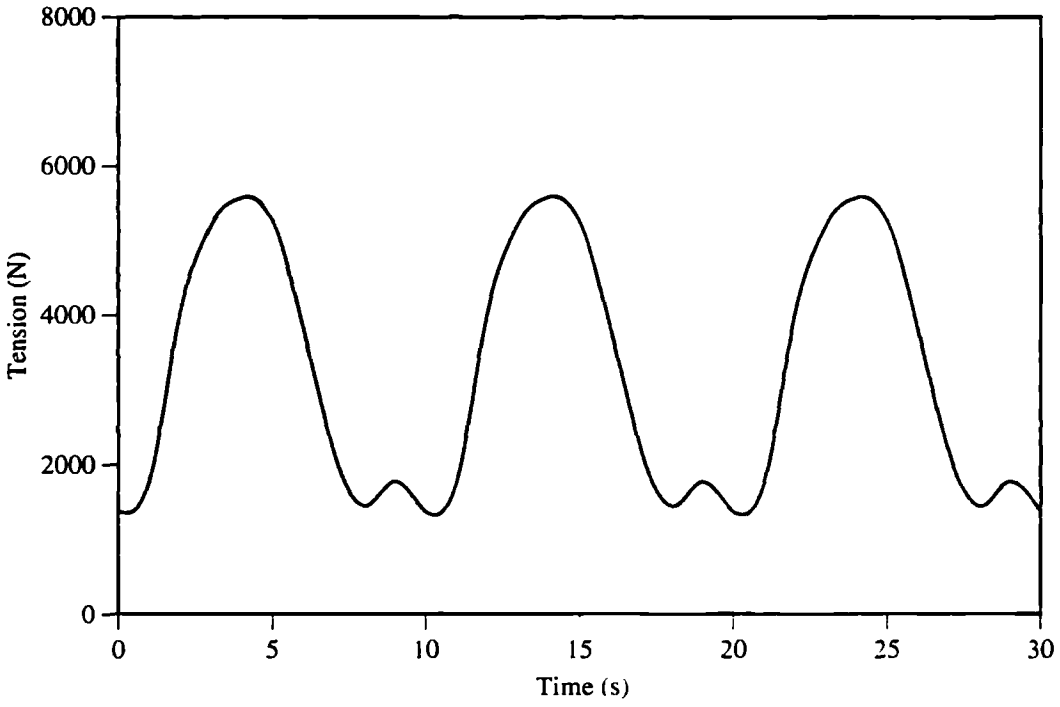

Figure 5.72 - Top tension versus time for simulation LWSL.

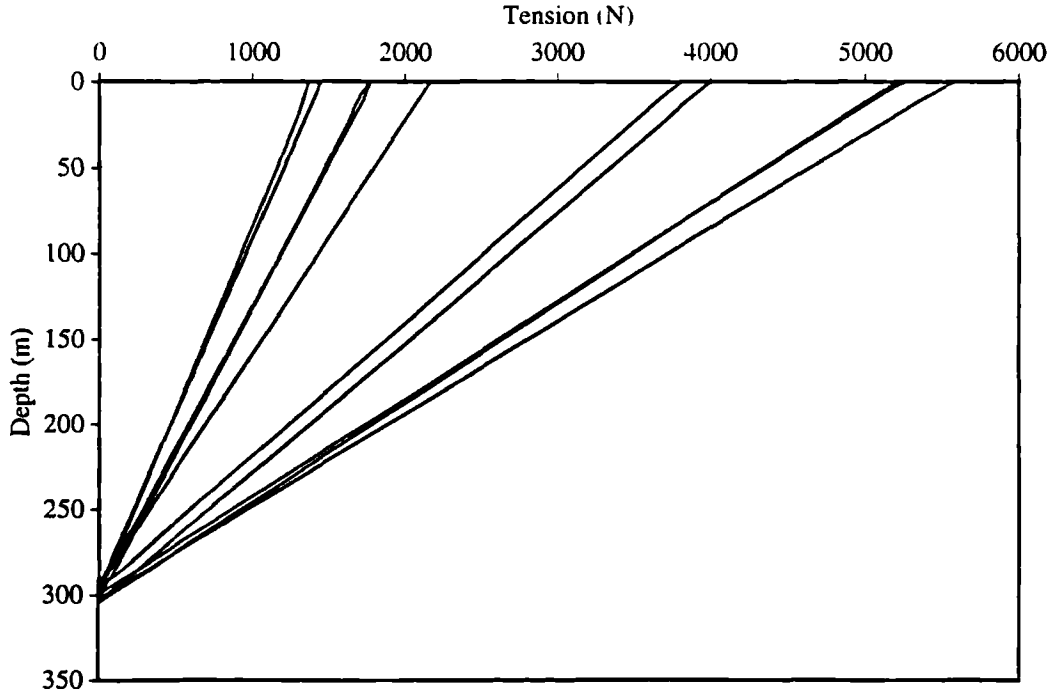

Figure 5.73 - Tension versus depth for simulation LWSL.

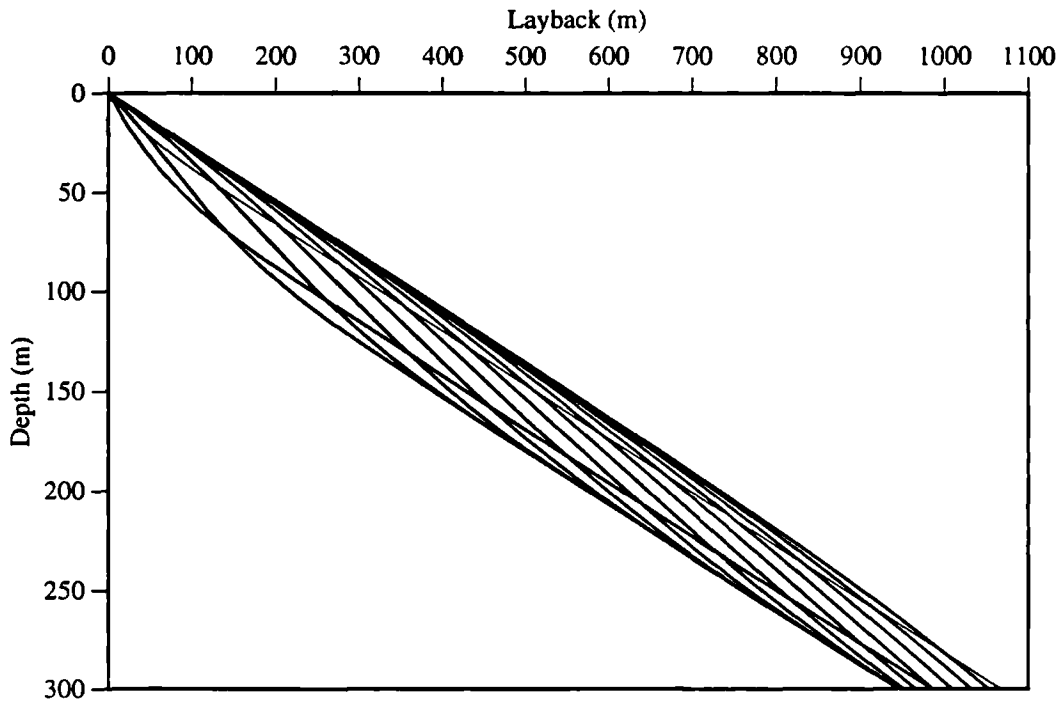

Figure 5.74 - Configuration for simulation HHSL.

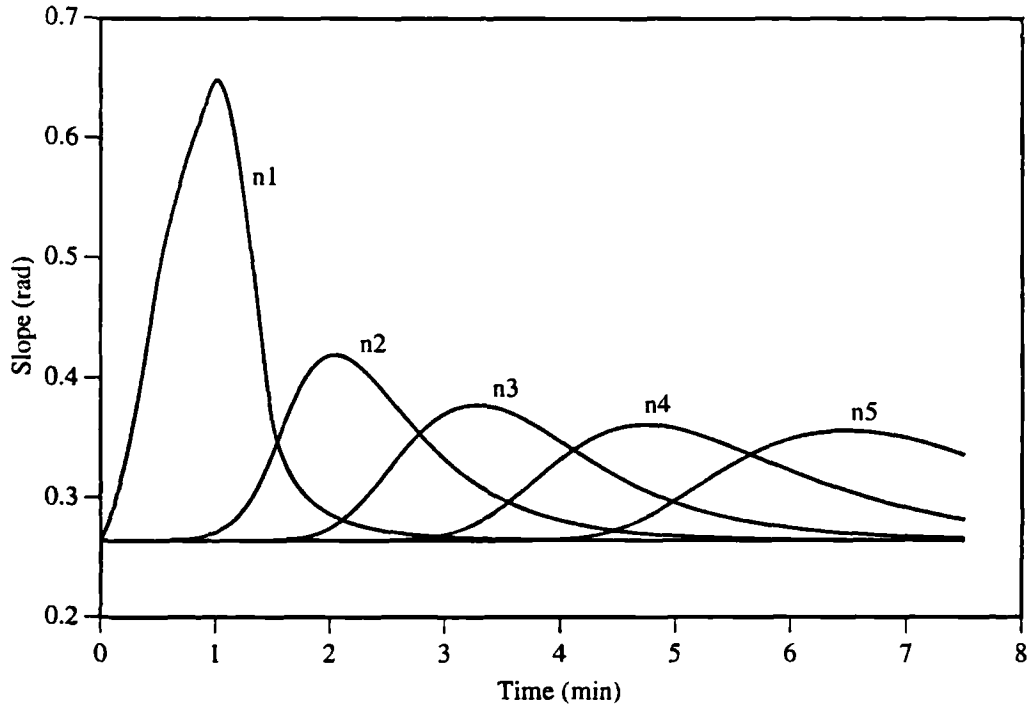

Figure 5.75 - Slope versus time for simulation HHSL.

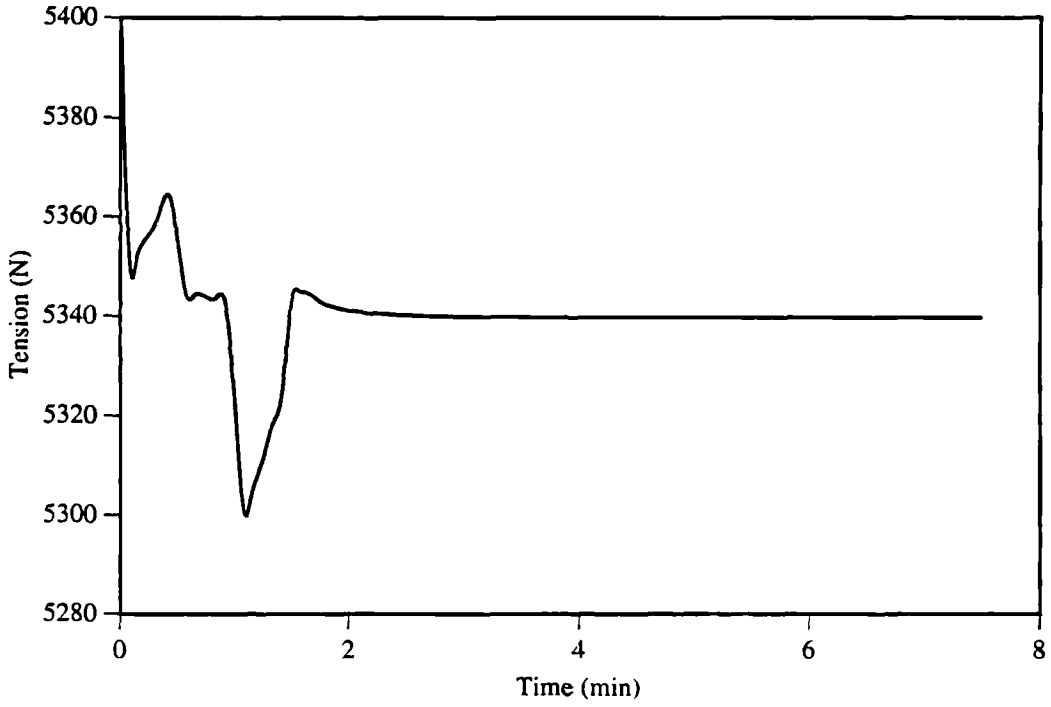

Figure 5.76 - Top tension versus time for simulation HHSL.

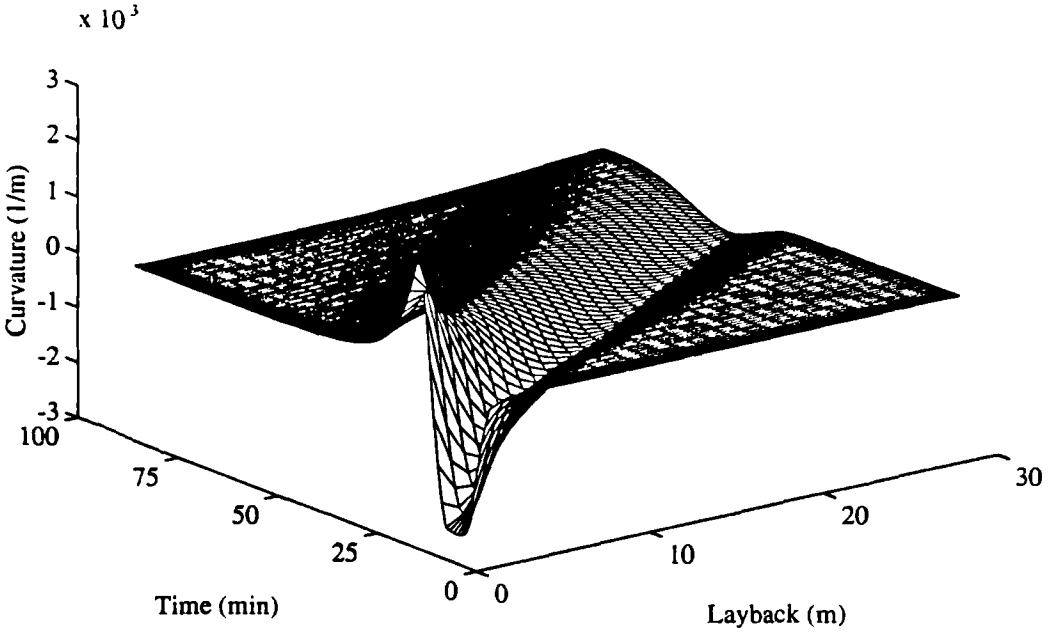

Figure 5.77 - Waterfall curvature for simulation HHSL.

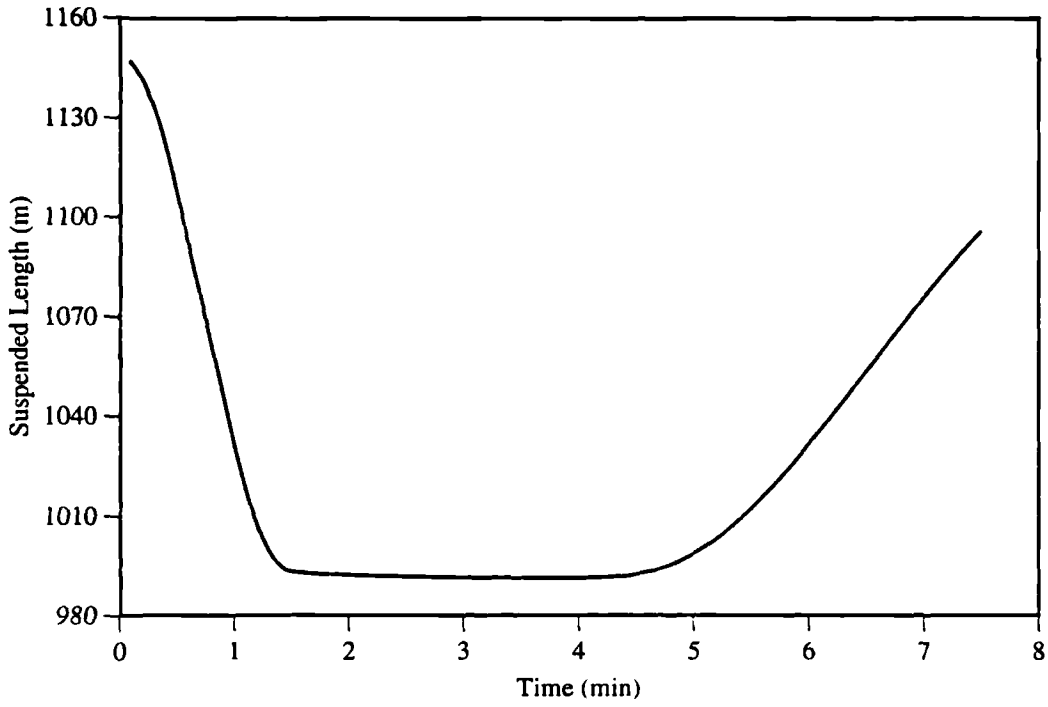

Figure 5.78 - Suspended length versus time for simulation HHSL.

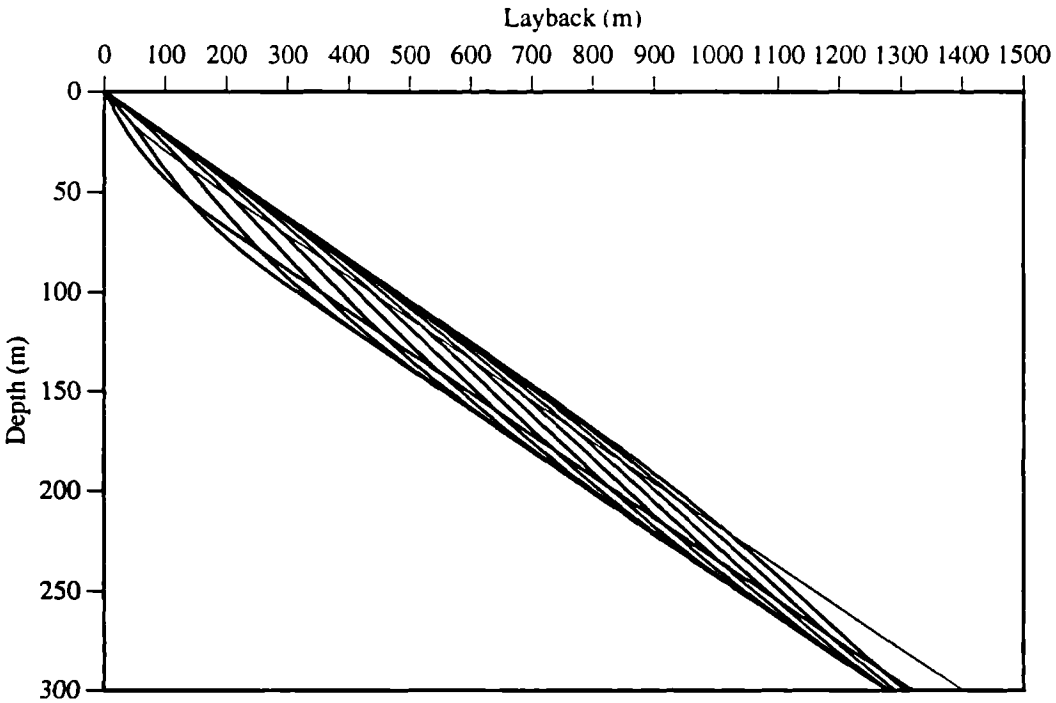

Figure 5.79 - Configuration for simulation LHSL.

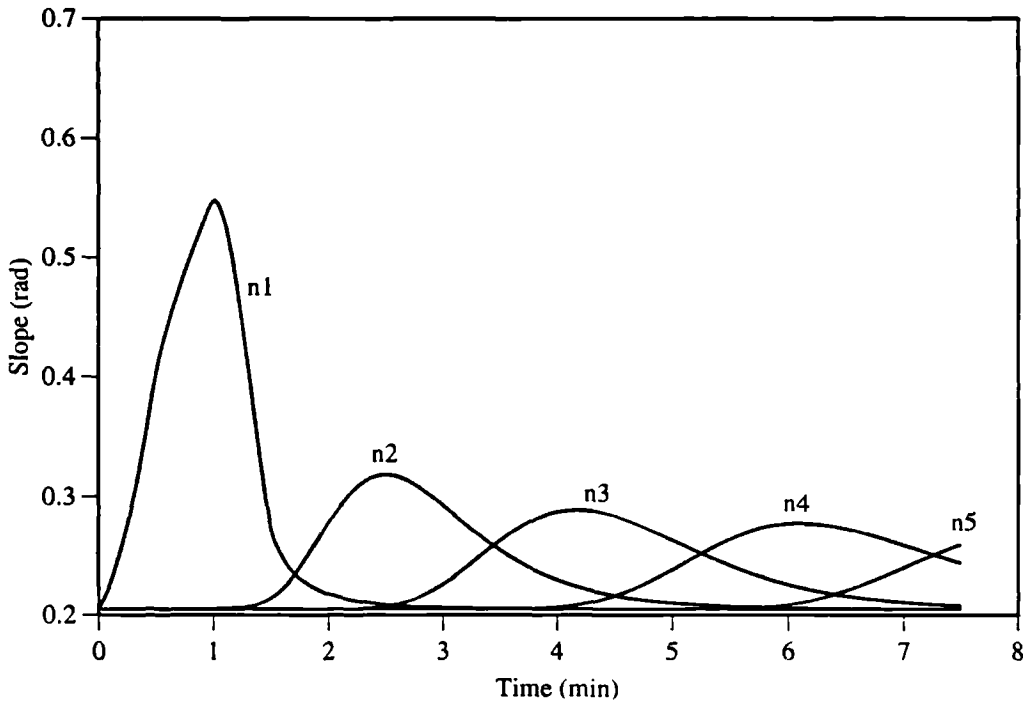

Figure 5.80 - Slope versus time for simulation LHSL.

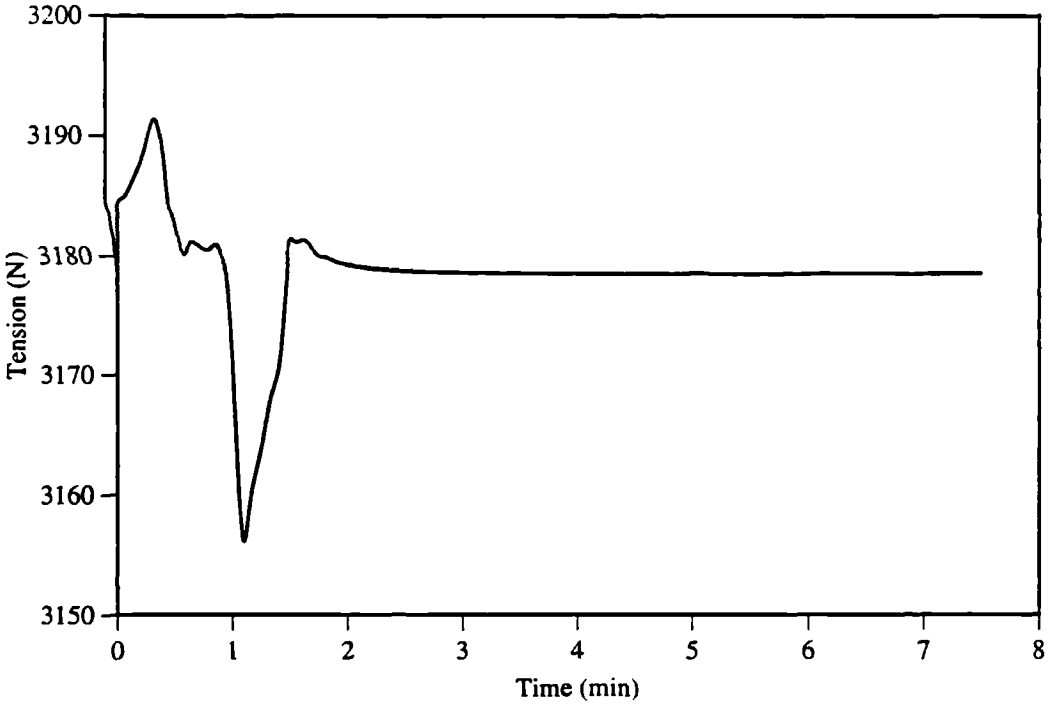

Figure 5.81 - Top tension versus time for simulation LHSL.

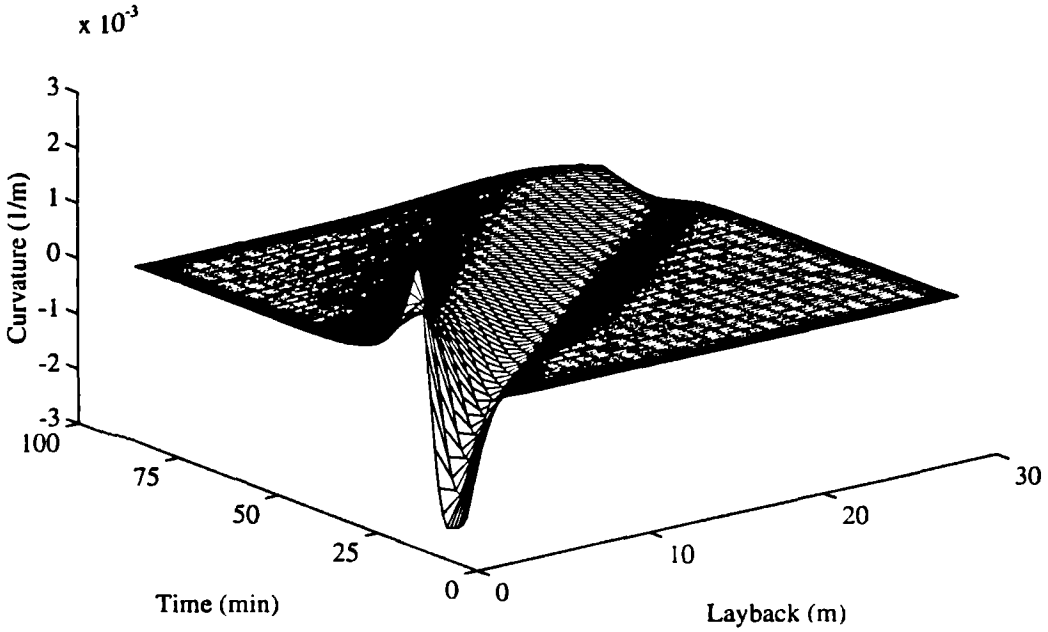

Figure 5.82 - Waterfall curvature for simulation LHSL.

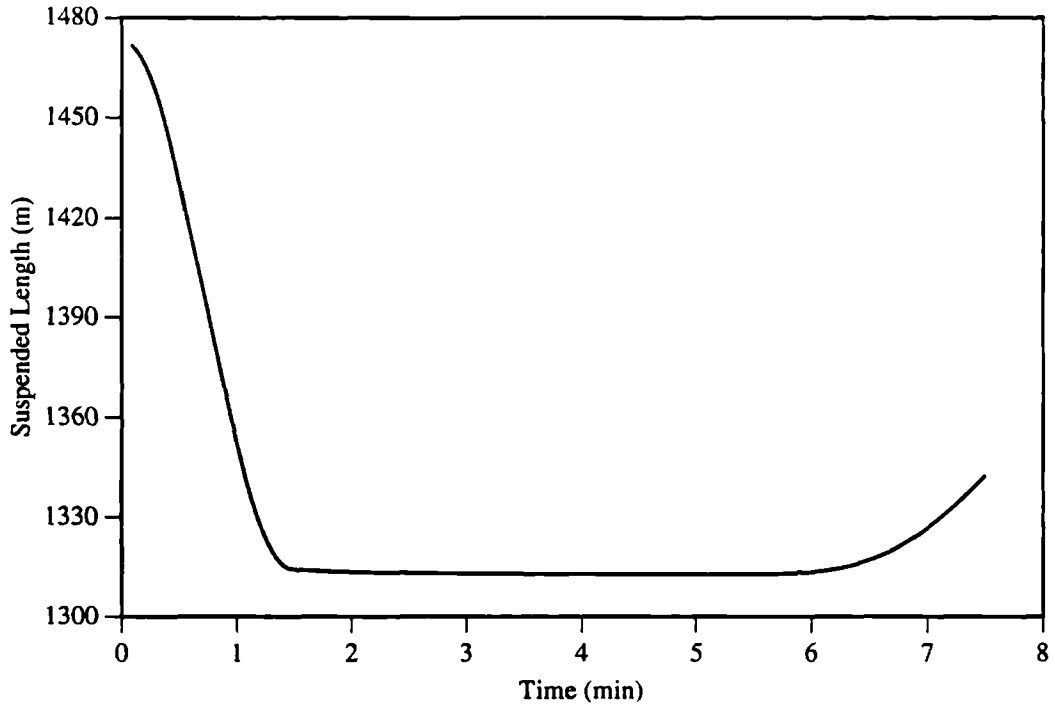

Figure 5.83 - Suspended length versus time for simulation LHSL.

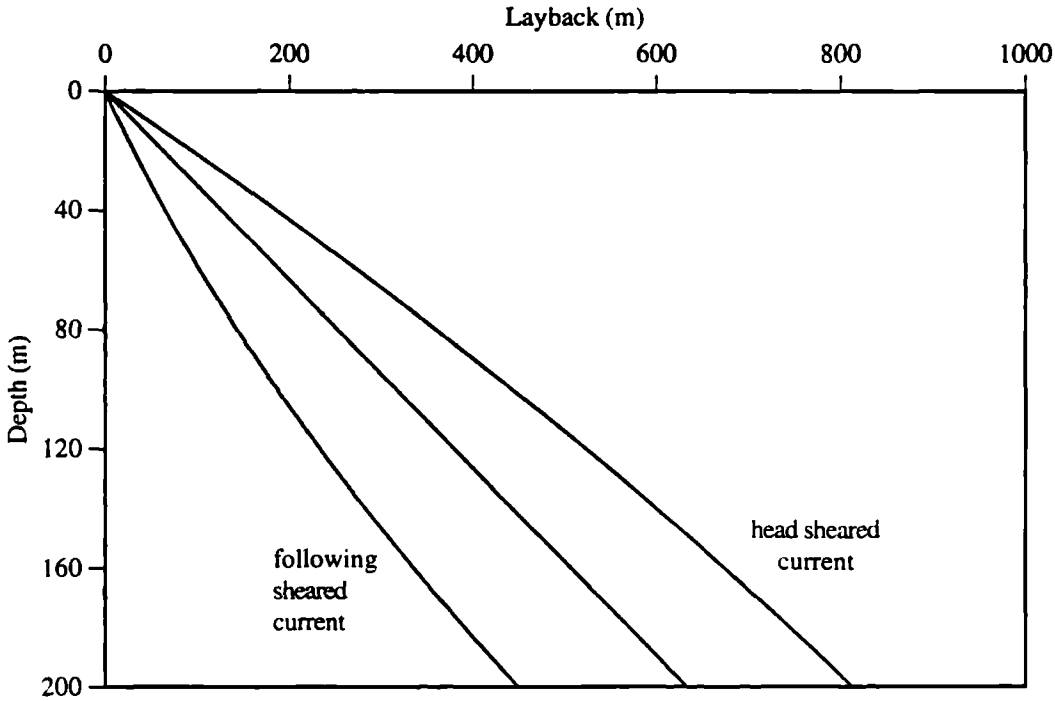

Figure 6.1 - In plane configuration envelope.

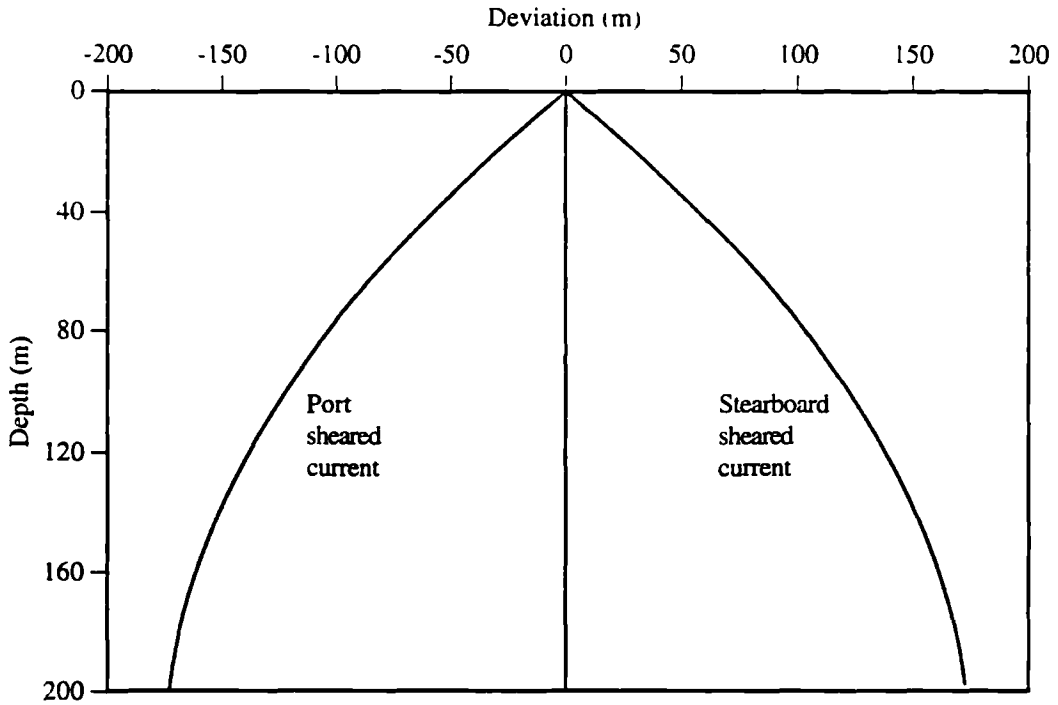

Figure 6.2 - Out of plane configuration envelope.

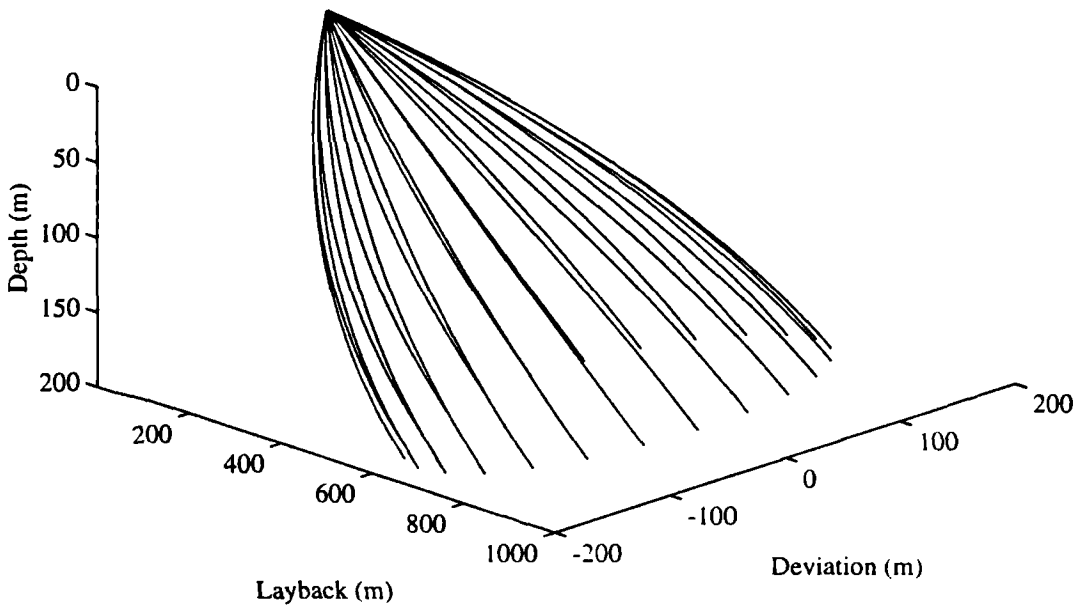

Figure 6.3 - Three dimensional configuration.

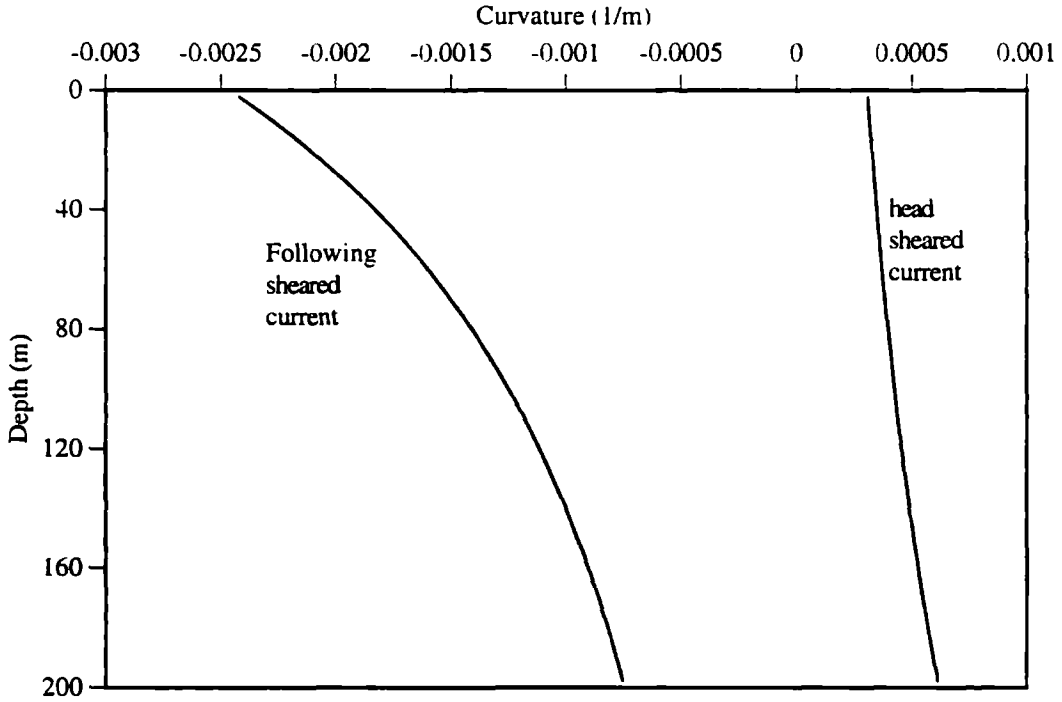

Figure 6.4 - In plane curvature envelope.

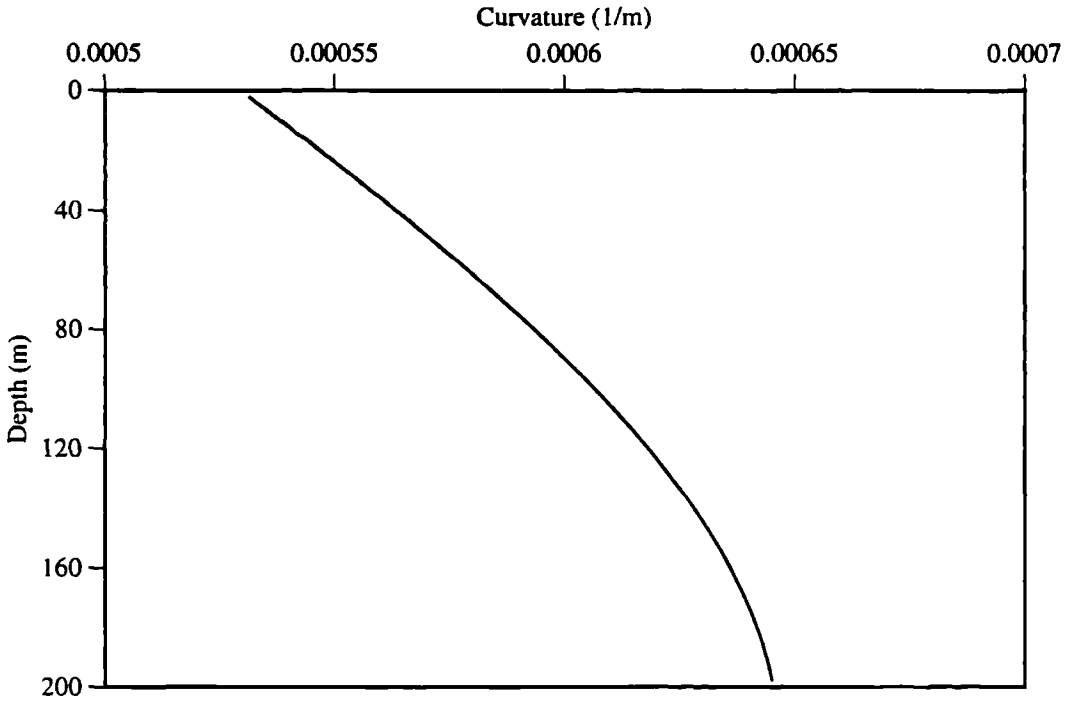

Figure 6.5 - Out of plane curvature.

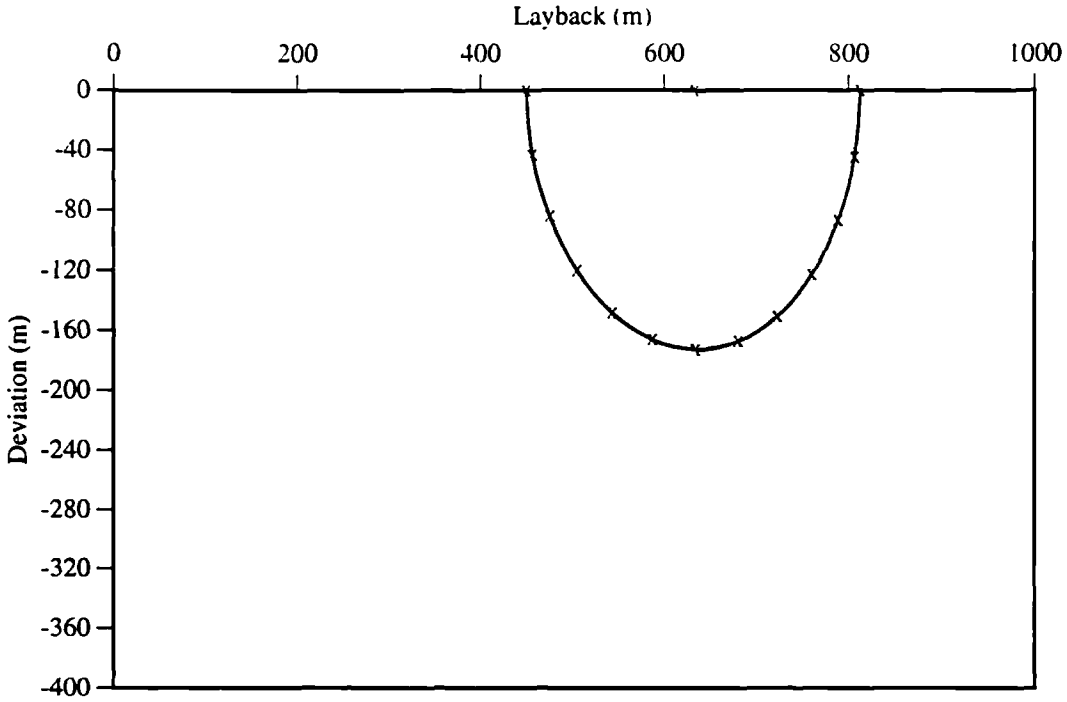

Figure 6.6 - Foot print diagram.